The University Of Sheffield.

Department Of Mechanical Engineering.

Numerical Modelling of Wind Borne Pollution Dispersion from Open Windrow Compost Sites

PhD Thesis

March 2014

Stylianos KATSANIS

BEng, MSc (Res)

Supervisors: Dr. S.B. CHIN and Dr. F.C.G.A. NICOLLEAU

Sheffield Fluid Mechanics Group

Thesis submitted to the University of Sheffield in partial fulfilment of the requirements for the degree of Doctor of Philosophy

Numerical Modelling of Wind Borne Pollution Dispersion from Open Windrow Compost Sites

Stylianos KATSANIS

PhD Thesis - The University of Sheffield - March 2014

Abstract

Open environmental flow is a multivariable, non-linear, unsteady flow system which presents a challenge to those who engage in understanding, monitoring and predicting it.

This thesis sets the foundation for future work and suggests best practice techniques for the numerical simulation of such flow taking into account important phenomena and assumptions. These factors include boundary conditions, location and size of the control volume and level of resolution. The use of more comprehensive techniques such as Computational Fluid Dynamics proposed herein, compared to those currently employed by regulating agencies, may take into account local meteorology and topography in order to provide a more accurate estimation of pollutant dispersion by site specific investigation.

Wind flow and effluent pollutant dispersion was examined for idealised flat and hilly terrains where topography was seen to largely influence wind flow phenomena and later pollution dispersion. These simulations assumed an incompressible, steady state air, flowing isothermally over vertical and horizontal line sources positioned near ground and upstream one or two sinusoidal axisymmetric hills in a single row. Results suggest that the wind speed increases on the upslopes of hills. Then the flow recirculates strongly on the downslope of a hill or the lee of any bluff body such as a house or trees.

Furthermore, a case study has been carried out for two locations in the UK, employing techniques and conclusions from idealised simulations. A proposed compost site, located in South Yorkshire was examined, where the local topography is characterised by sloping terrain and large woods; such factors were seen to influence wind flow and dispersion of particles and concentration. Results from the compost site were compared to results from a contrasting flat-land green waste processing plant in West Midlands. All simulations assumed an incompressible, steady state wind over three presumed compost piles.

For all cases studied herein, Lagrangian particle tracking was employed to show particle dispersion from the alleged compost piles and calculate average travel distances for trapped particles and entrapment probability. Particle tracking results show that particulate pollutants can get trapped at recirculation areas, in-between trees and village houses. Mass-less particles travel further before hitting an obstacle when released in low winds and their orbit is largely affected by topography when released from near ground sources.

In addition, Species Transport was enabled to examine the effect of topographical and meteorological conditions to pollutant concentrations. Species transport results for the examined composting sites show an increased number of particles trapped in-between rows of compost piles and a decrease of emissions to near background values within 200m from the source. However, it was evident that flat land favours the spread of species which can reach nearby houses at larger percentages.

Keywords: Computational Fluid Dynamics, Wind Flow, Effluent Pollution Dispersion, Idealised Terrain, Complex Topography, Open Windrow Composting.

To my family...

Acknowledgements

Every PhD thesis is a complicated piece of work. Although there is only a single name on the cover page many people came together and worked hard to make this thesis possible and worth reading.

Therefore, I would like to express my gratitude to:

Dr. S.B. Chin, for giving me the opportunity to undertake a PhD. His supervision, continuous help and father-like patience all those years during my BEng, MSc and PhD studies will never be forgotten. He has been a great help breaking down the complicated environmental modelling problem, explaining fluid mechanics principles, how CFD works and always pointing to the right direction when things were getting difficult or complicated.

Dr. F.C.G.A. Nicolleau, for his supervision and support during all those years; all the time he spent explaining mathematical equations to me and supplying key literature. His insight about particle behaviour and guidance on the mathematical part of this thesis was key to its completion. He has also helped me meet very interesting and well-known people in the field of fluid mechanics.

Dr. W.A. Bullough, for coming up with the original problem of air pollution from open windrow composting operations and giving ideas on how to approach the air pollution dispersion subject. He has also been our contact to the outside world getting in touch with the Environment Agency and the Health and Safety officials.

Mr. A. Viz, for taking part in our research work and looking into the complicated air pollution dispersion problem; therefore completing 2D simulations of idealised terrain for his MEng thesis. His useful results and conclusions are used and referenced in this work as a valuable step towards 3D approaches and simulations.

Special thanks go to my parents, John and Elisabeth for their moral and most importantly financial support during all my student years. Occasionally, they have been a shoulder to sob on when things were not going as planned.

I would also like to thank all undergraduate and postgraduate students who undertook their final year projects with us. Their questions about CFD helped me improve my work and presentation. They have been the most useful reviewers of my work.

Finally, special thanks go to all those who helped in their own special ways and most likely don’t know about it!

Kind Regards,
Stelios Katsanis

Nomenclature

English Symbols

$\overline{q_z}$	Vertical mean heat flux	W m^{-2}
$\overline{u_h}$	Mean velocity magnitude at reference height h	m s^{-1}
$\overline{u_p}$	Mean wind velocity at point P	m s^{-1}
$\overline{q}$	Mean specific humidity	-
$\overline{u}$	Mean wind velocity	m s^{-1}
$\overline{u}_x$	Mean wind velocity in the x direction	m s^{-1}
$\overline{u}_{inlet}$	Mean wind velocity at the inlet boundary	m s^{-1}
A	Surface area	m^2
a_{LSD}	Constant for the LSD method	-
A_{mp}	Amplitude	m
B	Constant for the LSD method	-
C	Trace concentration	kg m^{-3}
$C_{1\varepsilon}$, $C_{2\varepsilon}$, $C_{3\varepsilon}$	Turbulence model constants	-
c_d	Drag coefficient	-
c_e	Energy coefficient	-
c_{mi}	Mass concentration of species i	ppm
C_p	Pressure coefficient	-
c_p	Specific heat of air	J kg^{-1} K^{-1}
c_{vi}	Volumetric concentration of species i	kg m^{-3}
C_μ	k-ε turbulence model constant	-
C_w	Empirical wall constant	9.793
D	Hill diameter	m
d_p	Particle diameter	m
$D_{q,m}$	Diffusion coefficient for species q in the mixture	m^2 s^{-1}
e	Internal energy	J kg^{-1}
E	Specific total energy	J
f_c	Coriolis parameter	s^{-1}
F_D	Drag force	N
f_H	Flux of heat	J m^{-2}
f_m	Flux of momentum	N s m^{-2} s^{-1}
f_M	Flux of moisture	% m s^{-1}
G	Variable for the LSD method	-
g	Gravitational force	m s^{-2}
G_b	Generation of turbulent kinetic energy due to buoyancy	kg m^{-1} s^{-3}
G_k	Generation of turbulent kinetic energy due to mean velocity	kg m^{-1} s^{-3}
H	Hill height	m
h	Specific enthalpy	J kg^{-1}
h_{IL}	Inner layer height	m
h_{ref}	Reference height (for ABL)	m

H_{req}	Required height of the domain simulated	m
J_q	Diffusion flux of species q	kg m^{-2} s^{-1}
K	Wave number	m^{-1}
k	Turbulent kinetic energy	m^2 s^{-2}
k_{eff}	Effective thermal conductivity	kg m^{-3} s^{-3} K^{-1}
K_h	Turbulent exchange coefficient for heat	-
K_{ij}	Second order tensor	-
K_m	Turbulent exchange coefficient for momentum	-
k_P	Constant of proportionality	-
k_p	Turbulent kinetic energy at point P	m^2 s^{-2}
K_q	Turbulent exchange coefficient for moisture	-
l	Turbulent intensity	%
L_{ch}	Characteristic hill length	m
L_{MO}	Monin-Obukhov length	m
L_{req}	Required length of the domain simulated	m
L_v	Latent heat of evaporation	kJ kg^{-1}
m_i	Mass of species i	kg
n_{LSD}	Constant for the LSD method	-
p	Pressure	Pa
p_{LSD}	Constant for the LSD method	-
p_{stat}	Static pressure	Pa
Q	Source of trace gas	kg s^{-1} m^{-2}
R	Hill radius	m
$R*$	Gas constant	J kg^{-1} K^{-1}
Ra	Ideal gas constant for air	J kg^{-1} K^{-1}
Rc	Energy released from chemical reactions (or other processes)	J
Re	Reynolds number	-
R_b	Richardson bulk number	-
R_f	Richardson flux number	-
R_i	Richardson number	-
R_q	Net rate of production of species q	kg s^{-1} m^{-2}
S_{Ct}	Turbulent Schmidt number	-
S_h	User defined heat source of heat from chemical reaction	K
S_k	Turbulent kinetic energy, user defined source term	kg m^{-1} s^{-3}
S_ε	Turbulent dissipation rate, user defined source term	kg m^{-1} s^{-4}
S_M	Modulus of the mean rate of strain tensor	s^{-2}
S_q	Rate of creation at source for species q	kg s^{-1}
T	Absolute temperature	K
T_L	Lagrangian integral time	s
T_o	Ground temperature	K
u'	Instantaneous velocity	m s^{-1}
u_*	Surface friction velocity	m s^{-1}
u, v, w	Cartesian velocity components	m s^{-1}

u_p	Particle velocity	m s^{-1}
V	Volume	m^3
x, y, z	Cartesian coordinates	m
y_p	Distance from point P to wall	m
y^+	y plus value	-
Y_q	Mass fraction of species q	-
z	Vertical height above ground level	m
z_0	Surface Roughness height	m
z_{ABL}	Height of ABL	m

Greek Symbols

$\overline{\theta}$	Mean temperature	K
Γ	Gamma function (see Eulerian pollution dispersion models)	-
ΔS	Speed up ratio	-
ΔS_{max}	Maximum speed up ratio	-
ε	Turbulent dissipation rate	m^2 s^{-3}
ζ	Normally distributed random number	-
κ	Von Karman constant	0.4
μ	Dynamic viscosity	Pa s
μ_t	Turbulent viscosity	kg m^{-1} s^{-1}
v_θ	Thermal viscosity	m^2 s^{-1}
ρ	Density	kg m^{-3}
ρ_{air}	Density of air	kg m^{-3}
ρ_p	Density of particle	kg m^{-3}
σ	Shear stress tensor	N m^{-2}
$\sigma_k, \sigma_\varepsilon$	Turbulent Prandtl numbers for k and ε	-
σ_y	Transverse pollutant spread	m
σ_z	Vertical pollutant spread	m
τ_x, τ_y, τ_z	Wind shear stress for the three Cartesian directions	N m^{-2}
τ_{eff}	Effective shear stress	kg m^{-1} s^{-2}
Φ_E	Earth's latitude	deg
Ω	Angular velocity (earth rotation rate)	rad s^{-1}
∇	Nabla symbol defined as $\nabla = \begin{pmatrix} \frac{\partial}{\partial x_1} \\ \frac{\partial}{\partial x_2} \\ \frac{\partial}{\partial x_3} \end{pmatrix}$	-

Acronyms

2D	Two Dimensional
3D	Three Dimensional
ABL	Atmospheric Boundary Layer
AF	Aspergillus Fumigatus
CBL	Convective Boundary Layer
CERC	Cambridge Environmental Research Consultants

CFD	Computational Fluid Dynamics
CFU	Colony Forming Unit
DEFRA	Department for Environment, Food and Rural Affairs (UK)
DNS	Direct Numerical Simulation
E	East
EA	Environment Agency (UK)
EC	European Community
ENE	East North East
ESE	East South East
EU	European Union
HSE	Health and Safety Executive (UK)
k-ε	k-epsilon (turbulence model)
LES	Large Eddy Simulation
LSD	Speed up over hill calculation method by Lemelin et al., 1988
LSM	Lagrangian Stochastic Model
ML	Mixed Layer
N	North
NE	North East
NECPI	National Emission Ceilings Policy Instruments Group
NNE	North North East
NNW	North North West
NS	Navier Stokes
NW	North West
PMx	Particulate Matter of diameter x (microns)
R&H	Richards and Hoxey (1993) approach
RANS	Reynolds Averaged Navier Stokes
RNG	Re-Normalisation Group
RWM	Random Walk Model
S	South
SBL	Stable Boundary Layer
SE	South East
SL	Surface Layer
SSE	South South East
SSW	South South West
SW	South West
TRY	Test Reference Year
UDF	User Defined Function
UDP	User Defined Profile
UK	United Kingdom
UoS	The University of Sheffield
US	United States
US EPA	United States Environmental Protection Agency
VOC	Volatile Organic Compound
W	West
WNW	West North West
WSW	West South West

Table of Contents

List of Figures

List of Tables

Thesis Roadmap

Environmental flow and effluent pollution dispersion from industrial scale windrow composting sites are two complex problems examined in this work. Chapter 1 introduces the air pollution problem and outlines the aims and objectives of this thesis. Chapter 2 describes the structure of the lower atmosphere, in which air pollution from ground sources takes place, with the Atmospheric Boundary Layer characteristics largely influencing wind flow and pollutant dispersion from near ground sources. Other important factors that influence those problems have also been included herein such as topography, weather conditions together with source type and emission rate.

Available mathematical models for effluent pollutant dispersion are described in Chapter 3 amongst which is the Gaussian plume model. This rather simple model is employed by the well accepted ADMS program for calculating pollutant spread and is also approved for risk assessment by the UK Environment Agency.

Chapter 4 introduces the Computational Fluid Dynamics (CFD) technique as a more suitable tool for examination of pollutants released in the wind near ground level. The mathematical modelling and relative parameters adopted are also explained with all necessary assumptions for the numerical modelling technique, including a literature review for the choice of boundary conditions by the author of this paper.

The necessity for examination of wind flow and pollution dispersion over idealised terrain to establish the appropriate CFD procedure given the available tools is examined in Chapter 5. A neutral ABL was first simulated over a flat plane to reproduce results from other authors and prove the ability of the CFD program FLUENT to model such open environmental flow. Ideal axisymmetric sinusoidal 2D and 3D hills were also simulated. Studies for domain size and mesh density helped decide on the necessary boundary positions and the essential high-density near-ground resolution respectively. On the other hand, in order to solve the wind flow problem the researcher employed the RANS equations as well as the Lagrangian particle tracking and Species Transport equations to figure out the pollutant dispersion problem.

Implementing the procedure and conclusions from ideal terrain simulations in Chapter 5, a case study was undertaken including two industrial open windrow composting sites in the UK. Chapter 6 includes topographical descriptions of these two contrasting sites (Site A has a hilly terrain and Site B has a nearly flat terrain) and examines wind flow along with pollution dispersion from a group source of three simulated compost piles. Actual weather conditions were taken into consideration by statistically processing wind speeds and directions for South Yorkshire from the weather station situated at Weston Park Museum in Sheffield, UK.

Chapter 7 discusses challenges and difficulties in the CFD modelling technique adopted and presented in Chapter 4, comments on the results for ideal terrain presented in Chapter 5 and finally further explains results for the two open windrow composting sites modelled in Chapter 6. Topography effects to the wind flow are further discussed and results from the two methods employed for effluent pollutant modelling (Lagrangian Particle Dispersion and Species Transport) are combined to give a better understanding of the behaviour of particulate pollutants when released from near-ground sources like open windrow compost piles.

Finally, conclusions of this work are presented in Chapter 8. Suggested future work, different approaches and recommended combinations of cases to examine in the future are given in Chapter 9.

Note to the reader:

This thesis follows a bottom-up approach from simple to complex when it comes to explaining theory, physics and background information. The same approach has been followed with all CFD simulations herein, starting with the simplest two-dimensional ideal terrain cases and by gradually adding complexity, concluding with a couple of three-dimensional real life open windrow composting case studies.

Chapter 1

INTRODUCTION

1.1 Environmental Air Pollution

“The word *pollution* comes from the Latin *pollutus*, which means made foul, unclean, dirty” [Arya, 1999]. It is commonly used in everyday life to describe an atmospheric condition in which the concentration of several substances is higher than the normal background level (clean atmosphere). Pollution exists everywhere, even in the most remote locations. However, it is worse in high or over-populated cities and industrial zones where it can affect people, animals, vegetation and even materials.

Environmental air pollution is one of the major and growing concerns within the last decade, largely contributing to climate change. It has become an increasing problem over the last years due to growing population and industrialization. The environment is a very complicated and continuous changing natural system, difficult to understand and protect. Air pollution is a multi-variable problem consisting of gases, smoke, odours, dust, toxic and radioactive waste, and so on. Pollutants are not only emitted directly from a process but can also form in the air when primary pollutants react; these are called secondary pollutants.

Different types and scales of environmental air pollution problems exist. These can be summarised in Table 1; three main types of problem are listed (I, II and III) and categorised according to the vertical and horizontal scales of the problem.

Type of problem		Horizontal Scale	Vertical Scale	Temporal Scale	Type of Organization
I	Indoor	10^{-2}-10^{-1}km	Up to 10^{-1} km	10^{-1}-10^{0} hr	Family/business
	Local	10^{-1}-10 km	Up to 3 km	10^{-1}-10 hr	Municipality/county
	Urban	10-10^{2} km	Up to 3 km	10^{0}-10^{2} hr	Municipality/county
II	Regional	10^{2}-10^{3} km	Up to 15 km	10-10^{3} hr	State/country
	Continental	10^{3}-10^{4} km	Up to 30 km	10^{2}-10^{4} hr	Country/world
III	Hemispheric	10^{4}-2 x 10^{4} km	Up to 50 km	10^{3}-10^{5} hr	World
	Global	4 x 10^{4} km	Up to 50 km	10^{3}-10^{6} hr	World

Table 1 : Types and scales of air pollution problems.
[Arya, 1999]

Each of the types of pollution mentioned above is determined by the emission source, the atmospheric conditions and the relevant receptors (all will be described later in this paper). Understanding these factors and their interactions is a multi-disciplinary task requiring groups of scientists, engineers and environment agencies.

Air pollution sources can be broken up into three main categories: (i) urban and industrial, (ii) agricultural and other rural and finally, (iii) natural emissions. These can be further sub-divided as seen in Table 2.

Urban and Industrial Sources	**Agricultural and Other Rural Sources**	**Natural Emissions**
Power Generation	Dust Blowing	Wind Erosion
Industrial Facilities	Slash Burning	Forest Fires
Transportation	Soil Emissions	Volcanic Eruptions
Process Emissions	Pesticides	Sea Spray & Evaporation
Waste Disposal	Decaying Waste	Soil Microbial Processes
Construction Activities	Waste Processing	Natural Decay of Organic Matter

Table 2 : Sources of air pollution [Arya, 1999].

From a closer look, this thesis deals with the numerical simulation of environmental wind flows and spreading/transfer of particulate pollutants released from green waste processing plants in the lower layer of the atmosphere. The physics and mathematics describing such wind flow are introduced and explained, including assumptions and necessary simplifications. Available atmospheric dispersion models are also described followed by all significant factors that should be considered when modelling complicated terrains and taking into account meteorological phenomena.

Green waste processing sites have become more common since the European Union Landfill Directive 1999/31/EC calls for a rapid decrease of the amount of waste going to landfill. Following this directive and in order to deal with the increasing number of plants for the alternative handling of waste in the United Kingdom, the Department of Environment, Food and Rural Affairs (DEFRA) published its Waste Strategy for England (2007) that sets a distance of 250m below which and in the presence of sensitive receptors, a full environmental risk assessment is required to be carried out [Okuniewski and Dennis, 2007: EA Policy no.405_07].

Inappropriately operated and maintained green waste processing sites are known to cause pollution, harm to health and nuisance through noise, odour, leachate and potentially harmful bioaerosols [Taha et al. 2005, 2006, 2007]. Mennink-Kersten et al. (2006) found that infections due to *Aspergillus* spores are nowadays a common cause of the death amongst immunodepressed people. Such diseases can be caused by the harmful spores of the heat tolerant *Aspergillus fumigatus* fungi that can penetrate the respiratory system because of their small size. Such spores occur naturally in the atmosphere at low densities but may be released at very high densities from green waste processing facilities and especially from open windrow composting plants when compost is shredded or turned during pre and post open windrow processes.

A Computational Fluid Dynamics (CFD) technique is introduced as an alternative approach to already established but simple models that simulate air pollutant dispersion. The commercially available CFD program ANSYS FLUENT is employed herein by using the Reynolds averaged Navier-Stokes (RANS) models for wind flow modelling, Lagrangian particle tracking and Species Transport models to supply more information on the effects of complex local topography and meteorological conditions in order to assess the spread of effluent pollutants more accurately.

At first, simulations include wind flow and pollutant dispersion over a flat plane and later two dimensional and three dimensional axis-symmetric hills to initially simplify the problem and understand the behaviour of the available models. Multiple hills are also examined by using several hill geometries to further show the influence of topography and wind speed to pollution spread.

In order to apply the above technique in the real world, a case study is carried out for a proposed open windrow compost site for green waste in South Yorkshire where the local topography has a strong influence on the dispersion of bioaerosols. Results are compared to an existing open windrow site where complaints from neighbouring residents have been reported.

1.2 Thesis Aims

This work aims to:

1. Examine the complications encountered in the numerical simulation of wind flow and effluent pollution dispersion in the open environment (lower atmosphere).
2. List all important phenomena and assumptions that should be taken into consideration by utilising Computational Fluid Dynamics as an alternative and enhanced tool compared to programs employed by several environment agencies.
3. Examine wind flow and pollution dispersion over the idealised terrain to understand the multivariable problem of wind flow and pollution dispersion in the open environment.

4. Apply the suggested approach to a real life problem for a proposed open windrow composting plant at a hilly location in South Yorkshire and compare results to an existing compost site at a flat location in West Midlands where complaints by nearby residents have been reported.

1.3 Thesis Objectives

This work was broken down into the following parts:

1. Project Planning:
    a. Definition of project aims.
    b. Definition of project objectives.
2. Literature Survey:
    a. Physics of environmental wind flows.
    b. Physics of pollutant dispersion in the lower atmosphere.
    c. Techniques and programs to simulate wind flow and pollutant dispersion in the environment.
    d. Open windrow composting and its effect to the environment.
    e. Legislation, regulation and complains for areas in South Yorkshire, UK where proposed composting or green waste processing sites exist.
3. CFD Simulation of Idealised Terrain:
    a. Definition of the idealised terrain and reason for use.
    b. Boundary condition, domain size and mesh density studies.
    c. Flat terrain (wind flow and pollutant dispersion).
    d. Single 2D hill (wind flow and pollutant dispersion).
    e. Single 3D hill (wind flow and pollutant dispersion).
    f. Double 3D hills (wind flow and pollutant dispersion).
4. CFD Simulations of Real Terrain:
    a. A proposed open windrow composting facility in South Yorkshire, UK.
    b. An existing open windrow composting facility in West Midlands, UK.
5. Presentation and Discussion of Results, Conclusions and Recommendations:
    a. Final thesis writing.
    b. Thesis presentation and viva.

Chapter 2

OPEN WINDROW COMPOSTING

2.1 Introduction

Air pollution is a common problem all around the world with regulators, legislators and citizens trying to minimise and control it when and where possible. For the European Union the latest directive on ambient air quality and cleaner air for Europe was published in 2008 [2008/50/EC]. The European Union together with the National Emission Ceilings – Policy Instruments group (NECPI) have also regulated a directive [2001/81/EC] regarding the National Emission Ceilings (NEC) for certain atmospheric pollutants. However, in many cases the European Union directives do not set actual limits and thus let each country decide on dangerous pollutant levels and relevant actions. In the United States, air pollution levels were significantly reduced over the last 30 years due to 'Clean Air Acts' set by the US Congress and adapted by individual US states and later on by the European Union.

The air pollution problem on the local/urban scale consists of various components which are presented in Figure 1. All connections between factors and how these interact with one another are shown: from an emission source to possible receptors and probable reactions. The key to low emission rates and thus less complaints and affected receptors is to be proactive as suggested by environment agencies around the world. Unfortunately, in many cases regulations are formed after problems have occurred or are recognised and established. In some cases, regulation requires long and time consuming research which forces countries to pay large fines to the European Union when failing to meet directive targets and reaching pollution concentrations above the limits.

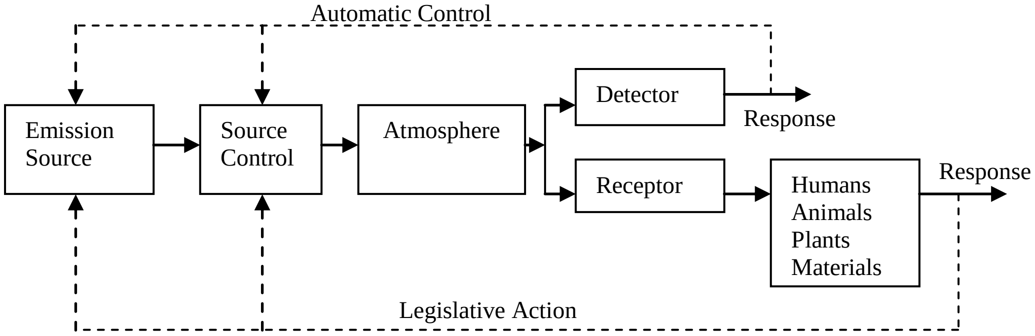

Figure 1 : Various components of the air pollution problem on a local/urban scale. [Adapted from Arya, 1999]

In the United Kingdom, air quality targets are set by the Department for Environment, Food and Rural Affairs (DEFRA) with the help of the Environment Agency (EA) and the Health and Safety Executive (HSE). Legislation exists for general air quality and more precise documentation is available for cases that have a high level of pollutant release and require specialised attention. DEFRA in conjunction with the BBC Weather Service have developed a banding method which is used to create a daily warning system that designates air pollution levels.

2.2 Waste Management and Regulation in the UK

In the UK, the Environment Agency has issued the Waste Strategy for England 2000 following the EU Landfill Directive 1999/31/EC which places targets for the amount of biodegradable waste going landfill and the obligation of pre-processing of all wastes before reaching any landfill site.

The composting process provides the solution for a wide range of biodegradable waste: house waste (e.g. vegetables, egg shells, paper, cardboard), agricultural waste (e.g. manure, straw, sawdust) and green waste (leaves, yard trimmings, etc). Compost plants can differ in size from personal (green compost bin in the back garden) to industrial, where production of compost is a business (multiple compost piles of hundreds of meters in length). For such large scale facilities, two main process types are adopted: the in-building composting and the open air windrow composting. The latter is much more common due to lower costs involved but the potential harmful emissions (bioaerosols, pathogens, fungi) are believed to be greater as these are directly released to the environment; the in-building composting takes place in a controlled environment (most of the times huge warehouses) from which the expelled air is first filtered to remove particles and bioaerosols. Other emissions with possible dangers to the environment, nearby residents and animals are: leachate and drainage after high amounts of rain and odour, dust and noise from the heavy machinery. All potentially harmful emissions form and arise at high densities from pre and post processes such as handling, turning, screening etc. Figure 2 gives a typical layout of an open windrow composting site with nearby receptors, houses, trees and possible harmful emissions.

The composting process is actually a speeded up natural process: biological decomposition. It is characterised by the physical and chemical breakdown of the organic matter from invertebrates and microorganisms respectively [Ward, 2002]. Most of the microorganisms (80-90%) in the compost consist of bacteria, Actinomycetes and fungi that break down the organic material within the compost pile. During this process heat is generated with the compost reaching temperatures above 60°C which must be maintained for the full length of the decomposition process [Ward, 2002]. The resulting compost material has many uses such as: fertiliser (necessary for organic farms), landscaping applications, soil regeneration and even growing mushrooms as it naturally contains all necessary nutrients.

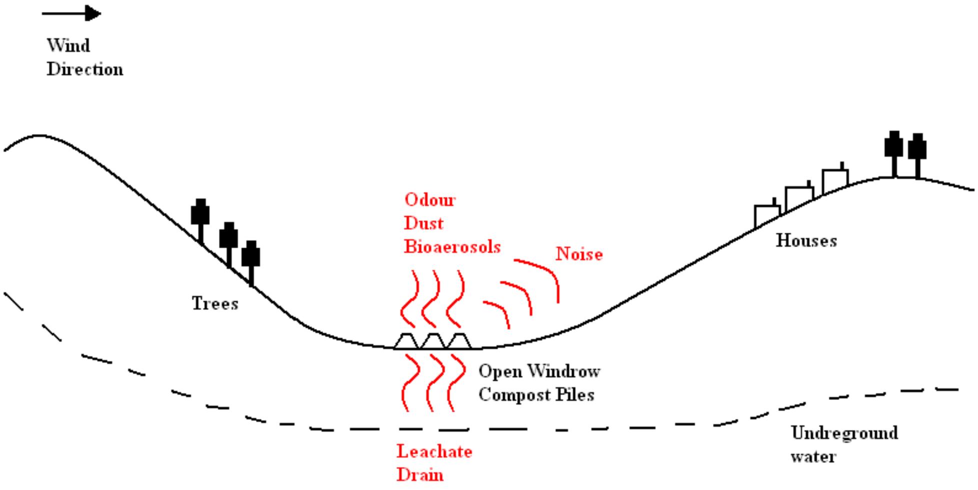

Figure 2 : Typical layout of an open windrow composting facility, possible harmful releases and nearby receptors.

Industrial composting has seen a rapid increase over the last decade with a rapid increase in the UK between the years 1990-2000 (Figure 3). It is predicted that by 2020 nearly 30 million tonnes per annum will be diverted from landfill to meet the EU landfill directive targets [Slater and Frederickson, 2001].

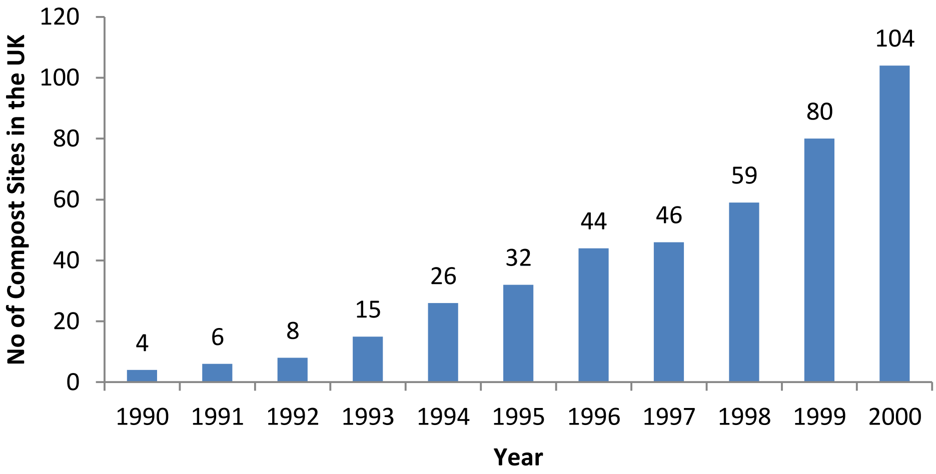

Figure 3 : Cumulative number of composting facilities in the UK during 1990's. [Slater and Frederickson, 2001]

Due to the increased number of compost plants and the rapid spread of the epidemic Foot and Mouth Disease (FMD) across Britain during the first quarter of 2001, reports from several UK compost sites showed that procedures and standards were not enough to guarantee hygienic operation and required the attention of plant managers, experts and more importantly regulators. Site managers, workers and public were (and in some cases still are) unaware of ways to protect themselves from possible dangers. Thus, in order to deal with these problematic circumstances, the HSE, DEFRA and EA have issued new, updated and more comprehensive guidelines over a period of several years.

In the early 2000’s the EA published the Technical Report P1-315/TR [Wheeler et al., 2001] on the health effects of composting operations after researching and comparing experimental data from three different sites; two of them were open windrow-turned green waste composting plants and the third was an in-vessel municipal waste composting plant. All three sites were apparently challenging to on-site monitor as surrounding factors can influence the sampling process. Such factors were: nearby motorway junctions, large trees influencing wind and creating unfavourable wind phenomena, crop farms and land depressions. Concentrations of bioaerosols at the facilities were found to be higher than ‘background levels’ (reference values according to the EA are: total bacteria of 1000cfu m^{-3}, total fungi of 1000cfu m^{-3} and Gram-negative bacteria of 300cfu m^{-3}). It was recommended that no sensitive receptors should be situated at distances smaller than 250m from the compost plant; that incoming waste has to be processed as soon as possible (preferably indoors) to minimise uncontrolled anaerobic digestion, potential odour and bioaerosol releases; finally it was recommended that applications for waste management licences and planning permissions should be considered simultaneously in order to ensure a multi-factor judging of the suitability of the plant (factors include location, equipment, structural and operational aspects).

An attempt was also made in the numerical modelling of the problem but it was soon found that the challenges and assumptions were too big at that stage for meaningful results mainly due to the biological complexity of bioaerosols (life-time, chemical composition). As suggested later by Drew et al. (2006), an important missing factor from all dispersion programs is the lack of ability to simulate properties of bioaerosols like their viability and their ability to aggregate and form clumps, which would affect the dispersion rate. Technical Report P1-315/TR was soon followed by a publication from the EA on Technical Guidance on Composting Operations (2001) to promote the best practise in the operation and regulation of composting facilities.

In 2003, the HSE published Research Report 130 [Swan et al., 2003] on the exposure and potential health effects from composting in order to review published literature on the subject. Cross-checking of results was difficult as data regarding health problems of compost workers is rare and a scientific connection of nearby receptors, who reported *Aspergillosis* type diseases, to the composting bioaerosol releases is non-existent. However, there are concerns by the regulating agencies regarding foot and mouth deceases and cases of respiratory failure which need to be evaluated and presented to the public. On the subject of numerical modelling of effluent bioaerosols, further work was suggested on the necessary assumptions for the concentration at source release. This is still a sizzling matter as data is rare to find and in most cases relative to the size of another/different compost site (in most cases bioaerosol dispersion modelling is required during planning stages and risk assessments of a plant). The same report recommends the change of the ‘250m rule’ until further research is completed, although there is no evidence that harmful bioaerosols are not able to travel further than this distance.

The framework published by the EA for the environmental risk management for composting facilities in the UK and Wales [Pollard et al., 2004] contained many necessary guidelines. An example of quantitative risk assessment was given by using numerical modelling and employing the program AERMOD. Amongst the most important factors to consider were the meteorological data and terrain effects. It is suggested that weather data from previous years must be examined and used (data that would create favourable conditions for maximum dispersion of bioaerosols or larger concentrations than normal) to predict near ground concentrations. It is stated that complex terrain can influence the spread of pollutants but this is significant and should be taken into account only when the slope is larger than 1 in 10.

In 2007, the new Waste Strategy for England 2007 was published by DEFRA as the previous strategy was outdated; some targets were partially met but others were not achieved. In-between the two publications, recycling and composting nearly quadrupled in the UK since 1996-97 reaching 27% in 2005-06.

Specifically for composting operations, the Environment Agency has released further guidelines; these covered risk assessments for organic waste facilities [Drew et al., 2008], methods to measure and derive source releases from compost sites [Crook et al., 2008 and Cartwright et al., 2009] and a report on dust and particulate effluent bioaerosols from agricultural processes that could affect human health [Scaife et al., 2008]. This latest report described known factors increasing emissions and suggested monitoring techniques and advised on further work to amplify knowledge and understanding of the problem. However, none of them suggest or mention the use or the appropriate use of numerical modelling for predicting bioaerosol dispersion.

The latest official publications were formed in 2009 by DEFRA on good practice guidelines regarding composting and odour control [Parker and Gibson, 2009] and by the HSE in 2010 on bioaerosol emissions from waste composting and potential risks to workers [Stagg et al., 2010] which is an updated and additional version to Swan et al. (2003). After monitoring multiple compost sites at distances downwind 250m from the source, results showed that concentrations did not exceed 'background levels' [Stagg et al., 2010]. However, it should be noted that no information is supplied on the position of these sites or on any nearby topographical factors that could alter or influence the sampling process. Moreover, in the conclusion it is mentioned that bioaerosol emissions from waste composting activities will continue to be a health concern for workers and nearby residents since further research is necessary to gather more information on this subject.

2.3 Bioaerosol Releases from Composting Facilities

Large concentrations of microorganisms are known to be present at compost plants. Controlling these airborne organisms is vital for the safety and health of workers and also for the local residential environment [Byeon et al., 2008]. Agitating processes during pre and post processing stages like shredding, turning and screening can make these microorganisms airborne forming bioaerosols [Swan et al., 2002]. Bioaerosols released include Fungi, Bacteria, Actinomycetes, Endotoxins, Mycotoxins, Glucans and Volatile Organic Compounds (VOCs). Note that high temperatures necessary for decomposition are known to favour growth of Actinomycetes and Fungi [Fischer et al., 1998]. These are recognized to be potentially dangerous to nearby receptors and especially to immunodepressed people with previous conditions such as leukaemia, lymphoma, diabetes etc.

Long term studies have been performed on composting facilities with the aim to measure bioaerosol concentrations using sampling methods (commonly used Anderson air samplers) and to investigate downwind concentrations. Most of the studies concluded that concentrations of bioaerosols reach ‘background levels’ at 100 to 500m with many within 250m [Swan et al., 2002]. Measurements by Sanchez-Monedero and Stentiford (2003) for plants in the UK and by Fracchia et al. (2006) for plants in Italy, respectively, showed that bioaerosol concentration reached normal levels within 300m from the compost site and that bacterial concentrations are highly dependent on the season. Chiang et al. (2003) have monitored emissions from a sludge composting facility on the east coast of the USA. Aerobic bacteria were seen to have high concentrations even at 1500m downwind the compost plant, 40% of which were smaller than 8μm and potentially harmful to humans due to ease of entry to the respiratory system.

Sampling at an open windrow composting plant in Grenchen, Switzerland was undertaken by Fischer et al. (1998) during the turning processes, with results showing that daily or weekly turned compost piles had lower surface counts of *Aspergillus fumigatus* (AF) than those turned monthly; this happened because in the frequently turned piles temperature was rising faster eliminating the AF spores. Thus, a frequent turning of the compost to speed up the decomposition process could be beneficial compared to a non-frequently turned compost pile which could release larger concentrations of AF. Fischer et al. (2008) conducted an analysis of airborne microorganisms and odour surrounding composting facilities in Germany; they emphasized on considering topographical and meteorological conditions during sampling – this also applies to numerical modelling. Herr et al. (2003) have also published concentration results from sampling at a different compost facility in Germany: these showed that at distances between 150 to 300m concentrations were 100 to 1000 times higher than ‘background levels’. The total bacteria count was much higher (5000cfu m^{-3}) compared to the recommended levels in Denmark or Sweden (100 - 700cfu m^{-3}) [Nielsen et al., 1995]. They emphasized on the fact that the sampling process took place during typical metrological conditions for the area and not during ‘worst case scenario’ weather phenomena.

Herr et al. (2003) also undertook a health-status study on residents living at a distance of 500m from the facility. The residents were asked to voluntarily answer questionnaires regarding their health and any other possible symptoms and later they had an interview with an independent doctor; unexposed people from other locations were also asked to participate as a control sample. Figure 4 shows some of the results from the health study. Residents within the 150-200m range have experienced shortness of breath, wheezing, cough on rising, itching eyes, nausea or vomiting and excessive tiredness in rates higher than the unexposed control. It is worth mentioning that even residents outside the ‘250m buffer zone’ were experiencing similar conditions at larger percentages than the unexposed control.

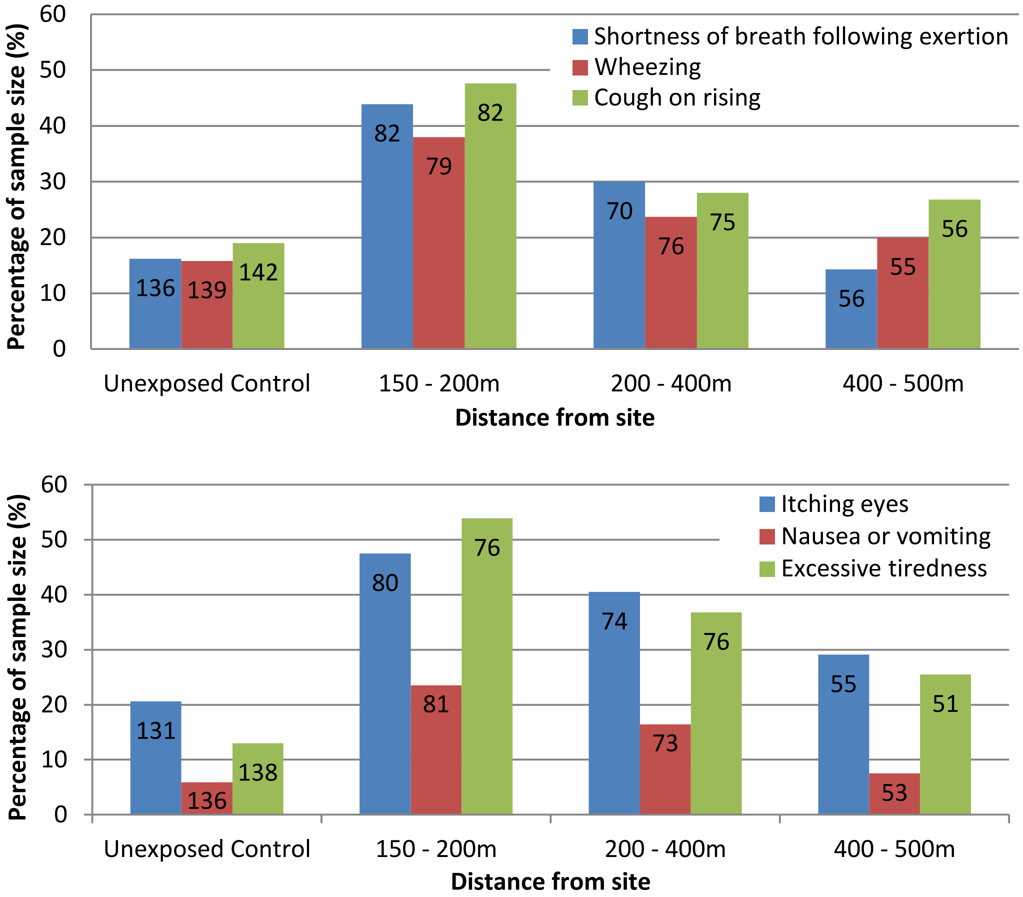

Figure 4 : Reported health complaints near a composting facility in Germany. Numbers on bars give sample size [Herr et al., 2003].

Taha et al. (2005) employed a portable wind tunnel to capture bioaerosols released from the surface of a compost pile in South East England by trapping them within the tunnel using filter samplers. Concentrations of AF and Actinomycetes in the ambient air measured were much higher than suggested background levels: 77000cfu m^{-3} and 10300cfu m^{-3}, respectively. Following that, Taha et al. (2006) have measured again the bioaerosol releases from (probably the same) green waste composting facility during agitation activities. This time sampling showed that concentrations of AF and Actinomycetes were much higher during the turning process than other processes like loading or screening. Results were imported to SCREEN3 dispersion program to model concentration values downwind of the composting site: depletion curves suggested that AF concentration values would decrease bellow 1000cfu m^{-3} before reaching 300m and below 100cfu m^{-3} before 500m. Taha et al. (2007) have further compared bioaerosol emissions from green waste composting during several stages of the compost decomposition (1, 2, 4, 6, 8, 12, 16 weeks) with the wind tunnel method. Concentrations did not show a distinctive trend relative to the compost age but measurements directly above the pile showed increased concentration during the early stages of the compost and a gradual increase by week 8. However, at week 16 concentrations increased again; the authors believe this was due to the weather conditions. Sampling results were used to model the concentration curves downwind of the site. Programs, SCREEN3 and ADMS3.3 were both used and compared with ADMS3.3 predicting concentration drop immediately (0m) after released at the source. The modelling process showed that SCREEN3 could not model multiple sources compared to ADMS3.3 which could present a more realistic scenario.

It is important to mention that although Taha et al. (2005, 2006, and 2007) have used dispersion modelling for concentration curves downwind the composting plant, little or no information is given regarding topographical features and weather conditions that could influence the spread of bioaerosols. Taha et al. (2007) mentioned that neither SCREEN3 nor ADMS3.3 were set to account for complex terrain or nearby buildings (it is unknown if this was due to the absence of such factors). Undoubtedly, the sampling method undertaken is extremely useful in order to give a clear view of bioaerosols released from compost piles and emission rates during the aging process of the compost (similar data are difficult to find). Sampling during agitating activities gives a clear indication that bioaerosol release increases during turning and screening and that these could be used as worst case scenarios. It was also noted by the authors that the "filter sampler" method reports an order of magnitude more than Anderson samplers which was also the observation of Wheeler et al. (2001). Thus, the suitability of these methods is in question as it seems that they do not catch all bioaerosols going through. However, it is recognised that these are the best methods for onsite sampling available at the moment.

Recommendations from several authors of the above mentioned publications regarding bioaerosol releases and high concentrations downwind of composting plants, with possibly affected nearby residents, call for improved practices of numerical modelling to aid towards a better decision tool for the planning process.

The guidance by the UK Environment Agency for risk assessments when receptors lie in the vicinity of 250m from the composting plant might not be sufficient, especially when literature suggests that dispersion of such dangerous bacteria, fungi etc. is relevant to topography and meteorological conditions and in some cases the relative spread exceeds those limits. Source data, emission rates and particle size distribution play an important role to bioaerosol dispersion and thus need to be further investigated [Wheeler et al., 2001 and Pollard et al., 2006]. Consequently, site specific investigation for wind flow and pollution dispersion modelling is required.

2.4 Examination and Prediction of Bioaerosol Releases

Advanced numerical modelling of bioaerosol releases is only mentioned a few times in the previously referred official UK guidelines. ADMS and AERMOD, two regulator-approved programs, are employed in some cases together with onsite sampling techniques. On-site measurements are usually done by using Anderson samplers or other methods that trap bacteria and fungi and later counted after an incubation period. Such methods are time consuming and expensive and relative parameters such as weather, topography and emission rates can never be ideal and identical, especially when comparing site measurements. During planning stages for new facilities, concentration figures from other ‘similar’ sites are projected in order to give an idea of the figures to planning officers. It is also recognized that there is no official general guidance on modelling pollution dispersion of bioaerosols stating which assumptions and factors are necessary to be taken into account for acceptable results.

Naturally, every site requiring a risk assessment is ‘unique’ and creates new and dissimilar challenges to the modeller. Thus, universal guidance on numerical modelling of pollution dispersion originating from processes such as composting operations is almost impossible.

Several guidelines on numerical modelling have been published by researchers and modellers over the last twenty years, as there has been a recognised need for more guidance on the subject and certainly greater accessibility to resources due to the continuously growing computer capabilities. These include the simulation of wind flow in lower atmosphere as well as transfer of pollutants by air at close proximity to the source or further downwind and are mentioned later in this work in relevant chapters.

The present work suggests the use of Computational Fluid Dynamics as an alternative numerical approach to two well-accepted programs: ADMS and AERMOD (briefly described later herein). These depend on external programs for the critical wind flow simulation and use Gaussian plume models to calculate the spread of effluent bioaerosols. Such models are limited due to the lack of in-program fluid flow modelling, grid size and resolution limits and most importantly due to the dispersion model employed (mostly a single Gaussian model in every program). However, their main advantages are turnaround time: i.e. results are given within hours, even minutes in some cases; ease of use and cost: both operational and infrastructural as neither special computers nor personnel are required.

Computational Fluid Dynamics programs combine the ability to solve flow fields and dispersion problems at the same time. There is a variety of proven turbulence models that can be implemented and puff, plume and particle dispersion type modelling is also available. Grid size and resolution is manually set by the modeller according to need and accuracy targets. CFD can account for complicated terrain including buildings, hills and other natural wind breaks and can take into consideration meteorological data which are either constant or changing over time. CFD is also the appropriate tool for systematically modelling the influence of complex topography on pollutant dispersion [Parker and Kinnersley, 2004]. All advantages are mentioned later analytically after explaining all important factors to computationally simulate wind flow and effluent pollution dispersion.

CFD has been extensively used for examining wind flow and pollution problems in the urban environment. Neofytou et al. (2008) have used ANDREA-HF to model pollution dispersion of NO_x, NO_2, $PM_{2.5}$ and PM_{10} in a street canyon in Helsinki; they compared their results to experimental measurements showing that there was good agreement except in two cases of under prediction due to limitations of the software to calculate traffic induced turbulence and chemical transformation. Results showed that the generated vortices due to buildings cause increased dispersion of street level pollution. Related work was done by Gousseau et al. (2011) for near-field dispersion modelling for neutral atmospheric conditions in downtown Montreal: two different modelling approaches where compared (RANS and LES) to wind tunnel results. Comparison showed that results had good agreement with both numerical approaches sharing the same grid and RANS underestimating concentration in some cases – LES was closer to wind tunnel results but more time consuming.

Mandas et al. (2004) have examined the use of an artificial hill for prevention of effluent coal particles from storage piles at a power station in Italy. They used CFD program FLUENT to model different hill geometries and heights in 2D and later 3D. Results presented a potential decrease of the wind flow magnitude at low elevations behind the proposed artificial hill; although particulate modelling was not done, this wind speed reduction is considered to be favourable for smaller particulate matter quantities flying away from coal piles.

Effluent dispersion modelling from storage piles (similar to the work herein) has also been previously investigated: Pelegry et al. (2009) simulated wind flow and dust emissions from open storage piles by using the CFD program CFXv10. It was shown that higher wind speed at the edges of the pile meant greater dust emissions. A real life simulation for a coal and iron ore sea terminal with two parallel piles was also undertaken. It was concluded that the first pile which was situated perpendicular to the wind released 5% more dust than the second pile and that most of this dust was trapped at the second pile.

Turpin and Harion (2009b) have looked into the three-dimensional effects of the surrounding buildings to storage piles at an industrial site. They simulated different wind directions (perpendicular and at different angles to the piles) and several pile geometries to suggest the type of pile that would give the lowest emissions.

The above raise questions towards different formations and shapes of storage piles to help reduce emissions and decrease the spread of pollutants. The effect of topography to wind flow and pollutant dispersion will be examined later in this work with the help of CFD.

Chapter 3

WIND FLOW AND EFFLUENT POLLUTION DISPERSION MODELLING

3.1 Introduction

Before modelling air pollution dispersion, it is necessary to understand the fluid mechanics of wind flow in the lower part of the earth's atmosphere. The concept of the Atmospheric Boundary Layer is explained in this chapter with all essential assumptions for neutral flow conditions featuring stability, characteristics and profiles for velocity and turbulence parameters. The effect of complex terrain on wind flow is also discussed as this is one of the major factors that could influence effluent pollution dispersion.

With the accurate simulation of wind flow further description of the problem of pollution dispersion can follow. Pollutants are carried by wind and their distribution in the environment mainly depends on the type and concentration of pollutants at a source, combined with prevailing weather and topographical conditions. Available dispersion models are discussed herein with all the factors that should be taken into account or neglected according to the accuracy required. These factors are explained with the aid of fluid mechanics, meteorology and mathematical modelling.

Finally, commonly used programs for effluent pollution dispersion are listed with more details on ADMS and AERMOD which are those mostly employed by regulators. The application of Computational Fluid Dynamics for modelling Atmospheric Boundary Layer flows and pollutants transferred by air, is also discussed.

3.2 Atmospheric Boundary Layer

3.2.1 Structure of the ABL

The Atmospheric Boundary Layer (ABL) is formed within the atmosphere and consists of the lower layer of the atmosphere close to the planetary surface. It responds to surface changes in a timescale of around an hour. The mean flow properties in this layer experience their sharpest gradients within the first 10 to 100 metres within a region called Turbulent Surface Layer. Although the ABL covers only the lowest part of the atmosphere (~1%), it corresponds to 20% of the atmospheric mass (Figure 5). This is mainly due to the exponential decrease of pressure with height [Rotach, 2008].

Flow in the ABL is greatly dependent on the earth's surface friction. It influences the wind's variable profiles close to ground level. Also, atmospheric radiation interacts with the surface, which leads to large gradients of temperature near the ground. Both surface friction and radiative energy make the flow unstable at small scales and cause turbulence. Flow in the ABL is turbulent and in most cases dominated by turbulence.

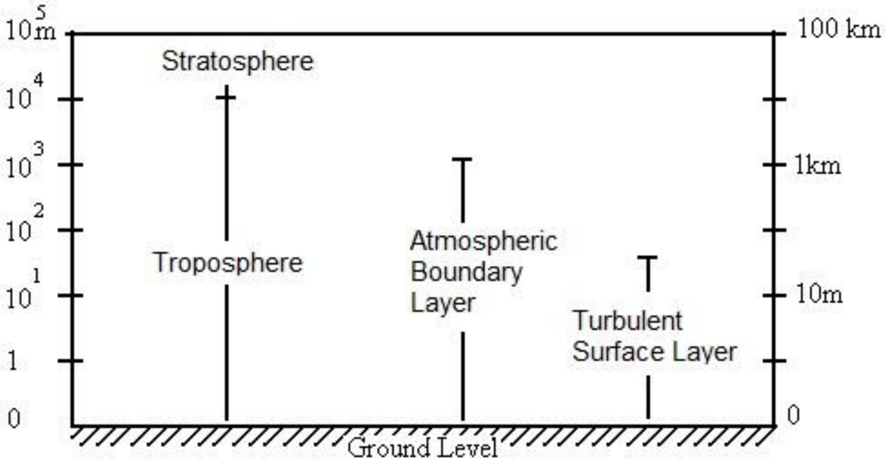

Figure 5 : Vertical structure of a homogeneous Atmospheric Boundary Layer. [Adapted from Rotach, 2008]

As the flow in the ABL is turbulent, momentum, energy and mass transportation exist within the flow. In the ABL, turbulent transport mainly takes place in the vertical direction because of strong vertical gradients close to the surface.

3.2.2 Basic ABL Assumptions

In order to tackle the flow characteristics of a two dimensional (2D) vertical ABL, assumptions towards simplification have to be introduced. The first one is horizontal 'homogeneity'. Under such assumption, properties of the flow vary only in the vertical direction disregarding changes in the horizontal direction for mean derivatives [Kaimal and Finnigan, 1994]. To further simplify the problem, 'stationarity' is assumed (no change of variable properties over time) disregarding the derivatives of time in the governing equations.

Following the above mentioned assumptions, the problem is considered steady state and time averaging can be employed to characterize properties of the fluid flow. That way, well understood theories and empirical equations originating from full scale and wind tunnel environmental studies can be employed to obtain realistic results (e.g. variable logarithmic velocity and turbulence profiles, surface roughness, etc.).

3.2.3 The Height of ABL

The ABL can be separated into two layers: the Surface Layer and the upper layer which are similar to the inner and outer layers seen in laboratory flows. The lower, Surface Layer (SL) vertically covers the first hundred meters of the atmosphere and has a constant shear stress. In this layer the fluid flow is not affected by the rotation of the earth. However, temperature variation and surface friction are the major factors that describe the flow structure. The upper layer (up to 1000m) has a variable shear stress and the fluid flow is also affected by earth's rotation, temperature variation and surface friction. The ABL height z_{ABL} can be expressed in terms of the exchange coefficient of momentum and the Coriolis parameter that provides the earth's rotation effect. This is described by Equation 3.1 [Sutton, 1953].

$$z_{ABL} = \pi \left(\frac{2K_m}{f_c}\right)^{1/2} \tag{3.1}$$

where:
K_m is the exchange coefficient for momentum.
f_c is the Coriolis parameter.

The Coriolis parameter f_c is given by the angular velocity of the earth and the latitude as described by Equation 3.2. Such a parameter is often not included in the governing equations of fluid flow as its effects are on the outer layer of the ABL and are difficult to correctly implement. However, the absence of such term means that horizontal homogeneity in the ABL cannot exist creating thus the necessity for the parameters of the top boundary of the control volume to include the Coriolis forces.

$$f_c = 2\Omega sin\phi_E \tag{3.2}$$

where:
Ω is angular velocity (earth rotation rate).
ϕ_E is latitude.

When warm eddies (convective air) rise from the SL and reach the inversion zone, they enter and finally mix with air from the free troposphere (above 1000m) causing intense vertical turbulent mixing, forming the Convective Boundary Layer (CBL). Major changes in the variable properties of the flow take place in the lowest part of the CBL (10%); the upper part (90%) is characterised by mixing which cancels (flattens) all variations and eventually drives the wind speed, direction and temperature to the values of the free atmosphere. This is illustrated in Figure 6 for a stable and convective boundary layer. It is important to mention that the height of the inversion layer is different during day-time and night-time.

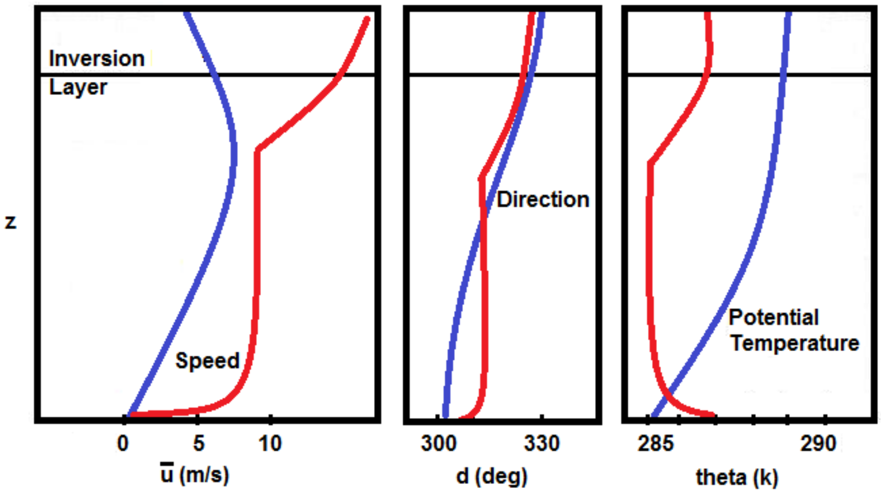

Figure 6 : Mean vertical profiles of wind speed, wind direction and potential temperature in the convective boundary layer (red lines) and stable boundary layer (blue lines). [Adapted from Kaimal and Finnigan, 1994]

3.2.4 Surface Layer Characteristics

Using the assumptions of horizontal homogeneity and stationarity mentioned earlier and based on theories of molecular diffusion in laminar flows, turbulent transport characteristics in the lower atmosphere can be described. Fluxes of momentum f_m, heat f_H and moisture f_M are described by the equations below in terms of gradients in the vertical direction and are counterparts of viscosity, conductivity and diffusivity in laminar flow. By contrast, their magnitudes are around three times larger [Kaimal and Finnigan, 1994].

$$f_m = K_m \rho_{air} \frac{\partial \overline{u}}{\partial z} \tag{3.3}$$

$$f_H = -K_h \rho_{air} c_p \frac{\partial \overline{\theta}}{\partial z} \tag{3.4}$$

$$f_M = -K_q \rho_{air} \frac{\partial \overline{q}}{\partial z} \tag{3.5}$$

where:
K_m, K_h, K_q are turbulent exchange coefficients for momentum, heat and moisture, respectively.
ρ_{air} is density of air.
$\overline{u}$, $\overline{\theta}$, $\overline{q}$ are mean values for streamwise wind component, temperature and specific humidity, respectively.

The momentum flux is characterised by components of stress in the vertical and horizontal direction. However, the shear stress variation in the vertical direction is considered negligible and the same applies to the horizontal direction because of homogeneity. Thus, for the Surface Layer:

$$\tau_z = \tau_0 \, , \tau_x = 0$$

Friction velocity u_* can now be defined to account for the effects of wind stress τ_0 on the ground. It depends on the surface roughness and the wind velocity magnitude.

$$\tau_0 = \rho {u_*}^2 \tag{3.6}$$

3.2.5 ABL Velocity Profile

The velocity profile for the lower part of the atmosphere can be described by a logarithmic formula that originates from the surface friction velocity, the height and the turbulent exchange coefficient for momentum. It is only valid for a neutral ABL.

The exchange coefficient for momentum K_m can be expressed in terms of friction velocity and height.

$$K_m = k_P u_* z \tag{3.7}$$

where:
k_P is a constant of proportionality.

Substituting Equation 3.3 for momentum flux into Equation 3.7 we get:

$$\frac{\partial \overline{u}}{\partial z} = \frac{u_*}{kz} \tag{3.8}$$

Finally, by integrating we get the logarithmic ABL profile:

$$\overline{u}(z) = \frac{u_*}{\kappa} ln\left(\frac{z}{z_0}\right) \tag{3.9}$$

where:
κ is the von Karman constant (= 0.4).
z_0 is the roughness height constant.

Richards and Hoxey (1993) suggest the use of such logarithmic velocity profile at the inlet boundary of numerical simulations combined with profiles for turbulent kinetic energy k and dissipation rate ε; given by Equations 3.10b to 3.10c. These should be combined with the standard k-ε turbulence model to numerically model constant ABL characteristics for a flat domain. They have also verified these profiles with full scale experiments at the Silsoe Research Institute in 1988. A comparison of the neutral velocity profile to those for stable and unstable ABL is shown in Figure 7.

$$\overline{u}(z) = \frac{u_*}{\kappa} ln\left(\frac{z+z_0}{z_0}\right) \tag{3.10a}$$

$$k = \frac{{u_*}^2}{\sqrt{C_\mu}} \tag{3.10b}$$

$$\varepsilon = \frac{{u_*}^3}{\kappa(z+z_0)} \tag{3.10c}$$

$$\text{with} \quad u_* = \frac{\kappa \overline{u_h}}{ln\left(\frac{h+z_0}{z_0}\right)} \tag{3.10d}$$

where:
C_μ is k-ε turbulence model constant.
$\overline{u_h}$ is mean velocity magnitude at reference height h.

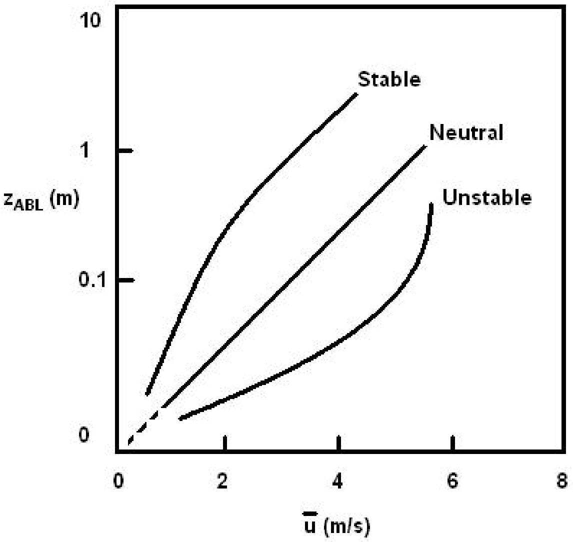

Figure 7 : Logarithmic velocity profiles for stable, neutral and unstable ABL.

3.2.6 Stability of the ABL

The ABL stability varies with day, night and season of the year. Temperature differences and thus heat transfer between the ground surface and the air affect the lower layer of the ABL and its variables. Stability is described through buoyancy and shear stress in turbulence and is defined with the help of a dimensionless parameter, the Richardson number R_i.

$$R_i = \frac{\left(\frac{g}{\overline{\theta}}\right)\left(\frac{\partial \overline{\theta}}{\partial z}\right)}{\left(\frac{\partial \overline{u}}{\partial z}\right)^2} \tag{3.11}$$

where:
g is gravitational acceleration.
$\left(\frac{g}{\overline{\theta}}\right)$ is a buoyancy parameter.

When R_i is positive the stratification is stable; when R_i is zero the stratification is neutral; and finally when R_i is negative the stratification is unstable. Table 3 gives basic properties of idealized states of the ABL.

Stratification	**Turbulence**	**Vertical Extension**	**Heat Transport**	**Occurrence**
Stable	+ Mechanical - Thermal	Shallow	Down	Night, snow, Ice cover
Neutral	+ Mechanical	Medium	Nil	Strong wind (idealised)
Unstable	+ Mechanical + Thermal	High	Upward	Day

Table 3 : Basic properties of idealised states of the ABL. Column 'turbulence' refers to turbulence production (+) and suppression (-) [Adapted from Rotach, 2008].

To further describe stability of the ABL in the lower layer and close to the ground, the flux Richardson R_f and bulk Richardson R_b numbers are sometimes used. As this work only deals with neutral ABL flows, these numbers are not described here; full definitions can be found in Kaimal and Finnigan (1994).

3.2.7 ABL Flow Characteristics over Hills

The introduction of uneven, non-flat terrain in the wind flow problem may rapidly change the characteristics of the ABL with velocity and pressure fields mostly affected. Airflow structure around a hill mostly depends on the hill's shape and size. In most cases, only the lowest part of the ABL is influenced by a hill (referring to hill heights less than 100m). However, there are cases of high altitude hills that influence the full height of the ABL causing disturbances to the stable atmosphere above (hills above 500m are considered mountains herein).

For a neutral ABL wind flow over a two-dimensional hill, the wind decelerates toward the foot of the windward face of the hill before it accelerates towards the top. For steep hills, depending on the geometry a small recirculation zone could form at the foot of the windward face. Maximum wind velocity is reached just above the hill top before it arrives at the leeward face of the hill where it starts to decelerate. For steep hills - always in conjunction with geometrical factors - a recirculation bubble occurs at the foot of the leeward hill face. Turbulent wakes exist at the recirculation zone until reattachment of the recirculated wind to the main flow occurs. This is illustrated in Figure 8 for wind flow over a two-dimensional axisymmetric hill for which there is no deceleration at the foot of the windward face [Kaimal and

Finnigan, 1994]. This is because of the 'smooth' geometry of the hill that favours the attachment of the flow to the windward face.

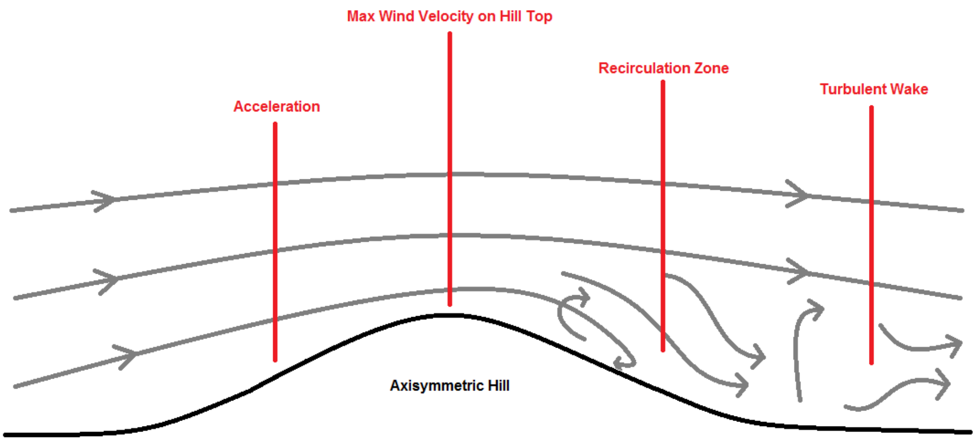

Figure 8 : Wind flow over a two-dimensional axisymmetric hill.

Vertical velocity profiles at the top of the hill and the windward and leeward faces are presented in Figure 9. Horizontal velocity profiles are also presented in Figure 9 for the inner and outer layer of the flow above the hill. This separation in layers is necessary because of the different dynamical process in each of these layers; the inner layer is characterised by turbulent regions because of the recirculation zone; the outer layer is almost unaffected by the inner layer with minimum disruption to the flow [Kaimal and Finnigan, 1994].

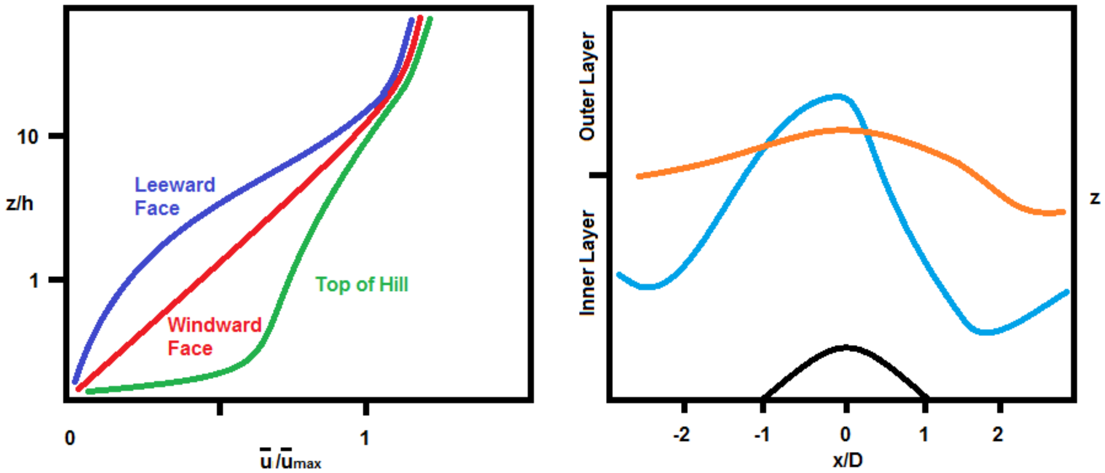

Figure 9 : Vertical (left) and horizontal (right) velocity profiles for wind flow over a two-dimensional axisymmetric hill.

Jackson and Hunt (1988) suggest the use of Equation 3.12 to calculate the height of the inner layer h_{IL} which depends on the surface roughness length z_0 and the Von Karman constant κ. Equation 3.12 applies only to low hills with no significant flow separation. For larger hills, this formula can approximate the height of the inner layer but should be used in conjunction with other numerical or experimental techniques.

$$\frac{h_{IL}}{L_{Ch}} \ln\left(\frac{h_{IL}}{z_0}\right) = 2\kappa^2 \tag{3.12}$$

where:
h_{IL} is the inner layer height.
L_{Ch} is the characteristic length equal to the horizontal distance between hill vertical axis and the upstream point where the height of the hill is H/2.

3.2.8 Speed Up Effect over Hills

The vertical velocity profile at the top of a hill is characterised by an increased velocity magnitude at the lower part; this is called the speed-up effect and is caused by air parcels being forced to pass above the hill. This is similar to flow through a converging-diverging nozzle. For three-dimensional axisymmetric hills, this speed-up effect would have a lower magnitude as air parcels would be able to move and travel also sideways the hill and not only over it.

A simple approximation of the speed-up effect of wind flow over a two-dimensional or a three-dimensional hill is suggested by Lemelin et al. (1988) based on computational data and compared to wind tunnel experimental results. It is described by Equations 3.13a, 3.13b and 3.13c.

$$\Delta S(x,z) = \Delta S_{max}\left(\frac{1}{1+3(x/n_{LSD}L_{Ch})^{p_{LSD}}}\right)^2\left(\frac{1}{1+a_{LSD}(z/L_{Ch})}\right)^2 \tag{3.13a}$$

where:
ΔS is the speed-up ratio.
ΔS_{max} is the maximum speed–up ratio.
n_{LSD}, a_{LSD}, p_{LSD} are constants given below.
x is the horizontal distance between the point on the hill where the speed up is required and the hill's axis (see Figure 10).

For 2D hills:

$$\Delta S_{max} = 1.3G \tag{3.13b}$$

H/D	G	L_{Ch}	a_{LSD}		n_{LSD}	p_{LSD}
≤ 1.0	H/D	D	2.0	x≤0	1.0	2.0
				x>0	5.0	1.0
> 0.4	1.0	H	0.6	x≤0	0.5	2.0
				x>0	10.0	1.0

Table 4 : Variables and constants for calculation of speed-up over 2D hill according to the LSD method [Lemelin et al., 1988].

For 3D hills:

$$\Delta S_{max} = 2.3G\left(\frac{B/L_{Ch}}{(B/L_{Ch}+0.4)}\right) \tag{3.13c}$$

where:
B is the horizontal distance between the hill's axis and the point sideways where the hill height is equal to H/2 (see Figure 10).

H/D	**G**	$\mathbf{L_{Ch}}$	$\mathbf{a_{LSD}}$	$\mathbf{n_{LSD}}$	$\mathbf{p_{LSD}}$
≤ 0.4	H/D	D	2.0	2.0	2.0
> 0.4	0.4	2.5H	2.0	2.0	2.0

Table 5 : Variables and constants for calculation of speed-up over 3D hill according to the LSD method [Lemelin et al., 1988].

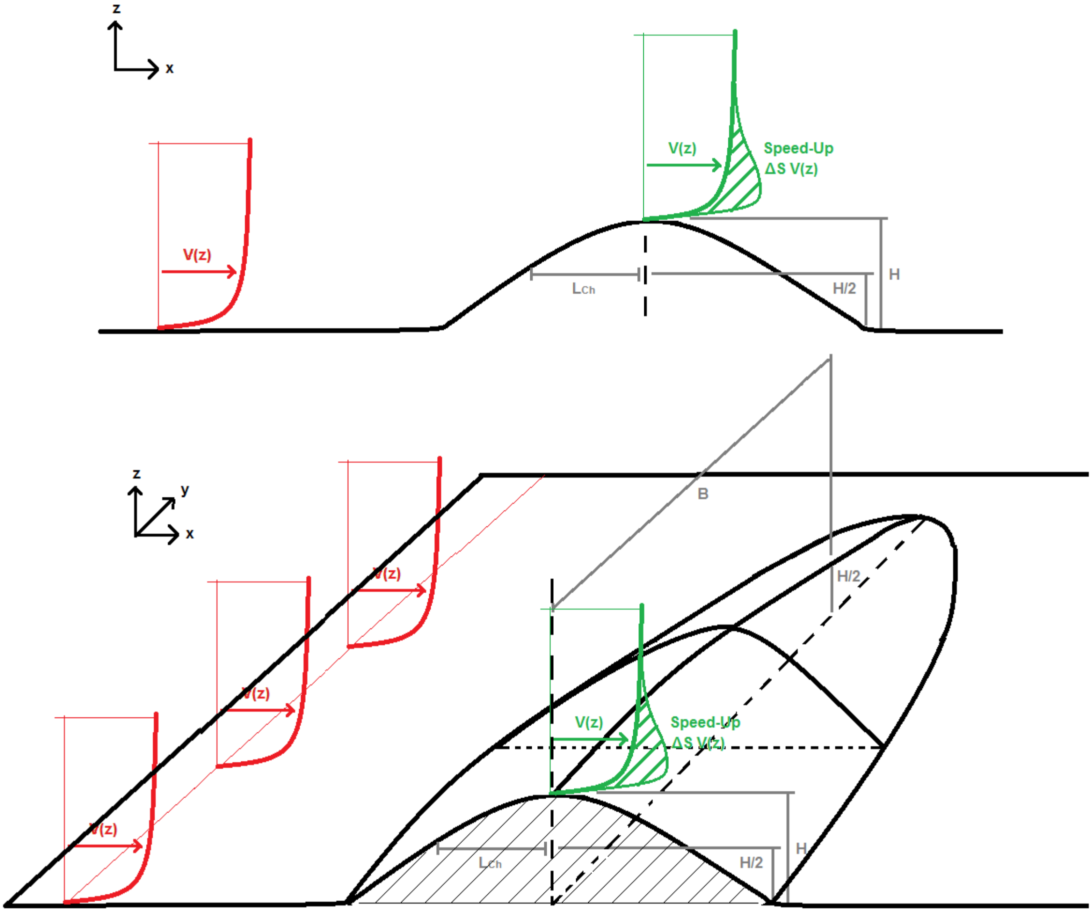

Figure 10 : Definitions for wind speed-up over 2D (top) and 3D (bottom) hill. [Adapted from Lemelin et al., 1988]

3.3 Reynolds Averaged Navier Stokes Equations

For the mathematical solution of wind flow problems, the Navier Stokes set of equations is regularly employed. Hydrodynamic flows are characterised by conservation equations for mass, energy and momentum. Due to the nature of open environmental flows, turbulence variables continuously change, resulting in temporal results from these differential equations. For practical reasons the Reynolds averaging method is employed for an averaged result by using approximations based on known properties of turbulence. The resulting set of equations is called Reynolds Averaged Navier Stokes Equations (RANS) and is given in Table 6. Conservation of momentum for a rotating earth is assumed with conservation of energy for the Atmospheric Boundary Layer.

However, this set of non linear coupled differential equations does not have an analytical solution. Thus a solution is possible only if some terms are neglected or closed. Subsequently, a numerical solution can be obtained. This numerical approach is adopted for atmospheric flows and examination of climate change, weather prediction and even prediction of localised phenomena.

Having more unknown variables than equations that describe a 3D incompressible flow, a closure problem exists where the exact mathematical approach can never provide enough equations to match the number of unknowns. Thus, a turbulence modelling approach has to be used [Chin, 2005] as described in the next section.

Momentum	$\frac{\partial \overline{u_i}}{\partial t} + \overline{u_j}\frac{\partial \overline{u_i}}{\partial x_j} + \frac{\partial}{\partial x_j}(\overline{u_i' u_j'}) = -\delta_{i3} g + f_c \varepsilon_{ij3}\overline{u_j} - \frac{1}{\overline{\rho}}\frac{\partial \overline{p}}{\partial x_i} + \nu \frac{\partial^2 \overline{u_i}}{\partial {x_j}^2}$	(3.14)
Energy	$\frac{\partial \overline{\theta}}{\partial t} + \overline{u_j}\frac{\partial \overline{\theta}}{\partial x_j} + \frac{\partial}{\partial x_j}\left(\overline{u_j'\theta'}\right) = \nu_\theta \frac{\partial^2 \overline{\theta}}{\partial {x_j}^2} + \frac{1}{\overline{\rho} c_e}\overline{Q R_C}$	(3.15)
Trace Gas	$\frac{\partial \overline{C}}{\partial t} + \overline{u_j}\frac{\partial \overline{C}}{\partial x_j} + \frac{\partial}{\partial x_j}\left(\overline{u_j' C'}\right) = \overline{Q}$	(3.16)
Mass	$\frac{\partial \overline{u_j}}{\partial x_j} = 0 \quad ; \quad \frac{\partial {u_j}'}{\partial x_j} = 0$	(3.17)
Equation of State	$\overline{p} = R_a \overline{\rho}\overline{T}$	(3.18)

Table 6 : RANS and other equations for mean variables in turbulent atmospheric flows. [Rotach, 2008]

where:
$-\delta_{i3} g$ is acceleration due to gravity (only in the vertical z direction).
f_c is Coriolis parameter (Equation 3.2).
ε_{ijk}=1 if (i, j, k) cyclic, =1 if (i, j, k) anti-cyclic and zero otherwise.
p is pressure.
ν_θ is thermal viscosity.
c_e is energy coefficient.
R_C is energy released from chemical reactions (or other processes).
C is trace concentration.
Q is source of trace gas (positive if source, negative if sink).
R_a is ‘ideal gas’ constant for air (R/Ma = 286 $J\ kg^{-1}\ K^{-1}$, where Ma is the molecular weight of dry air).

3.4 Turbulence Modelling

A specific turbulence model can be used for a range of problems but it must be accurate, simple and economical to use [Versteeg and Malalasekera, 1995]. Table 7 lists the main categories of turbulent models. Common models use RANS equations as these are widely employed in fluid flow modelling and commercial programs. Their use has been repeatedly proven for different types of flows by comparison to full scale or wind tunnel experimental results.

RANS	1. Zero equation model – mixing length model 2. Two equation model – k-ε model 3. Reynolds stress equation model 4. Algebraic stress model
Direct Numerical Simulation	NS equations with no turbulence model
Large Eddy Simulation	Based on space filtered equations

Table 7: Common turbulence models.

The most commonly used turbulence model is the k-ε model which includes two transport properties selected to represent the turbulent characteristics of the flow and focuses on variables affecting the turbulence kinetic energy. The first transport variable is turbulence kinetic energy k and the second is the rate of dissipation ε. These determine the energy and scale of turbulence of the flow respectively.

Kim et al. (2000) simulated wind flow over four real hilly locations (2D Cooper's Ridge, 3D Kettles hill, 3D Askervein hill and 2D Sirhowy valley) and employed RANS equations with the standard and RNG k-ε turbulence model for mathematical closure. Numerical results were compared to wind data for velocity profiles and reattachment lengths presenting small differences. The authors concluded that the chosen numerical model was suitable for reliable prediction of local scale wind flow over hilly terrain. The standard k-ε model was used in this work because of its long proved accuracy and effectiveness in a variety of applications.

3.5 Numerical Modelling of the Atmospheric Boundary Layer

Numerical modelling of the ABL is sometimes complicated and time consuming. Over the last twenty years, there have been many studies towards simulating the ABL as accurately as possible. These lead to several releases of guidelines on how to best approach such problems.

One of the most interesting and useful studies was administered by the team of Richards and Hoxey (R&H thereafter). They conducted full scale experiments for a 6m cube at the Silsoe Research Institute in the late 80s [Richards et al., 1997, 2000, 2008]. R&H used numerical modelling to examine fluid flow characteristics around a cube [Richards and Hoxey, 1992] and later published a paper on appropriate boundary conditions for numerical modelling of ABL flows using the k-ε turbulence model [Richards and Hoxey, 1993]. The team also compared their data to results from wind tunnel experiments [Richards et al., 2007]. Following the work of these authors, several papers were published examining appropriate boundary conditions for ABL modelling.

Hargreaves and Wright (2007) followed the R&H approach to model the ABL using commercial CFD codes FLUENT and CFX employing the standard wall function to examine how well these programs perform. They concluded that although necessary, the use of user defined profiles (by R&H) and the default turbulence parameters alone are not appropriate for maintaining constant ABL variables of mean velocity, turbulence kinetic energy and dissipation rate. They proposed suitable changes to the wall function of the lower boundary (ground) and the application of shear stress to the top boundary (sky) by making use of User Defined Profiles (UDPs). They also suggested that if modellers do not have the time or ability to apply such parameters and need to use the standard k-ε turbulence model with the standard wall function, extra care should be taken to maintain the ABL profile characteristics by choosing the shortest domain size possible but long enough to include all flow phenomena.

A similar approach to Hargreaves and Wright (2007) is suggested by Ishihara and Hibi (2002) to model wind flow behind a 3D steep hill (20%) using the standard k-ε turbulence model and Shih’s nonlinear model. They used numerical modelling to compare 2D vs. 3D flow characteristics around the hill and later evaluated numerical results to wind tunnel data. Both these works are discussed further, later in this paper.

Yang and Zhang (2009), also following the R&H work, have exploited different wall treatments and versions of the k-ε turbulence model (standard, realizable, RNG) in the CFD code FLUENT for the best simulation and preservation of the ABL. They have concluded that the inlet profiles, turbulence model, wall function and grid discretization affect the horizontal homogeneity and therefore should be carefully selected. Yang et al. (2009) have adapted their turbulence modelling approach based on the R&H initial recommendations. They successfully maintained a constant ABL velocity profile along their simulated domain using FLUENT with minor changes between the inlet and the outlet profiles.

Ohya and Uchida (2008) carried out both laboratory and numerical studies for modelling stable ABLs. They used a thermally stratified wind tunnel to model the velocity and temperature fluctuations. Numerically they approached the problem using Direct Numerical Simulation (DNS) that solved Navier Stokes equations without turbulence modelling. Comparison of results showed good agreement between the two methods. They recorded changes in the vertical turbulence profiles due to ABL stability effects and found connections to a neutral ABL for the transfer of momentum and heat fluxes.

Based on the ability of CFD to accurately simulate ABL characteristics further studies have taken place for urban environments. Blocken et al. (2007a) used FLUENT to study wind conditions and localised effects in passages between buildings and suggest ways to improve pedestrian comfort.

Later, Blocken and Persoon (2009) examined pedestrian wind comfort around the ‘Amsterdam Arena’ stadium and the effects of that to the surrounding buildings by simulating a 3D steady flow using RANS equations in FLUENT; the numerical results were then compared to full scale measurements for validation purposes – there was good agreement with a small over-prediction by CFD.

Furthermore, Di Sabatino et al. (2007 and 2008) presented the use of the k-ε turbulence model in FLUENT to model wind flow for the purpose of pollutant dispersion within idealised urban-type geometries. Results showed that after correctly specifying turbulence parameters in CFD the wind flow was accurately simulated. This is a very important factor for meaningful results of pollution dispersion which were in agreement with data from pollution dispersion program ADMS.

3.6 Dispersion Modelling of Effluent Pollutants

The term *dispersion* originates from the word *disperse* which means to go or distribute in different directions or over a wide area, thin out and eventually disappear. It should not be confused with *diffusion* which refers to mixing of different substances by the movement of particles.

Ensuring the best possible and accurate solution for wind flow in the ABL using numerical techniques is vital, methods available for modelling effluent pollution dispersion can now be discussed. These methods are introduced in sequence (first wind flow and secondly pollution dispersion) but they are often used in parallel (coupled) during the solution process to give the most accurate results. Several sophisticated models include the interaction of air flow with pollutants and vice versa to help understand how high concentrations of pollutants can influence the air flow in open or closed environments.

In order to express concentration of pollutants in the atmosphere two main units are engaged: either in terms of the volume of species per unit volume of air (ppm) or in terms of the mass of species per unit volume of air (kg m^{-3}). Conversion between these two units can be achieved by using the ideal gas model and expressing both in terms of molar concentration (moles per unit volume of air) [Arya, 1999]; as shown by Equation 3.19.

$$c_{vi} = \frac{R^{*}T}{pm_i} c_{mi} \tag{3.19}$$

where:
c_{vi} is volumetric concentration of species *i*.
c_{mi} is mass concentration of species *i*.
R^{*} is the universal gas constant.
T is absolute temperature.
p is pressure.
m_i is mass of species *i*.

Table 8 gives ambient concentrations of normal atmospheric and pollutant gases in the atmosphere. However, these numbers are subject to location, time and measurement precision. A general classification of gaseous pollutants based on their chemical properties can be found in Appendix 2.

Further to gas pollutants, particulate pollutants also exist in the atmosphere. Particle pollutants are released from natural sources such as ground dust, volcanoes, anthropogenic activities, fuel combustion etc. Some are formed by gas to particle conversion in the atmosphere due to natural or forced causes. Their diameter varies between a few nanometers (10nm) to a few micrometers (100μm) [Drew et al., 2006]; however, their size and composition can change by evaporation, condensation of vapour species, clustering of particles, chemical reactions etc.

Normal Atmospheric Gas	**Average Concentration (ppm)**	**Pollutant Gas**	**Average Concentration (ppm)**	**Approximate Residence Time**
N_2	780,840	$C0_2$	355	15 years
O_2	209,460	CH_4	1.7	7 year
Ar	9,340	N_2O	0.3	10 year
Ne	18.2	CO	0.05-0.2	65 days
Kr	1.1	SO_2	10^{-5}-10^{-4}	40 days
Xe	0.09	NH_3	10^{-4}-10^{-2}	20 days
He	5.2	NO_x	10^{-6}-10^{-2}	1 day
H_2	0.58	HNO_3	10^{-5}-10^{-3}	1 day
H_2O	Variable	O_3	10^{-2}-10^{-1}	

Table 8 : Clean atmosphere concentrations of normal atmospheric and pollutant gases. [Seinfeld, 1986]

Particle pollutants are removed from the atmosphere by two natural mechanisms: dry deposition (deposition at the Earth’s surface) or wet deposition (incorporation into cloud droplets during formation of rainfall) [Seinfeld and Pandis, 2006]. Because of the above mentioned natural removal of particle pollutants, their lifetime is short having a residence time from a few days to a few weeks.

On the other hand, gas pollutants have lifetimes ranging from few seconds to hundreds of years [Seinfeld and Pandis, 2006]. Table 9 displays some particle elements that exist in the atmosphere. Furthermore, a comparison of ambient and fine particles is given in Appendix 2.

		Concentration (ng m^{-3})		
Element	**Fine or Coarse Distribution**	**Remote**	**Rural**	**Urban**
Fe	F and C	0.6-4,200	55-14,500	130-13,800
Pb	F	0.01-65	2-1,700	30-90,000
Zn	F	0.03-450	10-400	15-8,000
Cd	F	0.01-1	0.4-1,000	0.2-7,000
As	F	0.01-2	1-28	2-2,500
Cu	F and C	0.03-15	3-300	3-5,000
Mn	F and C	0.01-15	4-100	4-500
Hg	-	0.01-1	0.05-160	1-500
Ni	F and C	0.01-60	1-80	1-300
Sb	F	0-1	0.5-7	0.5-150
Cr	F and C	0.01-10	1-50	2-150
SE	F and C	0.01-0.2	0.01-30	0.2-30

Table 9 : Concentrations and size distribution of various elements found in atmospheric particles. [Schroeder et al., 1987]

Modelling results have many probable uses:

- verification of emissions with regulations and standards
- design of new facilities
- calculating and designing stack heights
- accessing existing emissions
- air monitoring networks
- identifying large air pollution sources
- effectiveness of emission standards
- forecasting pollution releases
- forecasting accidental hazardous pollutants
- studying terrain elevation, presence of water bodies and land use factors
- scientific research including design of experiments
- saving cost and time over monitoring

Even though dispersion models have many prospective applications, there are limitations that should be always taken into account [Bluett et al., 2004]. Uncertainty originates from the lack of truthful and exact source information, meteorological data and the appropriateness of the chosen model for the task.

Air pollution dispersion modelling procedure contains four main steps as illustrated in Figure 11. All errors involved in each step should be known and taken into consideration when reaching the final stage of modelling and presenting results.

For each specific problem the appropriate dispersion model should be chosen by taking into account the complexity of dispersion (e.g. weather phenomena and terrain effects) and the potential scale and significance of effects including the sensitivity of the receiving environment (e.g. human health versus amenity effects).

Dispersion models are categorised by their dimensionality. The simplest case is a zero-dimensional (0D) box model, where the atmospheric domain is contained in a single box in which concentrations are the same everywhere. One-dimensional (1D), two-dimensional (2D) and three-dimensional (3D) models consist of a set of boxes aligned in the relevant Cartesian coordinates.

There are no rules on how to select dispersion models. However, certain models are known to work better than others when looking into specific applications. Figure 12 gives a chart of appropriate models according to complexity of dispersion and effects.

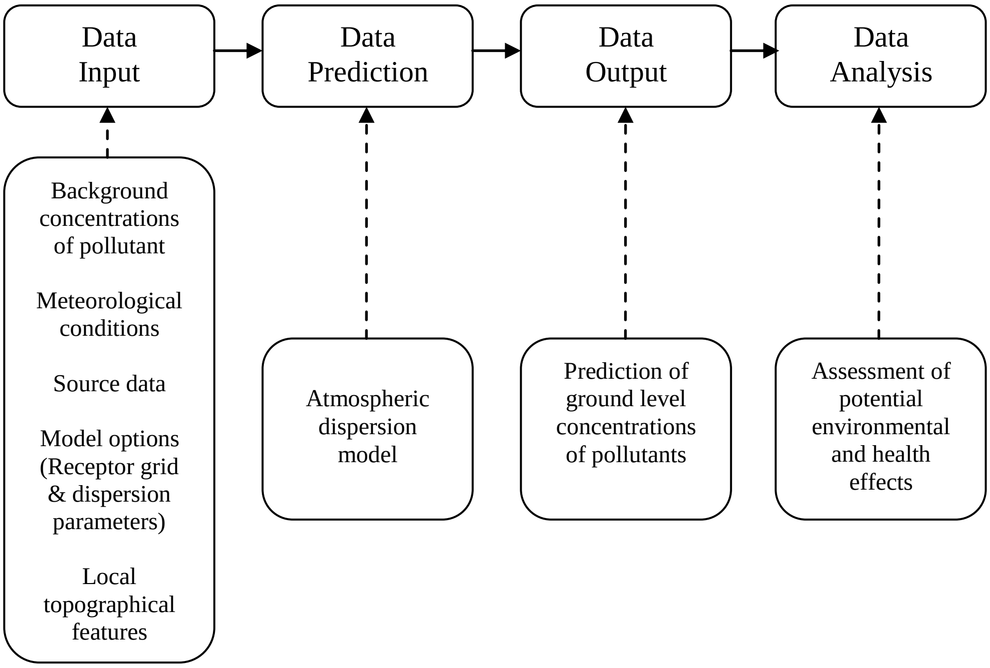

Figure 11 : Air pollution modelling procedure.[Adapted from Bluett et al., 2004]

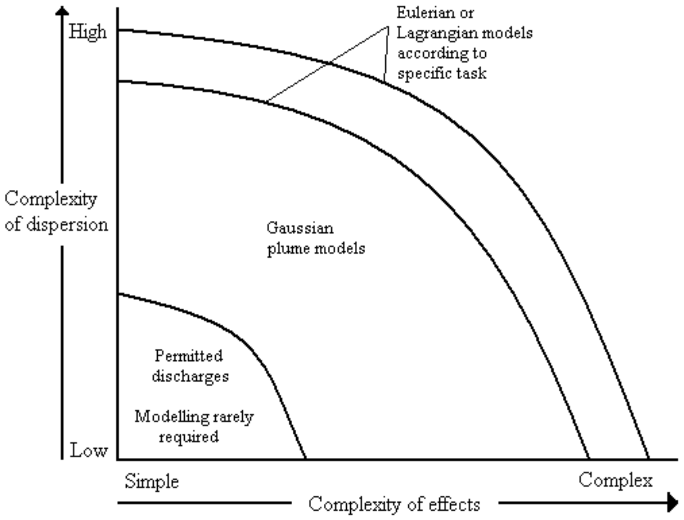

Figure 12 : Type of model typically applied according to the complexity of the problem. [Adapted from Bluett et al., 2004]

For cases of low complexity (simple geometry in small domains with well understood pollutant), source modelling is usually not required. Regulators and risk assessors can analyse the problem with experience, the use of past data or data from similar cases. Nevertheless, when dispersion complexity increases Gaussian models are mostly used. On the other hand, when complexity of effects is high, special application models are utilised. In the case of high complexity and requirement of great accuracy, Eulerian or Lagrangian models are chosen and applied with the help of advanced programs. Finally, airshed programs are used for high complexity cases due to their ability to be adapted by certain studies and include multiple factors that other model types cannot.

Gouesbet and Berlemont (1999) have published work of their group research on Eulerian and Lagrangian models of over two decades. They concluded that both approaches are valid for predicting particle behaviour in turbulent flows with the Lagrangian model performing better in cases of complex geometries and fluid-pollutant interaction.

3.6.1 Eulerian Dispersion Models

Eulerian dispersion models were named after the Swiss mathematician Leonhard Euler (1707-1783) and are based on the Eulerian frame of reference as the name suggests. This frame of reference is fixed in space and has specified origin. The equation for the conservation of mass of the tracer to be dispersed is used in order to get dispersion modelling results [Rotach, 2008].

One important assumption usually made for such type of models is that the flow field and the turbulence phenomena is independent of the pollutant concentration and the concentration is not affected by the fluid flow; the pollutant does not affect the fluid flow and vice versa - either thermodynamically or chemically. For cases where the flow field interacts with the traced pollutant, any possible reactions should be studied (e.g. by using a chemical module).

In a fixed Eulerian frame of reference, the air pollutant concentration is described by the Reynolds averaged mass conservation equation as described earlier.

$$\frac{\partial \overline{C}}{\partial t} + \overline{u_j}\frac{\partial \overline{C}}{\partial x_j} + \frac{\partial}{\partial x_j}\left(\overline{u_j{}'C'}\right) = \overline{Q} \qquad (3.16)$$

For solving the above equation flow field data are required. These are obtained by methods such as numerical modelling. Turbulence characteristics are also necessary in order to establish the turbulent flux divergence term.

By using first order closure, the flux divergence term can be expressed as:

$$\overline{u_j{}'C'} = -K_{ij}\frac{\partial \overline{C}}{\partial x_i} \qquad (3.20)$$

where:
K_{ij} is a second order tensor and its elements are referred to as ‘eddy diffusivities’.

Equation 3.16 reduces to Equation 3.21 by using Equation 3.20. The dispersion process described by Equation 3.21 is called 'Fickian' (note that K_{ij} was replaced by K_j for simplicity).

$$\frac{\partial \overline{c}}{\partial t} = -\overline{u_j}\frac{\partial \overline{c}}{\partial x_j} + \frac{\partial}{\partial x_j}\left(K_j \frac{\partial \overline{c}}{\partial x_j}\right) + \overline{Q} \tag{3.21}$$

There are many analytical solutions of the Eulerian transport equation. The most common is the Gaussian plume formula which is described later in this work.

According to Rotach (2008), for an idealised case Equation 3.21 can be analytically solved and reduced to Equation 3.22. Assumptions include: homogeneous conditions in cross wind direction; stationary flow; no mean vertical flow; no sinks; only one constant source at x_1=0.

$$\overline{u_1}\frac{\partial \overline{c}}{\partial x_1} = \frac{\partial}{\partial x_3}\left(K_3 \frac{\partial \overline{c}}{\partial x_3}\right) \tag{3.22}$$

For flow variables:

$$\overline{u_1} = (\overline{u_1})_0\left(\frac{x_3}{x_{3,0}}\right)^p \tag{3.23a}$$

$$K_3 = (K_3)_0\left(\frac{x_3}{x_{3,0}}\right)^m \tag{3.23b}$$

For boundary conditions:

$$\overline{C} \to 0\ for\ x_1, x_3 \to \infty \tag{3.23a}$$

$$\overline{C} \to \infty\ for\ x_1 + x_3 = 0 \tag{3.23b}$$

$$K_3\frac{\partial \overline{C}}{\partial x_3} \to 0\ for\ x_3 \to 0, x_1 > 0 \tag{3.23c}$$

Thus, the final solution is:

$$\overline{C}(x_1, x_3) = \frac{Qr}{2x_{3,0}(\overline{u_1})_0\Gamma(s)}\left[\frac{(u_1)_0{x_{3,0}}^2}{r^2(K_3)_0x_1}\right]^S exp\left\{-\frac{(u_1)_0{x_{3,0}}^2}{r^2(K_3)_0x_1}\left(\frac{x_3}{x_{3,0}}\right)^r\right\} \tag{3.24}$$

where:
Q is the source strength.
Γ is the Gamma function $r=m-p+2$ and $s=(1+m)/r$.

The solution given by Equation 3.24 was derived by Roberts (1923). It is called 'Robert's solution' and is only valid for $m-p+2 > 0$. The vertical distribution of mass is given by an exponential function. Typical values of *m* and *p* can be determined from turbulence theory or observations: representative values are given in Table 10.

Parameter	**Neutral Smooth Surface**	**Neutral Rough Surface**	**Moderately Unstable**
p	1	1	1.1
m	0.14	0.4	0.1
r	0.14	1.4	1
s	1	1	1.1

Table 10 : Typical values of p and m parameters for analytical Eulerian model. [Rotach, 2008]

There are Eulerian models of first, second and higher order closures, with several different approaches for each type. The most common for first order closure is the K-theory model in which it is assumed that pollutants are uniformly mixed in each cell. Advantages include that wind, turbulence fields and emission source combinations can be included.

Pollutants can be modelled in any of the three following common phases: gas, liquid or solid. In most cases meteorological data are acquired from numerical meteorological models. K-theory models should not be used for dispersion of pollutants in unstable meteorological conditions as in such cases the pollutant plume size is bigger than the size of the turbulent eddies [Zannetti, 1990].

In second order closure models, dispersion equations depend on the components of the turbulent flux. The number of models with second order closure is limited at the moment and are not frequently used because of the vast computing power required for solution.

3.6.2 Gaussian Dispersion Models

Gaussian plume models are widely used by regulators and risk assessors. They are often referred to as ‘Steady State models’ because of the use of steady state assumptions as they represent a collection of data over a time average. Another important detail is that constant meteorological conditions are assumed, even though plume characteristics change over time depending on changing emissions, prevailing winds and other meteorological data. Concentrations are calculated by using emission and meteorological conditions which are homogeneous across the modelling domain. Figure 13 gives a typical representation of a Gaussian plume from an elevated source (e.g. stack). The pollutant follows a normal probability distribution which could be described as having a conical shape.

Gaussian dispersion models are widely used for pollutants with simple chemical characteristics, when the topographical complexity is low and weather conditions are constant and uniform. Their main advantages include the ease of use; their scientific approval; the small meteorological, topographic and computer requirements; and their accurate results for low or / near ground level sources.

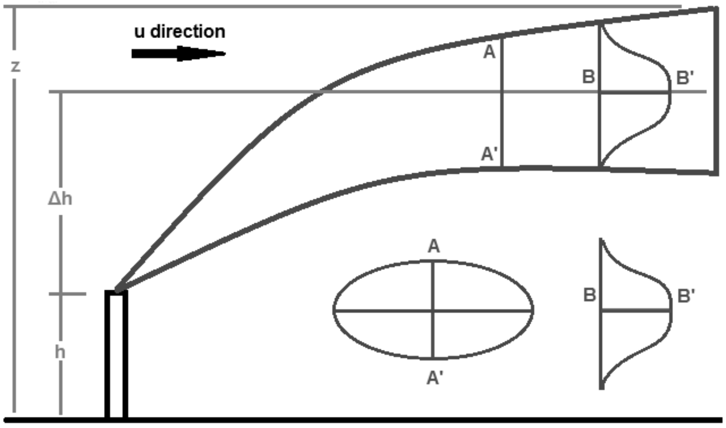

Figure 13 : Typical Gaussian plume from an elevated source.
[Adapted from Markiewicz, 2006]

Pullen et al. (2005) studied airborne agents in urban areas by utilising a Gaussian model. Results were found to be valid in the far field and at several building heights above ground. They emphasized on the importance of high resolution, spatial and temporal wind data for the accuracy of results.

Starting from the Robert's solution (Equation 3.24), and assuming that mean wind speed and exchange coefficient do not vary with height then, $m = p = 0$. Also assuming that, together with stationary flow, no diffusion occurs in the longitudinal direction, no sinks and with a constant point source (at 0, 0, H), Equation 3.21 can be reduced to:

$$\overline{u_1}\frac{\partial\overline{c}}{\partial x_1} = K_j \frac{\partial^2\overline{c}}{\partial {x_j}^2}, \quad j = 2,3 \tag{3.25}$$

For a 3D problem, the boundary conditions are:

$$\overline{C} \to 0\ for\ x_2 \to \pm\infty\ \ and\ \ x_3 \to \infty \tag{3.26a}$$

$$K_3 \frac{\partial \overline{C}}{\partial x_3} \to 0 \; for \; x_3 \to 0 \tag{3.26b}$$

For an initial condition of:

$$\overline{C}(x_1 = 0,\; x_2 = 0,\; x_3 = H) = \frac{Q}{u_1} \; \delta(x_3 - H)\delta(y) \tag{3.26c}$$

For plume characteristics of σ_y and σ_z, according to Equation 3.27 to relate the plume width and height to the basic variables:

$$\sigma_i{}^2 = 2K_i x_1 / u_1 \tag{3.27}$$

The final solution is given by:

$$\overline{C}(x_1, x_2, x_3) = \frac{Q}{2\pi\sigma_y\sigma_z\overline{u_1}} \, exp\left\{-\frac{1}{2}\left(\frac{x_2}{\sigma_y}\right)^2\right\}\left[exp\left\{-\frac{1}{2}\left(\frac{x_3-H}{\sigma_z}\right)^2\right\} + exp\left\{-\frac{1}{2}\left(\frac{x_3+H}{\sigma_z}\right)^2\right\}\right] \tag{3.28}$$

The second pair of rectangular brackets in Equation 3.28 exists due to the second mirrored source at $x_3 = -H$; which in terms of a real source is placed below ground level and is taken into account by the corresponding mass fraction of the mirrored source. This is shown in Figure 14. The Gaussian plume is represented by the green solid line and the corresponding vertical concentration distribution by the blue line from a source above ground. The mirror plume and concentration are each represented by dashed lines. Total concentration is given by the red solid line.

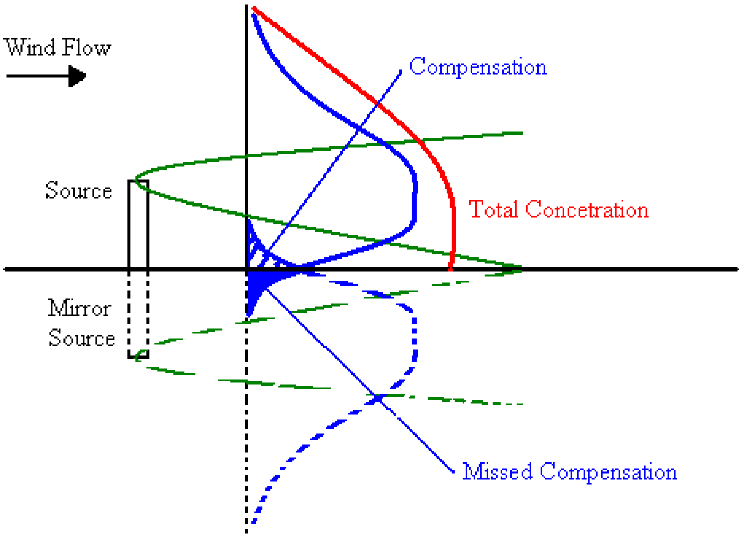

Figure 14 : Gaussian plume sketch [Adapted from Rotach, 2008].

While Gaussian models are easy to implement they have limitations that should be understood and taken under consideration before proceeding to any modelling. These mainly exist due to the fixed flow field assumptions and the absence of solving Navier Stokes equations.

The most important assumptions are [Bluett et al., 2004]:

- Causality effects: pollutant material is transported in a straight line instantly to receptors that could be hours away from the source. These do not take into account wind speeds (e.g. if wind blows at 1ms^{-1}, the pollutant will travel only 3.6km within the first hour) thus causality effects are not accounted for.
- Low wind speeds: Gaussian models can produce worst case scenario results at low wind speeds for calm conditions or low wind speeds. For most cases a minimum wind speed of 0.5 or 1ms^{-1} is required and any value below that is neglected due to the almost non-moving wind.
- Straight line trajectories: Gaussian models do not take into consideration the turning or rising wind due to terrain characteristics, thus underestimate terrain effects during stable conditions.
- Spatially uniform meteorological conditions: the uniform meteorological conditions assumed rarely occur. Terrain features, surface characteristics and natural windbreaks affect the boundary layer that influences the possible pollutant transport and dispersion.
- No memory on previous hour’s emissions: every time concentration calculations are conducted all previous results are discarded thus neglecting factors such as fumigation, morning inversion break up and daily recycling of pollutant of cities.

3.6.3 Lagrangian Dispersion Models

The Lagrangian approach is recognised by modellers to be more fundamental. It uses the Lagrangian frame of reference named after Joseph Louis Lagrange (1736-1813). In this case, the observer follows individual fluid particles as they move through space and time. Particle trajectories are given by plotting the position of each particle through time.

Lagrangian modelled trajectories can be calculated by two methods: the first one requires the calculation of the mean and turbulent velocities; for example - the Eulerian method using NS equations. The second one uses the Lagrangian Stochastic Model (LSM) to calculate the turbulent fluctuating values from mean input data. The first method requires longer processing time and greater CPU power and therefore it is only adopted by a small number of researchers. The second method only requires mean input values from empirical equations or experimental techniques. LSM uses stochastic differential equations to define turbulent velocities, being the major factor distressing accuracy of results. Dixon and Tomlin (2007) used a Lagrangian Stochastic Model to test results against two sets of wind tunnel measurements taken by other authors. Simulation results were close to experimental results, showing that simplicity of the model aids dispersion predictions for complex, three dimensional terrains. However, comparison with urban experiments was complicated as field data was difficult to obtain.

Graham and James (1996) have looked into turbulent dispersion of particles using a Lagrangian eddy interaction model in a homogeneous stationary turbulence. They also examined one-dimensional dispersion of non-fluid particles and the influence of the fluid velocity auto-correlation along the particle path. Results showed that long term dispersion of non-fluid particles can exceed that of fluid particles with conventional eddy interaction models not able to predict such cases.

Lagrangian puff models are different from plume models in several aspects: they always calculate mean concentration distributions and cannot cope with non-stationary conditions. Puff models simulate dispersion more accurately than plume models as they track pollutant dispersion in small, growing puffs as in Figure 15.

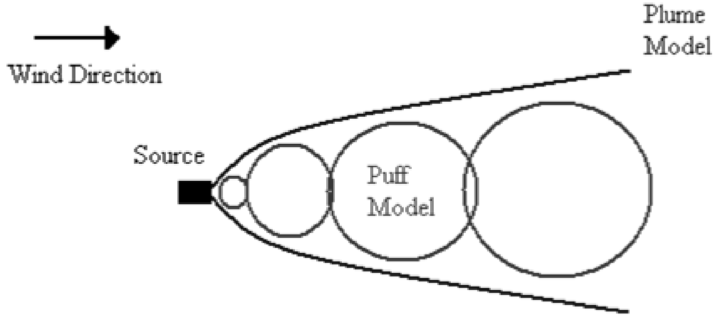

Figure 15 : Comparison of puff and plume models.

The growth of the initial puff can be modelled as suggested by Smith and Hay (1961) using two particle statistics:

$$\frac{d\sigma^{puff}}{dx} = 0.22l, \quad where\ l = \frac{\sum_{i=1,3} \sigma_{u_j}}{\overline{u_1}} \tag{3.29}$$

where:
l is turbulent intensity.
σ^{puff} grows linearly with distance from source; or with time based on Taylor hypothesis.

Puff models are mostly appropriate for complex topographies (where high resolution flow and turbulence fields exist) and instantaneous concentration values. A single puff would correspond to an accidental release or explosion of an instantaneous release (e.g. chemical plant accident). Alternatively, a continuous release of puffs corresponds to a continuous source (e.g. a waste process).

For the employment of Lagrangian particle dispersion modelling, the flow field must be known either by numerical simulation or by parameterisation techniques. All particles are assumed to behave like fluid particles and follow the same mean trajectories (i.e. 'mass-less') but each one has an individual path due to turbulence. Individual paths are based on stochastic models and particle history. For each particle and at each time step, acceleration is calculated to update the position. Thus for a concentration result, the number of particles can be calculated for a specified line, area or volume.

The general equation describing the air pollution dispersion in Lagrangian models is:

$$C(r,t) = \int_{-\infty}^{t} \int p(r,t \mid r',t')\, S_c(\, r',t')dr'd't \tag{3.30}$$

where:
$C(r,t)$ is the ensemble average pollutant concentration at the point r for time t.
$S_c(\, r',t')$ is the term describing the sources and sinks of the pollutant in the atmosphere.
$p(r,t \mid r',t')$ is the probability density function that the hypothetical parcel moves at time t’ from point r’ to the point r at time t.

3.7 Source Modelling

In order to model pollutant dispersion as accurately as possible, the source must be defined correctly. Sources for air pollution modelling can be broken up in four categories. The most accurate representation of the real life scenario is chosen and fully specified by the user. Multiple sources of same or different types are often used.

Mousiopoulos et al. (2009) have studied the importance of source treatment on numerical results together with wind tunnel measurements. They concluded that both type and strength of source have an influence on results and that clear source modelling guidelines should be available to modellers. In case that the characteristics of sources are not known and measurements are impossible, both worst and best case scenarios should be modelled.

Types of sources available in dispersion models are briefly described below and presented in Figure 16:

- Point source: such type of source is used for discharges from small openings such as stacks or vents. It requires several variables to be defined such as: exit velocity, emission rate and temperature.
- Area source: this type is mostly used for sources with large surface areas of irregular shapes. A set of polygons or squares is used to represent the pollutant source as accurately as possible such as landfill surfaces, piles of materials and even liquid surfaces including lakes, lagoons etc.
- Line source: this type of source is used for highways, narrow buildings etc. It releases the pollutants from a virtual line in the modelling domain.
- Volumetric source: this type of source can be created by combining area sources in both vertical and horizontal directions. It is often used for pollutant releases from within buildings.

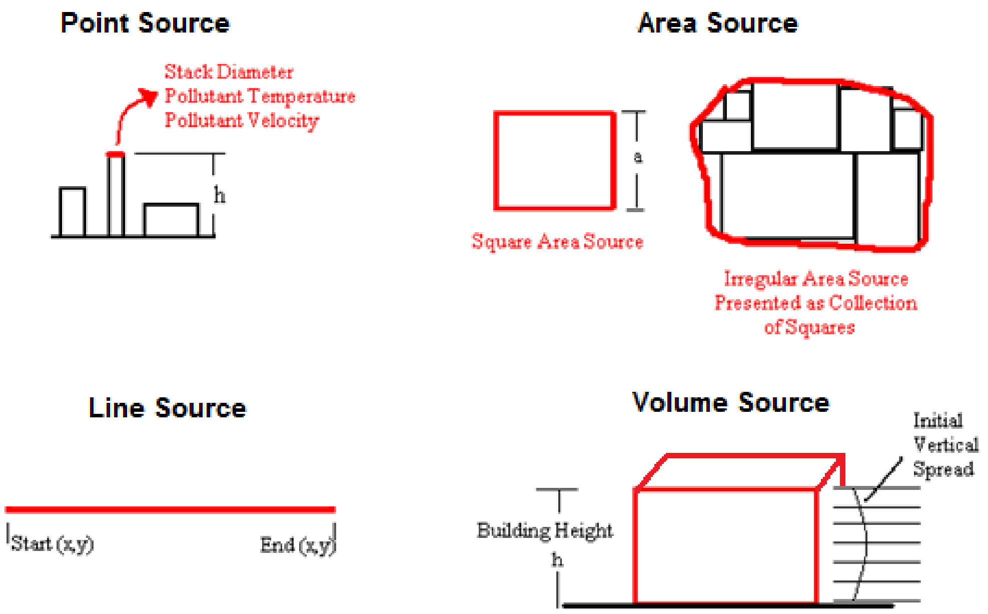

Figure 16 : Source types used by dispersion models.
[Adapted from Bluett et al., 2004]

Emission rate is also an important factor for correctly modelling source releases. Uniform emission modelling may be inappropriate [Mohan et al., 2009]. In most cases, the source does not emit pollutants at a constant rate. Emission rates often vary in time: pollutant release from a process that does not operate 24 hours a day or 7 days a week is not constant. Another example is the variable emissions due to the rate of process within working hours (e.g. rate of production). Season and temperature can also affect pollutant emission rate, with every pollutant type behaving differently according to its properties.

Another factor that could influence variable emission rate is the source type. Large area sources often produce uneven pollutant releases over the surface and in some cases even because of the wind magnitude over that surface. For consideration of such source behaviour, unsteady inlet conditions and source emissions are taken into account. Examples of such cases would be: power station effluents according to electricity demand; waste processing site effluents around the day etc.

Emission data can be obtained by experimental methods as well as from monitoring organisations and government bodies. However, data should be used cautiously as averaged values could lead to massive over-predictions of pollutant dispersion, especially when combined with worst case weather scenarios.

3.8 Topographical Influence

Terrain elevations and topographical characteristics are very important and could rapidly affect pollution dispersion. Wind breaks such as hills, trees and buildings may alter the wind flow and pollutant dispersion. Wind flow velocity reduces rapidly in dense built-up areas due to the blocking effect of buildings compared to flow in the open environment where wind behaviour may be affected by low houses or trees [Huang et al. 2008]. Such windbreaks can also absorb pollutant particles, therefore reducing the spread length or area. Lakes, rivers and trees can even reverse wind and pollutant direction due to localised phenomena such as recirculation and ‘dead areas’. Turpin and Harion (2009b) simulated a three dimensional wind flow over coal stockpiles near a power station. They found that the topography of the site and shapes of stockpiles were of high importance, affecting the flow structure above and around the industrial site.

3.8.1 Sloping Terrain

Sloping terrain is also an important factor as it drives air down or up hillsides due to vertical temperature differences. In general, wind accelerates while travelling on the windward face of the hill and decelerates on the leeward face; static pressure decreases and increases respectively. Kim et al. (2001) examined a two-dimensional flow and dispersion when hills and buildings are present, concluding that both play an important role to the vertical spread and average height of a plume. Slope of hills is often described in percentage values (e.g. 10%, 20% etc.) but in some cases it is given as the right angle relationship of vertical height to horizontal length (e.g. 1:10, 1:15 etc.). The larger the run in a slope ratio, the gentler the angle of the incline will be (a slope of 1:16 would be less steep from that of 1:12).

The complexity of modelling increases rapidly when terrain characteristics are taken into consideration. In general, the more complex the problem is, the higher the probability for poorer results. Puff models are in most cases more appropriate for complex terrain scenarios. Their non-steady state includes casual effects and non-straight trajectories, which are disadvantages of plume models.

3.8.2 Surface Roughness

Terrain features such as buildings, trees etc. are represented in some programs with the use of surface roughness; other programs include such features with the combination of 3D geometry and roughness. Surface roughness strongly affects wind flow separation and recirculation at hilly terrains [Lun et al., 2003]. Vertical mixing of a pollutant plume increases with surface roughness as mechanical turbulence exists over the ground. Common values exist for typical surfaces (Table 11), although most models use specific values that are known to work better according to each physical model employed.

Ground Surface Type	**Surface roughness length (m)**
Urban	1.0–3.0
Coniferous forest	1.3
Cultivated land (summer)	0.2
Cultivated land (winter)	0.1
Grassland (summer)	0.1
Grassland (winter)	0.001
Water	0.0001

Table 11 : Surface roughness lengths for typical surfaces [Schnelle and Dey, 1999].

3.9 Weather Influence

Weather conditions play an important role in atmospheric dispersion modelling. Pollutants can travel large distances because of strong winds and delivered to ground receptors much faster because of rain. Weather conditions are spatial and temporal in complicated, hilly terrains. Ground level pollutant concentrations are mainly affected by wind direction and speed - for transport - and turbulence and mixing height of the boundary layer - for dispersion [Rotach, 2008].

Each dispersion model requires different types and amounts of meteorological data with Lagrangian models being the most demanding. In some cases a dispersion model is selected after considering possible weather phenomena and checking available data. The Royal Meteorological Society (1995) has issued guidelines on the justification and use of models for atmospheric dispersion modelling and the communication and reporting of results. Mandurino and Vestrucci (2009) have examined the importance of meteorological data in environmental analysis by looking at two different approaches: the classical statistical approach (multi-year and long term data) and an environmental Test Reference Year (TRY) approach. The latter was found to give more accurate results as it uses a set of real, contemporaneous data taken from an hourly series of at least 10 year recordings.

Calm conditions should also be given great consideration. They form stable conditions that rapidly decrease horizontal and vertical mixing especially when modelling near-ground sources and having sensitive receptors at a close distance.

Temperature effects should also be modelled where appropriate. Temperature inversions are caused by several factors and are favoured by cold nights and low wind speeds. Possible inversion layers above valleys could trap pollutants and result in high concentrations. When modelling sources near large pockets of water, sea and land breezes should also be taken in to account. Land heats and cools faster than water, creating temperature differences that cause localised wind flow and recirculation.

Data should be obtained from the nearest meteorological office or weather station to enhance validity. Most studies use wind roses; nevertheless this is not always feasible due to the absence of weather stations at some areas. In this case, statistics are applied to previous and new data available and mean values are calculated.

Ideally, weather phenomena and pollutant dispersion should be simulated together. Practically, the cost involved is prohibitive. One approach is to look at the half life (residence time) of the pollutants and decide on the appropriate duration (time) of the simulation, the distance (spatial dimensions) and hence the amount of meteorological data required at boundaries.

The turbulent state of the Atmospheric Boundary Layer and its vertical extension are both affected by the instability of the net radiation from the Earth's surface. During the day, the surface is heated due to the positive net radiation, the positive heat flux and the well mixed CBL. At sunset the surface loses thermal energy and the process is reversed. This causes the rise of a Stable Boundary Layer (SBL) originating from the Earth's surface and going up to 200 metres as illustrated in Figure 17. Thus, effects of the daily cycle to air pollution dispersion are more severe during sunrise and sunset making it difficult to monitor and record profiles of layers.

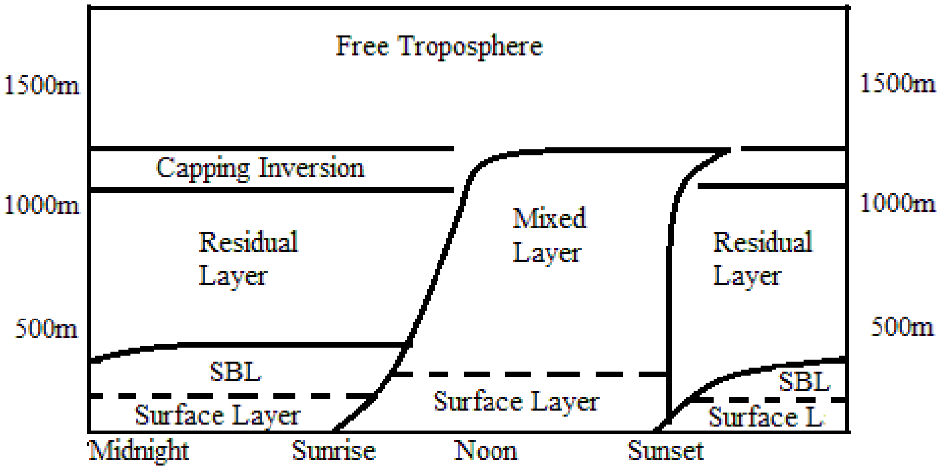

Figure 17 : Daily cycle of the ABL.
[Adapted from Rotach, 2008]

Figure 18 illustrates different valley and slope winds during the day. Wind direction is seen to change from night to morning with winds blowing down and up the valley respectively. Wind flowing down or up the slopes is also seen with inverse direction between sunrise and sunset. Effects like these should be taken into consideration when modelling hilly topographies. As suggested by Katestone Scientific (1998), significant valleys can restrict horizontal movement and dispersion and encourage the development and persistence of drainage flows.

Other important factors to consider would be the wind type and direction according to month or season. These can be modelled by using variable meteorological conditions in the same simulation process. Such approach would clearly display the effect of the season. However, such simulation would require large sets of weather data which would need processing for input to the relevant wind flow modelling program - a time consuming and sometimes expensive process.

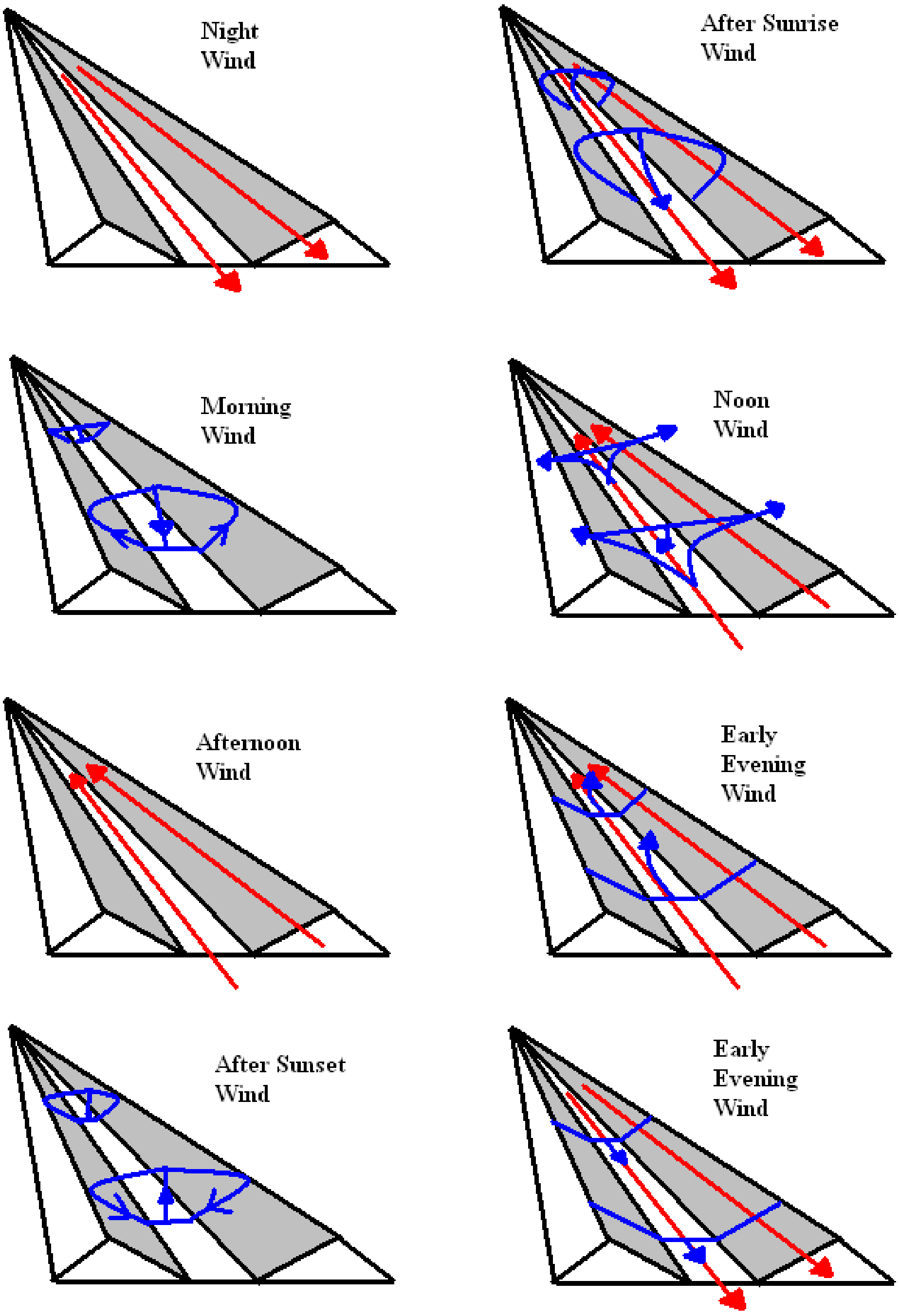

Figure 18 : Different stages of valley and slope wind during a day.
[Adapted from Rotach, 2008]

3.10 Programs for Effluent Dispersion Modelling

3.10.1 Introduction

Air pollution dispersion programs are widely used in different countries around the world, but only a few studies have been made to validate results and compare accuracy. For complicated urban terrains, gas and particle dispersion differences are noteworthy when comparing to relatively flat-land sites. Furthermore, most models are assumed to support particle dispersion modelling, but these are mostly limited to $PM_{2.5}$ and PM_{10} (Particulate Matter of 2.5 and 10 micrometers respectively) and cannot give results for particle concentrations [Holmes et al., 2006]. Thus comparison and validation is difficult and in some cases impossible.

In general, dispersion programs are categorised between ‘advanced’ and ‘airshed’. These are described below, including their main application and some advantages and disadvantages. Commonly used programs such as ADMS and AERMOD are also described herein.

3.10.2 Advanced Dispersion Programs

Advanced dispersion programs are mostly used for research purposes and lately have been adopted in the regulatory sector as a more advanced alternative to programs using Gaussian models. As these programs include multiple factors, they have higher demands in human, data and computational resources.

Such dispersion programs can be categorised by the type of pollutant release in the computational domain. In most modelling cases, a combination of those is used and adopted in an effort to increase accuracy and precision [Bluett et al., 2004].

- Particle release: in this case pollutants are released and represented by a stream of particles (gases and/or liquids) which is affected by the wind and turbulence phenomena. Particle models are probably the best choice for pollutant concentration close and around the source. However these require high computational power and a high number of released particles (at least 10^5).
- Puff release: a series of puffs is often used to represent pollutants that are transported by weather phenomena. Each puff could represent a release of a certain pollutant amount in a given amount of time.

- Grid Point release: in this kind of model, a three dimensional (3D) computational domain is used to represent and calculate pollutant dispersion and concentration. The most common problem with this type of modelling is the extent of computational requirements and the frequent case of the pollutant release scale to be smaller than the chosen grid spacing.

The main difference between advanced dispersion programs and those using Gaussian models is the requirement of the first for three dimensional meteorological data and not only single-point measurements. Furthermore, the use of advanced codes requires the knowledge of boundary layer meteorology, turbulence and particle dynamics. Specialised pre and post processing software on high-end computers is also a necessity, with the ability to run for hours (even days or weeks in some cases) and handle large jobs.

Such types of programs described in this section are known to be more precise and accurate. However, it should be noted that in some cases models used in advanced programs perform equally to Gaussian models. Those cases often include: grid point models near source of pollutants; near-field receptors under non-convective conditions and near field receptors for wind speeds over $1ms^{-1}$ [Bluett et al., 2004].

Every case requires its own ‘angle of attack’, letting the modeller choose the appropriate model according to the requests of the client or the research topic (in some cases quality is not as important as quantity). A comparison of the capabilities of each model is often the starting point for a pollutant dispersion work, followed by possible validation. Finally, model misuse or misinterpretation of results is quite often due to modellers having a better knowledge of steady state models.

Comparison between models and programs is difficult and in many cases insignificant. Each model was designed for specific tasks and thus the limitations are known. On the other hand, cost is one of the most important factors considered by modellers when choosing the model that best suits their problem and application. Staff expertise is the most common setback: time and costs for training are significantly higher due to the complexity of advanced dispersion codes. In such case external experienced modellers are brought in to consult or even manage the work.

Three-dimensional topographical and meteorological data are required for advanced programs. This, rapidly increases the amount of data for input and processing. Especially in cases of high terrain or weather complexity, advanced programs are employed. For simple terrain geometries, a plume model would be more appropriate. Configuration and processing time of all models is likely to be more complicated for advanced programs due to the multiple factors taken into account. Processing time increases by the complexity of terrain, weather conditions etc., but can be handled by most high-end personal computers. Dimov et al. (2004) looked into the difficulties of numerical treatment of large air pollution models, concluding that parallel computing is a necessary tool which allows modellers to increase complexity and accuracy of most problems studied.

3.10.3 Airshed Dispersion Programs

Airshed dispersion programs are used for modelling pollutant dispersion and concentration over larger areas or when multiple sources are required. Gaussian and advanced codes cannot achieve accurate results when dealing with large computational domains. However, airshed programs are not able to run on personal computers and often require supercomputers and/or parallel processing.

Airshed capable programs are mostly used for modelling air quality and pollutant dispersion of entire regions, including all topographical characteristics and relevant features of the region. Common applications include: emissions from a city, from a waste process and even potential terrorist attacks. This complicated technique divides the computational domain into small cells and models pollutants as they move from one cell to another. (Gaussian and advanced dispersion programs track and follow the pollutants from a single point source - or line or area.) The wind flow is modelled in each cell separately, but all cells together form the final result. There are different choices of grid sizes and time steps according to the needs of the problem. Grid sizes often reach hundreds of kilometres and variable time steps can be included in a single simulation.

One of the great advantages of airshed programs is that they take into account all phenomena (weather and pollutant related) in the vertical structure of the atmosphere. Thus, a range of different sized-cells is used to accurately model the lower layers close to the ground. The height of the computational domain always includes the atmospheric boundary layer (1 to 2km) and in some cases it even covers the entire troposphere (up to 30km) [Bluett et al., 2004].

Information for two main features is required in particular before using an airshed dispersion program: all relevant data on emission of pollutants and meteorology conditions. Emissions of all pollutants released from every source in the domain are most critical. Emissions records or measurements are often required for every particular time step to be examined. All possible sources (domestic, industrial, natural) should be accounted for and have their source type selected (point, line or area).

Contaminant details are often required by models to perform accurately. Most models require CO, SO_2, NO_x, and other particulates. These are important for modelling possible chemical reactions in the examined domain. An hourly time resolution is often suggested as any smaller intervals would be non-practical. The period of source modelling depends on the application but in most cases is suggested to cover at least two periods: one for 2-3 days and another one at longer intervals (e.g. monthly or yearly).

Meteorological conditions are also very important for accurate modelling of pollution dispersion. Data is required for all three dimensions of the domain but in most cases the complete set comes after estimation of missing values using mathematical techniques like linear interpolation.

There are only a few limitations to airshed programs and these often exist due to lack or inconsistency of input data. The modeller can choose the type and presentation of results from a wide variety of choices and tools according to the needs of the problem. Charts and multi-dimensional graphs are often employed to best represent results and help non-experts understand the outcome.

Accuracy is much higher using such codes. However, this is affected by input data and the modeller’s knowledge. It is recognised that Gaussian and advanced programs are less accurate in cases of extreme complexity and when multiple factors are considered. On the other hand, airshed programs achieve accurate results but require long processing times, high computational power and user experience in multiple scientific fields. Most of the times, such type of modelling is used by research groups that consist of multiple experienced specialists so that everyone can contribute in a specific field of the modelling process.

3.10.4 The Commonly Used ADMS Dispersion Program

There are several well-known and accepted programs for effluent pollution dispersion with common programs and their main characteristics listed in Table 13. Advanced programs ADMS and AERMOD are the most popular and are briefly described here (a comparison table for these two can be found in Appendix 2).

ADMS is a FORTRAN language dispersion code developed by Cambridge Environmental Research Consultants (CERC) in collaboration with the UK Meteorological Office, National Power Plc. and the University of Surrey. The first edition was released in 1993 and the latest edition ADMS 4 in 2009 (described in this paper). It is widely used for environmental impact assessments, regulatory purposes and emergency planning both in the United Kingdom and overseas. It was designed to model the dispersion of buoyant or neutrally buoyant particles and gases [Carruthers et al., 1994].

ADMS can give a long term average and peak hourly pollutant concentrations taking into account alternating wind directions and speed over different topographies. However, it has some limitations which are briefly discussed below with the most important being: problematic representation and pollutant dispersion prediction at low wind speeds and especially below $1ms^{-1}$ [Mohan et al., 2009], limitation on number of required for modelling buildings in-between which pollutants could be trapped and some resolution problems in case the domain examined is large.

ADMS uses the mean wind profile and the Monin-Obukhov length to calculate boundary layer heights and then uses a skewed Gaussian concentration distribution to calculate dispersion under convective conditions. It employs the Runge-Kutta algorithm to solve conservation equations for estimating plume rise including buoyancy, momentum and boundary layer inversions. This code can also model dry deposition (calculated using gravitational settling and deposition velocity) which is assumed to be proportional to the near-surface concentration and wet deposition which is approximated using a washout coefficient [Holmes et al., 2006]. Furthermore, it can account for time varying emissions, odours, NO_x chemistry and radioactive decay.

Information data regarding the meteorological conditions for the area examined in ADMS is primarily calculated by the Met Input Module which uses ‘met files’. Such data is available through the Met Office and could include weather data for one or more hours or longer periods. The Met Input Model calculates data hourly checking that there is no data missing, calculating and adding meteorological quantities where necessary. The effects of topographical features and non-uniformities in the surface properties are neglected and it is assumed that boundary layer characteristics can be expressed at any instant in terms of the values of the surface characteristics; further assumptions regarding the Met Input model can be found in ADMS 4 Technical Specification - P05/01P/09.

The boundary layer structure is calculated in ADMS by using variables and quantities calculated by the Met Input Module. This calculation uses the mean wind profile – based on the surface roughness length at the source site - and the Monin-Obukhov length L_{MO} which originates from the Monin-Obukhov similarity theory which is used for non-adiabatic atmospheric conditions – also known as stratified atmospheric conditions.

Similarity theories (like Monin-Obukhov) are based on dimensional analysis and have been developed using approximate theories and experimental measurements in order to help calculate the vertical mean velocity profiles in the atmospheric boundary layer [Seinfeld and Pandis, 2006]. For calculating mean velocity profiles in the non-adiabatic surface layer and assuming that variations in the surface roughness length z_0 only shift (do not affect) the velocity profiles, the problem has four dimensions: mass, length, time and temperature. For such system and according to the Buckingham π theorem there are two dimensionless groups governing the behaviour of the system: the flux Richardson number (*Rf*) given by Equation 3.31 and the dimensionless velocity gradient $\frac{\kappa L_{MO}}{u_*}\frac{\partial \overline{u_x}}{\partial z}$ [Seinfeld and Pandis, 2006].

$$Rf = -\frac{\kappa g z \overline{q_z}}{\rho c_p T_0 u_*^3} \tag{3.31}$$

where:
c_p is specific heat of air.
T_0 is the ground temperature.
$\overline{q_z}$ is the vertical mean heat flux.

The flux Richardson number is a function of the distance from the ground and is equal to the ratio of the production of turbulent kinetic energy by buoyancy to its production by shear stress [Seinfeld and Pandis, 2006]. As it is dimensionless, it can be also written in a dimensionless length form:

$$Rf = \frac{z}{L_{MO}} \tag{3.32}$$

The Monin-Obukhov length L_{MO} is defined as the height at which the production of turbulence by both mechanical and buoyancy forces is equal and provides a measure of the stability of the surface layer [Seinfeld and Pandis, 2006]. Equation 3.33 describes the Monin-Obukhov length.

$$L_{MO} = -u_*^3 \frac{\rho c_p T_0}{\kappa g \overline{q_z}} \tag{3.33}$$

Both Richardson number and Monin-Obukhov length describe the stability of the atmospheric boundary layer and have an inverse relationship. Thus, when $Rf > 0$ then $L_{MO} > 0$ and when $Rf < 0$ then $L_{MO} < 0$ (stable and unstable atmosphere respectively).

In many applications, empirical forms of the Monin-Obukhov similarity functions have been determined from micrometeorological experiments at various flat homogeneous sites [Arya, 1999]. Commonly used values of the Monin-Obukhov length for different atmospheric stability conditions are given below.

Monin-Obukhov L_{MO}		**Stability Condition**
Very large negative	$L_{MO} < -10^5$ m	Neutral
Large negative	-10^5 m $\le L_{MO} \le -100$ m	Unstable
Small negative	-100 m $< L_{MO} < 0$	Very unstable
Small positive	$0 < L_{MO} < 100$m	Very stable
Large positive	100 m $\le L_{MO} \le 10^5$ m	Stable
Very large positive	$L_{MO} > 10^5$ m	Neutral

Table 12 : Monin-Obukhov length with respect to atmospheric stability. [Seinfeld and Pandis, 2006]

Turbulence profiles are calculated by formulae based on surface roughness and boundary layer height; they depend on the atmospheric stability characterised by the Monin-Obukhov length ratio h/L_{MO} that corresponds to different stratification stabilities. Turbulence length, time scales and energy dissipation rate are calculated assuming that the vertical length scale is determined by the local shear and the blocking effect of the surface and is limited by the boundary layer depth [P09/01U/09]. Other properties calculated are buoyancy frequency, pressure, specific humidity and potential temperature. Further details regarding boundary layer specification in ADMS are given by ADMS 4 Technical Specification - P09/01U/09.

The plume spread and mean concentration module uses a Gaussian plume that includes ground and inversion-layer reflections as described by Equation 3.34.

$$C = \frac{Q_S}{2\pi\sigma_y\sigma_z U} exp\left(\frac{-y^2}{2\sigma_y^2}\right)\left\{exp\left(\frac{-(z-z_S)^2}{2\sigma_z^2}\right) + exp\left(\frac{-(z+z_S)^2}{2\sigma_z^2}\right) + exp\left(\frac{-(z-2h+z_S)^2}{2\sigma_z^2}\right) + \right.$$

$$exp-(z+2h-zs)22\sigma z2+exp-(z-2h-zs)22\sigma z2 \qquad (3.34)$$

where:
σ_y is transverse spread.
σ_z is vertical spread.

Appendix 1 of P10/01V/09 states that the model has been derived and tested under UK meteorological conditions and that the upper limit for plume spread averaging time generally is 24 hours. Further information and equations regarding dispersion parameters and mean concentration according to atmospheric conditions can be found in ADMS 4 Technical Specification – P10/01V/09 and P12/01V/09.

ADMS has a separate module for taking under consideration complex terrain effects. In general and for slopes less than 1:10 the domain examined is considered flat. For slopes more than 1:10 the Complex Terrain Module should be enabled. This module uses FLOWSTAR to calculate flow field and turbulence parameters using linearised analytical solutions of the momentum and continuity equations [P14/01O/09]. It uses the same meteorological data as the main ADMS model and boundary layer variables are calculated with the same boundary layer structure module.

The terrain files can be of any grid size but the number of maximum data points should not exceed 5000. For every four points, a rectangle is formed for which an internal calculation grid is created. Three pre-defined spacings are available for that grid: 16x16 points (testing), 32x32 points (standard) and 64x64 points (large or complex domains). In the vertical direction the grid has ten vertical levels ranging from 1.3 times the minimum surface roughness to 2km [P14/01O/09]. These predefined spacing options could largely affect the resolution and final output of the program if terrain data is limited or not detailed. Thus, for two points, 320 metres apart the standard grid (32x32) would create cells of 10 metres while two points 100 metres apart would result to cell sizes of approximately 3 metres.

In the complex terrain module, hills affect the flow and are taken into account by simplifying terrain data to a single Gaussian shaped hill of circular cross section and height of the highest hill [P14/01O/09].

ADMS can also account for building effects by calculating the near field dispersion of pollution from sources close to large buildings or groups of buildings represented as a single effective building [P16/01S/09]. This single effective building is a single block with equivalent crosswind and vertical dimensions; the flow field consists of a recirculating flow at the leeward side where concentration is uniform.

ADMS 4 can model up to 300 sources with each source emitting up to 10 pollutants and each pollutant including up to 10 different particle sizes [P24/01H/09]. Point, line, area and volume type sources can be modelled with the concentration formulas adapted to the relevant dimensionality. For line, area and volume sources ADMS can model decomposition for each meteorological condition and each different output point. Further details for treatments of sources can be found in ADMS 4 Technical Specification – P25/03H/09.

AERMOD was formally approved by the US EPA in 2000. It is a near field steady state Gaussian plume model that uses the boundary layer similarity theory to define turbulence and dispersion coefficients as a continuum, rather than a discrete set of stability classes [Bluett et al., 2004]. It accounts for buoyant plumes and a method to approximate flows over complicated terrain. The model does not include wet or dry deposition of gases and only uses a simple treatment of dry deposition using a reflection algorithm [Holmes et al., 2006].

Furthermore, a short description of AERMOD by Viz (2011) can be found in Appendix 1.

Name	**Model Type**	**Scale**	**Grid Size**	**Resolution**	**Source Types**	**Pollutant**	**Building Effects**	**Topography**
ADMS	3D Gaussian Plume	Local Regional	3000 grid cells Up to 50km	No limits	Point Area Line	Gas Particle	Yes	Complex
AERMOD	Steady State Bi-Gaussian Plume	Local Regional	<50km	No limits	Point Area Volume	Gas Particle	-	Simple & Complex
CALPUFF	Multi Layer Non Steady Gaussian Puff	Regional	<200km	No limits	Point Area Line Volume	Gas Particle	Yes	Complex
MICRO CARGRID	CFD	Local	<10km	H: 1m V: 1m	Point Area Line Volume	Gas Particle	Yes	Simple & Complex
SCREEN3	Gaussian Plume	Regional	<50km	No limits	Point Area Volume	Gas Particle	Yes	Simple & Complex
TAPM CSIRO	Eulerian Lagrangian	Regional	<1000 x 1000 km	H: 0.3-30km V: >10m	Point Area Volume	Gas Particle	Yes	Complex

Table 13 : Characteristics of most commonly used air pollution dispersion programs [Adapted from Bluett et al., 2004].

Chapter 4

CFD NUMERICAL MODELLING APPROACH

4.1 Introduction

Simulating wind flow and effluent pollution dispersion with actual weather, topographical and source data can be a challenging and time consuming task. The need for simplifications and assumptions is apparent in order to gradually examine and develop all appropriate steps and parameters for modelling such problem with the help of CFD program FLUENT.

Computational Fluid Dynamics is known to perform well in modelling fluid flow in the Atmospheric Boundary Layer in which wind born pollution dispersion takes place. Yang et al. (2009) have studied boundary conditions in order to model the ABL by performing numerical simulations for an empty (feature-less) domain. Results showed that for correct modelling of the ABL, variables describing the inlet boundary conditions should be specified properly for the full height of the domain; the modelling of ground roughness must be realistic; the top (sky) boundary condition should be carefully chosen; and finally all parameters should be tuned relatively to each problem examined.

Blocken et al. (2007b) have further looked into wall function roughness chosen in CFD programs based on experimental data for sand grained channels. This factor can play an important role in the accuracy of the results and the comparisons made between CFD codes. They advised to always simulate an empty computational domain (prior to the actual simulation) with all appropriate boundary conditions in order to check and ensure the best available wind flow results which could later affect pollutant dispersion. CFD programs have also been used to simulate air pollution dispersion in canyons. Yang and Shao (2008) simulated 2D idealised canyons and a 3D canyon in Hong Kong Central area. Results supported previous data obtained by the same authors and successfully provided the complicated flow field phenomena in that region.

Comparison of CFD programs with other dispersion modelling programs has also been carried out. Pullen et al. (2005) compared the Gaussian puff model SCIPUFF to CFD code FAST3D-CT for several sites in Washington DC and Chicago. CFD was found to perform better for complicated terrains which produce hazard areas whose characteristics are sensitive to release location and meteorological conditions. Di Sabatino et al. (2007 and 2008) presented the comparison of CFD code FLUENT to operational air dispersion model ADMS URBAN. Both effects of street canyons and obstacle arrays were investigated with FLUENT achieving better results for complex geometries. However, turbulence diffusion may be adjusted by the use of Schmidt number (described later in this chapter) to mimic the effect of extra mixing in high building density. These conclusions are further supported by Riddle et al. (2004) who also compared FLUENT CFD code to ADMS and concluded that CFD is more appropriate for greater complexity problems that could not be solved in ADMS. Furthermore, CFD programs can account for low wind speeds, multiple buildings and sources with constant but also variable emission rates; all of which create challenges in ADMS [Mohan et al., 2009]. Authors examining CFD capabilities have mentioned the high cost, time and processing power required, emphasising on the use of CFD modelling programs by users with knowledge on fluid mechanics. They also advise on further research to examine the full potential and limitations of CFD.

In this chapter, the author introduces the concept of simulation of ideal terrain and also how this approach has been used in the past to represent topographical characteristics for open environmental flows. A description of the mathematical models employed with the help of CFD program FLUENT, to solve wind flow and particulate pollutant dispersion is given, followed by literature review on appropriate boundary conditions for accurately modelling wind flow in the neutral ABL. Finally, ideal terrain geometry and domain size used for preliminary simulations are defined.

4.2 Use of Idealised Terrain

The examination of simplified or idealised geometry is common practice in the early stages of numerical modelling of complicated flow phenomena (factors increasing modelling complexity of environmental flows are presented in Chapter 3). There are many reasons for simplifying the geometry including: removal of parts or features that would have negligible effects on the flow phenomena; coarse representation of features that do not affect the flow at the point/s of interest; and finally for obtaining the step by step, best practise and approach for understanding factors that influence results. Common examples of simulations which make use of simplified geometries are vehicles, trains and aeroplanes.

Regarding the case of environmental wind flow, ideal geometries have been extensively used to examine and improve modelling methods. Boxes are used to represent buildings [Blocken et al., 2007a] and street canyons [Gromke et al., 2008], large steps to represent canyons and escarpments [Xie et al., 2006] and arrays of cubes to represent urban built areas [Hu and Wang, 2005].

CFD has been extensively used to model wind flow and pollutant concentrations in street canyons [Chu et al., 2005] in order to compare results to experimental wind tunnel data [Mavroidis, 2000 and Chang et al., 2003]. Simulations showed that such dense built up areas can create localised phenomena and recirculation in-between buildings thus resulting in increased particles delivered to residents and high levels of concentration trapped at pedestrian heights. For large arrays of cubes, it was observed that localised dispersion patterns were formed; these were dependent on source position and neighbouring cubes.

For studies on wind flow around tall and geometrically complicated buildings, a simplified version of each building is often designed incorporating only major characteristics that would influence the flow. An example is given in Figure 19: a comparison between a CAD and a CFD model of the Arts Tower of the University of Sheffield.

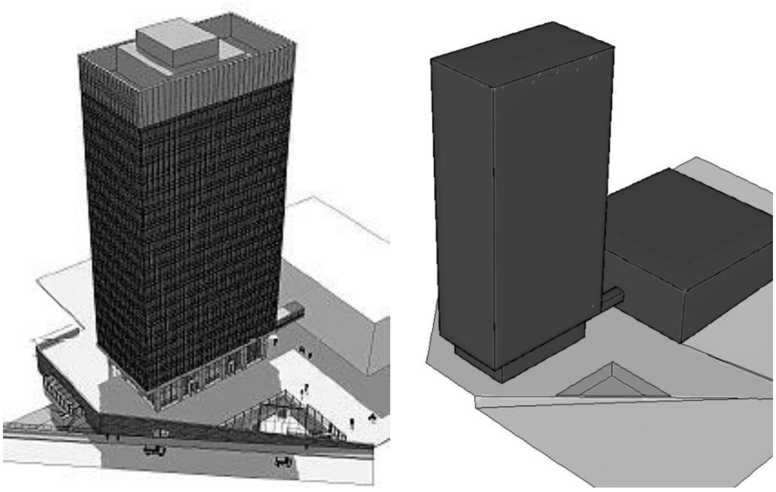

Figure 19 : CAD model (left) [UoS website] and simplified CFD model (right) [Banks, 2005] of the Arts Tower of the University of Sheffield, UK.

Moreover, numerical modelling of wind flow over complicated topographical terrain has been previously investigated by several authors. Kobayashi et al. (1994) used RANS to model turbulent wind flow over an ideal forest situated on a 2D ideal steep hill; results demonstrated the influence of forest trees on the wind flow profiles and were compared to experimental data showing good agreement.

Kim et al. (1997) have also utilised RANS with the standard *k*-*ε* turbulence model to study wind flow over single and double 2D hills and compared speed-up characteristics, recirculation areas and reattachment lengths to wind tunnel measurements. They found that this numerical technique is applicable for such modelling and concluded that the presence of a low hill upwind of a high hill did not affect mean velocity profiles. This was not the case for a high hill upwind of a low hill which had a strong influence to mean velocity profiles and recirculation trends.

Carpenter and Locke (1999) have investigated wind flow over 2D steep and shallow sinusoidal hills using experimental (wind tunnel) and numerical techniques (CFD). Multiple hill configurations showed lower mean wind flow magnitudes than for single hill cases. Comparison of the maximum mean wind magnitude atop hills showed little difference between configurations with the maximum value occurring above the second hill for simulations of multiple steep hills.

Castro et al. (1988) have looked into wind direction effects on pollutant dispersion from point source downwind 3D steep hills within the recirculation zone. They found the surface concentration to be sensitive to wind direction with concentration levels at maximum for a wind flow with angle of attack equal to 0° (along the axisymmetric hill centreline); this was therefore considered the worst case scenario. As the wind direction changed, concentration at the same point (where maximum values occurred for 0°) fell rapidly until it reached ‘background’ levels at an attack angle of 20°.

Kim et al. (2001) have simulated wind flow and pollution dispersion over 2D hills and buildings. Several hill slopes and building heights were modelled to study the influence of geometry (hills and cubes) on the streamline wind velocity and on pollutant concentration. They found the *k*-*ε* turbulence model to be appropriate for modelling such problem after comparing their results to previous studies. Two-dimensional simulations for domains that combined a single hill with two rectangular buildings (forming a canyon in-between) showed that the hill caused an increase to the recirculation area behind the canyon and decreased pollutant dispersion by reducing the height of the simulated plume above the canyon.

In this sense, Parker and Kinnersley (2004) used CFD program FLUENT to model fluid flow and particle dispersion from a point source on a flat plane and upwind a cone and a ridge. Regarding the solution of fluid flow, RANS equations were used with the RNG k-ε model for closure. For particle dispersion modelling, discrete phase modelling was employed using entrapment for the ground faces. Results were compared to wind tunnel data for the same geometries giving a closely similar pattern of dispersion.

Literature clearly suggests that terrain morphology and buildings can influence the wind flow and effluent pollution dispersion; thus the need for examination of their effects to the flow with the use of idealised geometries. Hills, canyons and arrays of cubes were seen to greatly influence wind flow, creating localised phenomena and recirculation zones that trap particulate pollutants. Results from numerical modelling have been compared to wind tunnel results for validation showing good agreement. Nonetheless, all of the herein sited authors emphasized on the correct choice of a turbulence model, domain size and dispersion model to accurately simulate effluent pollution dispersion according to the terrain simulated – consequently the need for site specific investigations, wind flow and pollution dispersion modelling for real life case studies arises.

4.3 Mathematical Modelling

Commercial CFD software, FLUENT, originally developed by Creare Inc. in the late 80’s, was employed to model wind flow and pollution dispersion in this work. FLUENT is widely used in the industrial and scientific communities for studying and solving engineering problems.

4.3.1 Wind Flow Modelling

In order to model wind flow in the open environment, Reynolds averaging is engaged to time-average the instantaneous values given by the Navier Stokes equations for turbulent flow. These solution variables can be decomposed into mean and fluctuating components for velocity (Equation 4.1), pressure and other scalar quantities (Equation 4.2).

$$u_i = \overline{u_i} + u_i' \tag{4.1}$$

$$\phi = \bar{\phi} + \phi' \tag{4.2}$$

where:
$\overline{u_i}$ is mean velocity component (i=1, 2, 3).
u_i' is fluctuating velocity component (i=1, 2, 3).
ϕ is a scalar (i.e. pressure, energy, species concentration).

Equation 4.1 and Equation 4.2 are substituted for a time average in both instantaneous continuity and momentum equations resulting to the Reynolds Averaged Navier Stokes (RANS) equations as described by Equation 4.3 and Equation 4.4 which are written in Cartesian tensor notation. The momentum equation contains Reynolds stresses represented by $-\rho\overline{u_i'u_j'}$ which can attain mathematical closure by the use of Equation 4.5.

$$\frac{\partial \rho}{\partial t} + \frac{\partial}{\partial x_i}(\rho\overline{u_i}) = 0 \tag{4.3}$$

$$\frac{\partial}{\partial t}(\rho\overline{u_i}) + \frac{\partial}{\partial x_j}(\rho\overline{u_i}\,\overline{u_j}) = -\frac{\partial p}{\partial x_i} + \frac{\partial}{\partial x_j}\left[\mu\left(\frac{\partial\overline{u_i}}{\partial x_j} + \frac{\partial\overline{u_j}}{\partial x_i} - \frac{2}{3}\delta_{ij}\frac{\partial\overline{u_l}}{\partial x_l}\right)\right] + \frac{\partial}{\partial x_j}\left(-\rho\overline{u_i'u_j'}\right) \tag{4.4}$$

where $\overline{u_i'u_j'}$ is closed as: $-\rho\overline{u_i'u_j'} = \mu_t\left(\frac{\partial\overline{u_i}}{\partial x_j} + \frac{\partial\overline{u_j}}{\partial x_i}\right) - \frac{2}{3}\left(\rho k + \mu_t\frac{\partial\overline{u_k}}{\partial x_k}\right)\delta_{ij}$ (4.5)

where:
k is turbulent kinetic energy.
μ_t is turbulent viscosity.

4.3.2 Turbulence Modelling

Turbulence modelling is used to time-average the instantaneous fluctuations in the flow governing equations by removing the small scales leading to less computationally expensive equations in terms of solving.

The Boussinesq hypothesis (Equation 4.5) calculates the Reynolds stresses from the mean velocity gradients. Turbulent viscosity μ_t is calculated as a function of the latter mentioned variables. While using the k-ε turbulence model, two additional transport equations must be solved for the turbulence kinetic energy k and the turbulence dissipation ε. The k-ε turbulence model assumes high Reynolds numbers and hence a separate model for near wall treatment is required where the flow occasionally becomes laminar, the standard wall function method is implemented (described later in this chapter).

As a result, the combination of RANS equations with the standard k-ε turbulence model employed in this work has been the suggested approach by several authors for simulating wind flow in the open environment [Richards and Hoxey, 1993; Kim et al., 1997; Parker and Kinnersley, 2004; Hargreaves and Wright, 2007]. It is a two-equation model developed by Launder and Spalding (1974) and is widely used for engineering flow simulations due to its reasonable accuracy within a reasonable processing time. It includes two transport equations for turbulence kinetic energy k and its dissipation rate ε. The respective equations in FLUENT are defined by Equations 4.6 and 4.7.

$$\frac{\partial}{\partial t}(\rho k)+\frac{\partial}{\partial x_i}(\rho k\overline{u_i})=\frac{\partial}{\partial x_j}\left[\left(\mu+\frac{\mu_t}{\sigma_k}\right)\frac{\partial k}{\partial x_j}\right]+G_k+G_b-\rho\varepsilon-Y_M+S_k \tag{4.6}$$

$$\frac{\partial}{\partial t}(\rho\varepsilon)+\frac{\partial}{\partial x_i}(\rho\varepsilon\overline{u_i})=\frac{\partial}{\partial x_j}\left[\left(\mu+\frac{\mu_t}{\sigma_\varepsilon}\right)\frac{\partial\varepsilon}{\partial x_j}\right]+C_{1\varepsilon}\frac{\varepsilon}{k}(G_k+C_{3\varepsilon}G_b)-C_{2\varepsilon}\rho\frac{\varepsilon^2}{k}+S_\varepsilon \tag{4.7}$$

where:
G_k is generation of turbulence kinetic energy due to the mean velocity gradients.
G_b is generation of turbulence kinetic energy due to buoyancy.
Y_M is contribution of the fluctuating dilatation in compressible turbulence to the overall dissipation rate.
$C_{1\varepsilon}$, $C_{2\varepsilon}$ and $C_{3\varepsilon}$ are turbulence model constants.
σ_k and σ_ε are the turbulent Prandtl numbers.
S_k and S_ε are user defined source terms.

Removing terms neglected, Equation 4.6 and Equation 4.7 for k and ε respectively are simplified and presented below:

$$\frac{\partial}{\partial t}(\rho k)+\frac{\partial}{\partial x_i}(\rho k\overline{u_i})=\frac{\partial}{\partial x_j}\left[\left(\mu+\frac{\mu_t}{\sigma_k}\right)\frac{\partial k}{\partial x_j}\right]+G_k-\rho\varepsilon \tag{4.8}$$

$$\frac{\partial}{\partial t}(\rho\varepsilon)+\frac{\partial}{\partial x_i}(\rho\varepsilon\overline{u_i})=\frac{\partial}{\partial x_j}\left[\left(\mu+\frac{\mu_t}{\sigma_\varepsilon}\right)\frac{\partial\varepsilon}{\partial x_j}\right]+C_{1\varepsilon}\frac{\varepsilon}{k}(G_k+C_{3\varepsilon}G_b)-C_{2\varepsilon}\rho\frac{\varepsilon^2}{k} \tag{4.9}$$

The turbulent viscosity μ_t in the k-ε turbulence model is modelled by calculating k and ε and is defined by Equation 4.10.

$$\mu_t=\rho C_\mu\frac{k^2}{\varepsilon} \tag{4.10}$$

where:
C_μ is a constant.

The turbulence constant values for the calculation of the k-ε turbulence model equations are given below as suggested by Launder and Spalding (1974):

$$C_{1\varepsilon}=1.44\quad C_{2\varepsilon}=1.92\quad C_\mu=0.09\quad \sigma_k=1.0\quad \sigma_\varepsilon=1.3$$

The above values for the k-ε turbulence model constants were also suggested by Richards and Hoxey (1993) for numerical modelling of wind flow while using their suggested logarithmic inlet conditions (as described in Chapter 3). All of these constants were used in this work with the exception of $\sigma_\varepsilon = 1.11$ which was the suggested value by Hargreaves and Wright (2007) for more accurate modelling of neutral ABL conditions in FLUENT in combination with the R&H approach.

The generation of turbulence kinetic energy due to the mean velocity gradients is defined by Equation 4.11 for the standard *k*-*ε* turbulence model.

$$G_k = -\rho \overline{u_i' u_j'} \frac{\partial \overline{u_j}}{\partial x_i} \tag{4.11}$$

And when following the Boussinesq hypothesis:

$$G_k = \mu_t {S_M}^2 \tag{4.12a}$$

$$\text{where: } S_M \equiv \sqrt{2 S_{ij} S_{ij}} \tag{4.12b}$$

where:
S_M is the modulus of the mean rate of strain tensor.

4.3.3 Particle Tracking

Lagrangian particle tracking is used to model particle's motion in numerical domains examined: both idealised and real. Trajectories of discrete phase particles can be predicted by integrating the force balance on each particle. The force balance is calculated for a Lagrangian reference frame and is equal to the particle inertia including forces acting on the particle. The mathematical representation of particle force balance is given by Equation 4.13a and is described by the equations of motion for a small rigid particle first derived by Maxey and Riley (1983).

$$\frac{du_p}{dt} = F_D(\overline{u} - u_p) + \frac{g(\rho_p - \rho)}{\rho_p} + F_x \tag{4.13a}$$

$$F_D = \frac{18\mu}{\rho_p d_p^2} \frac{c_d Re}{24} \tag{4.13b}$$

$$F_x = \frac{1}{2} \frac{\rho}{\rho_p} \frac{d}{dt} (\overline{u} - u_p) \tag{4.13c}$$

$$F_x = \left(\frac{\rho}{\rho_p}\right) u_{pi} \frac{\partial \overline{u}}{\partial x_i} \tag{4.13d}$$

where:
u_p is particle velocity.
$F_D(\overline{u} - u_p)$ is drag force per unit particle mass.
g is gravitational acceleration.
ρ_p is density of the particle.

ρ is fluid density.
d_p is particle diameter.
F_x is an additional acceleration force.
μ is molecular viscosity of the fluid.
c_d is the drag coefficient.
Re is the Reynolds number.

The drag force F_D included in the particle force balance equation is described by Equation 4.13b and depends on the molecular viscosity of the fluid, the density and diameter of the particle, the drag coefficient and the Reynolds number. Additional forces F_x can also be included in the original Equation 4.13a; these are necessary to be taken under consideration when modelling acceleration of the surrounding fluid because of the particle (Equation 4.13c) and when the particle density is lower than the fluid density ($\rho_p < \rho$) which causes an additional force due to the pressure gradient in the fluid (Equation 4.13d). Further description on all forces and variables in equations of motion for particles and their influence can be found in Abo El-Azm (2008).

The simplified version of Equation 4.13a employed for particle tracking in this work is presented below by Equation 4.14. Pollutant particles released from sources in both idealised and real domain simulations are considered to have identical characteristics (mass, diameter etc.) to the air particles used for wind flow – these particles were called ‘mass-less’ in this work.

$$\frac{du_p}{dt} = F_D\left(\overline{u} - u_p\right) \tag{4.14}$$

4.3.4 Stochastic Particle Tracking

For turbulent flow fields in the open environment, particle dispersion is modelled using the stochastic tracking model. Particle trajectories can be calculated by solving the trajectory Equation 4.14a for the mean fluid phase velocity.

The stochastic particle tracking approach, described by Baxter and Smith (1993), predicts dispersion under turbulent flow conditions by integrating the trajectory equation using the instantaneous velocity, $\bar{u} + u_p{}'(t)$ along the particle path. Random turbulence effects on particles are represented by setting an adequate number of particles to display (also known as number of tries). A stochastic method, the Discrete Random Walk Model (DRW) is employed to calculate the instantaneous gas velocity; this 'random' velocity is kept constant during the lifetime of the turbulent eddies. The DRW is characterised by: a Gaussian distributed random velocity fluctuation for values, u', v' and w' which are calculated based on the Gaussian probability distribution described by Equation 4.15a; and by the characteristic lifetime of an eddy τ_e which is defined in Equation 4.16a [Fluent 6.3 User's Guide, 2006].

$$u' = \zeta\sqrt{\overline{u'^2}} \tag{4.15a}$$

$$\text{where: } \sqrt{\overline{u'^2}} = \sqrt{\overline{v'^2}} = \sqrt{\overline{w'^2}} = \sqrt{2k/3} \tag{4.15b}$$

$$\tau_e = 2T_L \tag{4.16a}$$

$$\text{where: } T_L \approx 0.15\frac{k}{\varepsilon} \tag{4.16b}$$

where:
ζ is a normally distributed random number.
$\sqrt{\overline{u'^2}}, \sqrt{\overline{v'^2}}, \sqrt{\overline{w'^2}}$ are local RMS values of the velocity fluctuations.
T_L is the Lagrangian integral time.

4.3.5 Species Transport

In addition to Lagrangian particle tracking, pollution dispersion was also modelled using the species transport approach by calculating convection–diffusion as described by Equation 4.17. This equation is solved for *N-1* species where *N* is the total number of species in the fluid flow. The sum of the mass fractions of all species must be equal to unity; this *Nth* mass fraction is given from the sum of the *N-1* solved mass fractions [Fluent 6.3 User's Guide, 2006].

Analytical description of all equations for a mixture and the Lagrangian derivative of the mass fraction along a streamline of a particle can be found in Nicolleau (2009).

$$\frac{\partial}{\partial t}\left(\rho Y_q\right) + \nabla\cdot\left(\rho\vec{u}Y_q\right) = -\nabla\cdot J_q + R_q + S_q \tag{4.17}$$

where:
Y_q is the mass fraction of species q.
∇ is the nabla symbol used hereafter for shorter equations - see nomenclature for definition of the nabla symbol.
J_q is the diffusion flux of species q.
R_q is the net rate of production of species q.
S_q is the rate of creation by addition from the dispersed phase plus any user-defined sources.

For turbulent flows, the diffusion flux J_q is calculated using Equation 4.18a with a default Schmidt number of 0.7 in FLUENT [Fluent 6.3 User's Guide, 2006].

$$J_q = -\left(\rho D_{q,m} + \frac{\mu_t}{\mathrm{Sc_t}}\right) \nabla Y_q \tag{4.18a}$$

$$\text{where: } \mathrm{Sc_t} = \frac{\mu}{\rho D_{q,m}} \tag{4.18b}$$

where:
$D_{q,m}$ is the diffusion coefficient for species q in the mixture.
$\mathrm{Sc_t}$ is the turbulent Schmidt number (ratio of momentum and mass diffusivity).

4.3.6 Energy Equation

In case the fluid flow is non-isothermal, the energy equation has to be adopted to account for thermal effects; such is defined by Equation 4.19a. Terms on the right-hand side correspond to the energy transfer due to conduction, species diffusion and viscous dissipation respectively. Finally, S_h accounts for heat generated from chemical reactions or any other used-defined sources. While using the species transport equation (Equation 4.17), the energy equation (Equation 4.19a) is used to account for enthalpy transport because of species diffusion. In FLUENT, such term cannot be neglected and therefore is included in all species transport calculations by default [Fluent 6.3 User's Guide, 2006].

$$\frac{\partial}{\partial t}(\rho E) + \nabla \cdot \left(\vec{u}(\rho E + p)\right) = \nabla \cdot \left(k_{eff} \nabla \mathrm{T} - \sum_{\mathrm{i}} \mathrm{h_i} \vec{J_\iota} + (\overline{\overline{\tau_{\mathrm{eff}}}} \cdot \vec{u})\right) + S_h \tag{4.19a}$$

$$\text{where: } E = h - \frac{p}{\rho} + \frac{u^2}{2} \tag{4.19b}$$

$$\text{with enthalpy for an ideal gas: } h = \sum_i Y_i \, h_i \tag{4.19c}$$

$$\text{and enthalpy for an incompressible flow: } h = \sum_i Y_i \, e + \frac{p}{\rho} \tag{4.19d}$$

where:
E is specific total energy.
k_{eff} is effective thermal conductivity.
τ_{eff} is effective shear stress.
e is internal energy.

4.4 Boundary Conditions

Correct boundary conditions are necessary for an accurate solution of the wind flow problem. Wind flow has to be modelled as accurately as possible since effluent pollution dispersion modelling depends on it. The choice of boundary conditions has to be made based on which condition (available in the program used) better represents the actual physical phenomena of the simulated flow. Hence, during the initial planning stages of the simulation approach, many difficulties arise to convert the environmental wind phenomena into variable profiles of $\overline{u}$, k and ε and later specify these as boundary condition types and quantities. Literature review for the case of wind flow simulation using CFD programs has shown that authors adapt suitable boundary conditions primarily to the problem they try to model and secondarily to the different types of boundaries available in the program utilised.

Table 14 summarizes commonly used boundary conditions for open environment wind flows by several authors and research groups (in chronological order). Most of these authors have used the inlet conditions specified by Richards and Hoxey (1993). In some cases experimentally obtained values and profiles for mean velocity $\overline{u}$ (use of power law) were specified together with R&H logarithmic profiles for *k* and *ε*.

		Boundary Conditions				
Author (Year)	**CFD Program**	**Inlet Condition**	**Top (Sky) Condition**	**Bottom Condition**	**Side Condition**	**Outlet Condition**
Richards and Hoxey (1993)	Phoenix	R&H logarithmic profiles	Constant shear stress	Wall with standard wall function	- (2D)	Pressure outlet
Meroney et al. (1999)	Fluent	Experimental data	Symmetry	Non-slip wall	Symmetry	Outflow
Parker and Kinnersley (2004)	Fluent	Power law for *u*, R&H for *k* and *ε*	Symmetry	Non-slip wall (standard wall function)	Non-slip wall	Outflow
Hu and Wand (2005)	Phoenix	Power law for *u*, R&H for *k* and *ε*	Free slip	Smooth wall with log law function	Symmetry	Pressure outlet
Xie et al. (2006)	Phoenix	Experimental data	Pressure outlet	Wall	Symmetry	Pressure outlet
Blocken et al. (2007a)	Fluent	Experimental data	Slip wall	Non-slip wall (standard wall function)	Slip wall	Pressure outlet
Hargreaves and Wright (2007)	Fluent	R&H logarithmic profiles	Symmetry	Wall with surface roughness	Symmetry	Pressure outlet
Gromke et al. (2008)	Fluent	Experimental data	Symmetry	Wall with surface roughness	Symmetry	Outflow

Table 14 : Commonly used boundary conditions for simulating open wind flows.

For the top boundary (the most difficult to represent numerically) some authors choose the symmetry type when using FLUENT or the pressure outlet condition when using PHOENIX. Symmetry is considered as the most common boundary type for the sides of 3D domains, except for those simulations that replicate wind tunnel flow for which a no-slip wall is required. When it comes to the bottom boundary representing the ground, all authors use a wall type boundary with appropriate surface roughness values for the type of terrain they are trying to simulate. Outlet boundary conditions differ according to the application of modelling; to compare CFD results with experimental data, an outflow or a pressure outlet is mostly used.

Consequently, reviewing Table 14, literature review and after examining the capabilities of FLUENT in simulating a neutral ABL over a flat plane (later described), it was decided that the boundary conditions mentioned in Table 15, would apply to all domains for CFD simulations in this work. This choice was also supported by the absence of full scale or wind tunnel data. Thus, the logarithmic profiles according to the R&H approach are the best way to represent a neutral ABL flow at the inlet of the domain.

Boundary	**Condition Type in FLUENT**
Inlet	R&H logarithmic profiles for $\overline{u}$, k and ε
Top	Symmetry
Sides (3D)	Symmetry
Bottom	Wall with specified surface roughness
Outlet	Pressure outlet

Table 15 : Boundary conditions chosen for CFD simulations herein.

4.4.1 Inlet Boundary

The inlet boundary is specified as velocity inlet. This is the most appropriate boundary condition for defining the velocity magnitude and other relevant scalar properties. The default velocity direction was set to be normal to the boundary and further specified by a user defined profile.

The logarithmic equations describing the mean velocity, turbulence kinetic energy and dissipation rate according to Richards and Hoxey (1993) were defined at the inlet with the use of a UDF (User Defined Function) in FLUENT. Three mean inlet velocities were selected for inlet conditions; thus, resulting to three different logarithmic ABL inlet conditions for 2, 5 and 10ms^{-1} all at a reference height of 6m with a von Karman constant $\kappa = 0.4$ and a surface roughness height z_0=0.1m (for grass land). As an example, inlet profiles defined for mean velocity 5ms^{-1} at a reference height of 6m are presented in Figure 20.

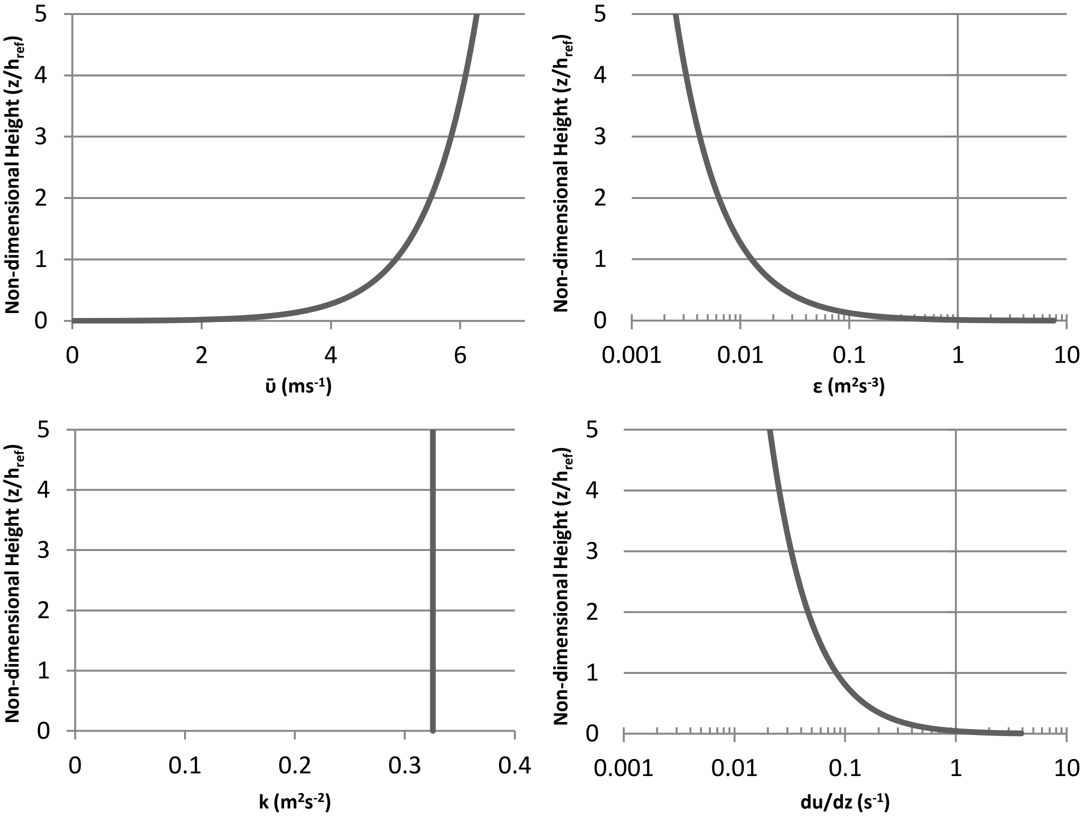

Figure 20 : Inlet profile of wind speed $\overline{u}$, turbulent kinetic energy k, dissipation rate ε and du/dz for up to non-dimensional height 5z_{ref} for neutral ABL profile with $\overline{u}$=5ms^{-1} at reference height 6m.

4.4.2 Top and Side Boundaries

Top and side boundaries (for 3D simulations) are set as symmetry boundaries for simplicity, processing and time saving after considering work of other authors (see Table 14). However, their most important characteristic was that they can act as zero shear slip walls.

4.4.3 Ground, House and Obstacle Boundaries

Regarding the ground and other important characteristics within the computational domain that would influence the flow, the boundary type selected was the wall boundary. By default, the standard wall function is enabled for all wall boundaries which for the mean wind velocity at the wall, relents to Equation 4.20a.

$$\bar{u} = \frac{1}{\kappa}\ln\left(C_w y^*\right) \tag{4.20a}$$

with: $$\bar{u} = \frac{\bar{u}_p C_\mu{}^{1/4}\ k_p{}^{1/2}}{\tau_w/\rho} \tag{4.20b}$$

and: $$y^* = \frac{\rho C_\mu{}^{1/4}\ k_p{}^{1/2}\ y_p}{\mu} \tag{4.20c}$$

where:
C_w is empirical wall constant (=9.793).
$\bar{u}_p$ is mean wind velocity at point P.
k_p is turbulent kinetic energy at point P.
y_p is distance from point P to the wall.
μ is dynamic viscosity of the air.

Further to the standard wall function in FLUENT, there is also an option for specification of surface roughness height K_s , and roughness constant C_s, for turbulent flows. This allows the representation of the type of surface modelled (refer to Table 11 for typical values). For all simulations herein the surface roughness height was set to $K_s \ = 0.2m$ and the roughness constant was left to the default value of $C_s = 0.5$. The specified value of $K_s \ = 0.2m$ was calculated after selecting a surface roughness height of 0.01m for a grass land (based on the case study later examined) and multiplying it by 20, as suggested by Hargreaves and Wright (2007) for correct representation of open environment roughness in FLUENT.

While simulating particle tracking, walls and other wall-type boundaries are set to absorb particles on collision. This was decided as bioaerosol particles are small enough (only a few microns in some cases) to get stuck to any obstacles with which they would collide with. Although, the biological behaviour of particles is not studied or modelled here, it was assumed that bioaerosol particles would die a short while after getting stuck to any surface. Consequently, even if released again these would be inactive and not considered dangerous; thus there was no reason for reflection or delayed re-release from any wall boundaries (ground, houses and trees).

4.4.4 Outlet Boundary

The outlet boundary was set as pressure outlet with zero gauge pressure allowing for a smaller domain in size for saving processing time and power required. Such boundary condition minimizes convergence difficulties by defining realistic turbulence conditions (profiles for k and ε) and any occurring backflow is assumed normal to the outlet face [Fluent 6.3 User's Guide, 2006]. All other quantities at the pressure outlet boundary are extrapolated from the interior of the domain.

4.5 Ideal Geometry and Domain Selection

Following approaches of other authors [Carpenter and Locke, 1999; Castro et al., 1988; Kim et al., 2001; Parker and Kinnersley, 2004], two sinusoidal hills were considered in this paper for all idealised terrain CFD simulations: a steep hill and a swallow hill. Both hills were symmetric around their vertical axis and their geometry was characterised by the function of a sinusoidal wave (Equation 4.21) with the amplitude A_{mp} defining the height *H* of the hill and *K* the wave number (Figure 21).

$$y(t) = A_{mp} \cdot \sin{(Kx)} \tag{4.21}$$

where:
A_{mp} is amplitude.
K is the wave number.

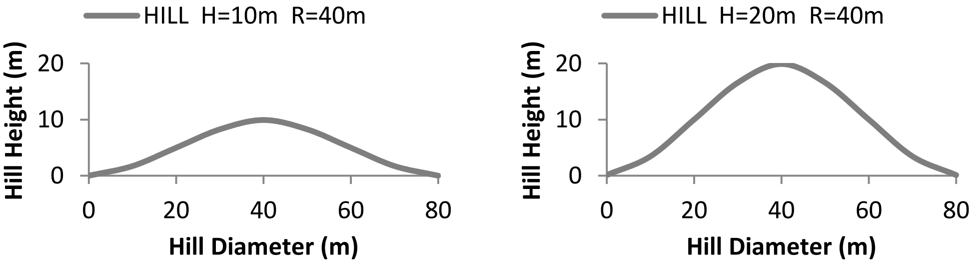

Figure 21 : Dimensions of shallow and steep sinusoidal hills used for idealised 2D and 3D simulations.

Following the specification of boundary conditions and hill geometry, the domain size was defined. For 2D simulations, the domain size choice was straight forward by specifying upwind and downwind distances to make sure that all wind phenomena will be visible and no interaction with the top boundary will occur.

For 3D simulations, in order to simplify simulations and reduce processing time and power required, only half the hill was simulated with the use of a symmetrical domain (Figure 22). This domain was reflected later during post-processing to display mirrored results for a full hill. Simulating half the domain is a significant assumption; wind flow phenomena or effluent pollutant dispersion would never be symmetrically similar around a hill. On the other hand, a perfectly axisymmetric hill does not exist in the environment – so there is no need for correct replication of terrain in this case. The geometry of the domain should be fully modelled if required later for unsteady simulations or for other simulating techniques-approaches.

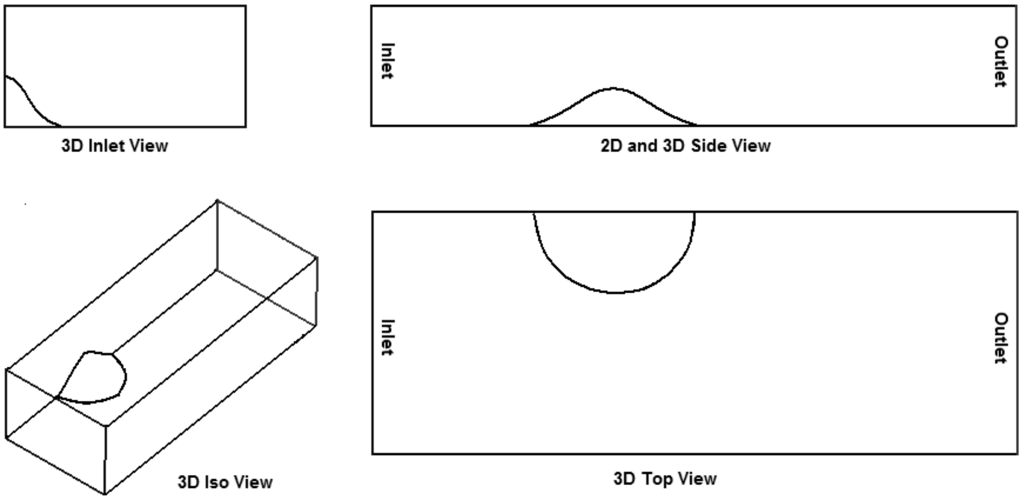

Figure 22 : Schematic diagram of 2D and 3D examined domains.

In order to simulate wind flow and later particle dispersion around an idealised hill, a domain size study for both 2D and 3D domains had to be undertaken. This helped towards defining minimum distances of the domain boundaries to the hill (or multiple hills) examined. All boundaries should be far enough from the hill so that they do not interfere with fluid flow. Also, using the smallest possible domain helps decrease processing time and power required.

Similarly, simulations for a number of combinations of domain dimensions were run. A file-naming system that helped identify the domain size was adopted. The boundary lengths from the hill were defined in multiples of the hill height for the top boundary and hill radius for the front, side and behind boundaries. An example of a domain size simulated is: F2-S2-A2-B4 where F refers to the distance in front of the hill, S to the side of the hill (equal to zero for 2D domains), A to above the hill and finally B to the distance behind the hill. Further description regarding geometry of hills is given in relevant parts in Chapter 5.

In order to merely examine and compare effects of domain size, all mesh intervals, boundary conditions and solver details were kept exactly the same for all domains. Logarithmic ABL profiles [Richards and Hoxey, 1993] for $\overline{u}$, k and ε were specified at the inlet of all domains for mean velocities of 2ms^{-1}, 5ms^{-1} and 10ms^{-1} at a reference height of 6m. These wind speeds were selected as representative values of calm, medium and windy conditions respectively in South Yorkshire, UK (based on meteorological data from the weather station at the Weston Park Museum in Sheffield for the year 2006 - analysis of weather data is available in Chapter 6).

Chapter 5

CFD SIMULATION OF IDEALISED TERRAIN

5.1 Introduction

Pollard et al. (2004) made the assumption of a flat terrain for slopes less than 1:10 when modelling environmental flows for risk assessment. This criterion was thereafter adopted by the EA for including ground morphology characteristics in numerical modelling. However, it is unclear what the limitations of this criterion are and when terrain topography should not be considered flat but hilly. Fluid flow phenomena and recirculation zones behind hills are known to greatly affect pollutant spread and concentrations as discussed later. Work in this chapter tries to answer these questions by examining wind flow and effluent pollution dispersion over idealised hills with variable slopes.

Firstly and before studying wind flow and pollution dispersion over hilly terrain, a good understanding of neutral ABL flow on a flat plane needs to be established. For this purpose, neutral ABL conditions are simulated over a flat domain. Difficulties related to program limitations on sustaining a neutral ABL with constant velocity and turbulence parameter profiles are raised during these simulations together with suggestions on how to maintain these profiles.

Preliminary CFD simulations of wind flow over a two-dimensional axisymmetric hill follow by examining necessary domain size, mesh density and turbulence parameters. Both particle tracking and species transport techniques are utilised for the study of pollutant dispersion from a source upstream of the 2D hill. Differences occur between 2D and 3D approaches and there is a need to examine and later discuss 3D simulations.

Finally, results from three-dimensional simulations of wind flow and pollution dispersion over axisymmetric hills (single and multiple hills) are presented accompanied by relevant studies for domain size, mesh independence and boundary positions. The effects of wind speed variation and hilly terrain are investigated and compared, showing the relation of effluent pollution dispersion to topography, important local characteristics such as trees and houses and weather conditions which could greatly influence pollutant spread and concentration.

5.2 Simulation of Neutral ABL on Flat Plane

As a starting point, a 3D domain as described by Hargreaves and Wright (2007) was created and simulated in commercial CFD code FLUENT in order to replicate results of neutral ABL on a horizontal flat plane. For that reason, the Richards and Hoxey (1993) approach was used with the suggested logarithmic ABL profiles for mean velocity magnitude $\overline{u}$, turbulent kinetic energy k and dissipation rate ε as previously described in Chapter 3. For both domain size and boundary conditions, the same parameters as used by Hargreaves and Wright (2007) were adopted: the domain size was 100m x 500m x 5000m; the top (sky) boundary was set as symmetry and so were the two side faces; inlet was set as velocity inlet in order to specify custom profiles for $\overline{u}$, k and ε and outlet as pressure outlet (Figure 23). The mean velocity of $\overline{u}_{\text{inlet}}$=10ms^{-1} at a reference height h_{ref}=6m was used; for the wall (ground) roughness a value of twenty times the surface roughness was set (0.2m). For closure of the RANS equations, the standard k-ε turbulence model with standard wall function treatment was enabled. Simulations were run using double precision to minimise round-of errors and second order spatial discretization to reduce truncation errors as suggested by ERCOFTAC CFD BPG (2000).

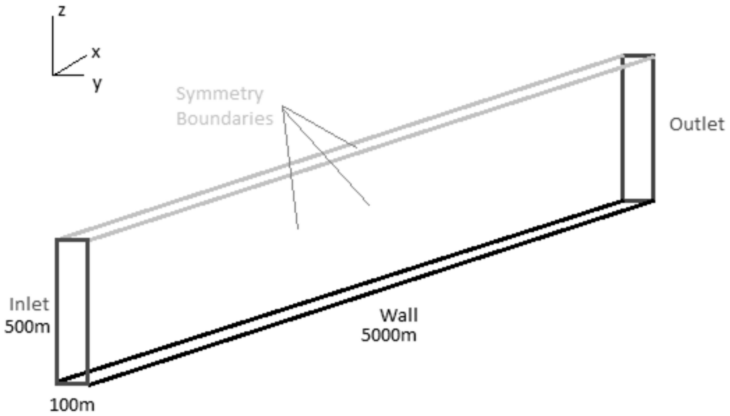

Figure 23 : 3D Domain and boundary conditions used for simulating neutral ABL on flat plane.

Results from the Hargreaves and Wright (2007) replication simulation showed that with the simple and straight forward choice of the standard k-ε turbulence model and standard wall function, constant ABL profiles can be maintained for the limited length of approximately 1500m – results are shown in Figure 24. After this length, the velocity profile started changing and the values of k and ε dropped and increased respectively. Turbulent kinetic energy k showed a decrease of 80%, an under-prediction that would definitely affect wind flow phenomena. To further maintain an ABL with constant variables, a different selection of top boundary type and wall function was necessary, as suggested by Hargreaves and Wright (2007) and Yang et al. (2009). However, the capability to simulate a neutral ABL on a commercial CFD software like FLUENT with constant characteristics is important. The application of user defined functions, custom wall treatments and modified turbulence models would be time intense and resource demanding – nevertheless their value towards increased accuracy should not be neglected. Consequently, the present author decided to further look into achieving a constant ABL simulation with the standard turbulence model, wall function and parameters already available in FLUENT.

For this purpose, two further cases were simulated with the same dimensional and numerical characteristics but with higher placement of the top (sky) boundary at 1000 and 1500m. Results showed an almost linear relationship between domain length and height to maintain constant ABL parameters and these data are given in Figure 25 and Figure 26 for the two sky heights respectively. Profile plots for these simulations show that mean ABL flow variables remain constant in the vertical direction; the domain with height 1000m has constant and overlapping (or very similar) profiles for up to 3000m; the domain with height 1500m keeps vertical profiles constant up to 4000m downwind.

Figure 27 shows comparison of turbulent kinetic energy along the domain length for different heights above ground. Downstream profiles of k values were chosen for comparison purposes as these were most affected by the domain height change. Profiles for $\overline{u}$ and ε showed minor changes that could be neglected. All profiles were seen to remain almost constant for distances up to 4000m downwind for the domain with the highest sky boundary: DH=1500m. It is clearly seen that the higher the top boundary of the domain is, the longer the values of k are retained downwind. Consequently, it was concluded that for simulating a neutral ABL over an ideal flat plane with a required domain length L_{req}, the minimum simulated domain height H_{req} should be at least one third of the domain length (Equation 5.1).

$$H_{req} = 1/3\, L_{req} \tag{5.1}$$

where:
H_{req} is required height of the domain simulated.
L_{req} is required length of the domain simulated.

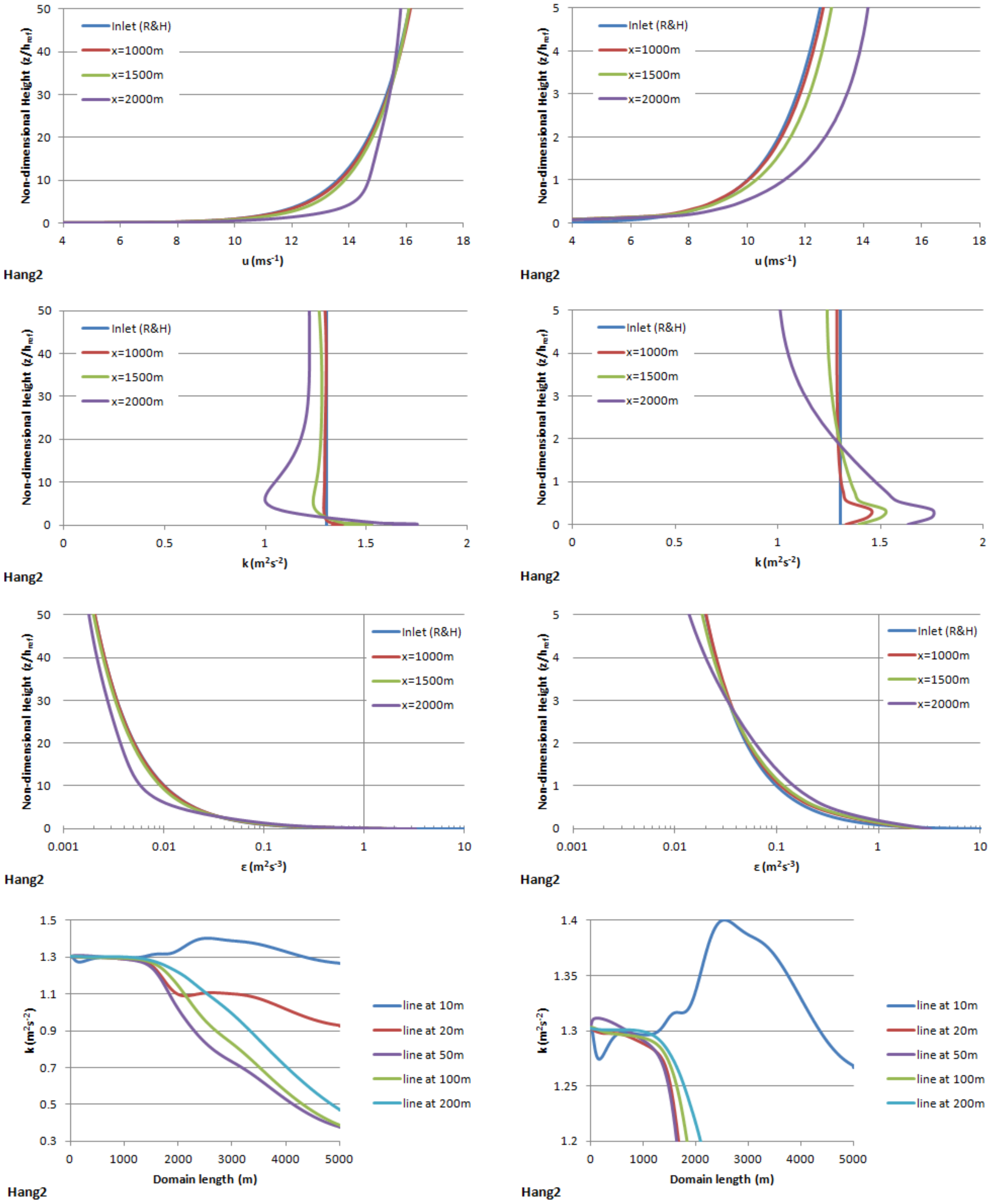

Figure 24 : Profiles of velocity magnitude $\overline{u}$, turbulent kinetic energy k and dissipation rate ε for up to non-dimensional heights of $50z_{ref}$ and $5z_{ref}$ and turbulent kinetic energy k along domain length for simulation with domain height DH=500m.

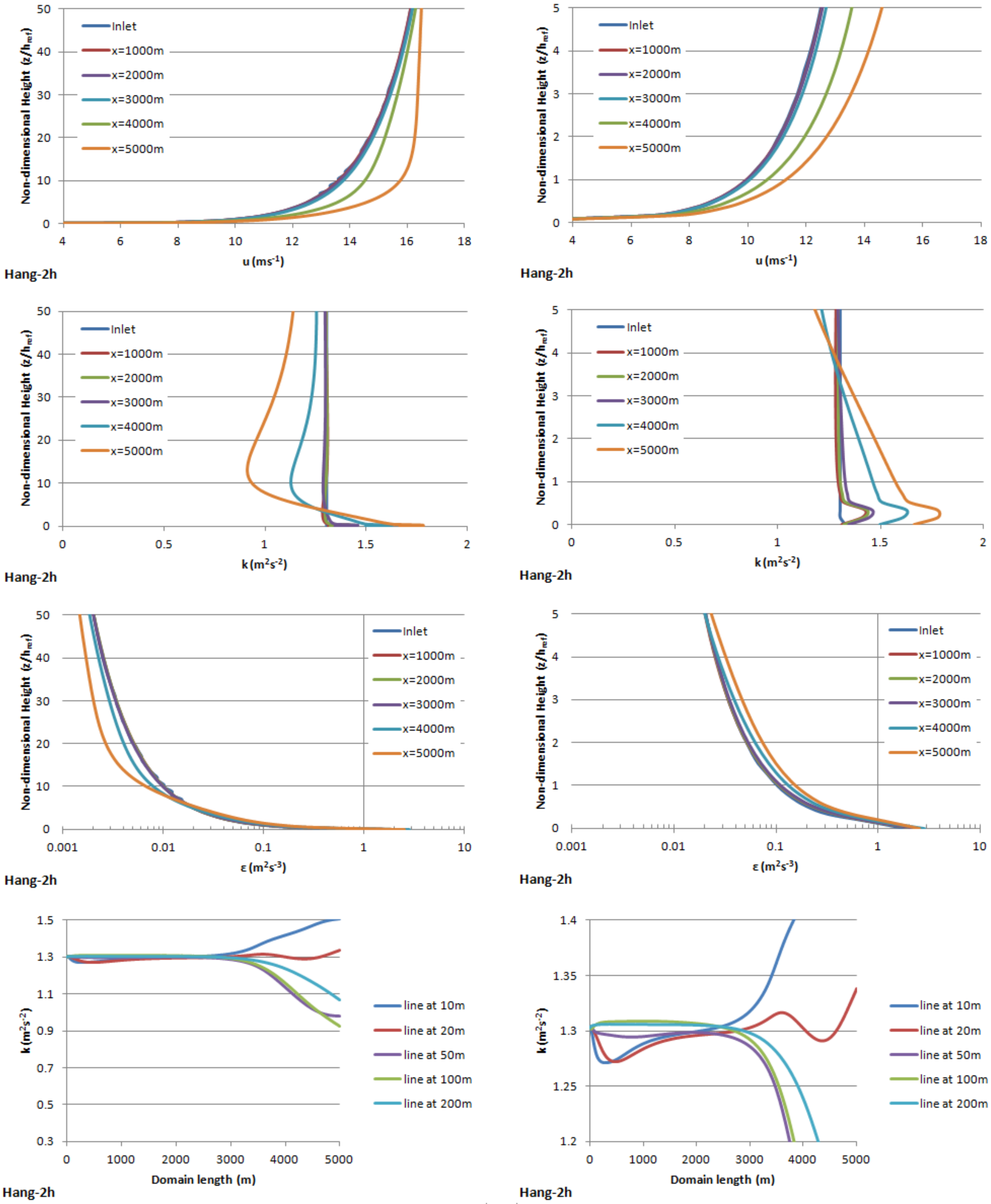

Hang-2h

Hang-2h

Hang-2h

Hang-2h

Hang-2h

Hang-2h

Hang-2h

Hang-2h

Figure 25 : Profiles of velocity magnitude $\overline{u}$, turbulent kinetic energy k and dissipation rate ε for up to non-dimensional heights of 50z_{ref} and 5z_{ref} and turbulent kinetic energy k along domain length for simulation with domain height DH=1000m.

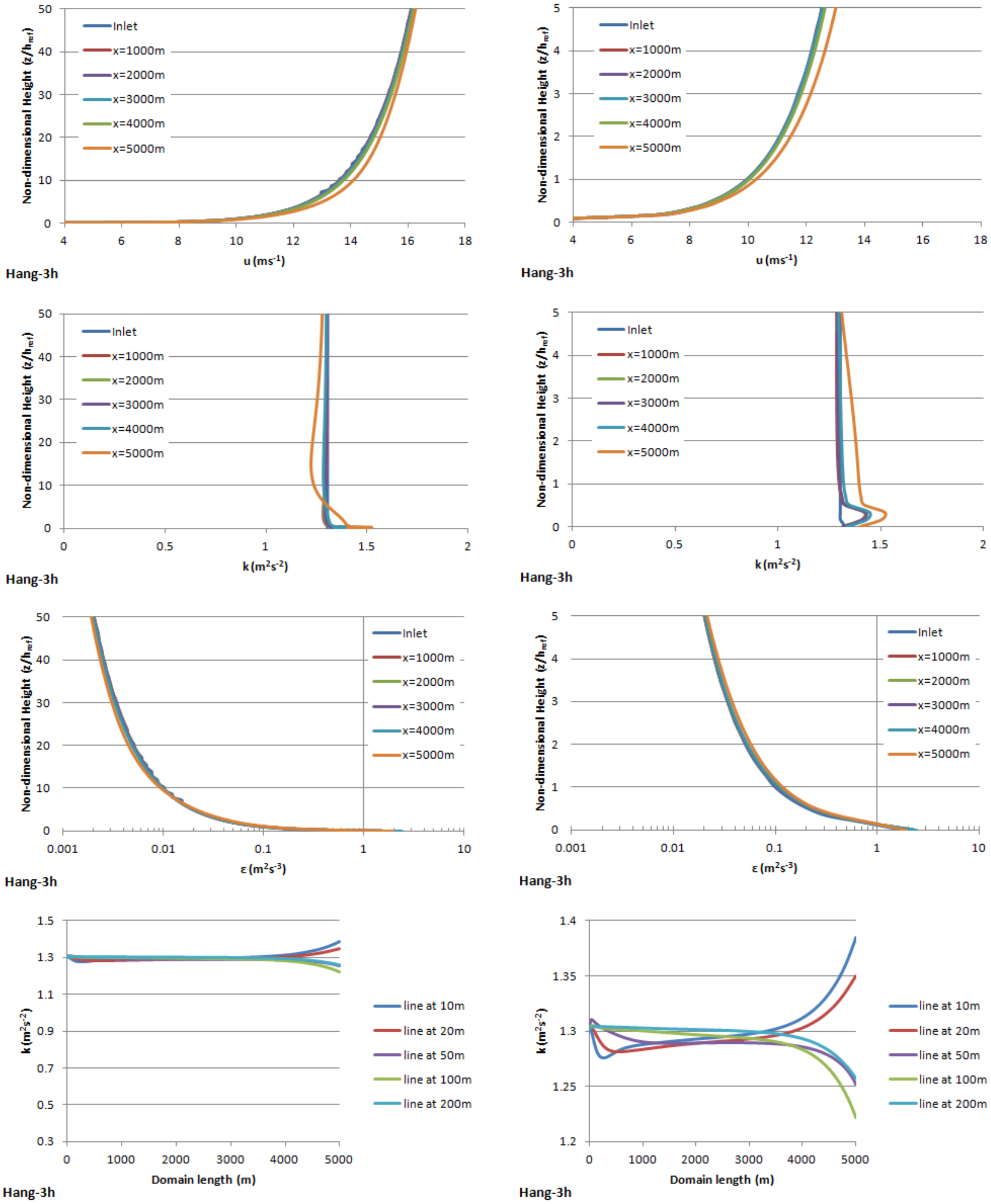

Figure 26 : Profiles of velocity magnitude $\overline{u}$, turbulent kinetic energy k and dissipation rate ε for up to non-dimensional heights of $50z_{ref}$ and $5z_{ref}$ and turbulent kinetic energy k along domain length for simulation with domain height DH=1500m.

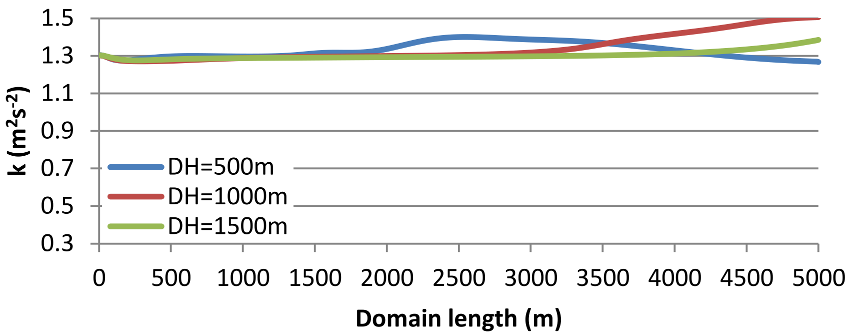

(a) Comparison Plot at height = 10m

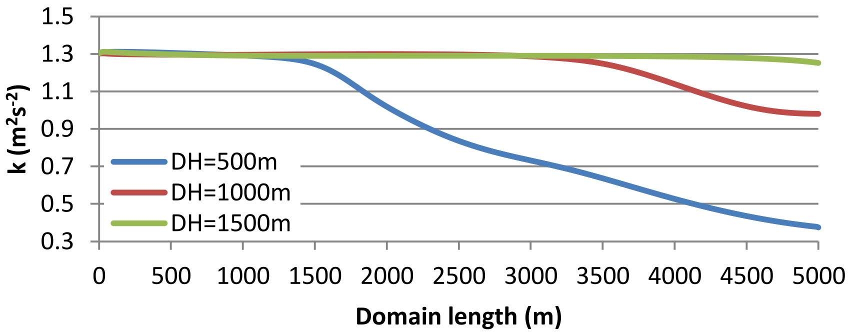

(b) Comparison Plot at height = 50m

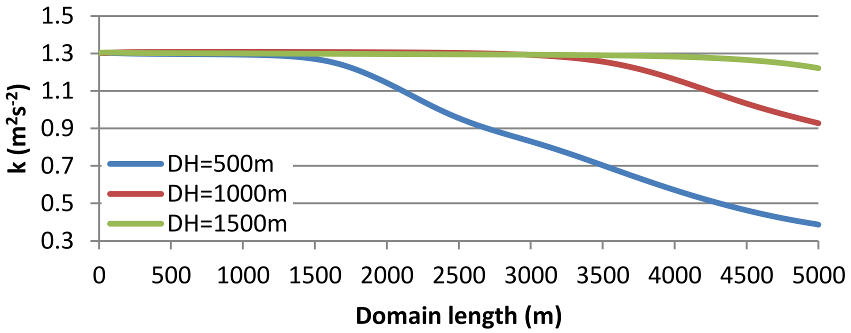

(c) Comparison Plot at height = 100m

Figure 27 : Comparison of turbulent kinetic energy k at height of (a) 10m, (b) 50m and (c) 100m above ground along domain length for flat plane simulations with different domain heights.

In real atmospheric flows there is no top boundary; variables and characteristics of the flow and the ABL profile change with height as described earlier in Chapter 3. However, in numerical simulations the definition of a control volume in which the flow will be studied is necessary. For a domain with symmetry condition for the top (sky) boundary the simulation is treated as if it was a channel flow – simulating half the channel.

During the iteration procedure, FLUENT develops the defined inlet profiles for $\overline{u}$, k and ε; this is achieved by a developing boundary layer within the flow field in the horizontal x-direction. When that boundary layer reaches the top of the domain it mixes with the symmetrically ‘assumed’ boundary layer from the other half. The higher the top boundary of the domain is, the longer it takes for the boundary layer to reach it, thus the longer the ABL characteristics can remain constant.

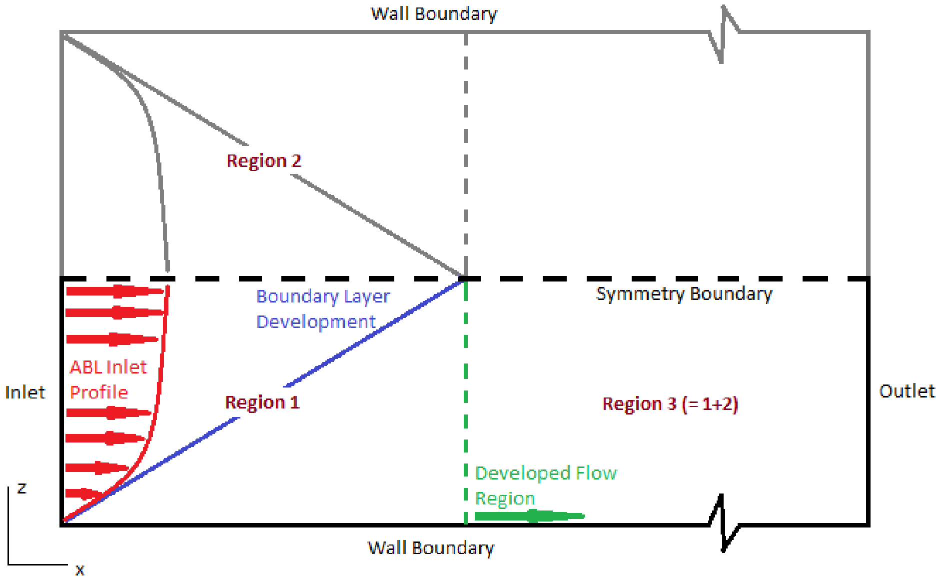

Figure 28 : Schematic of a typical simulated domain of a flat plane with symmetry conditions for the top boundary showing different flow regions.

All three regions of the flow are shown in Figure 28. Region 1 is the working and ‘useful’ part of the studied domain. For the full length of this region the ABL profiles for mean velocity magnitude u, turbulent kinetic energy k and dissipation rate ε stay constant; the exact same takes place in the symmetrical Region 2. At the end of Regions 1 and 2, the flow phenomena from both these regions meet and mix creating the new Region 3. In Region 3, the profile for mean velocity magnitude $\overline{u}$ develops, turbulent kinetic energy k decreases and dissipation rate ε increases. This leads to an ABL with developed characteristics (altered variable values) and much lower turbulent kinetic energy values than necessary for a neutral stability condition, mainly affecting wind flow mixing and as shown later pollution dispersion. This is also the conclusion by Gorle et al. (2009) who have studied the influence of turbulent kinetic energy to the concentration of 1μm particles; they have shown that a decrease of 40% for k would lead to an increase of the maximum concentration value by 90%.

Thus, when numerically modelling environmental flows and using neutral ABL profile parameters the appropriate location of the top (sky) boundary of the domain must be chosen. It was shown that when using the standard k-ε turbulence model with standard wall function a constant ABL can be achieved but only when choosing an appropriate height for the computational domain. For the case of commercial CFD software FLUENT this is approximately three times the length of the examined (modelled) area.

An additional problem arises with the selected settings in FLUENT for simulating environmental wind flow: the standard wall function on ground and hill edges gives highly irregular values (sudden jump in values) for the first cell near the ground. This is clearly illustrated in vertical profile plots for turbulence kinetic energy k for neutral ABL flow over flat plane (Figure 25, Figure 26 and Figure 27).

In order to gauge the quality of the grid, the function of y^+ is used in FLUENT with recommended values within the range of 30 to 100 [Fluent User's Guide, 2006]. When values of y^+ are higher than 100, the height of the first cell at the ground has to be decreased; on the other hand when values of y^+ are low, the height of the first cell can be increased. This ensures good prediction of turbulence parameters close to the wall where the flow is not fully turbulent.

Previous authors [Hargreaves and Wright, 2007; Yang et al., 2009] have noticed the difficulty of getting y^+ within the required range thus the need for custom wall functions. When such solution is not possible, due to time or resources limitation, the use of a very small (in height) first cell at the ground is suggested; this was the approach followed in this work. This minimises the effects of the wall to the flow and makes the irregularity in variables smaller.

5.3 Wind Flow and Pollution Dispersion over Single 2D Hill

5.3.1 Introduction

After modelling neutral ABL flow on a flat plane and before moving to 3D simulations of wind flow and pollution dispersion over hills, a procedure has to be established regarding boundary positions, mesh density, numerical solver, dispersion models, etc. Such studies would be time consuming and CPU power hungry if applied to 3D simulations, thus 2D simulations are first employed to start examining the problem of wind flow and air pollution dispersion over hilly terrain.

The problem of wind flow and particle dispersion over a single sinusoidal 2D hill has been previously studied by Viz (2011). His results showed that an ABL logarithmic profile should be used to minimise the upwind domain length and processing time and power required; a uniform inlet profile would require a certain distance to get developed before reaching the examined hill/s. For these simulations, wind flow was considered steady, incompressible and isothermal with boundary conditions as for the flat terrain described and modelled earlier. A steep hill was included in these simulations with dimensions of H=20m and D=40m. Logarithmic ABL profiles with mean velocities of 3, 5 and 10ms^{-1} at a reference height of 6m were specified at the inlet. Particles were released from a 3m tall vertical line source, 100m upwind the centre of the hill and were examined by employing the Particle Tracking technique in FLUENT with the Random Walk Model. This approach used the one-way coupling technique with particles influenced by the wind flow but not vice versa as particles were considered 'mass-less'. (For information on flow-particle coupling techniques see Fluent 6.3 User's Guide, 2006). Ground and hill boundaries were set to trap all particles on contact. Results for particle average distance travelled are presented in Figure 29 for all three examined ABL logarithmic inlet profiles.

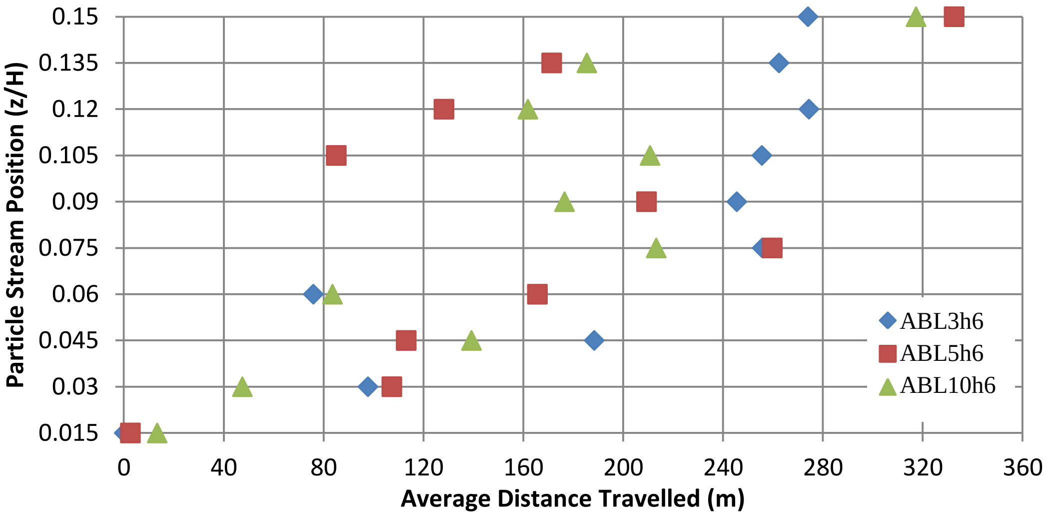

Figure 29 : Average distances travelled for particulates released from a 3m vertical line source 100m upwind 2D sinusoidal hill for three neutral ABL logarithmic inlet profiles [Data from Viz, 2011].

For neutral ABL inlet conditions of 3ms^{-1} particles were seen to travel further than of 5ms^{-1} and 10ms^{-1}. However, an inconsistency was noted for particles released from the middle of the vertical source (positions 0.105, 0.12 and 0.135) for a wind flow of 5ms^{-1}; these travelled shorter distances than those of a mean velocity for 10ms^{-1}. Such irregularity is probably due to the stochastic nature of the Random Walk Model combined with the numerical error and requires further examination [Viz, 2011].

5.3.2 Domain Size Study

A 2D domain size study was conducted for several domains (Table 16). The boundary location upstream, downstream and above a single 2D hill was varied so as to establish boundary positions which would not influence the fluid flow phenomena over the hill. All solver settings were similar to those used for wind flow over a flat plane and according to Hargreaves and Wright (2007). Logarithmic profiles for mean velocity of 10ms^{-1} at a reference height of 6m and a structured grid (square cells 1x1m throughout) were used for all domains.

Figure 30 shows mean velocity and coefficient of pressure profile plots for the top boundary of each domain. An ideal top boundary not influencing the wind flow over the 2D hill would give a straight line across the domain for velocity (constant mean velocity magnitude) and a linear drop for the coefficient of pressure.

2D Domain Sizes	
F3-S0-A3-B6	F4-S0-A4-B8
F5-S0-A5-B10	F5-S0-A8-B10
F5-S0-A10-B10	F5-S0-A12-B10
F5-S0-A14-B10	F5-S0-A16-B10

Table 16 : Dimensions of domains examined for 2D domain size study.

The effect of the hill on velocity and coefficient of pressure profiles on the top boundary decreased as this boundary was moved further away from the ground. Profiles for domains with a top boundary at A3, A4, A5 and A8 were clearly affected by the hill; domains with top boundaries at A10, A12, A14 and A16 gave a reasonable deviation in the values of velocity and coefficient of pressure. It is noteworthy that, inlet velocities slightly increase as the domain height increases; this is due to the logarithmic profile set for velocity. Velocity profiles for F5-S0-A12-B10, F5-S0-A14-B10 and F5-S0-A16-B10 are almost identical and would overlap for the same inlet conditions. A top boundary far enough and uninfluenced by the 2D hill would give approximately the same value of velocity at the outlet as at the inlet; this is the case for domains with a downstream distance of B10. Also significant is that the maximum deviation for both variables is not given at x/D=0 (atop the hill) but at an approximate distance of 0.25D after the hill; this is because of the distance it takes for the effect of the hill to reach the top boundary. This distance was seen to increase as the top boundary height was increased, reaching a distance of 1D for the highest domains (F5-S0-A14-B10 and F5-S0-A16-B10).

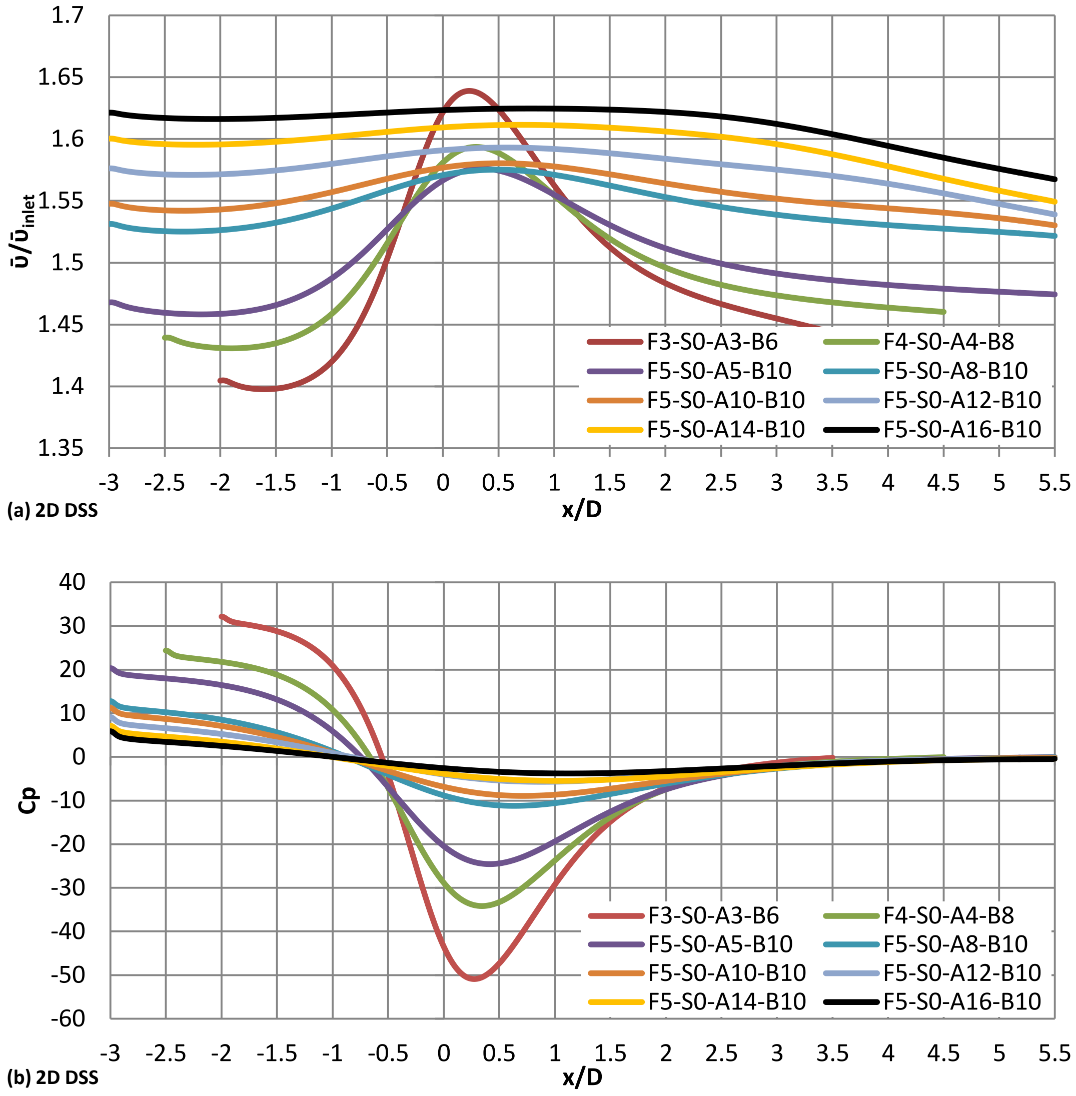

Figure 30 : Horizontal profile plots of (a) velocity and (b) coefficient of pressure along the top boundary for 2D ideal domain size study.

Hence, taking into consideration the small differences on top boundary profiles for the highest domains (F5-S0-A10-B10, F5-S0-A12-B10, F5-S0-A14-B10 and F5-S0-A16-B10) and the increased required processing time, it was decided that F5-S0-A12-B10 would be used as the recommended domain for the rest of the 2D simulations. Mean velocity magnitude and static pressure contour plots for the suggested domain are shown in Figure 31. Domain boundaries are clearly seen not to interact with the wind flow and no phenomena created by the hill are reaching the top boundary. The full recirculation zone is also visible and included in the domain; an important area to be examined later during pollutant dispersion modelling.

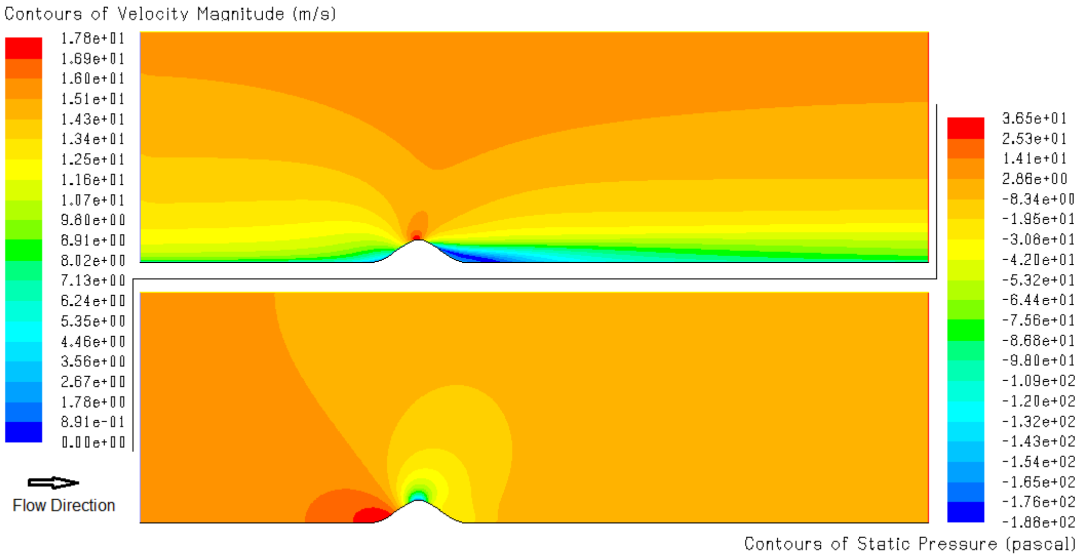

Figure 31 : Contour plots of mean velocity magnitude (top) and static pressure (bottom) for suggested 2D idealised domain.

5.3.3 Mesh Density Study

Mesh structure and density choice are important for accurate simulation results. A structured grid was used to examine the effects of mesh density on ABL wind flow over the 2D steep hill for the previous suggested domain size. Six different mesh densities were examined: three with square uniform mesh of interval size 0.5, 1 and 2 meters and three with expanding mesh density. For domains with growing mesh density, the 2D domain was separated into five areas (Figure 32) to allow higher mesh densities at points of interest (above hill and before/after hill). Areas 2, 3 and 4 had the highest mesh density with constant mesh intervals of 0.5, 1 and 2 meters. The mesh density gradually decreased towards the inlet and the outlet up to an interval size of 10 meters in the horizontal (x) direction. For the vertical (z) direction, a constant mesh density was set with intervals of 0.5, 1 and 2 meters; that allowed use of square cells at the areas of interest which are known to produce the most accurate results [ERCOFTAC CFD BPG, 2000]. Table 17 summarizes all domains created for the mesh density study.

The mesh density effect was studied using the same solver parameters as for the domain size study. All simulations were run to a convergence criterion of 10^{-5} for minimising the initial calculation error [COST Action 732, 2007]. Results were compared following the same technique as for the domain size study: velocity and coefficient of pressure profiles were plotted for the top boundary of the domain (Figure 33). Comparison between uniform and expanding meshes of the same interval size at areas of interest showed little difference in results. Expanding mesh densities reduces the processing time and power as such domains contain a smaller number of cells and a concentrated fine mesh at and around the hill. Differences between mesh intervals were also minor, with the smallest uniform interval of 0.5x0.5m giving a more detailed representation of required profiles. However, the much larger processing time for a double precision, second order solution (4 hours) made such high mesh density impractical for these 2D ideal simulations (compared to 2 hours and 1 hour for the uniform 1x1m and 2x2m meshes respectively).

Velocity magnitude and coefficient of pressure profiles were also plotted for a horizontal line at a height of 2H (two hill heights) above ground (Figure 34). Profile comparison showed a similar trend to that at the top boundary. The effect of the hill is clearly visible with maximum velocity magnitude above the hill's top; at the same point coefficient of pressure is minimum.

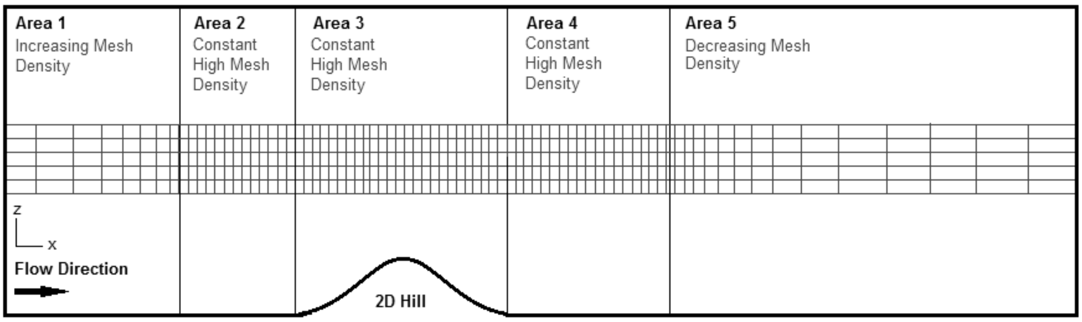

Figure 32 : Sketch of 2D domain with areas used for expanding mesh density study.

Domain Name	**Mesh Density Details** (horizontal × vertical, left to right)					
	Area 1	**Area 2**	**Area 3**	**Area 4**	**Area 5**	**No of Cells**
0.5x0.5m Uniform	0.5 x 0.5m	0.5 x 0.5m	0.5 x 0.5m	0.5 x 0.5m	0.5 x 0.5m	662,880
0.5x0.5m Expanding	10 x 0.5m to 0.5 x 0.5m	0.5 x 0.5m	0.5 x 0.5m	0.5 x 0.5m	0.5 x 0.5m to 10 x 0.5m	64,800
1x1m Uniform	1 x 1m	1 x 1m	1 x 1m	1 x 1m	1 x 1m	165,600
1x1m Expanding	10 x 1m to 1 x 1m	1 x 1m	1 x 1m	1 x 1m	1 x 1m to 10 x 1m	29,400
2x2m Uniform	2 x 2m	2 x 2m	2 x 2m	2 x 2m	2 x 2m	41,400
2x2m Expanding	10 x 2m to 2 x 2m	2 x 2m	2 x 2m	2 x 2m	2 x 2m to 10 x 2m	15,400

Table 17 : Interval size details for 2D domain mesh density study.

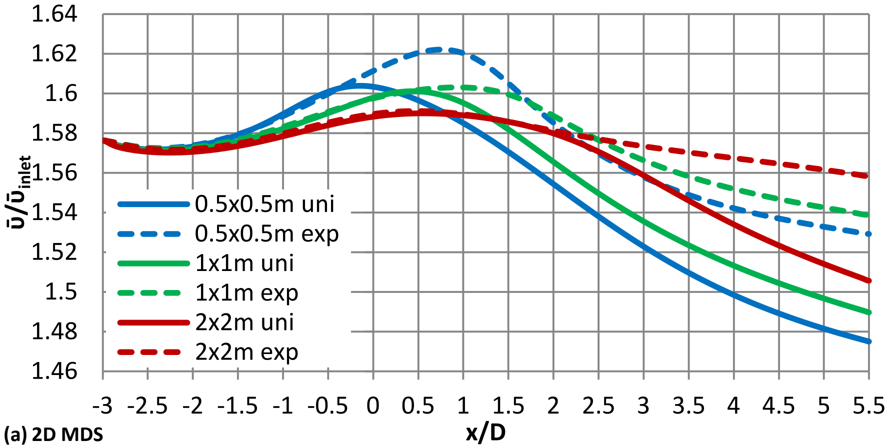

(a) 2D MDS

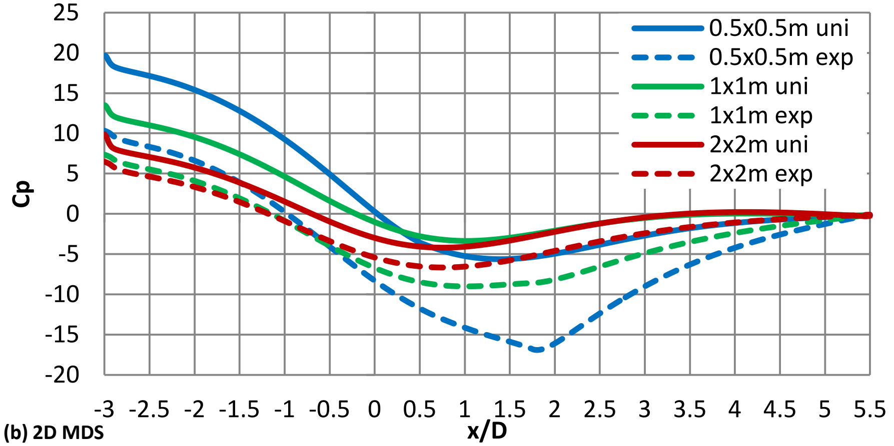

(b) 2D MDS

Figure 33 : Horizontal profile plots of (a) velocity and (b) coefficient of pressure along the top boundary for 2D ideal domain mesh density study.

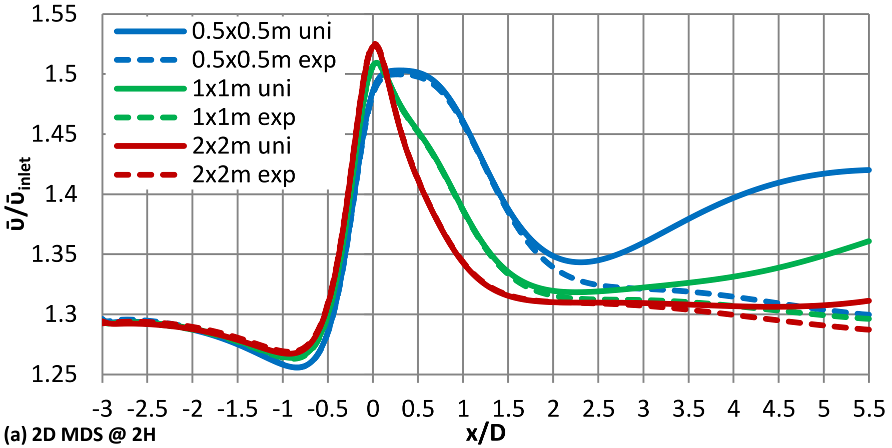

(a) 2D MDS @ 2H

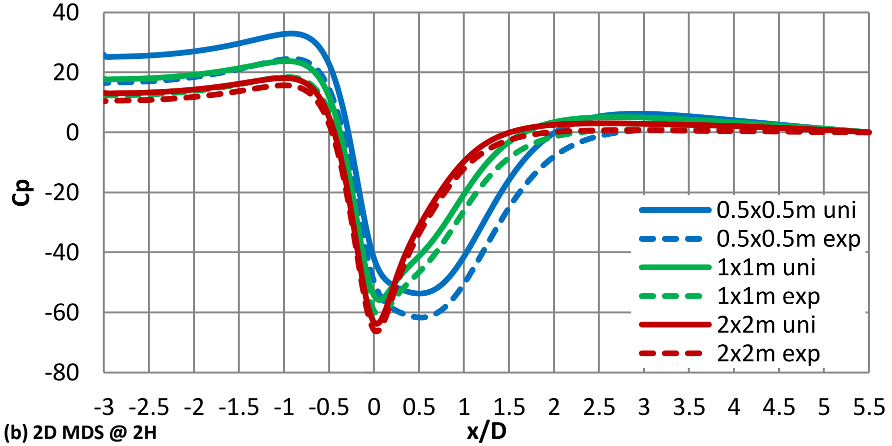

(b) 2D MDS @ 2H

Figure 34 : Horizontal profile plots of (a) velocity and (b) coefficient of pressure along a monitor line at 2H above ground for 2D ideal domain mesh density study.

Above hill (horizontal x positions from -0.5D to 0.5D), all mesh densities performed equally well with minor differences in both velocity and coefficient of pressure. Growing mesh densities were seen to underestimate velocity downwind the hill and closer to the outlet. However, the maximum error is seen at the outlet where little or no information is required regarding wind flow or pollutant dispersion.

Taking into consideration the similar performance of uniform and expanding mesh, the latter was employed for saving processing time. The fine mesh density (0.5x0.5m) was seen to perform better but was not adopted due to the high number of cells and time required for solution. Thus, the domain with the intermediate expanding mesh of 1x1m was selected for all 2D simulations in order to achieve good quality results in a reasonable amount of time.

5.3.4 Wind Flow and Species Transport over Single 2D Hill

Wind flow simulations were run for three ABL inlet conditions over a 2D sinusoidal hill based on the earlier described boundary and mesh studies. Horizontal velocity profiles were plotted at height H (hill top) and at height 2H (Figure 35). Results for the three ABL inlet conditions (2, 5 and 10ms^{-1}) were identical when plotted on non-dimensional graphs, showing that non-dimensional horizontal velocity variation does not depend on the mean velocity at the inlet but on the geometry of the hill. This is largely due to the small range of velocities simulated. Defining higher inlet velocities would not be representative of typical weather conditions nor would be physical for open environment studies (wind speeds during tornados, typhoons and other extreme weather phenomena would be much higher resulting in different conclusions but would also be much more difficult to numerically represent as such conditions are multi-directional with variable intensities).

Velocity profiles showed little difference between inlet and outlet boundaries. Velocity was seen to decrease as the wind flow approached the hill (-2.5D to -0.5D) and increase above the windward face of the hill (-0.5D to 0D). Above hill (at height H and 0D) velocity was seen to be maximum. Wind velocity dropped above the leeward face of the hill and stayed constant until the flow left the domain at 5.5D.

Velocity profiles for horizontal velocity u_x near ground were also plotted to establish reattachment length (Figure 35b). Again, these profiles were seen to overlap for all cases giving a wind flow reattachment length of 0.6D.

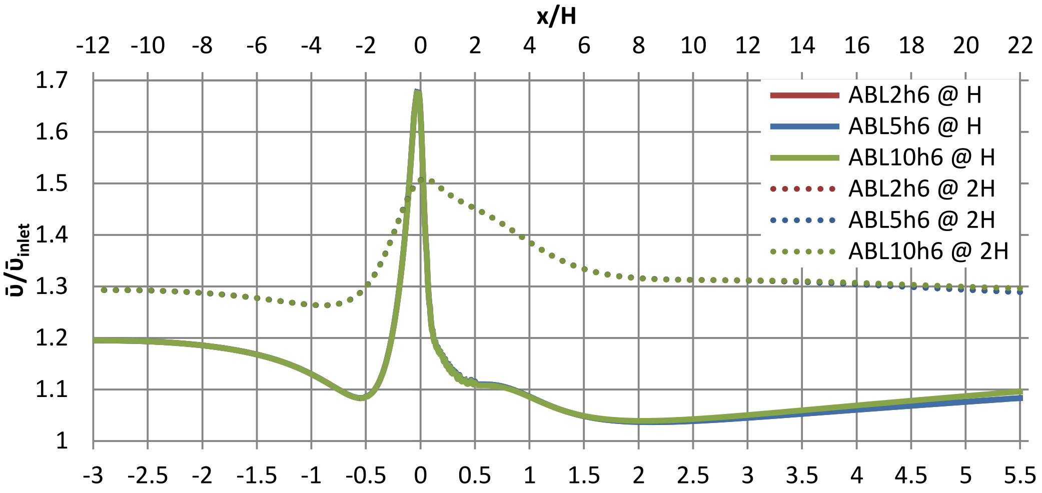

(a) $\bar{u}/\bar{u}_{inlet}$ 2D Comparison

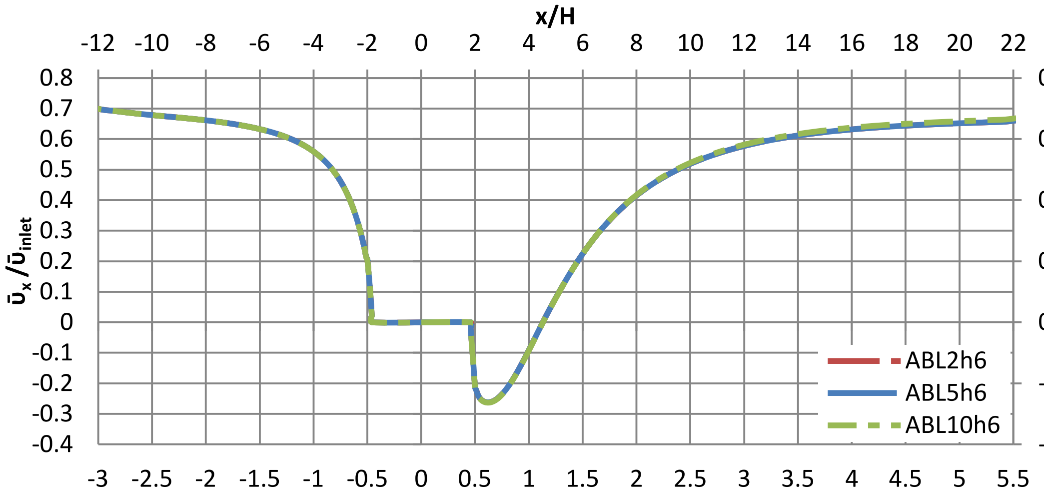

(b) $\bar{u}_x / \bar{u}_{inlet}$ 2D Comparison

Figure 35 : Horizontal profile plots of (a) velocity at H and 2H above ground and (b) velocity at first cell above ground level for wind flow over 2D sinusoidal hill.

Contours of mean velocity magnitude and turbulent kinetic energy for the 2D domain with an inlet condition of ABL10h6 are shown in Figure 36. The lowest part of the windward face was also seen to have low velocities but no flow separation took place. The recirculation zone at and just after the leeward face of the hill is clearly visible with the dark blue colours indicating the lowest mean velocity magnitudes. The recirculation zone is further presented in Figure 37 by superimposed wind pathlines and velocity vectors.

Following wind flow modelling, the species transport model in FLUENT was used as an alternative approach to particle tracking employed by Viz (2011) to model pollutant dispersion and to examine how the hill geometry can influence wind flow and thus pollutant concentrations. Species transport simulations were conducted for both flat and single hill terrains in order to examine the influence of the hill geometry to the pollutant concentration and spread. A ground source was defined 1.25D (100m) upwind to the centre of the hill releasing wood particles at a constant velocity of $1ms^{-1}$; for flat terrains the source was placed at an identical distance from inlet (illustrated in Figure 38). For details on the species transport model see Chapter 4; for full description see Fluent User's Guide (2006).

Comparing wood species release downwind flat terrains (Figure 39a) showed that for smaller mean inlet velocities (ABL2h6) the mole fraction is larger closer to the source. The percentage of wood mole fraction close to the source decreases as the mean velocity at the inlet increases, showing that wood species released in higher magnitude winds would travel further than wood species released in low winds; in this case species fraction would decay faster due to large percentages at and near the ground source.

Figure 39b and Figure 39c show the effect of the hill to the wood mole fraction for three ABL inlet conditions. Percentages of wood species were seen to drop faster for low wind speeds (ABL2h6) than for large wind speeds (ABL10h6). The hill was seen to act as a barrier to the wood species, reducing the mole fraction by approximately 10%, 5% and 2% for ABL2h6, ABL5h6 and ABL10h6 respectively. Thus, at lower mean velocities the effect of the hill increases, blocking a larger percentage of the species released.

Mole fraction comparison plots between flat and hill domains for individual inlet velocities are shown in Figure 40. Wood mole fraction plots for both flat and hilly terrains were identical until the species reached the windward face of the hill where percentages started decreasing at a higher rate. Just after the hill and on the leeward face, a sudden drop in mole fraction took place. This drop was larger for lower wind speeds. Results showed that wood mole fraction would reach background levels (in this case 0%) faster when the inlet wind speed was higher. In the case of the hilly terrain, a hill acted as a barrier to the flow and thus the species spread; this effect was seen to be greater for lower ABL inlet conditions.

The above raise questions regarding the EA guidelines to consider hilly terrains as flat when slopes are less than 1:10. This will be further examined with the help of the 3D modelling of wind and pollution over hilly terrains in the following parts.

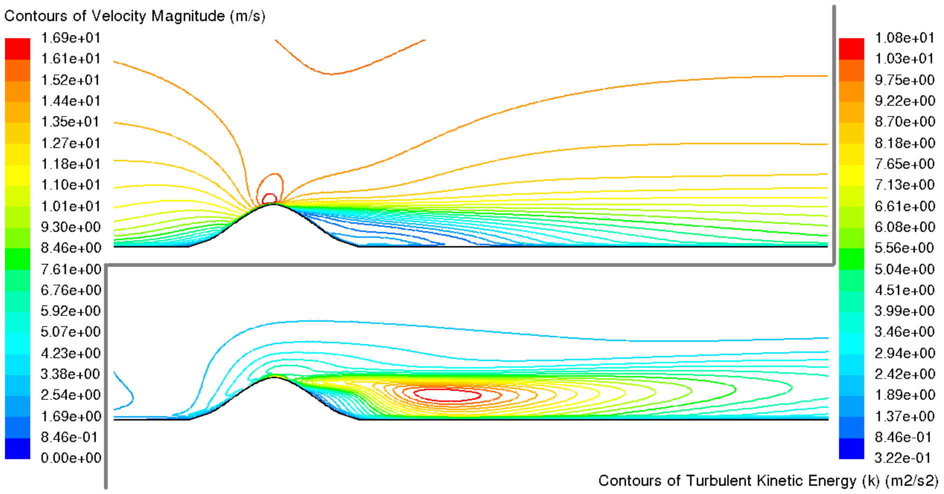

Figure 36 : Contours of mean velocity magnitude and turbulent kinetic energy for wind flow over single 2D sinusoidal hill with inlet ABL10h6.

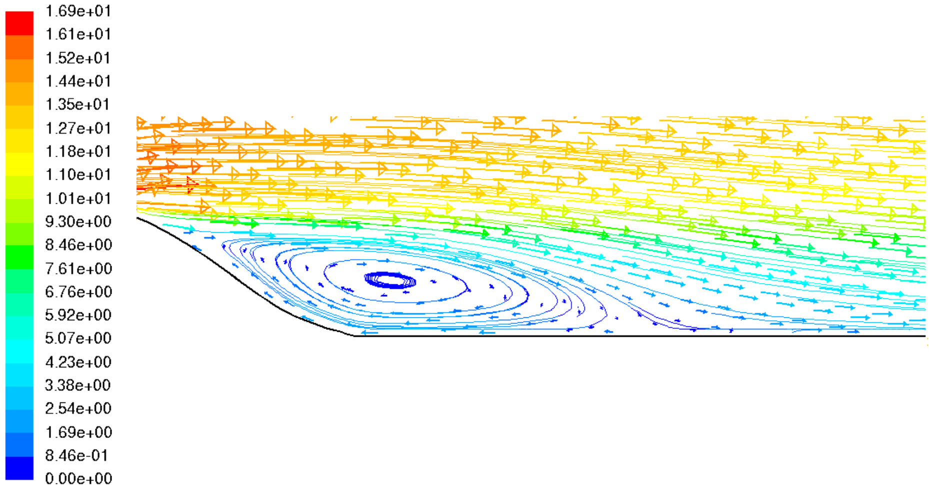

Figure 37 : Superimposed wind pathlines and vectors of mean velocity magnitude downstream 2D sinusoidal hill with inlet ABL10h6.

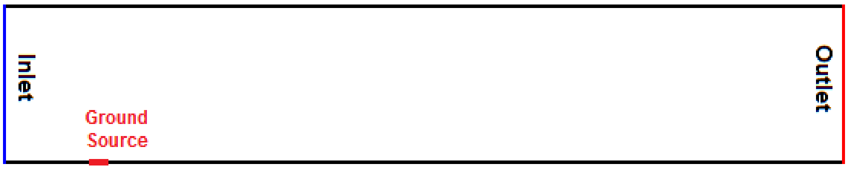

2D Flat Terrain

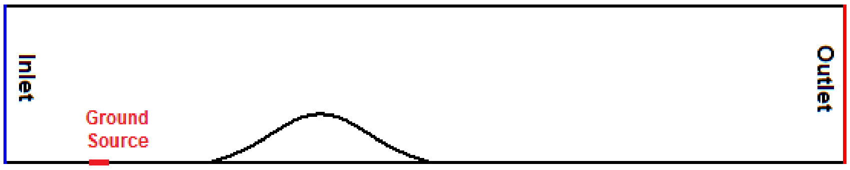

2D Sinusoidal Hill Domain

Figure 38 : Flat and single hill 2D domains with ground source simulated for species transport (same domain size and source placement).

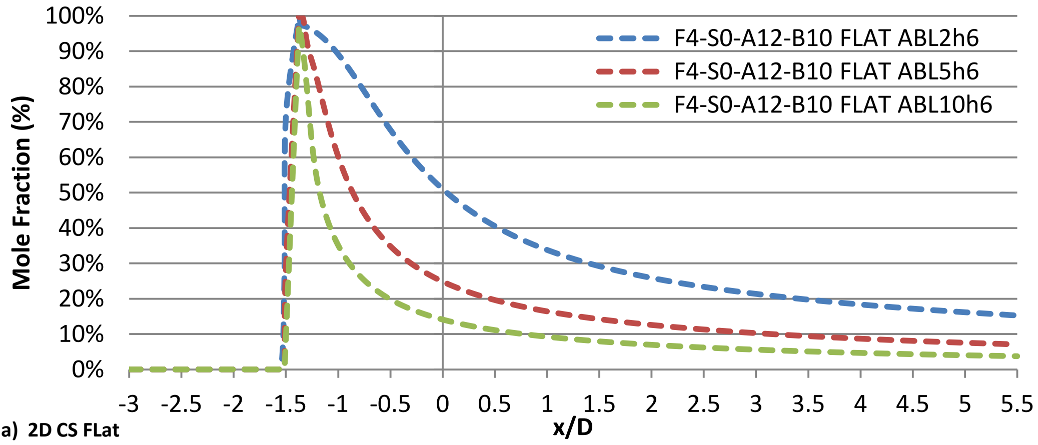

(a) 2D CS FLat

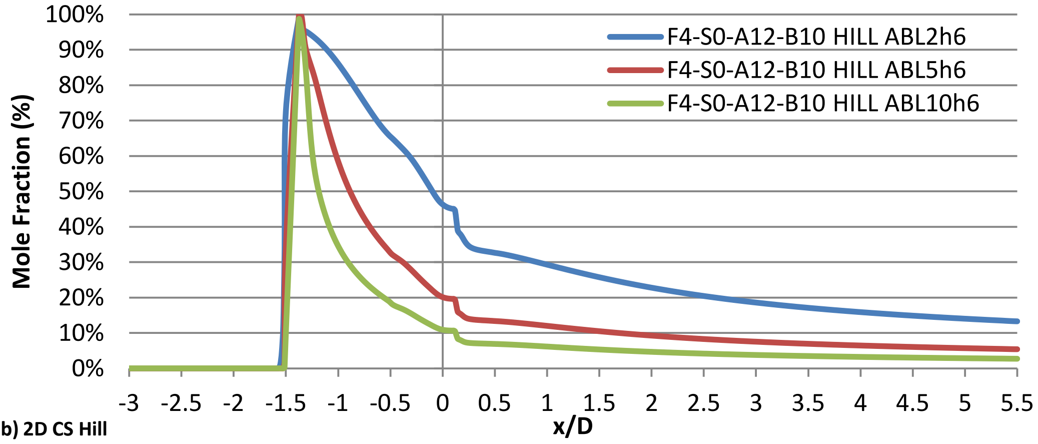

(b) 2D CS Hill

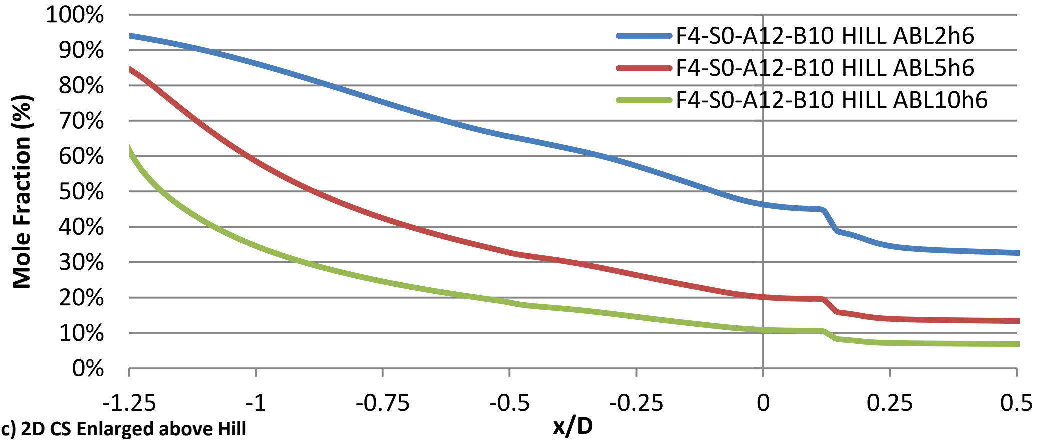

(c) 2D CS Enlarged above Hill

Figure 39 : Wood mole fraction comparisons at ground level for (a) 2D flat terrain, (b) 2D single hill terrain and (c) enlarged view of mole fraction over single 2D hill for three ABL logarithmic inlet profiles.
($\overline{u}$=2ms^{-1}, $\overline{u}$=5ms^{-1}, $\overline{u}$=10ms^{-1}, all at reference height h_{ref}=6m)

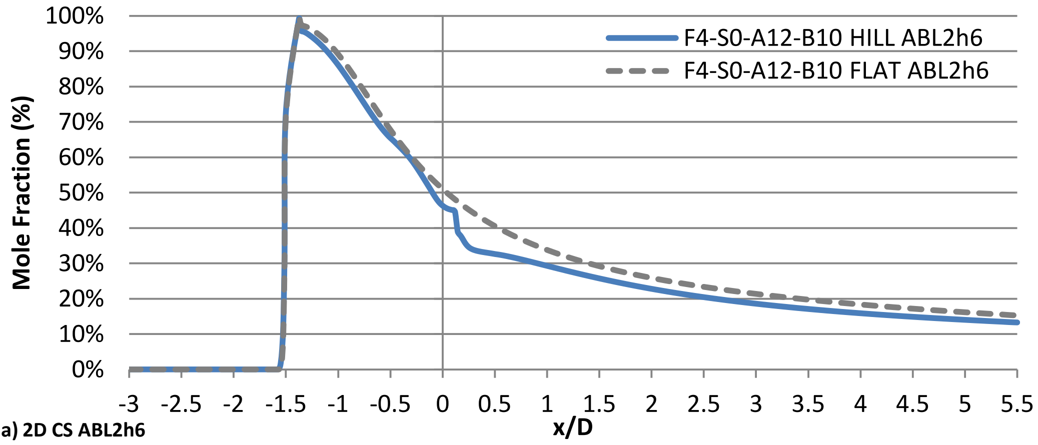

(a) 2D CS ABL2h6

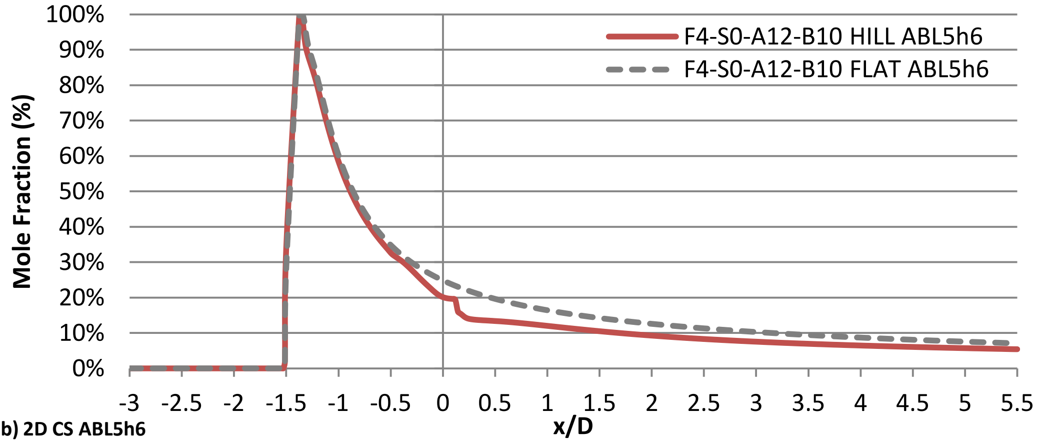

(b) 2D CS ABL5h6

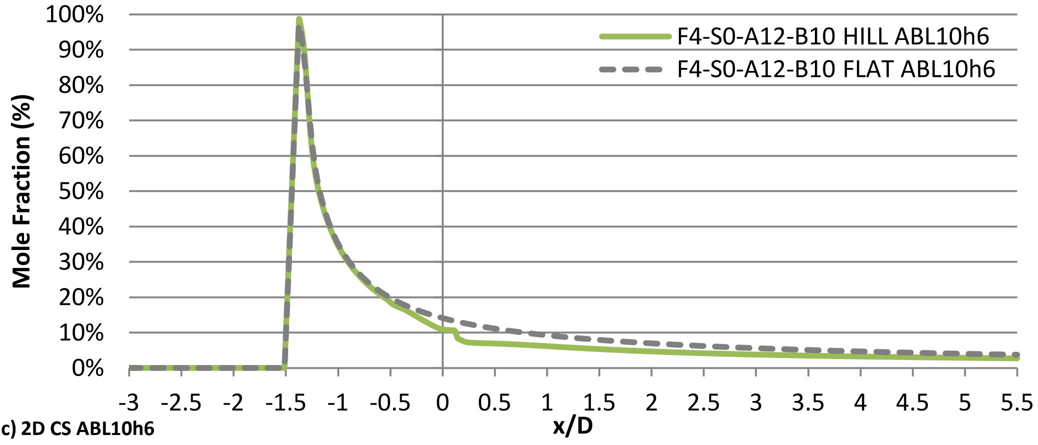

(c) 2D CS ABL10h6

Figure 40: Wood mole fraction comparisons at ground level for single 2D hill and 2D flat terrains for three ABL logarithmic inlet profiles.
((a) $\overline{u}$=2ms^{-1}, (b) $\overline{u}$=5ms^{-1}, (c) $\overline{u}$=10ms^{-1}, all at reference height h_{ref}=6m)

5.4 Wind Flow and Pollution Dispersion over Single 3D Hill

5.4.1 Introduction

Following ideal 2D simulations, 3D ideal hills were studied. Although similar to the 2D approach, these 3D domains required more time and processing power to give accurate results due to the large number of cells. Therefore, identical techniques during the pre and post processing stages were adopted for all 3D simulations to make production and comparison of results faster and more efficient.

Monitor lines and planes were created for all cases to plot the mean velocity, static pressure and coefficient of pressure on and around the hill. These helped show the effects of the idealised hill geometry to the wind flow and how the flow phenomena reach - or stay away from – the specified boundaries. Above hill monitor lines and planes were defined in multiples of hill heights and sideways monitor lines and planes were defined in multiples of hill radius. The first line and plane above the hill was at a height H equal to the hill height. The first line and plane sideways the hill was at a distance R equal to the hill radius; the sideways lines were at height H/2. Schematic diagrams of the monitoring lines and planes are shown in Figure 41.

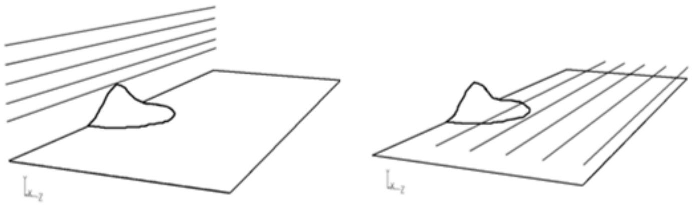

Figure 41 : Monitor lines used for 3D ideal domain comparison.

5.4.2 Domain Size Study

As mentioned earlier for 2D simulations, a domain size study was necessary before obtaining results. Once more, all boundary conditions, mesh intervals (1x1m at and around the hill) and solver details were identical in all cases. The sinusoidal hill used for the 3D domain study was similar to the 2D hill with a diameter D=80m and height H=20m. The examined domain sizes were simulated for ABL10h6 and are listed in Table 18.

3D Domain Sizes	
F2-S2-A2-B4	F3-S3-A3-B6
F4-S4-A4-B8	F5-S5-A5-B10

Table 18 : Dimensions of domains examined for 3D domain size study.

In order to compare the results of all domain sizes examined, velocity and coefficient of pressure profiles for the external line (furthest from the hill) were plotted for both above and sideways hill (Figure 43). These plots examined the influence of the hill to the wind flow and to what extent these phenomena reached the top and side boundaries. As for 2D simulations, ideally, the velocity profile on a longitudinal line far-away from the hill would give a straight horizontal line indicating that velocity is not affected by the hill's geometry; for coefficient of pressure the plotted curve for the same far-away line would give a linear drop. Velocity profiles above the hill show an almost linear drop of velocity with a small irregularity because of the hill. Coefficient of pressure profiles for the same -above hill- line show a similar trend with the boundaries of the largest domains being less affected by wind flow around the hill. Profiles for both velocity and coefficient of pressure at the furthest line sideways the hill show small differences between domains examined.

Comparison plots (Figure 43) and detailed domain size result plots show that a domain size of F4-S3-A4-B8 would be big enough to include all fluid flow phenomena with boundaries not interacting with the flow but small enough to optimise processing power and time (dimensions are shown in Figure 42). Such boundaries would allow all velocity and pressure flow phenomena, due to hill geometry, to be included and studied. It is worth mentioning that overall the domain dimensions for 3D simulations were smaller than for 2D – something that will be discussed later on.

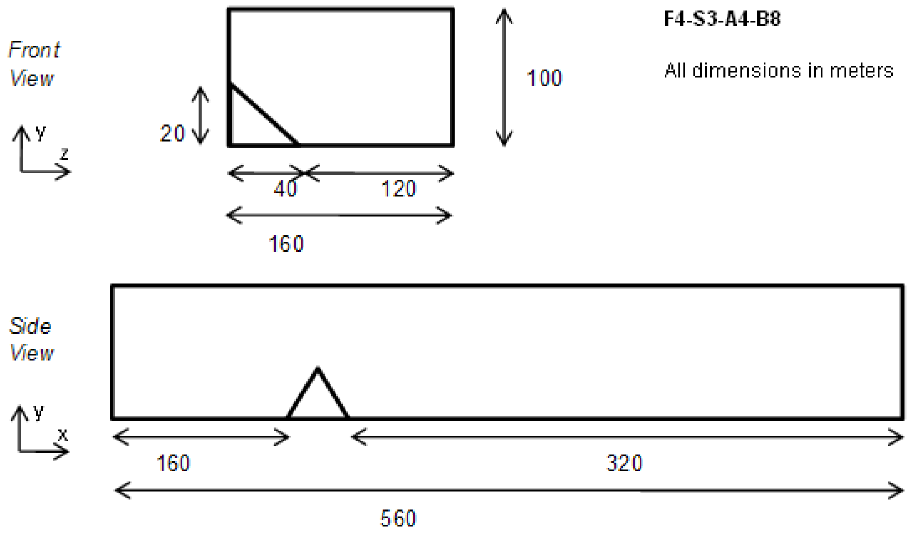

Figure 42 : Dimensions of suggested 3D domain size.

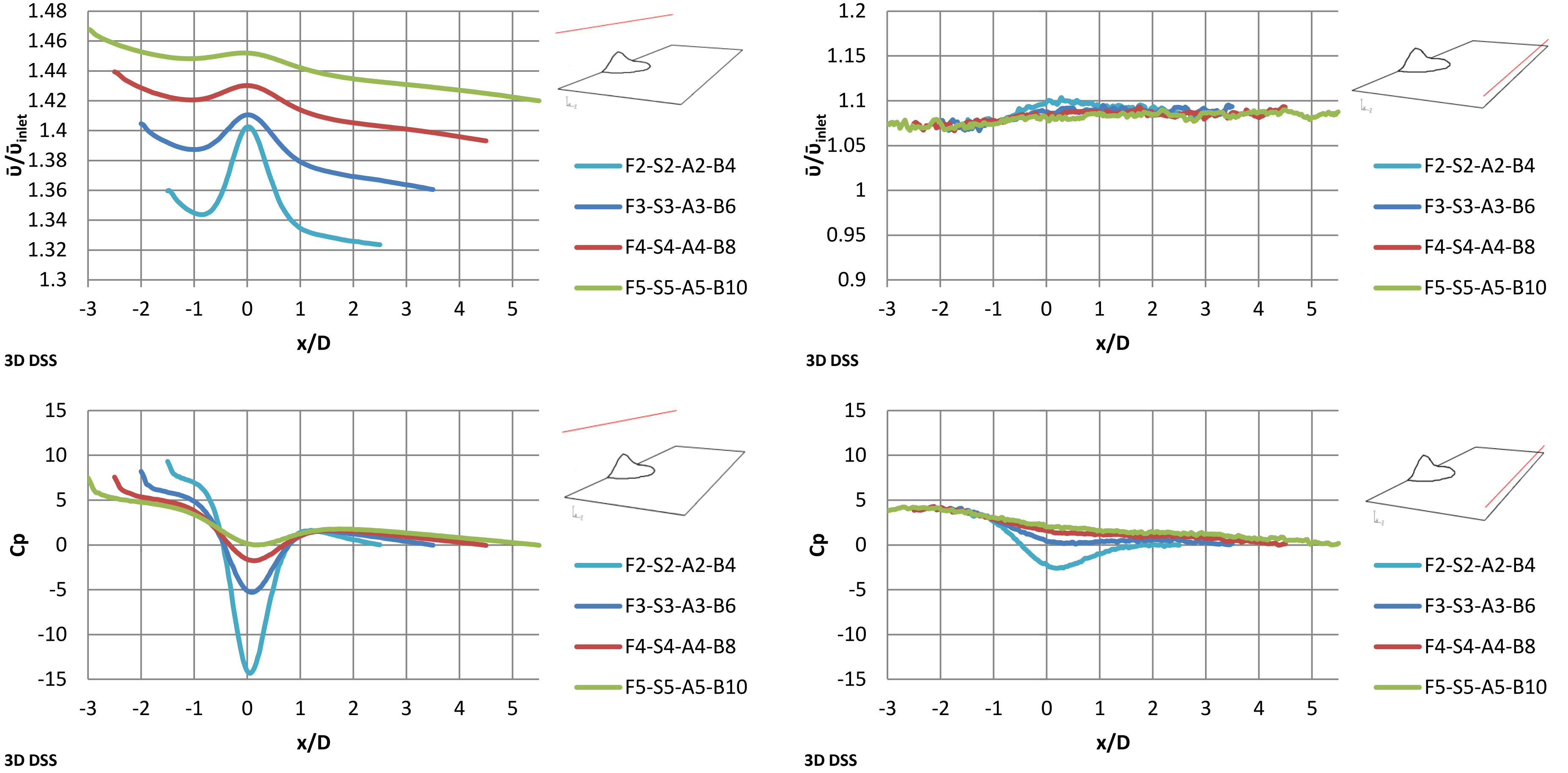

Figure 43 : Comparison plots of velocity and coefficient of pressure (left) above and (right) sideways hill for studied 3D domain sizes.

5.4.3 Mesh Density Study

For the examination of the effects of the numerical grid on the solution process, a mesh density study was carried out. All simulations were run using double precision to minimise round of errors and second order spatial discretization to reduce truncation errors [ERCOFTAC CFD BPG, 2000].

To further minimise errors, a hexahedral mesh type was employed as for 2D simulations. For the biggest part of the domain, skewness was zero with cells having 90° angles. All skewed cells were around the hill where the mesh required adaption of intervals and orientation to account for the circular base and the sine-curved face of the hill.

Three different mesh densities were studied and compared: 0.75m, 1m and 2m at the surface of the hill for an inlet ABL profile of $10ms^{-1}$ at reference height of 6m (Table 19 gives information on the number of cells for each mesh density).

The majority of cells were placed above and around the hill where the area of interest is; with the intervals getting larger towards the outer boundaries of the domain up to 10m at the inlet, outlet, sky and away-from-hill side. For this purpose, the domain was separated in multiple volumes as shown in Figure 44. A capture of the full $1m^3$ dense domain is shown in Figure 45 and a detailed view of the grid at the hill in Figure 46.

Mesh Interval on Hill Surface	**Number of Hex Cells**	**Case Name**
0.75m	2 455 560	MS-075m
1m	1 285 000	MS-1m
2m	715 200	MS-2m

Table 19 : Details of 3D mesh densities studied.

Figure 47 shows comparison plots of velocity and coefficient of pressure for above and sideways furthest-from-hill lines. Results for the examined mesh densities were similar for both monitor lines above and sideways the hill. As the mesh density did not have a major effect on results, the intermediate domain MS-1m with $1m^3$ cells at the hill was selected for these 3D simulations. This domain was seen to produce accurate results within a reasonable amount of time for the examination of wind flow and pollutant dispersion – full results are presented later in this chapter.

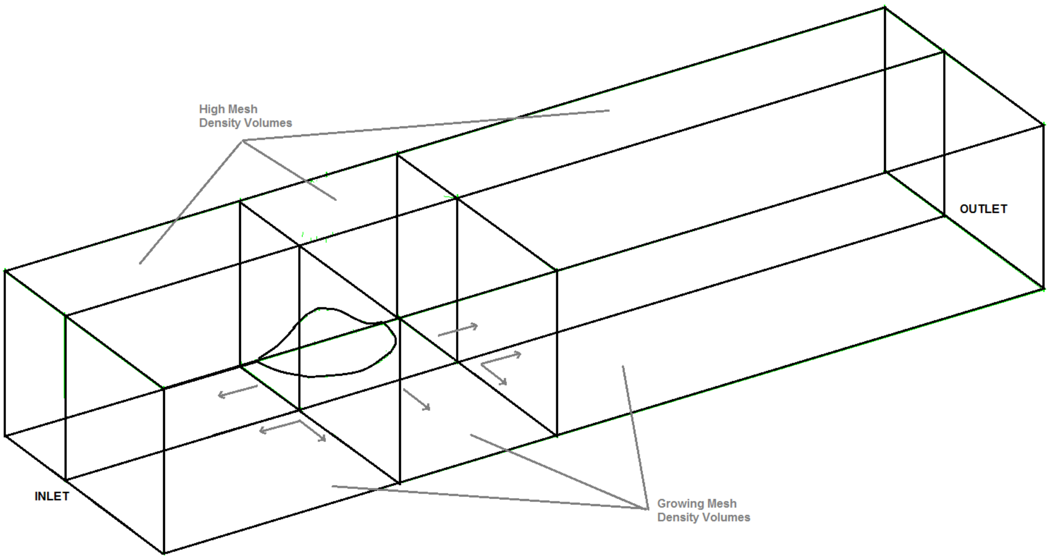

Figure 44 : Sketch of 3D domain with multiple volumes used for mesh density study (arrows indicate direction of expanding mesh density – fine to coarse).

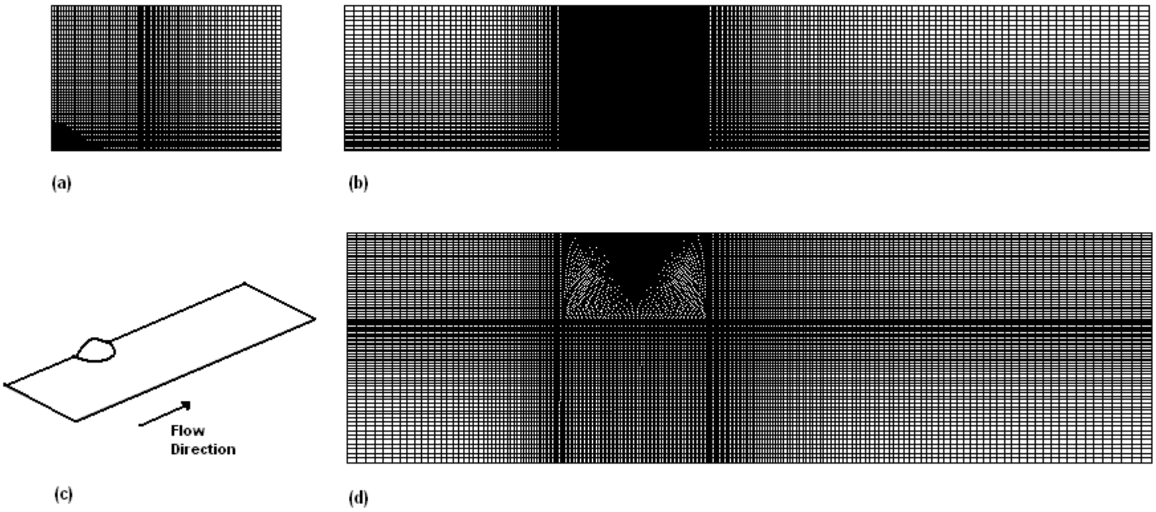

Figure 45 : Numerical grid used (1m on hill and ground faces) for mesh independence study, with (a) front view (inlet plane), (b) side view (symmetry plane), (c) isometric view of domain with flow direction and (d) top view (wall plane).

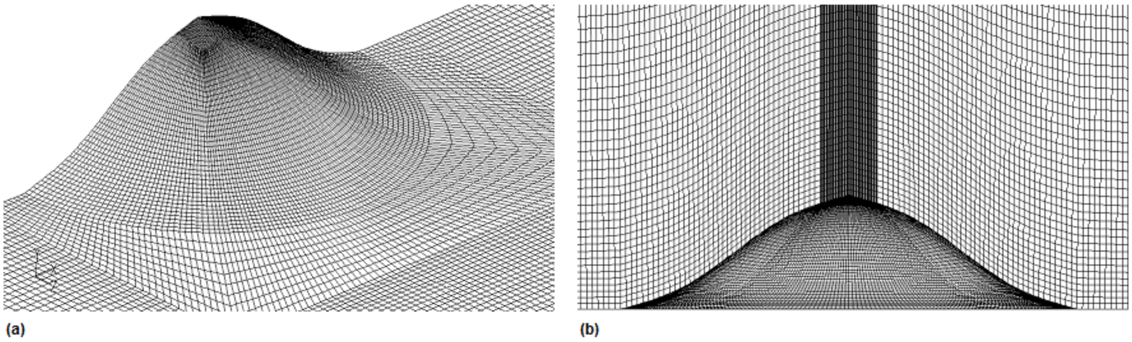

Figure 46 : Detailed hill view of numerical grid used (1m on hill and ground faces) for mesh independence study, with (a) isometric view of hill and (b) side view (symmetry plane).

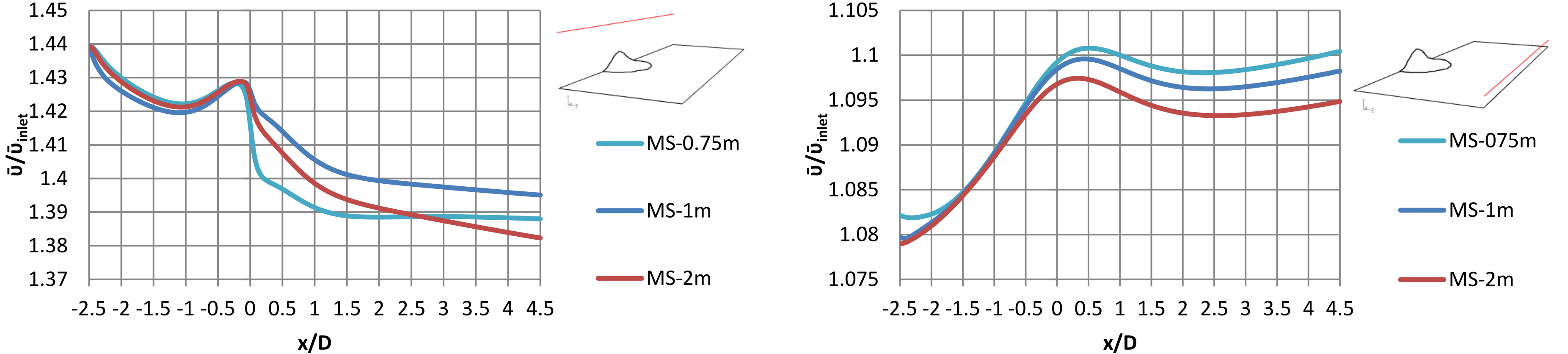

3D MDS @ 5H

3D MDS @ 4R

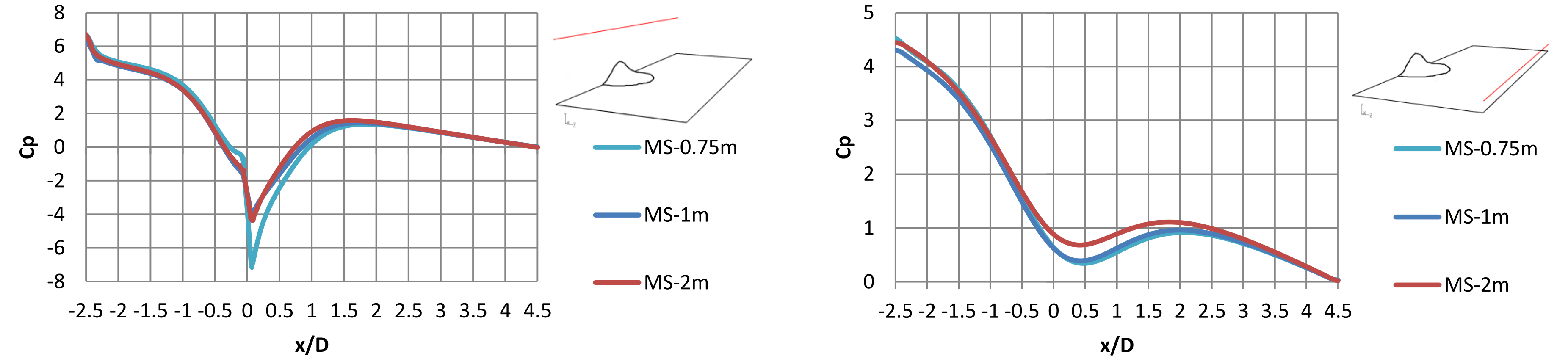

3D MDS @ 5H

3D MDS @ 4R

Figure 47 : Comparison plots of mean velocity magnitude and coefficient of pressure (left) at 5H above hill and (right) at 4R sideways hill for studied 3D mesh densities.

5.4.4 Wind Flow and Particle Tracking over Single 3D Hill

Following conclusions from previous parts of this chapter (boundary conditions, domain size and mesh density), the wind flow over a three dimensional single hill was simulated. The hill had a circular base of 80m diameter and 20m height as described earlier.

Three inlet conditions were specified according to the Richards and Hoxey (1993) approach and based on the available weather data to represent calm, medium and windy conditions; these were specified with logarithmic profiles for $\overline{u}$, k and ε with mean velocities of 2ms^{-1}, 5ms^{-1} and 10ms^{-1} at reference height of 6m as described in Table 20. Different wind directions will not be examined here as the hill is axisymmetric and any change in wind direction would be equal to moving the source from the centreline causing reduction of the effect of the hill to the wind flow [Castro and Snyder, 1982].

Case Name	**Mean Velocity $\overline{u}_{\text{inlet}}$**	**Reference Height h_{ref}**
SH-ABL2h6	2ms^{-1}	6m
SH-ABL5h6	5ms^{-1}	6m
SH-ABL10h6	10ms^{-1}	6m

Table 20 : Single hill 3D simulations conducted.

Figure 48 shows monitor lines utilised to compare results from simulations with different inlet conditions. Monitor lines on the mid-plane over hills were drawn as well as horizontal monitor lines at a height of 0.25H (5m) above ground.

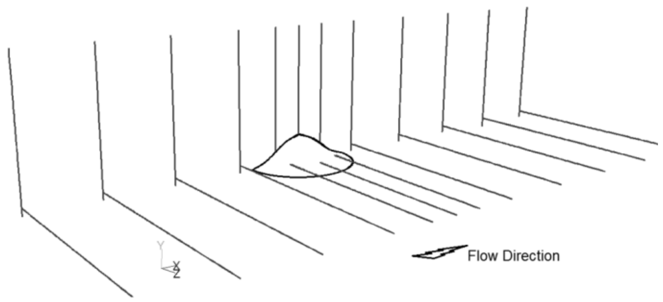

Figure 48 : Vertical and horizontal monitor lines used to plot variable profiles for 3D ideal hill simulations.

Velocity profiles downstream the domain for all three ABL inlet conditions are shown in Figure 49. For all ABL cases, velocity of the wind was seen to increase as it went up the hill (-0.5D to 0D) and when reaching the top (0D), replicating the speed up effect described earlier in Chapter 3.

Recirculation occurs behind the hill at the base of the leeward face with reattachment taking place after 0.65D from the top of the hill. Then, the velocity magnitude begins to slowly recover until it reaches the outlet.

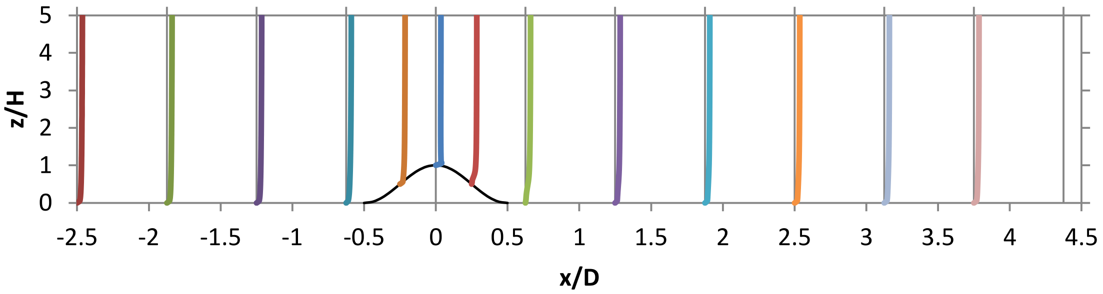

(a) SH-01-ABL2h6 ū Profiles

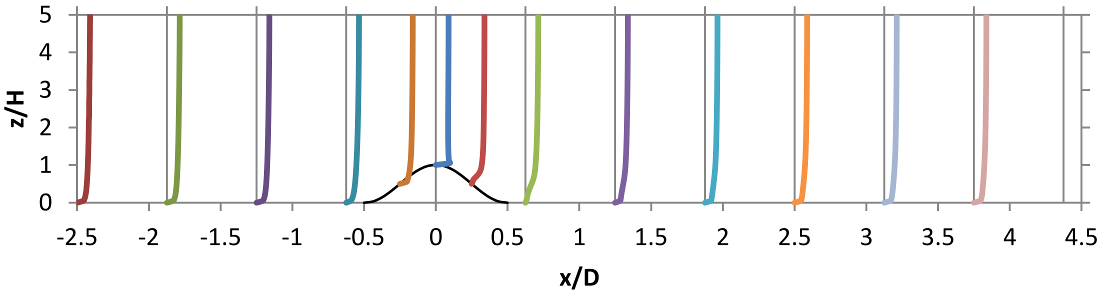

(b) SH-01-ABL5h6 ū Profiles

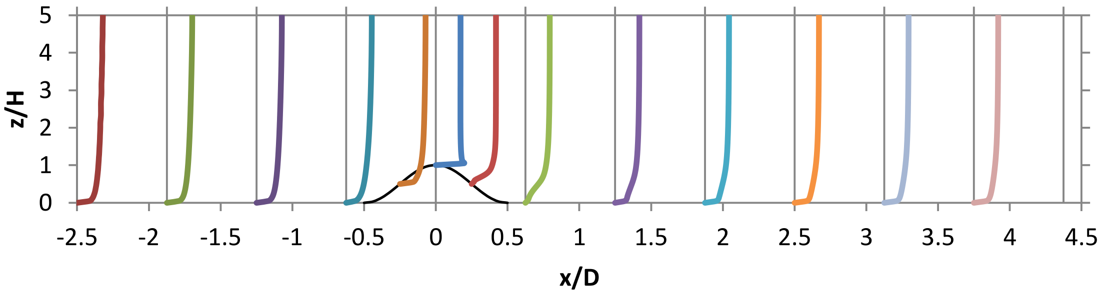

(c) SH-01-ABL10h6 ū Profiles

Figure 49 : Profiles of mean velocity magnitude for mid-plane (side view) over single 3D hill for three ABL inlet conditions (a) $\overline{u}$*=2ms*$^{-1}$*, (b)* $\overline{u}$*=5ms*$^{-1}$*, (c)* $\overline{u}$*=10ms*$^{-1}$*, all at reference height of* h_{ref}*=6m.*

Comparison plots for velocity profiles at heights H and 2H above ground on the symmetry plane are shown in Figure 50a. Comparison of velocity profiles for horizontal velocity u_x near ground are given in Figure 50b in order to examine the wind flow reattachment length: this was found to be 0.65D for all cases.

Velocity plots for all inlet conditions overlap as previously seen for 2D simulations due to the small range of velocities encountered in the open environment and thus simulated.

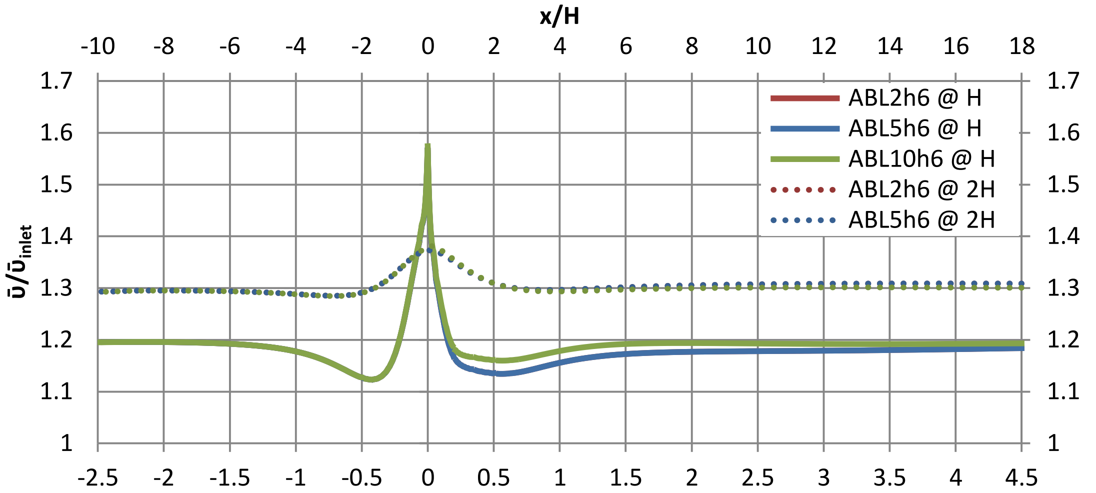

(a) $\bar{u}/\bar{u}_{inlet}$ 3D SH Comparison

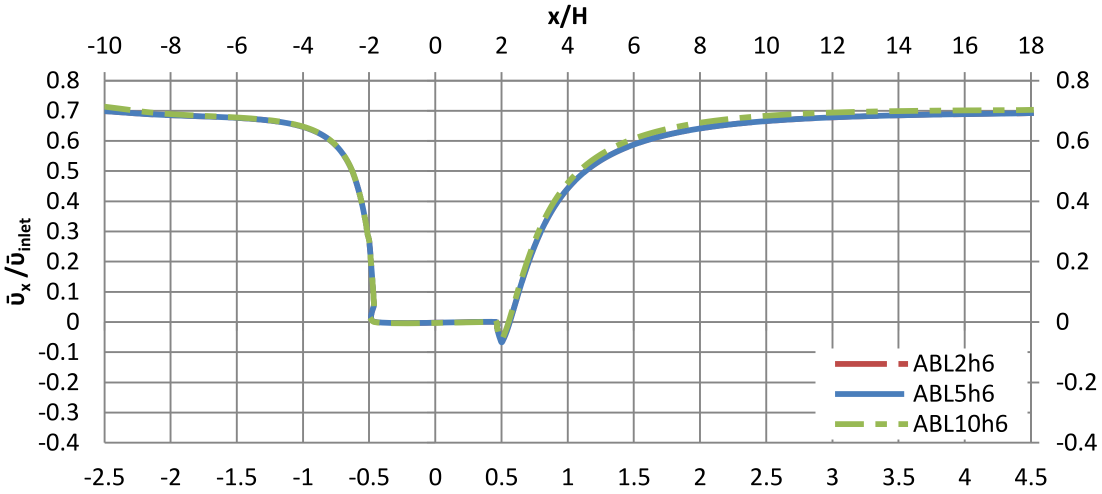

(b) $\bar{u}_x/\bar{u}_{inlet}$ 3D SH Comparison

Figure 50 : Horizontal profile plots of mean velocity at (a) H and 2H above ground and (b) first cell above ground level for wind flow over 3D sinusoidal hill.

Velocity and coefficient of pressure plots for multiple distances above and sideways the single hill with inlet ABL10h6 are presented in Figure 51. In addition, Figure 52 and Figure 53 use contour plots to display different views of the hill and ground faces; mid-planes at the hill are used to display variable contours above and sideways of the hill. Mean velocity, coefficient of pressure, turbulent kinetic energy and dissipation rate are also presented. Contours of mean velocity magnitude and coefficient of pressure show that as velocity increases on the windward face of the hill, pressure drops. At the highest point of the hill, velocity is maximum and pressure coefficient is minimum. Finally on the leeward face of the hill velocity drops (recirculation occurs) and the pressure coefficient increases again. Contours plots of k and ε show high values at the top of the hill where turbulence production takes place.

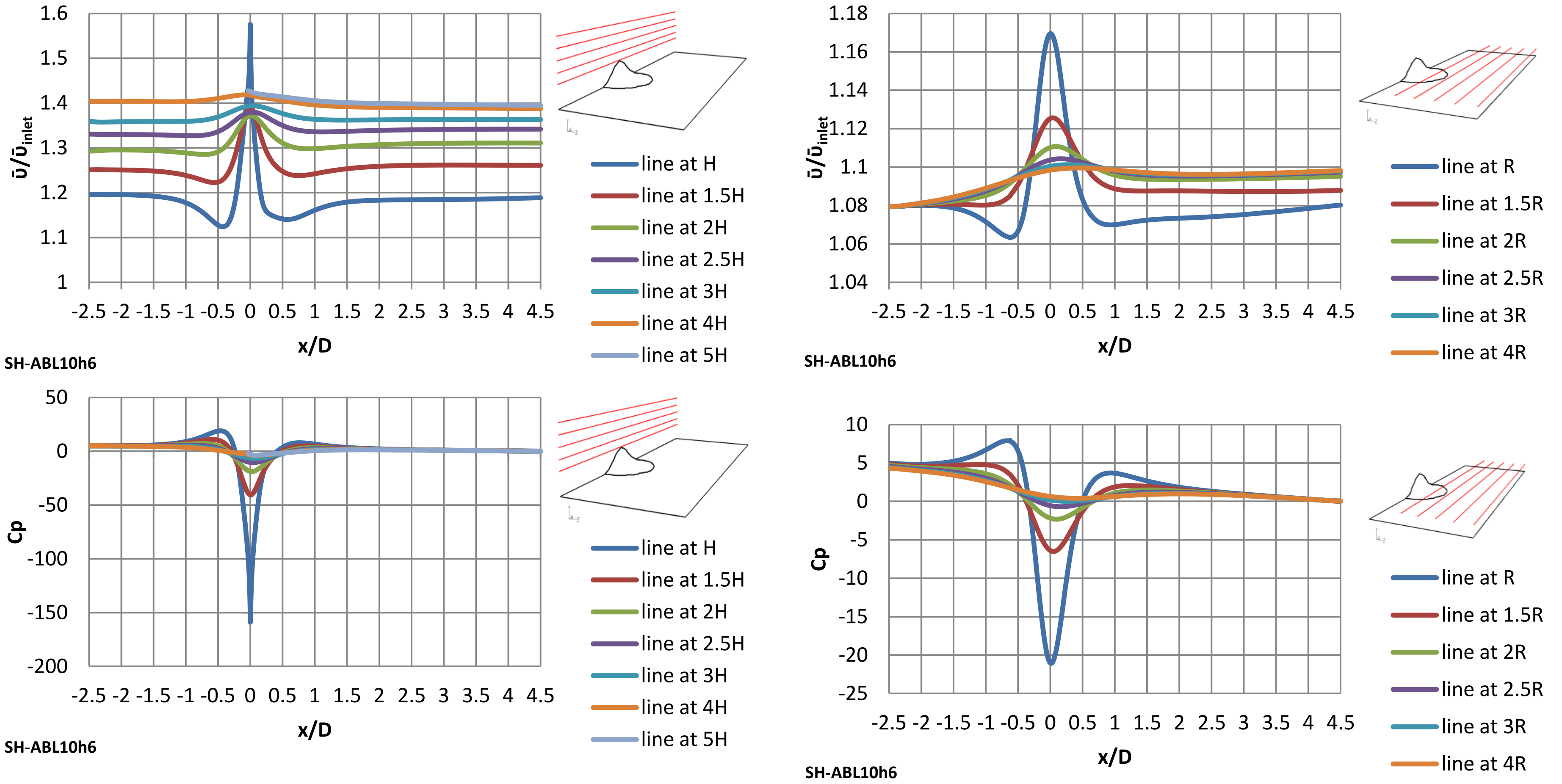

Figure 51 : Plots of velocity and coefficient of pressure (left) above hill and (right) sideways hill for wind flow over single hill with inlet condition ABL10h6.

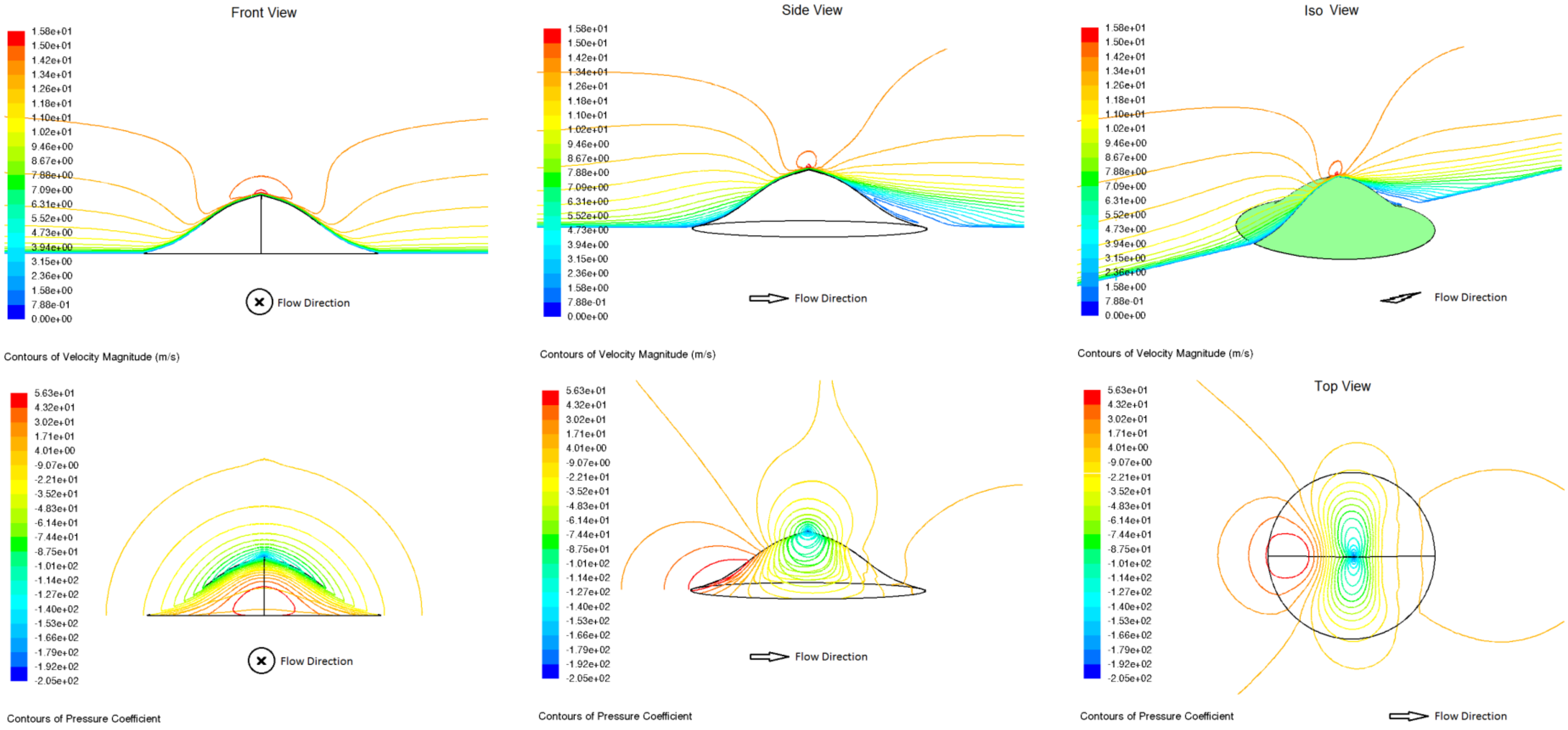

Figure 52 : Contour plots of mean velocity magnitude $\overline{u}$ and pressure coefficient C_p over single 3D hill for ABL10h6.

(Front and side views show contours on hill face and mid-planes and top views show contours on hill and ground faces)

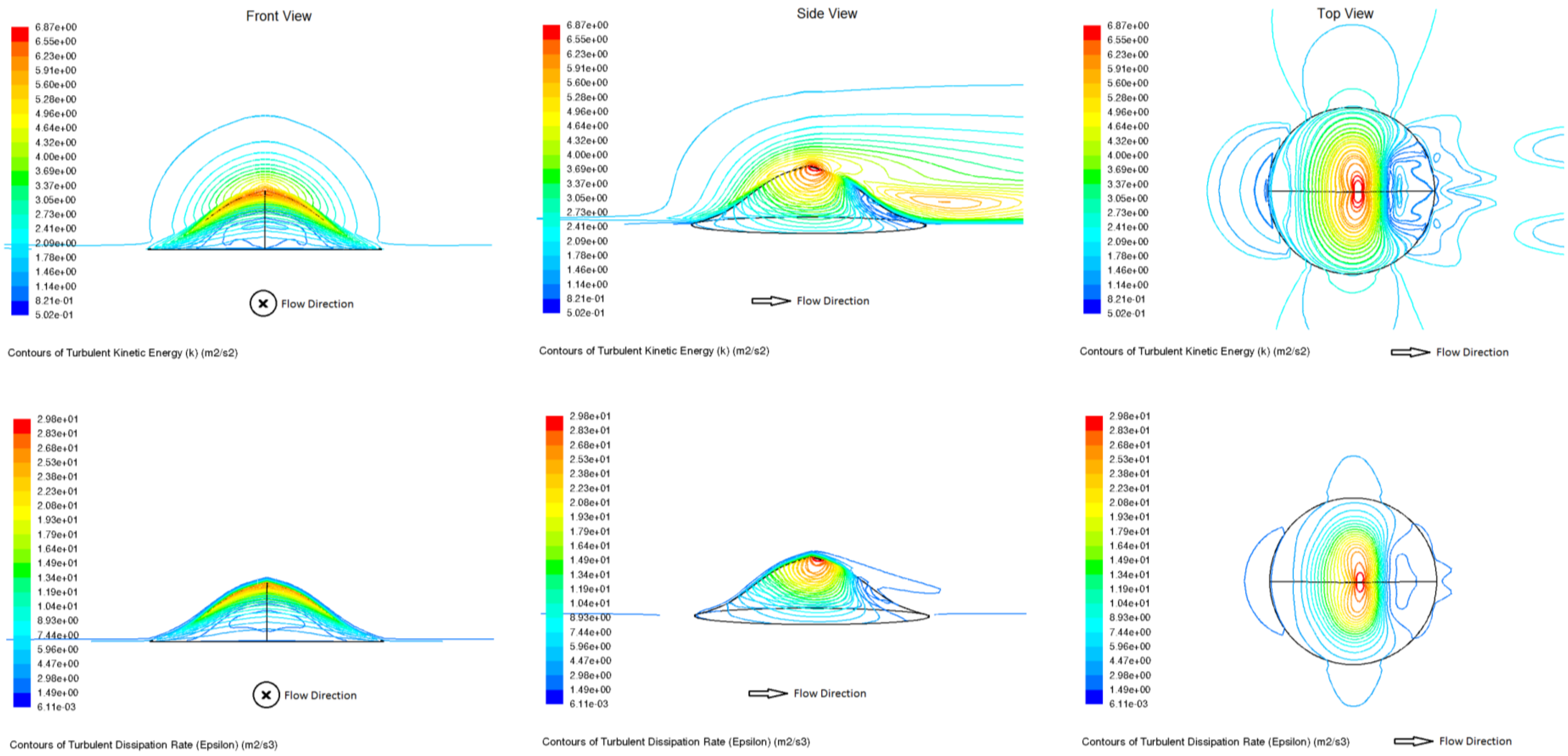

Figure 53 : Contour plots of turbulent kinetic energy k and dissipation rate ε over single 3D hill for ABL10h6.

(Front and side views show contours on hill face and mid-planes and top views show contours on hill and ground faces)

The Lagrangian particle tracking was enabled in FLUENT to model pollutant dispersion. The model used a one-way coupling technique with released particles influenced by the wind flow but not vice versa [Fluent 6.3 User's Guide, 2006]. Two line sources were defined for continuous release of ‘mass-less’ particles from ten equally spaced streams with zero initial velocity: a vertical and a horizontal source as presented in Figure 54. Both were placed 100m upwind of the hill centre with the vertical source extending from ground level (0m) up to 3m in height; the horizontal source was placed normal to the wind flow direction and centred with respect to the side boundaries, suspended 1m above ground and was 25m long (50m when mirrored due to the symmetrical domain approach).

Initially, the particle tracks overlapped with the wind flow pathlines. The Random Walk Model (RWM) was then enabled to introduce turbulence to the particle release as this is closer to what happens in the open environment due to turbulence and local recirculating eddies. The difference in particle tracks between these two different approaches can be seen in Figure 55 and Figure 56 with particles moving not only parallel to the wind flow direction but also sideways. Particles are also seen entering and exiting the recirculation zone at the leeward face of the 3D hill. Although the RWM stirred the simulation one step closer to reality, all particles released at source were reaching the outlet and exiting the domain. Furthermore, in actual pollutant dispersion in the open environment, particulate pollutants get trapped in trees, houses, the ground etc. momentarily or lastingly due to their small size (some pathogens and fungi are only a few microns in diameter). Thus, entrapment for the ground and hill faces was enabled in FLUENT with these boundaries trapping and absorbing particles on impact (Figure 57).

Results for particles released from each source stream were statistically handled to give average distance travelled of trapped particles and entrapment probability for a set of 10 tries per case. Particle data for the vertical line source (Figure 58) show that particles released at higher positions travel further than those released near ground level. For the horizontal line source (Figure 59) particles released near the symmetry plane were seen to travel further than those released away from the hill centre. However, particles released at or closer to the symmetry plane had greater chances of being trapped on the ground or hill faces after entering the recirculation zones. For both sources, higher inlet velocity was seen to carry particles for shorter distances.

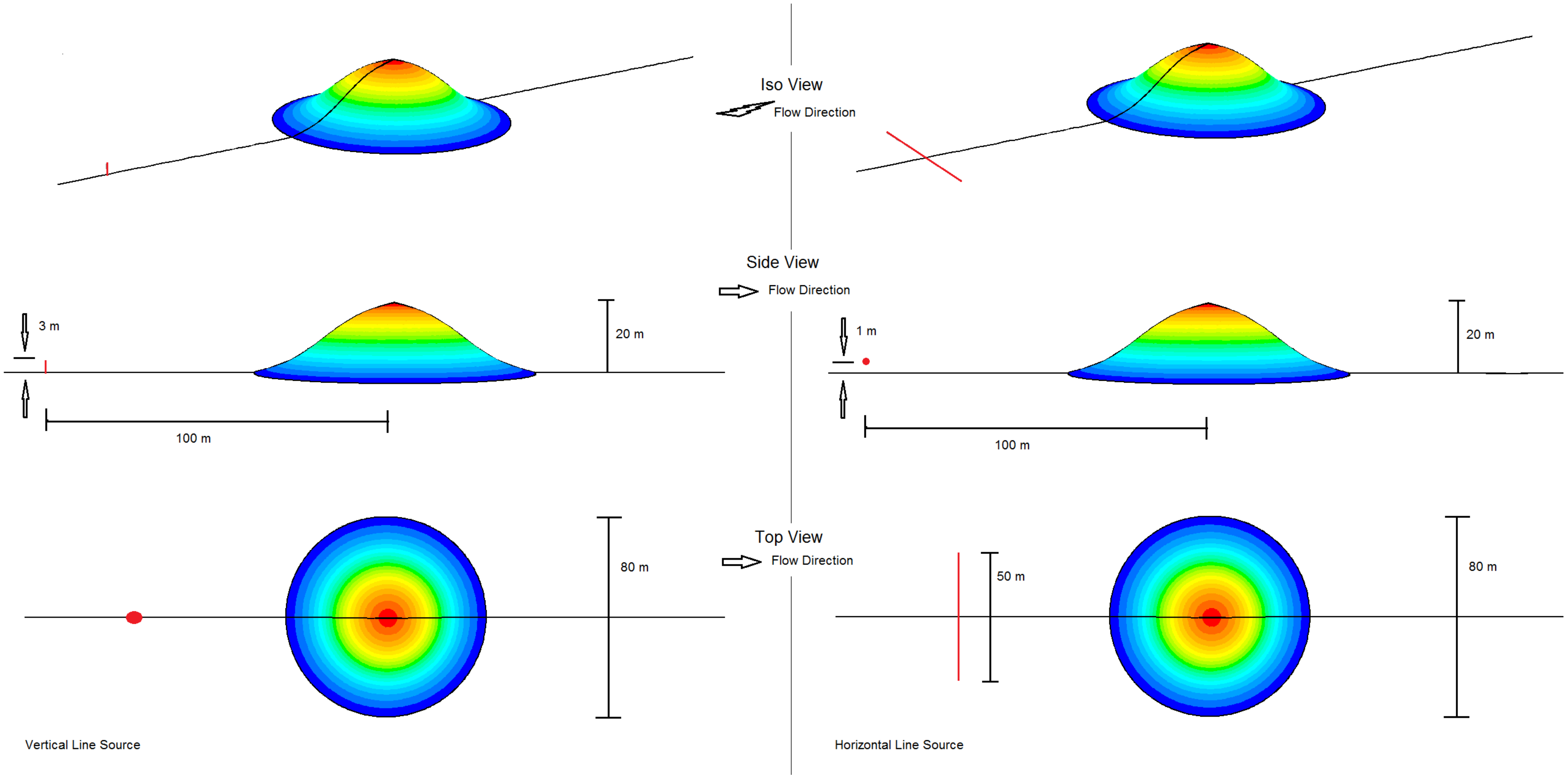

Figure 54 : Vertical (left) and horizontal (right) line source positions upstream 3D hill.

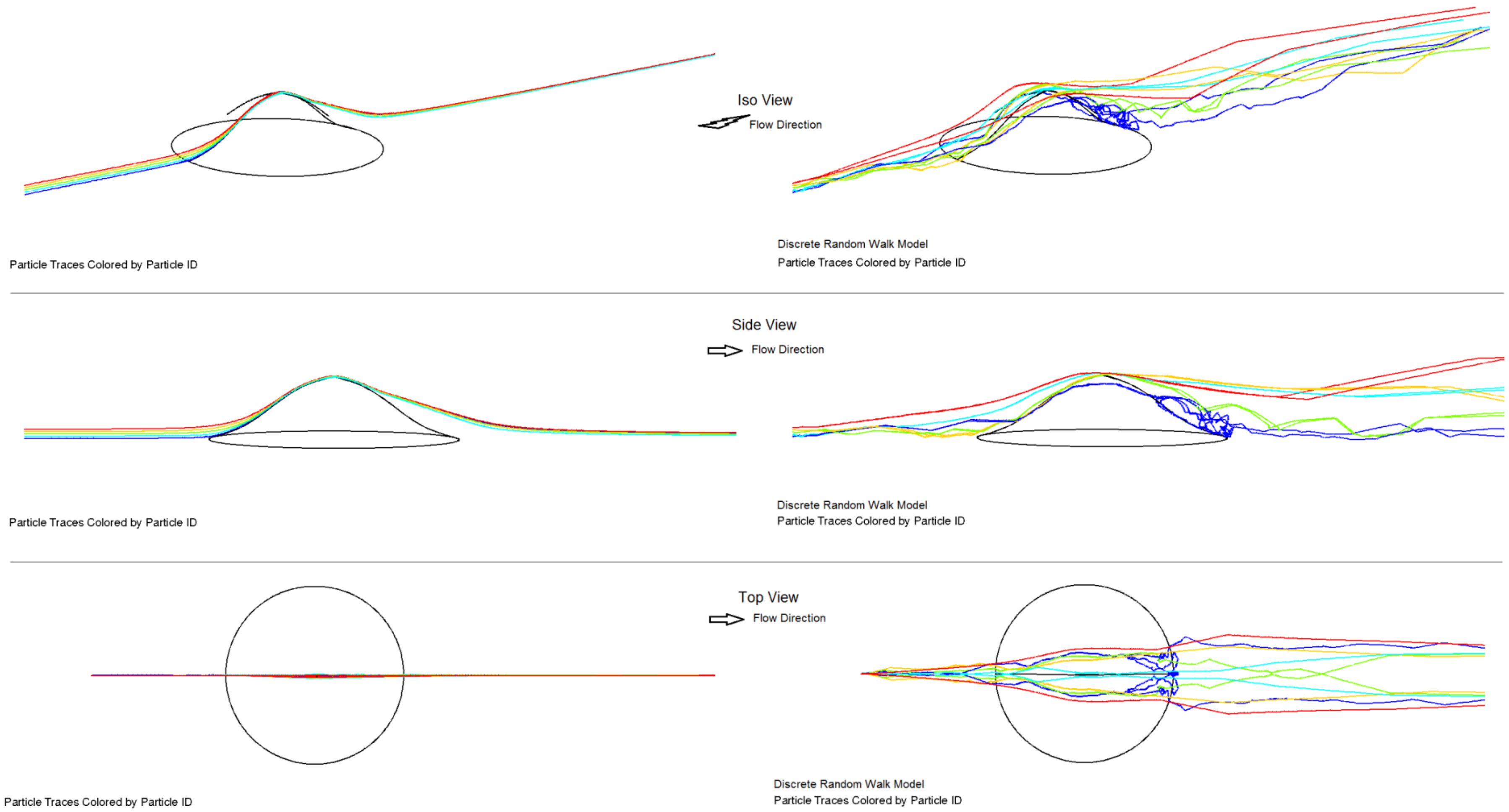

Figure 55 : Particle tracks coloured by particle ID for a vertical line source upstream single 3D hill.

(Plots show; left - standard particle tracking, right - random walk model)

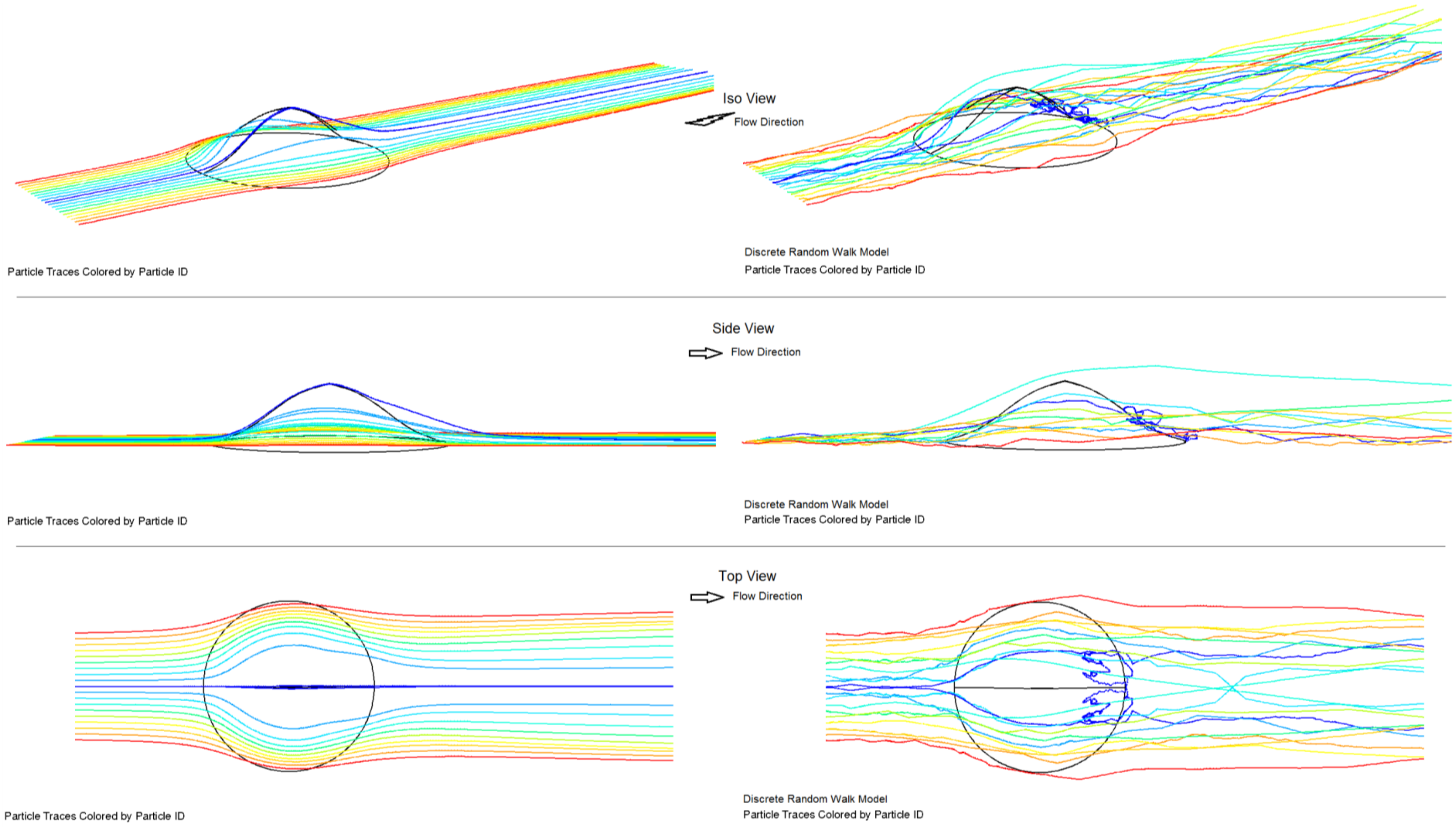

Figure 56 : Particle tracks coloured by particle ID for a horizontal line source upstream single 3D hill.

(Plots show; left - standard particle tracking, right - random walk model)

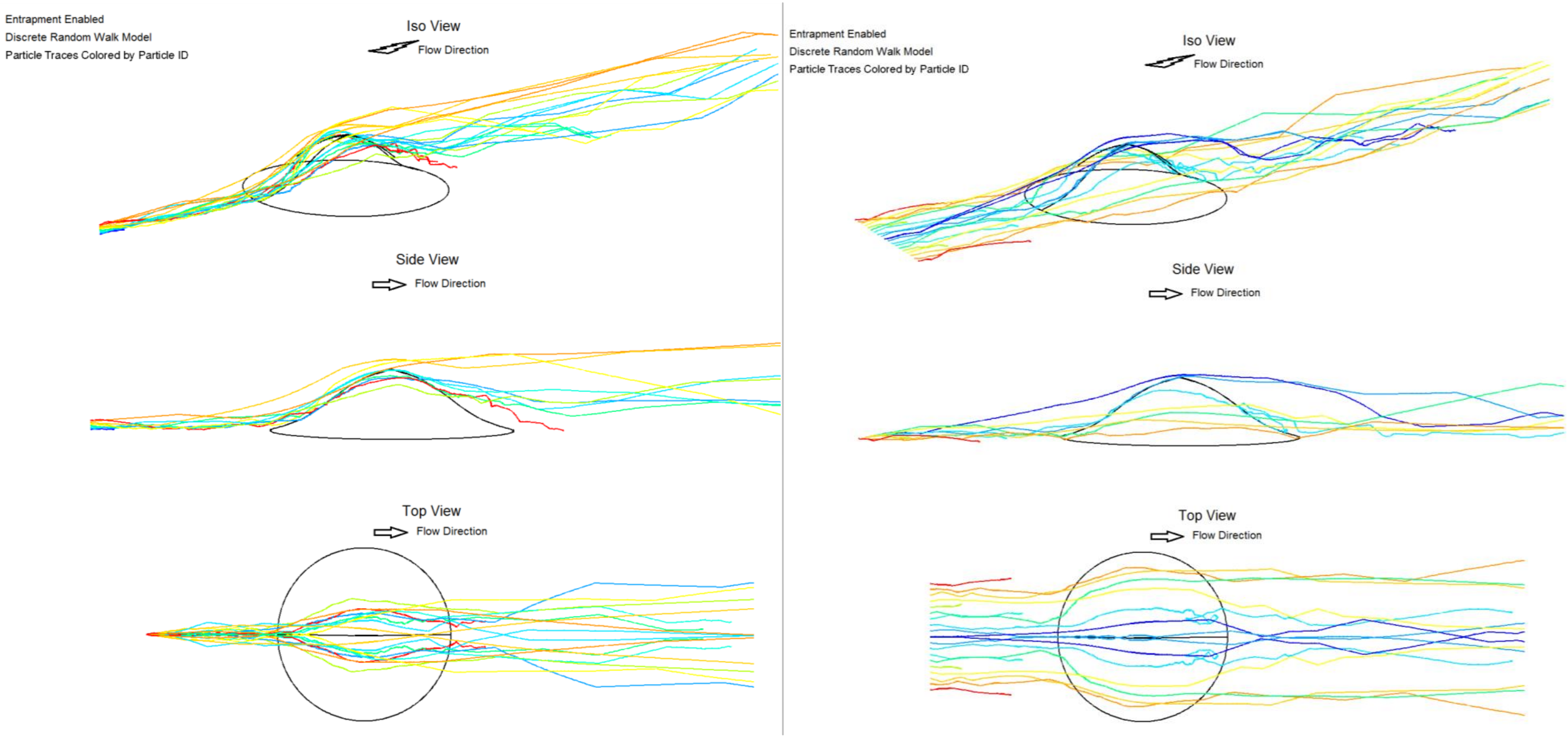

Figure 57 : Particle tracks coloured by particle ID for a vertical line source (left) and a horizontal line source (right) upstream single 3D hill.

(Random walk model and ground entrapment enabled)

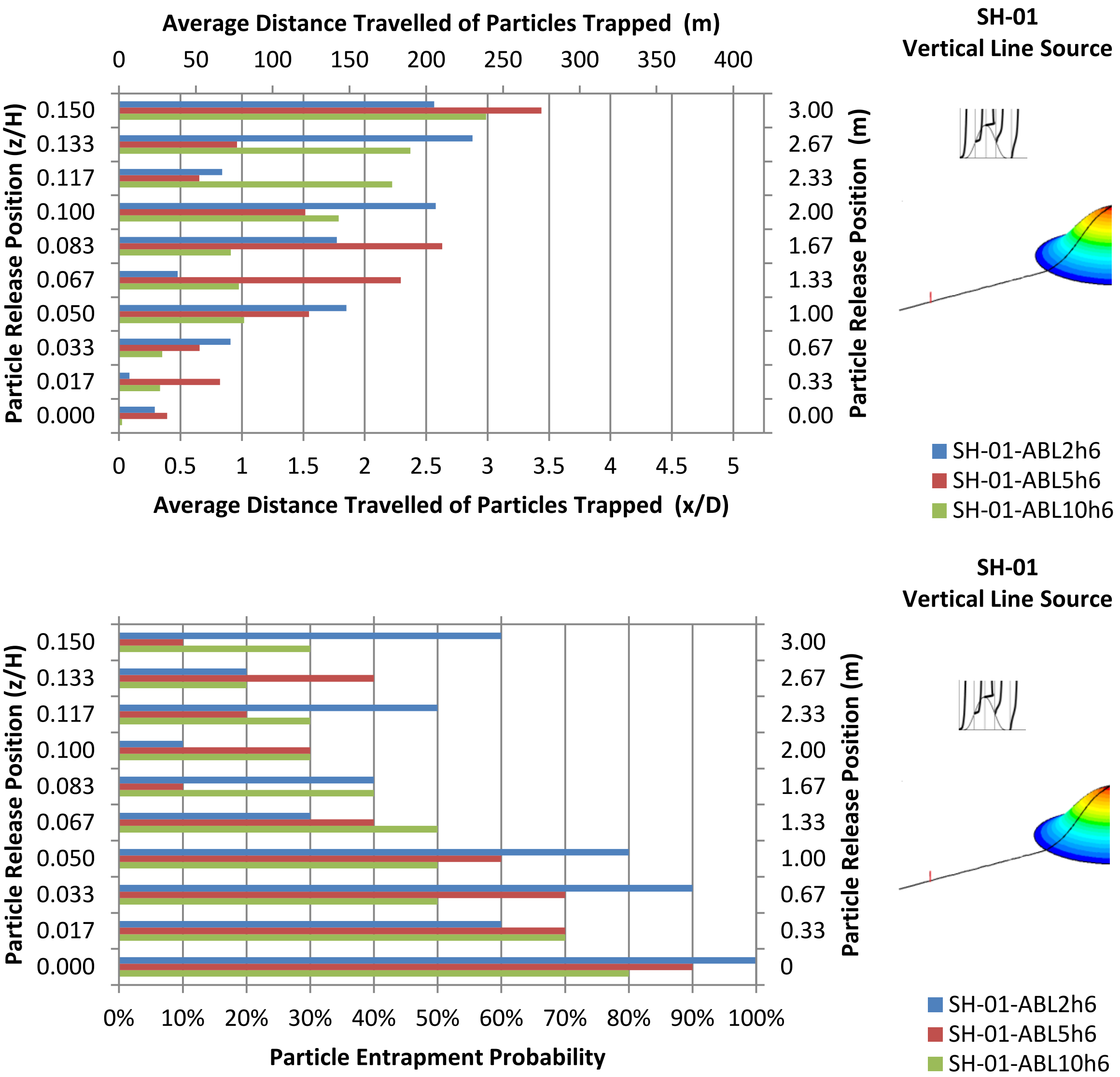

Figure 58 : Average distance travelled and entrapment probability for particles released from a vertical line source upstream single 3D hill for three ABL inlet conditions. (Random walk model and ground entrapment enabled)

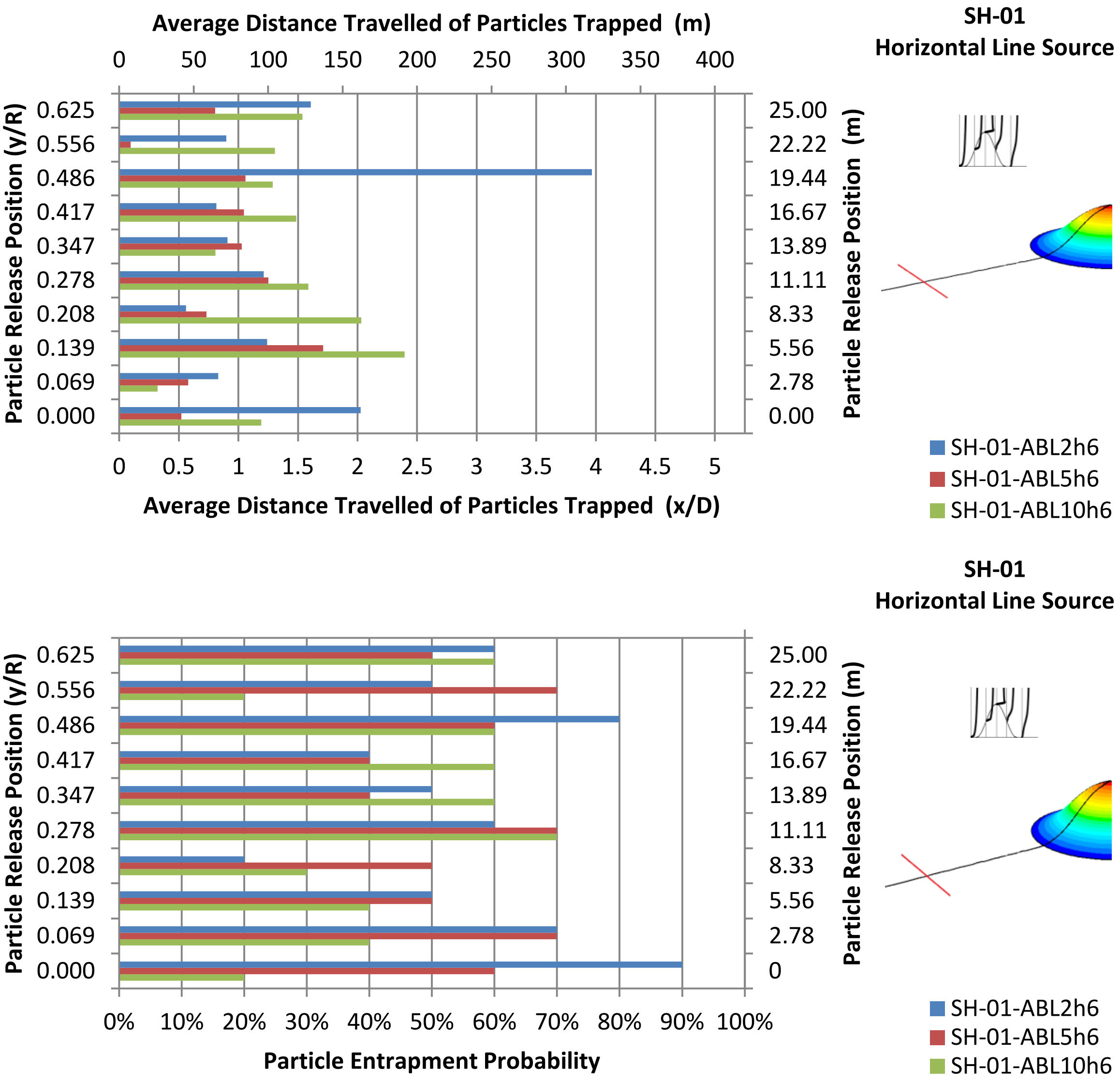

Figure 59 : Average distance travelled and entrapment probability for particles released from a horizontal line source upstream single 3D hill for three ABL inlet conditions. (Random walk model and ground entrapment enabled)

5.4.5 Species Transport over Single 3D Hill

To alternatively examine pollutant dispersion in hilly environments, species transport simulations were conducted for wind flow over a 3D hill, with settings and solver parameters similar to previously described 2D cases. A ground face source was created for these simulations and was placed 100m upwind the hill (Figure 60): it had a length of 5m and a width of 10m (20m when mirrored). Wood species were released from this area source with a constant mean velocity of 1ms^{-1}.

Comparison of wood mole fraction on the symmetry plane downwind the pollutant source for three ABL conditions shows that the lower the ABL mean velocity, the larger the effect of the hill on species mole fraction is (Figure 61). At the lowest mean inlet velocity (ABL2h6) wood mole fraction decreased by 13% on the windward face of the hill and by 4% on the leeward face of the hill. Mole fraction percentages for ABL2h6 were significantly larger than for the highest mean inlet velocity simulated: ABL10h6 (see Figure 62 for a closer wood mole fraction plot at the 3D hill). A comparison of mole fraction values on hill faces for all ABL conditions studied is given in Table 21 and contour plots for all three cases in Figure 63, Figure 64 and Figure 65.

Case Name	**Reduction of Wood Mole Fraction**		**Wood Mole Fraction 4D Downstream Hill**
	Windward Face	**Leeward Face**	
SH-ABL2h6	13%	4%	3.7%
SH-ABL5h6	10%	1.5%	1.5%
SH-ABL10h6	8%	1%	0.7%

Table 21 : Wood mole fraction percentages for mid-plane on hill faces and at 4D downstream single sinusoidal 3D hill.

Contour plots of wood mole fractions present horizontal slices of the wood species cloud for all cases and show that such species travel the maximum distance further from the hill for the lowest inlet condition of ABL2h6. This does not seem to be the case for ABL10h6 for which species reach background fraction as soon as they get to the windward face of the hill. Regarding vertical climb (in the z direction), and in all cases, wood species were seen to reach higher altitudes and travel above the hill height in the case of the lowest inlet velocity ABL2h6 than the highest inlet velocity ABL10h6. In all comparisons, ABL5h6 gave results in-between ABL2h6 and ABL10h6 as expected.

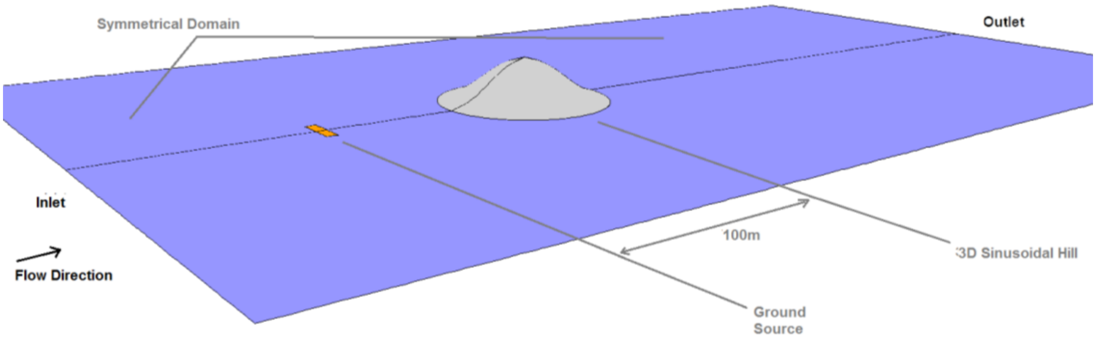

Figure 60 : Single hill 3D domain with ground source simulated for species transport examination.

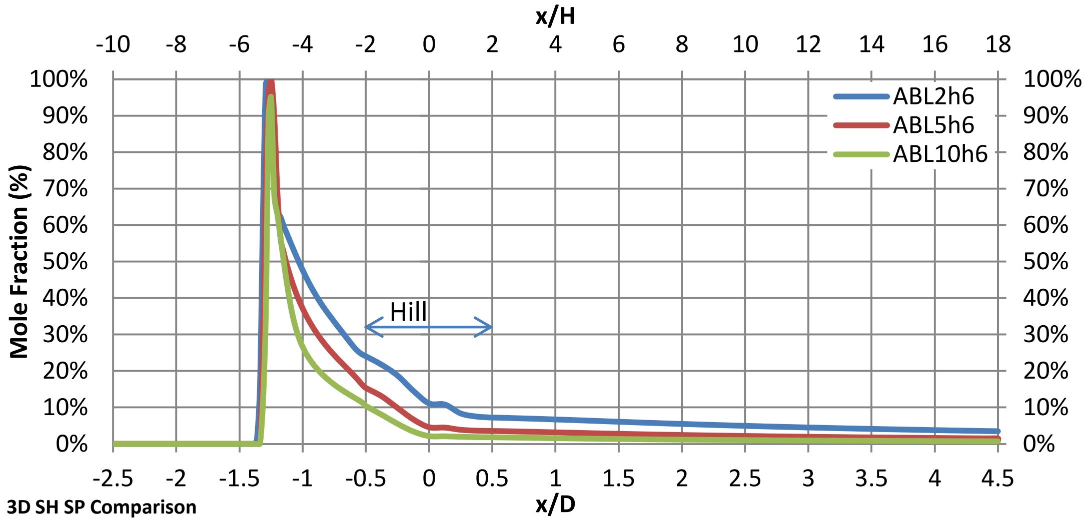

Figure 61 : Wood mole fraction comparisons at lower ground and hill faces on symmetry plane for 3D single hill for three ABL logarithmic inlet profiles. ($\overline{u}$=2ms^{-1}, $\overline{u}$=5ms^{-1}, $\overline{u}$=10ms^{-1}, all at reference height h_{ref}=6m)

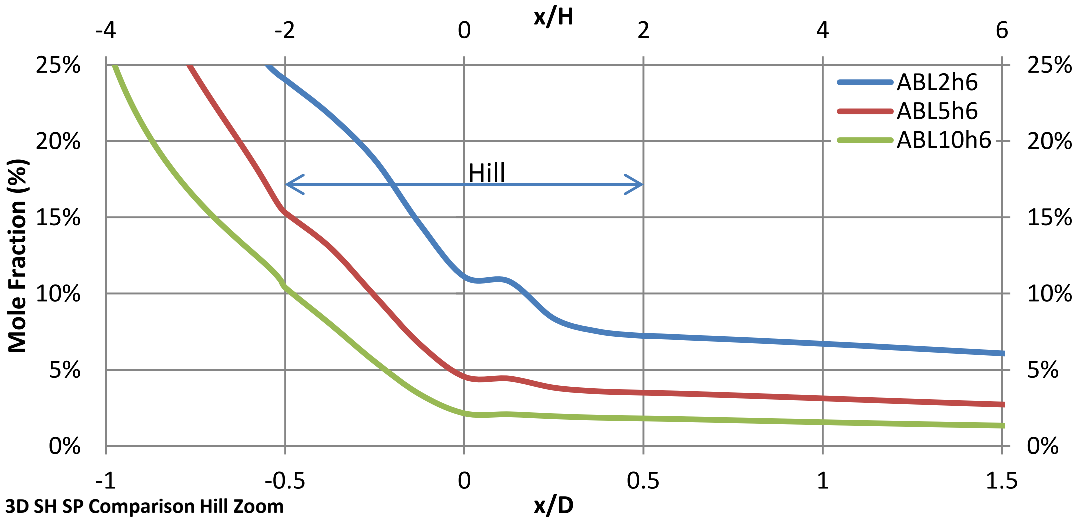

Figure 62 : Wood mole fraction comparisons at lower ground and hill faces on symmetry plane for 3D single hill for three ABL logarithmic inlet profiles (zoomed in view for comparison of hill effects).

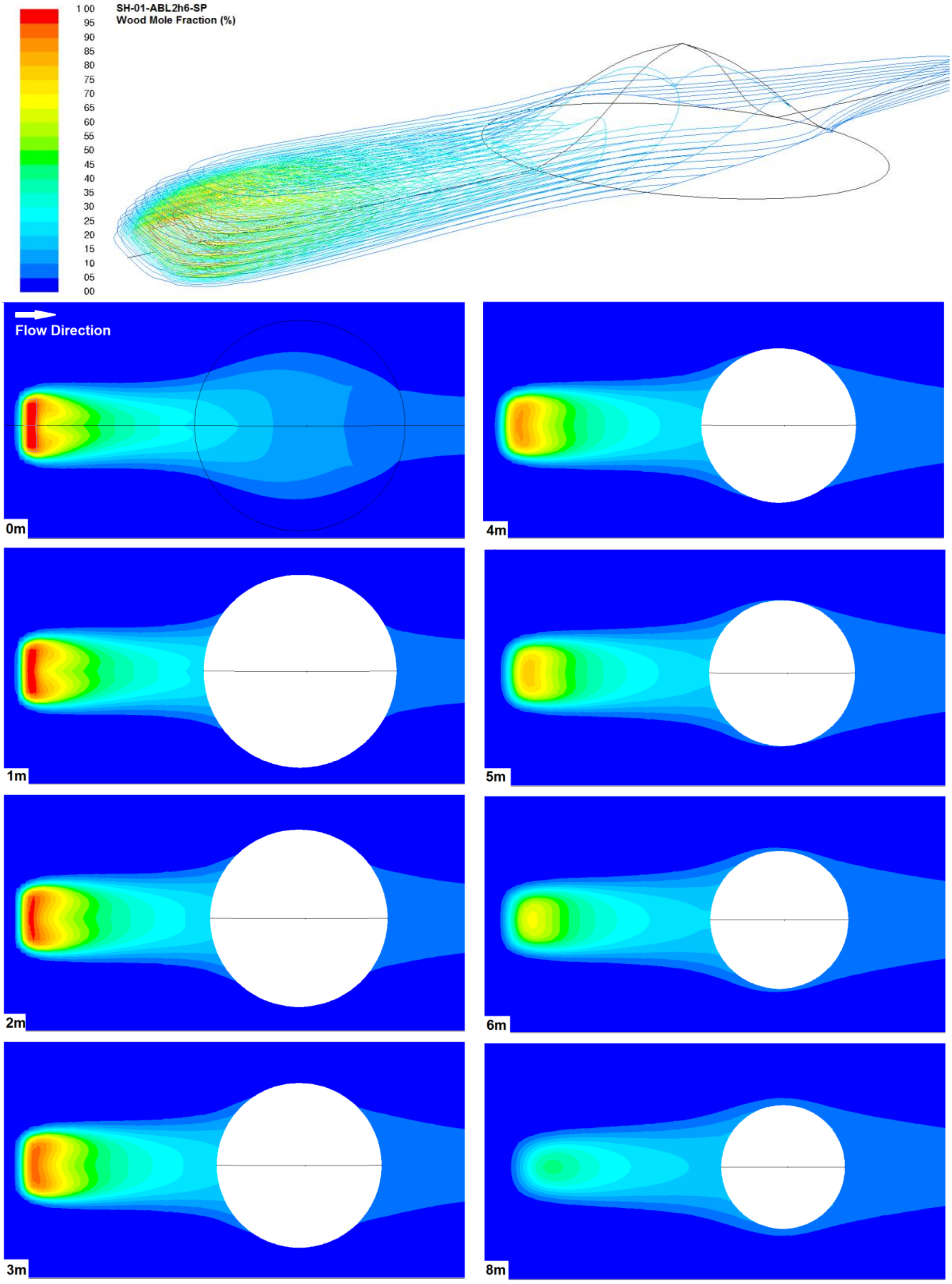

Figure 63: Contour plots of wood mole fraction (%) on and above ground level for single sinusoidal 3D hill with inlet ABL2h6 (isometric and top views).

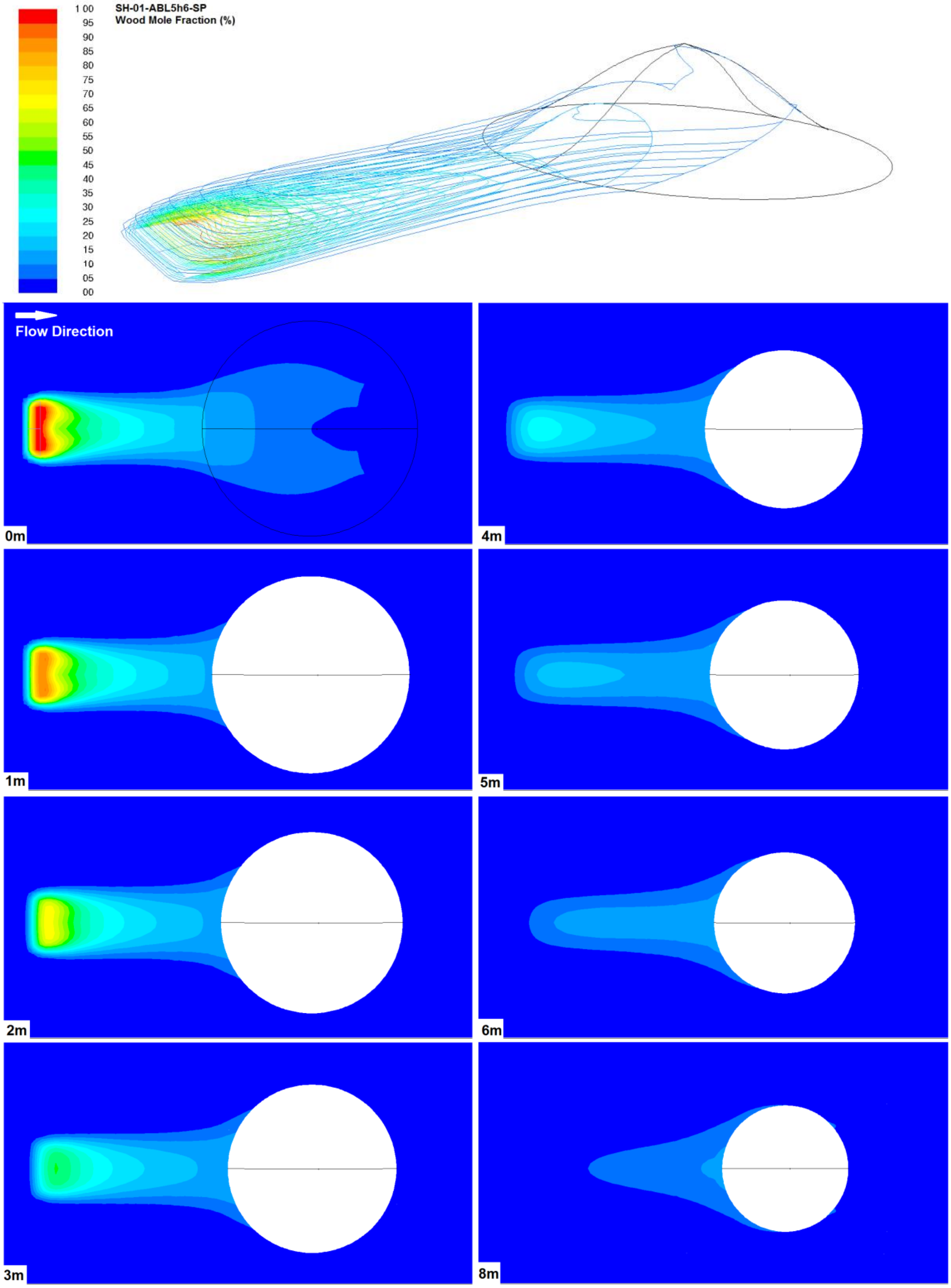

Figure 64 : Contour plots of wood mole fraction (%) on and above ground level for single sinusoidal 3D hill with inlet ABL5h6 (isometric and top views).

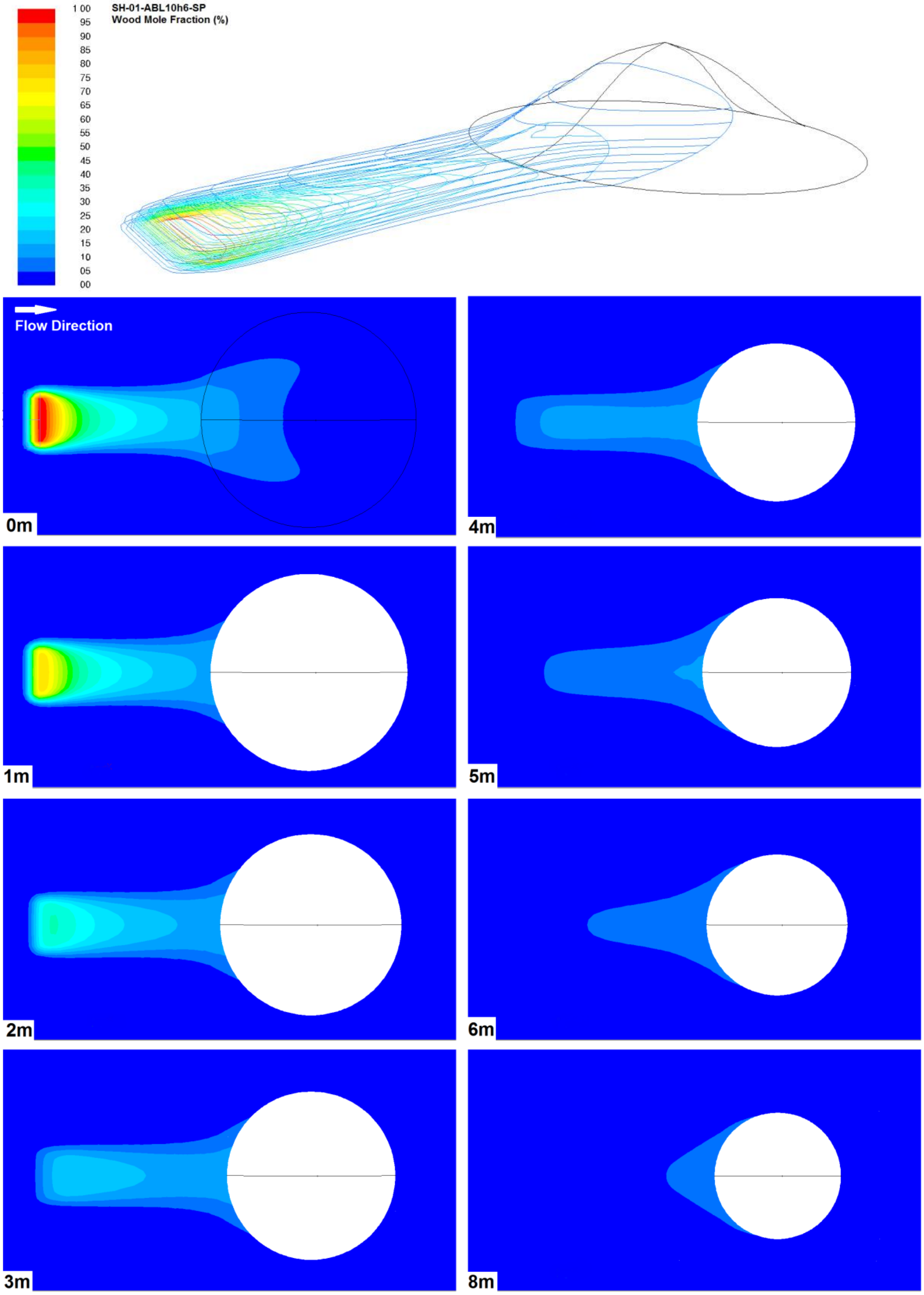

Figure 65 : Contour plots of wood mole fraction (%) on and above ground level for single sinusoidal 3D hill with inlet ABL10h6 (isometric and top views).

5.5 Wind Flow and Pollution Dispersion over Double 3D Hills

5.5.1 Introduction

To further examine effects of terrain geometry on wind flow and pollution dispersion, double 3D sinusoidal hills were simulated. These additional cases were all conducted with two hills which were distanced 2.5D (200m) apart. With the double hill approach, the wind flow effect of the first hill to the second hill was examined together with the hill effect on pollutant dispersion. Figure 66 shows a 2D side view of the three domains examined with steep and shallow sinusoidal 3D hills in a single row.

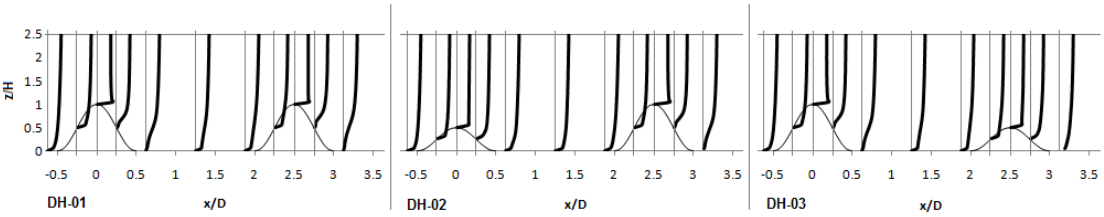

Figure 66 : Side view of 3D domains simulated with double hills.

Table 22 summarises all 3D double hill cases simulated. Variable profiles, contour plots, particle tracking information and species transport data are all presented for results comparison as previously shown for the case of wind flow and pollutant dispersion over single 3D sinusoidal hill.

Case Name	$\overline{u}$ at 6m Ref Height	1st Hill Info	2nd Hill Info	Orientation
DH-01	2ms^{-1}	H=20m D=80m	H=20m D=80m	In single row
DH-02	5ms^{-1}	H=10m D=80m	H=20m D=80m	In single row
DH-03	10ms^{-1}	H=20m D=80m	H=10m D=80m	In single row

Table 22 : Double hill 3D simulations conducted.

The domain size selection regarding three double hill simulations was based on the domain size study for the single 3D hill. Thus, the distance upwind the first hill was F4, downwind the second hill was B8, sideways was S3 and above the highest hill was A4 with the resulting domain being an extended version of the original domain for the single 3D hill case. The same applies for the mesh density with all three domains having the exact same characteristics of the proposed mesh with 1m interval size on hill and ground faces and a growing mesh up to 10m at boundaries.

All options in the pre-processing stage were set exactly as for the single 3D hill: all cases were solved for three inlet conditions (2, 5 and 10ms^{-1} R&H suggested logarithmic profiles) with particle tracking and species transport following the initial 3D wind flow solution.

5.5.2 Wind Flow and Particle Tracking over Double 3D Hills

Recirculation zones and reattachment length results from double hills were studied and compared to each other by plotting horizontal velocity variation along the ground and hill faces as well as at height H above ground, all on the symmetry plane (Figure 67). Mean wind speed profiles above hill for the vertical z direction referring to all three domain geometries are presented in Figure 68 for inlet condition ABL10h6.

Dimensionless velocity plots for all three inlet ABL conditions regarding the same hill geometry combination were seen to overlap as previously noted for the case of single 2D and 3D hills. The important difference in results was seen regarding the dissimilar hill combinations studied. In detail, for the case of double steep hills (DH-01), wind flow accelerated up the first steep hill reaching maximum velocity at the summit. Velocity plot at height H (Figure 67a) was seen to have two equal peaks above the two hill tops. Wind velocity dropped further on the windward face of Hill 2 than of Hill 1 and did not fully recover before the wind exited the domain. Velocity plots for the ground face (Figure 67b) showed that the recirculation zone after Hill 2 had lower velocities than Hill 1 with also a slightly larger reattachment length; 0.8D for Hill 2 and 0.7D for Hill 1.

In the case of steep and shallow hills (DH-02), Hill 1 being half the height of Hill 2 acted as a damper for the wind flow reaching Hill 2. Velocity plot at height H atop Hill 2 was larger than for Hill 1 as expected but reattachment length was smaller for Hill 2 when compared to DH-01: 0.7D.

In the case of steep and shallow hills (DH-03), the steeper and higher Hill 1 acted as a wind barrier to the shallower and lower Hill 2. The flow over Hill 1 was much the same as in DH-01 but the maximum wind speed on top of Hill 2 was much lower with no recirculation after the leeward face.

Contour plots for all cases simulated can be found in Appendix 3. These contain side views of the pressure coefficient and wind speed distributions above hills at the mid plane; top views of turbulence kinetic energy at a normal distance of 1m above ground and hills are also included. For DH-01, the acceleration of the wind up the slope created low pressure on the windward side of the hills. Pressure coefficient values were lower on the windward face of Hill 2 than that of Hill 1. Turbulence kinetic energy increased rapidly as the wind raced up the slope and its values remained high on the leeward face; its maximum values were reached on top of Hill 2. Distributions of pressure coefficient and turbulence kinetic energy in DH-01 were representative of the other two domains. In DH-03, the higher Hill 1 decreased the turbulence kinetic energy over Hill 2 by up to 30% compared with that in the other two cases.

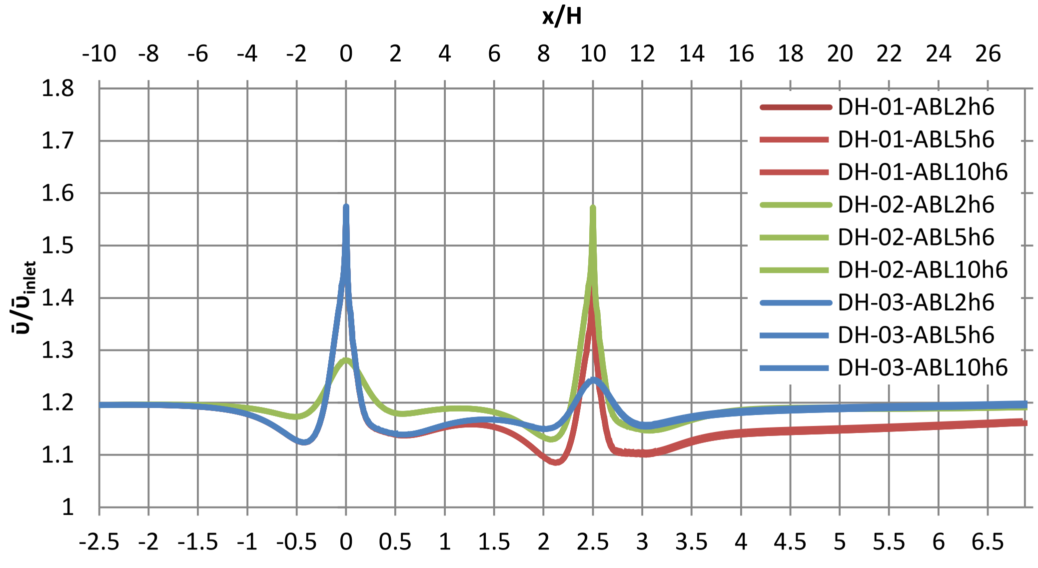

(a) $\bar{u}/\bar{u}_{inlet}$ 3D SH Comparison @ 1m

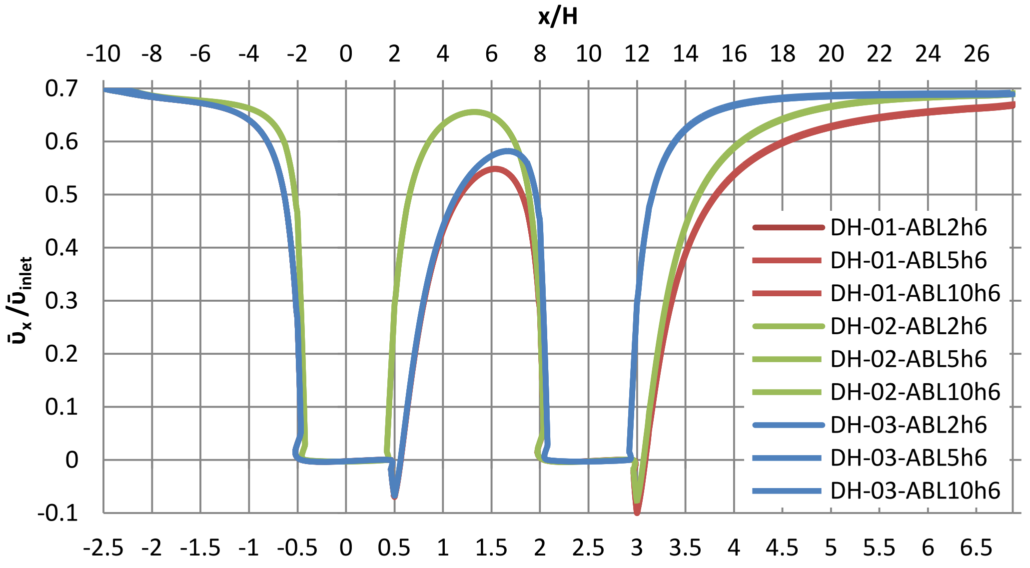

(b) $\bar{u}_x/\bar{u}_{inlet}$ 3D SH Comparison @ 1m

Figure 67 : Horizontal profile plots of (a) velocity magnitude at H above ground and (b) velocity at first cell above ground level for wind flow over double 3D sinusoidal hills.

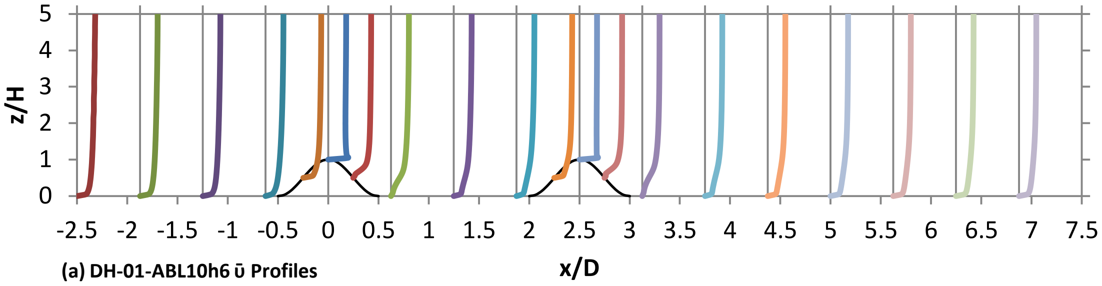

(a) DH-01-ABL10h6 ū Profiles

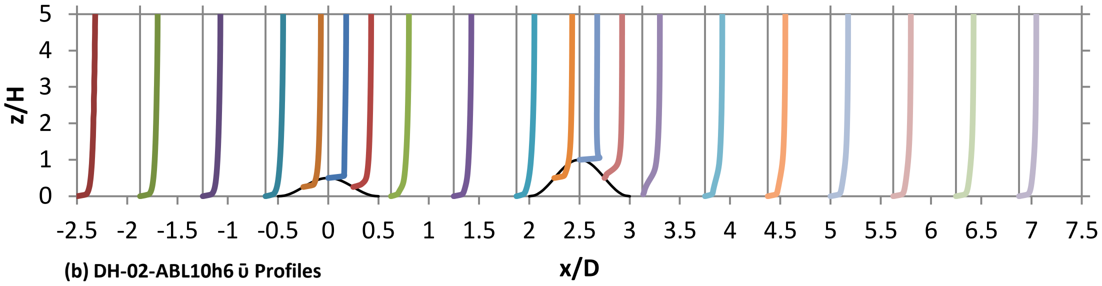

(b) DH-02-ABL10h6 ū Profiles

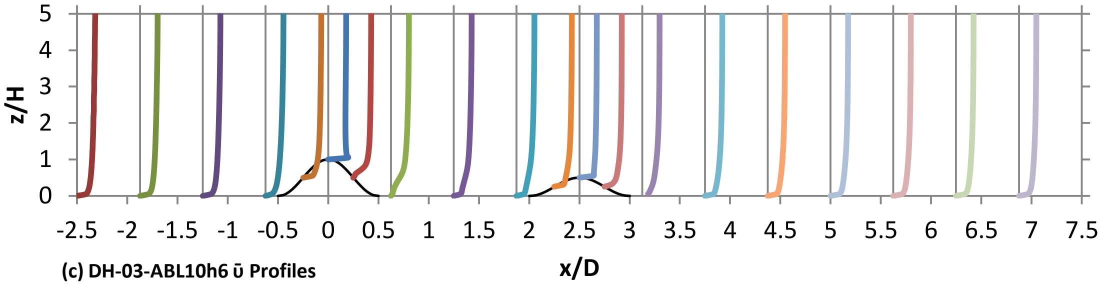

(c) DH-03-ABL10h6 ū Profiles

Figure 68 : Profiles of mean velocity magnitude for mid-plane (side view) over three combinations of double 3D hills studied with inlet condition ABL10h6.

As for the case of single 3D hill, one way particle tracking was enabled for 'mass-less' particles which were released from two line sources 100m upstream the first hill; a vertical and a horizontal line source as described earlier in this work. Results for both line sources and for all three ABL inlet conditions are presented in Figure 70, Figure 72, Figure 74, Figure 76, Figure 78 and Figure 80. These were statistically post-processed to give averaged travelled distance of trapped particles and entrapment probability percentages with respect to the initial release conditions.

The damping and obstructing effects of the shallow and steep hills respectively to the wind flow were found to also interact with the particle tracking results; particles were observed to travel further when Hill 1 was shallow than when Hill 1 was steep. The recirculation zones at the leeward side of steep hills drove particles to the ground face where these were trapped. When no recirculation zone existed (shallow hill), particles travelled larger distances before landing on ground faces and eventually getting absorbed.

For trapped particles released from the vertical line source, average distance travelled was found similar for all domains (Figure 70, Figure 74 and Figure 78). Particles released from the highest streams of the source travelled further than those released near ground positions which were more likely to get trapped either on the windward face of Hill 1 or in the recirculation zone of same hill if steep. In general, the higher the particle release position, the further particles were seen to travel. Particles released between 1m and 2m above the ground were most likely to be trapped on the windward face of Hill 1 or in the leeward recirculation of the same hill if steep. For domains DH-01 and DH-02 which include a steep Hill 2, particles released from 2 to 3m above ground were trapped on the windward face of Hill 2 and in its recirculation. This was not the case for domain DH-03 which had a shallow Hill 2.

On the other hand, for trapped particles released from the horizontal line source, the average distance travelled was similar for domains with steep Hill 1 (DH-01, Figure 72 and DH-03, Figure 80) but dissimilar for the domain with shallow Hill 1 (DH-02, Figure 76). All the results show that particles spread mostly sideways around the hills and only those released from positions at or close to the symmetry plane travelled above the hills. This was probably due to the low vertical distance (height) of the horizontal source from the ground.

For all three domains, particles released closer to the symmetry plane (centre of hill) at positions 0 to 8m travelled the shortest distances as these were trapped on the windward face of Hill 1 or in the recirculation zone of Hill 1 when steep. Particles released from positions 10 to 14m travelled short distances as they were trapped on the windward face of Hill 2 or in its recirculation zone when steep. In particular, DH-01 and DH-03, both having a steep first hill, showed a similar pattern of average trapped particle distances and entrapment probability. In the case of DH-02 which had a shallow Hill 1, probability of particles getting trapped when released from the horizontal source was smaller than for DH-01 and DH-03. In the case of DH-03, most of the particles were trapped on the leeward face of steep Hill 1 or in its leeward recirculation, with only a few particles reaching the shallow Hill 2.

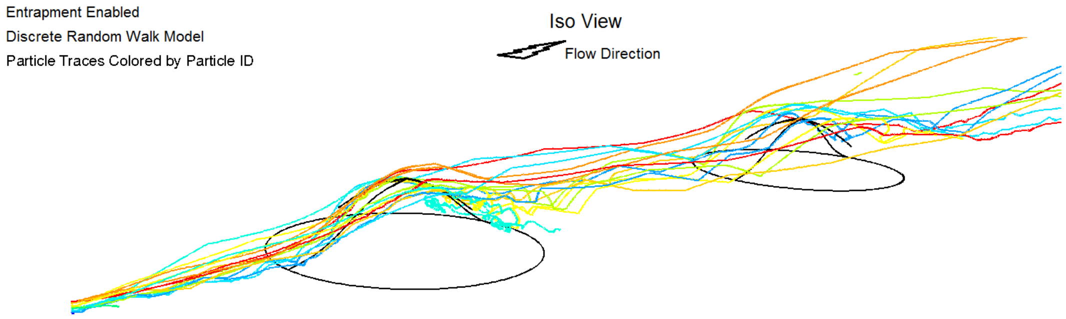

Figure 69 : Isometric view of particle tracks coloured by particle ID for a vertical line source upstream two steep 3D hills.

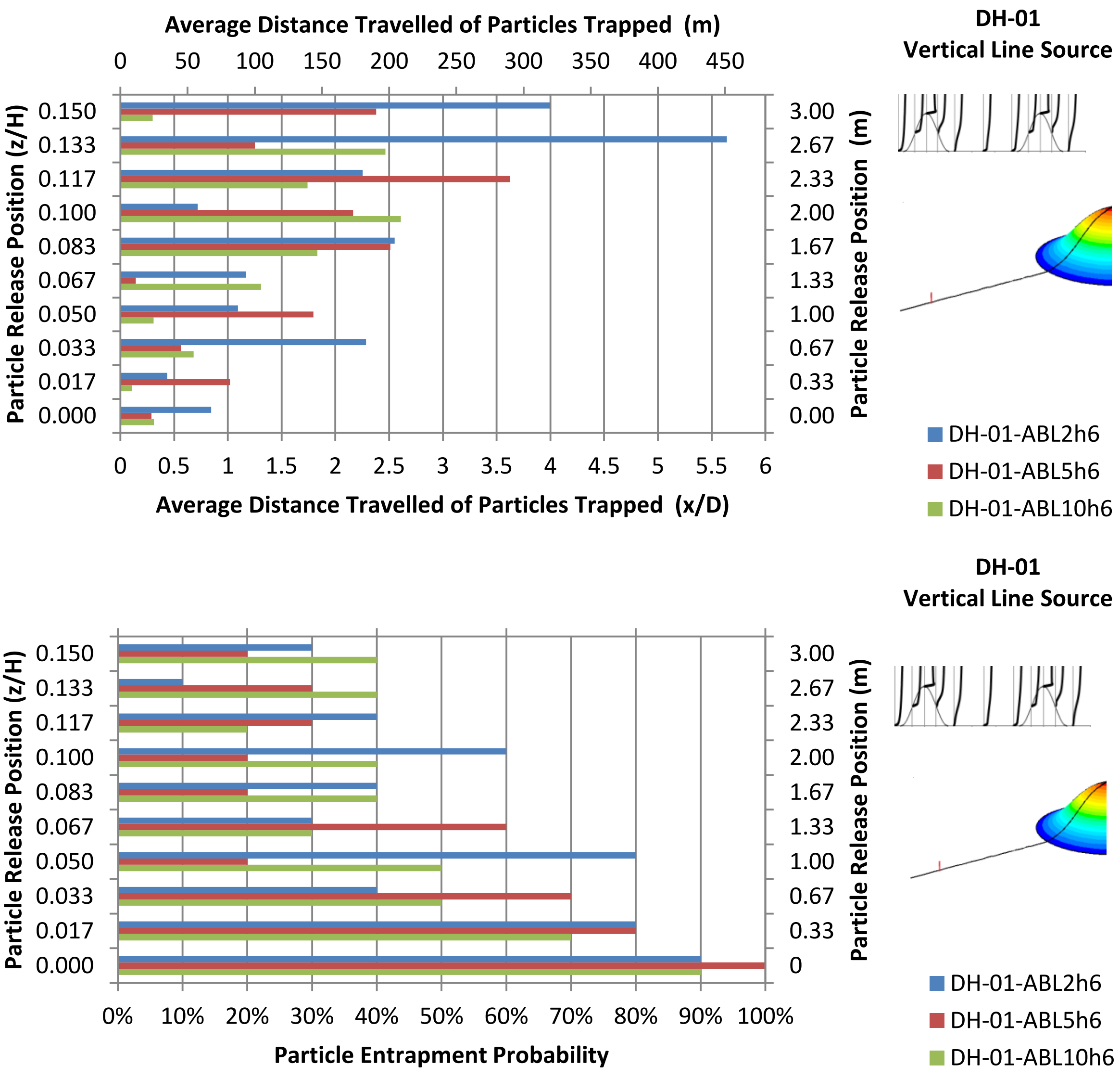

Figure 70 : Average distance travelled of particles trapped (top) and particle entrapment probability (bottom) plots for particles released from a vertical line source upstream two steep 3D hills for three ABL inlet conditions.

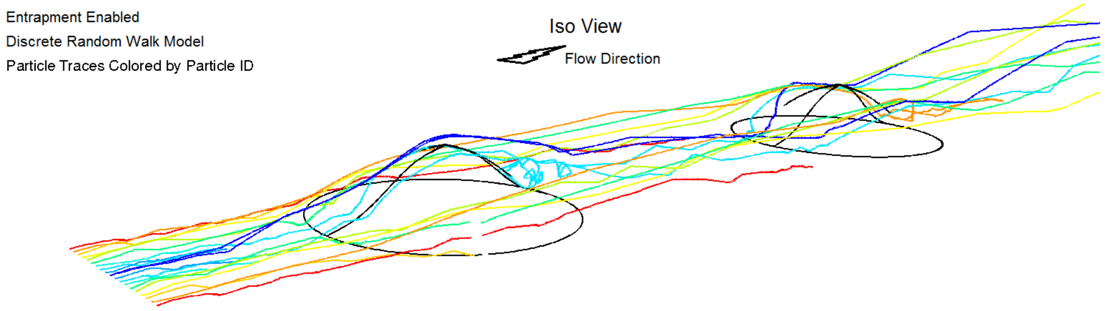

Figure 71 : Isometric view of particle tracks coloured by particle ID for a horizontal line source upstream two steep 3D hills.

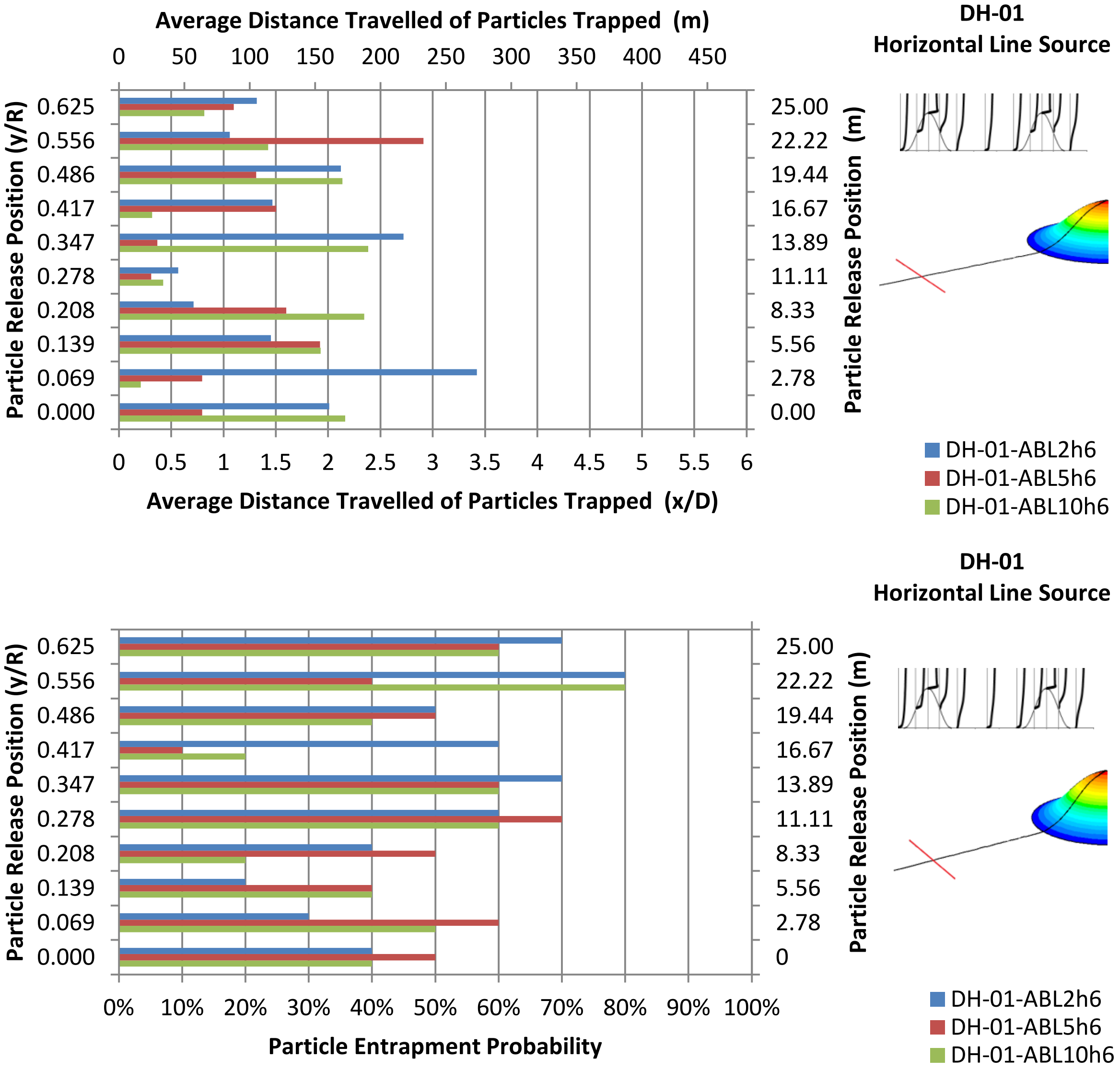

Figure 72 : Average distance travelled of particles trapped (top) and particle entrapment probability (bottom) plots for particles released from a horizontal line source upstream two steep 3D hills for three ABL inlet conditions.

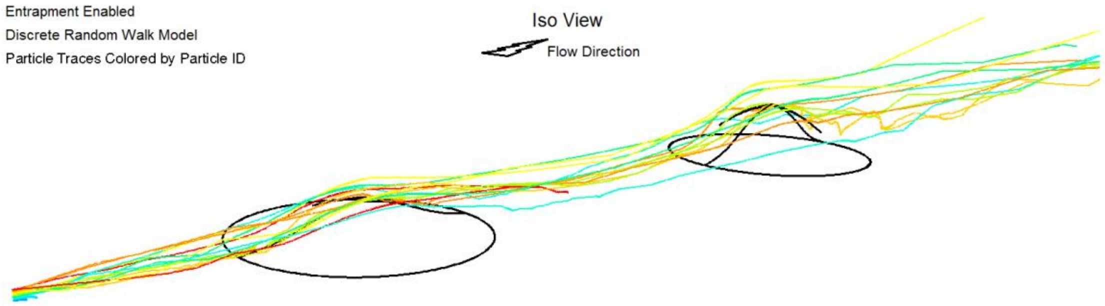

Figure 73 : Isometric view of particle tracks coloured by particle ID for a vertical line source upstream shallow and steep 3D hills.

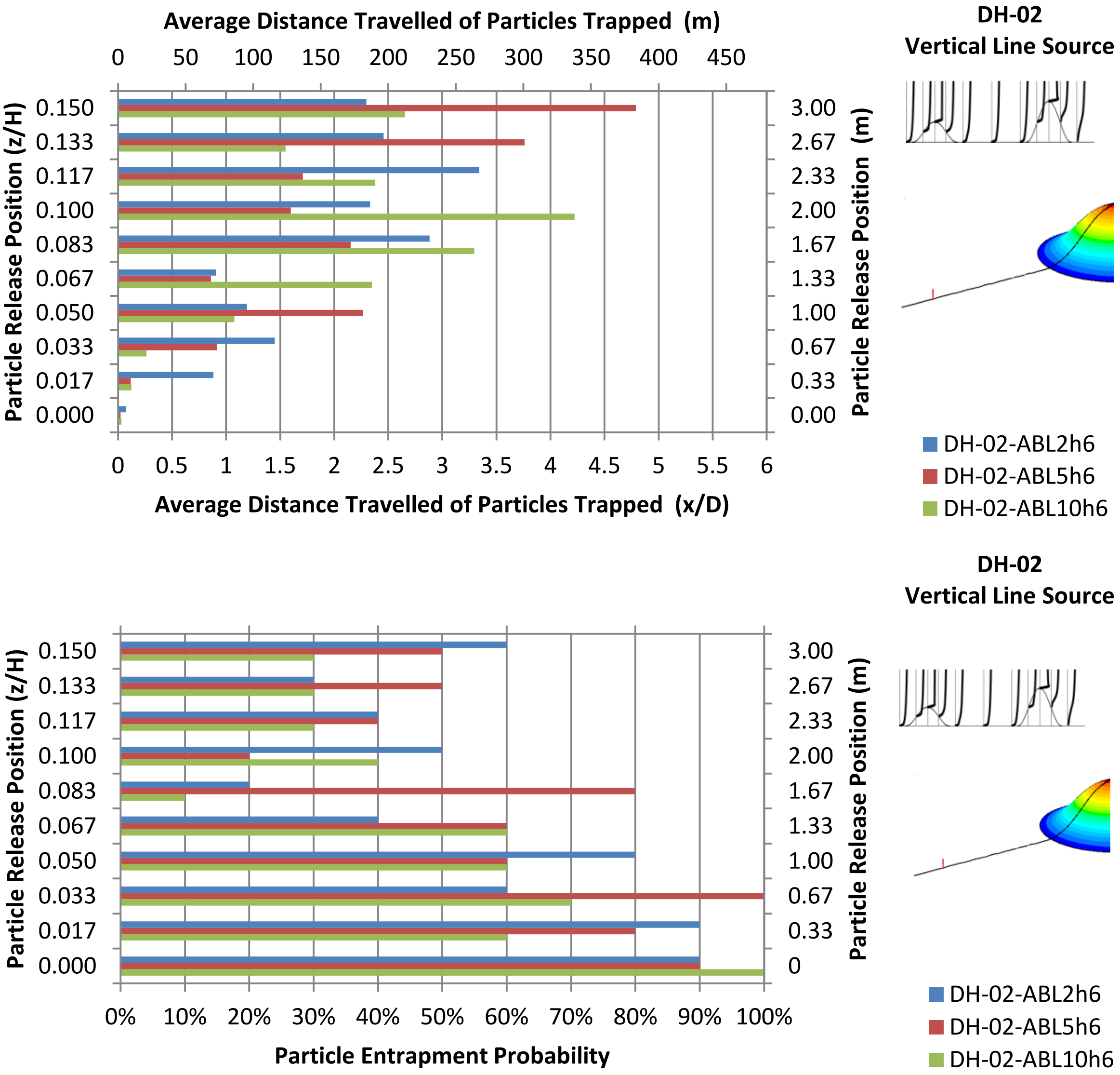

Figure 74 : Average distance travelled of particles trapped (top) and particle entrapment probability (bottom) plots for particles released from a vertical line source upstream shallow and steep 3D hills for three ABL inlet conditions.

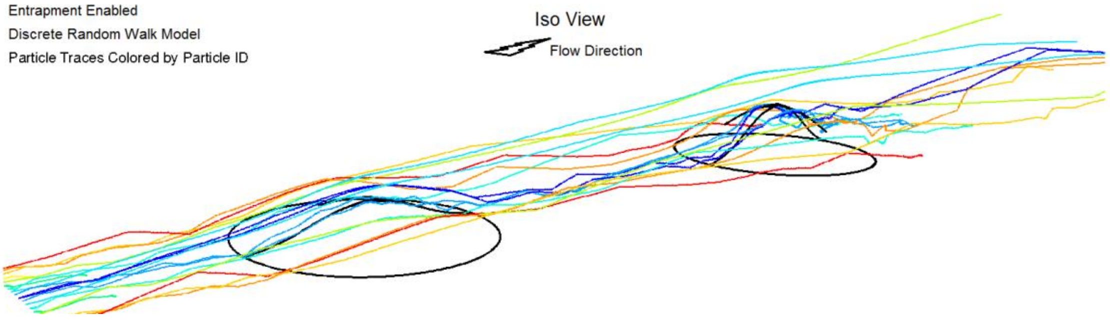

Figure 75 : Isometric view of particle tracks coloured by particle ID for a horizontal line source upstream shallow and steep 3D hills.

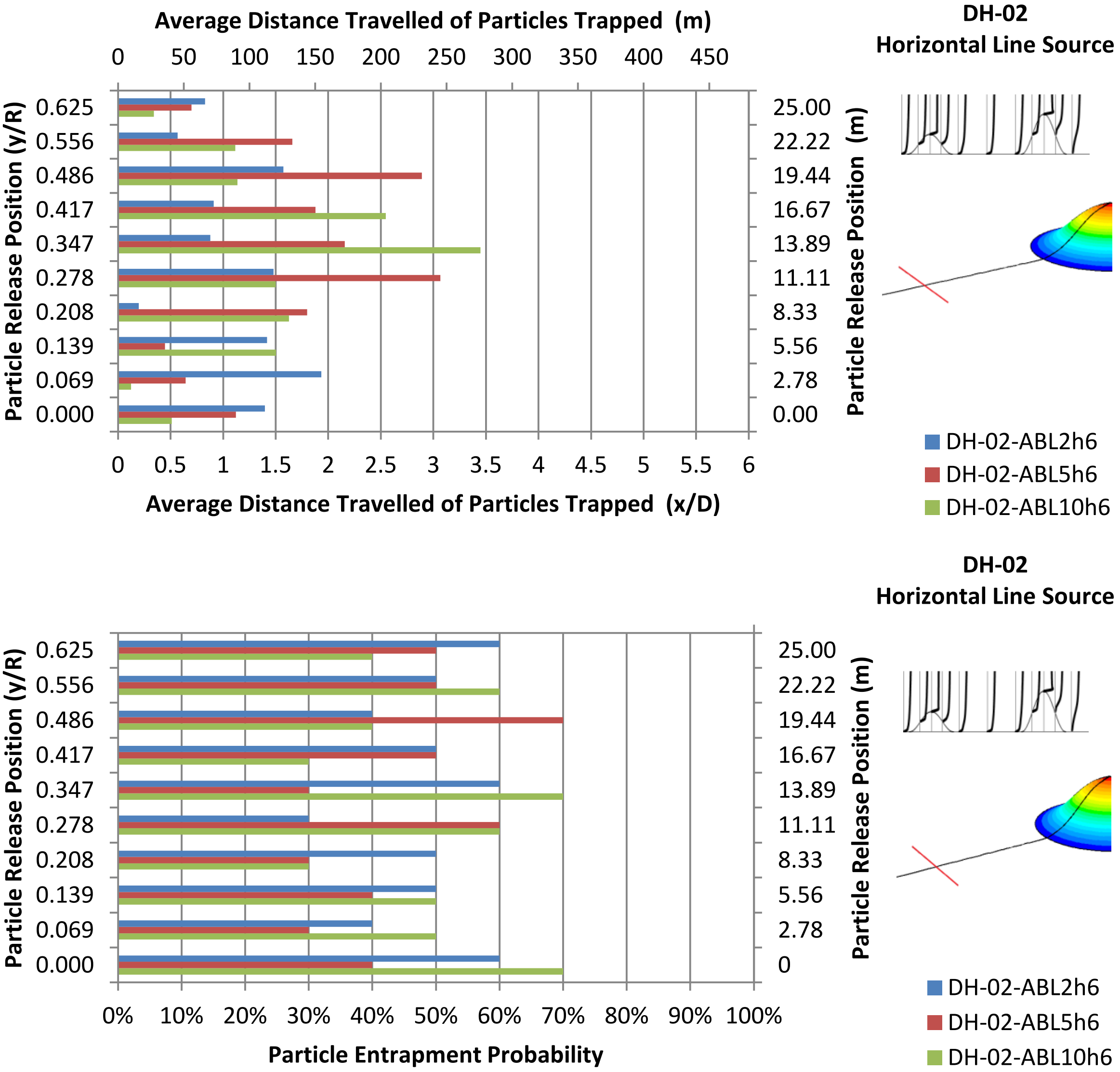

Figure 76 : Average distance travelled of particles trapped (top) and particle entrapment probability (bottom) plots for particles released from a horizontal line source upstream shallow and steep 3D hills for three ABL inlet conditions.

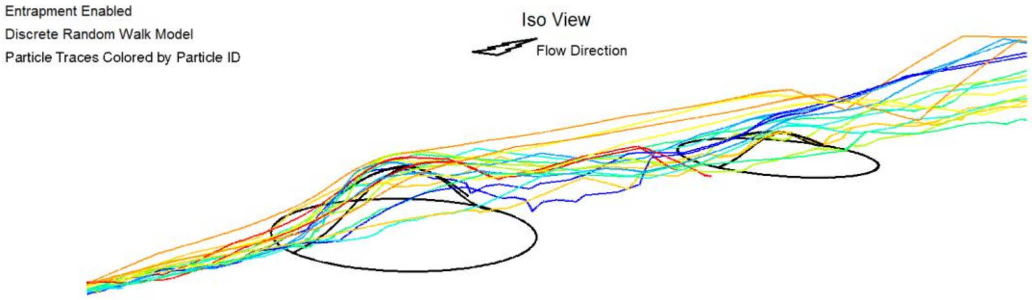

Figure 77 : Isometric view of particle tracks coloured by particle ID for a vertical line source upstream steep and shallow 3D hills.

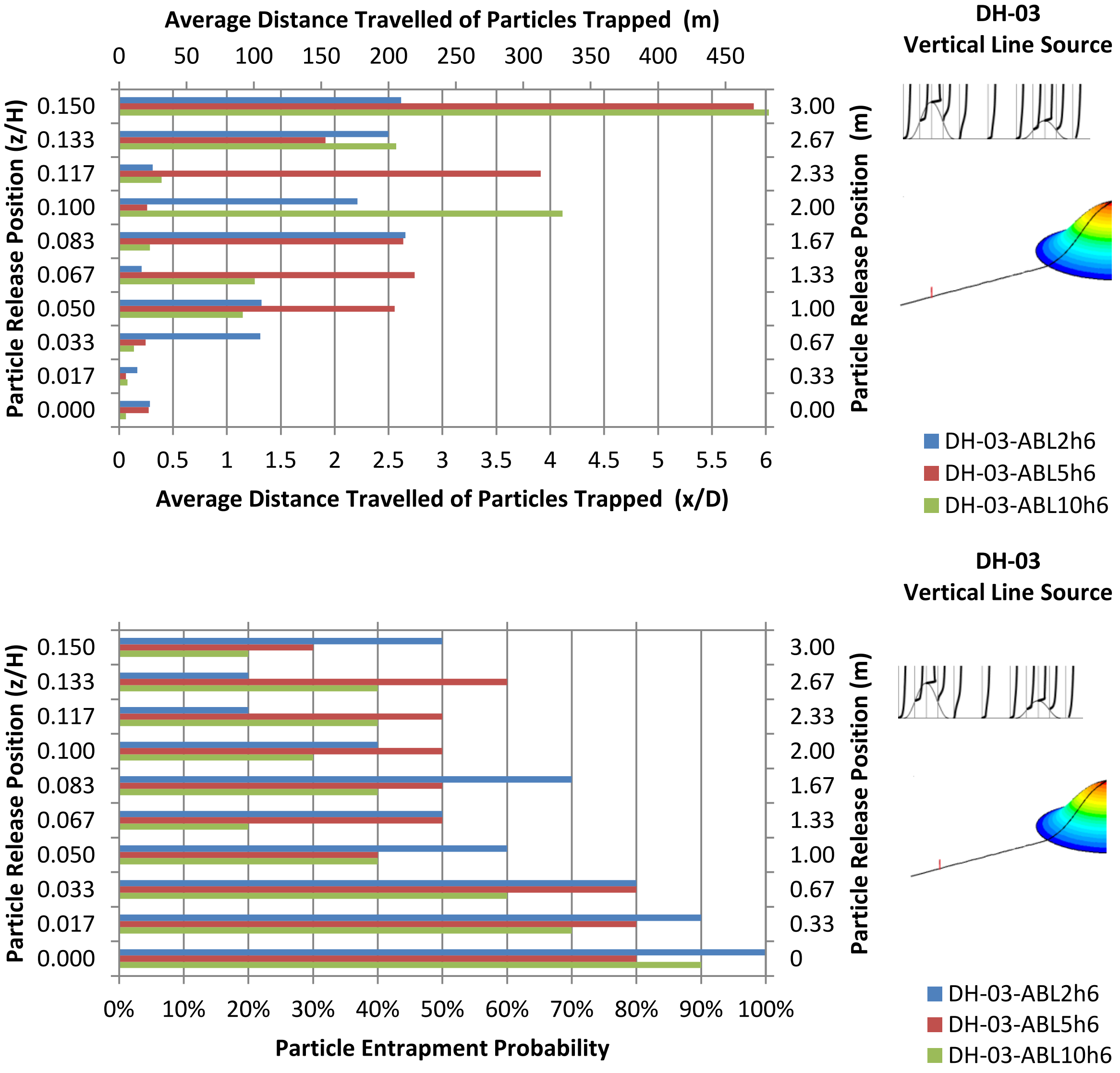

Figure 78 : Average distance travelled of particles trapped (top) and particle entrapment probability (bottom) plots for particles released from a vertical line source upstream steep and shallow 3D hills for three ABL inlet conditions.

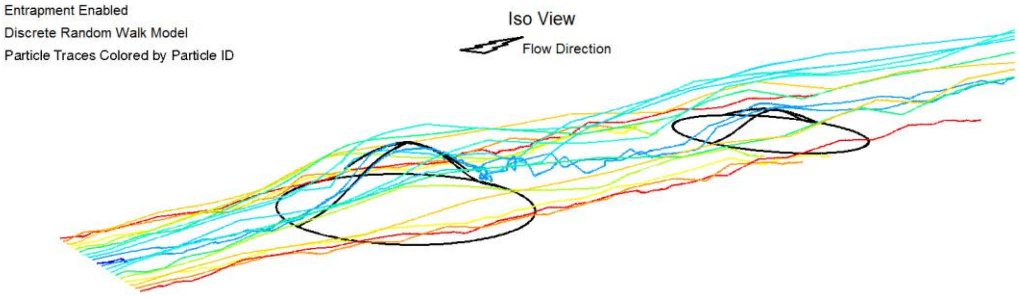

Figure 79 : Isometric view of particle tracks coloured by particle ID for a horizontal line source upstream steep and shallow 3D hills.

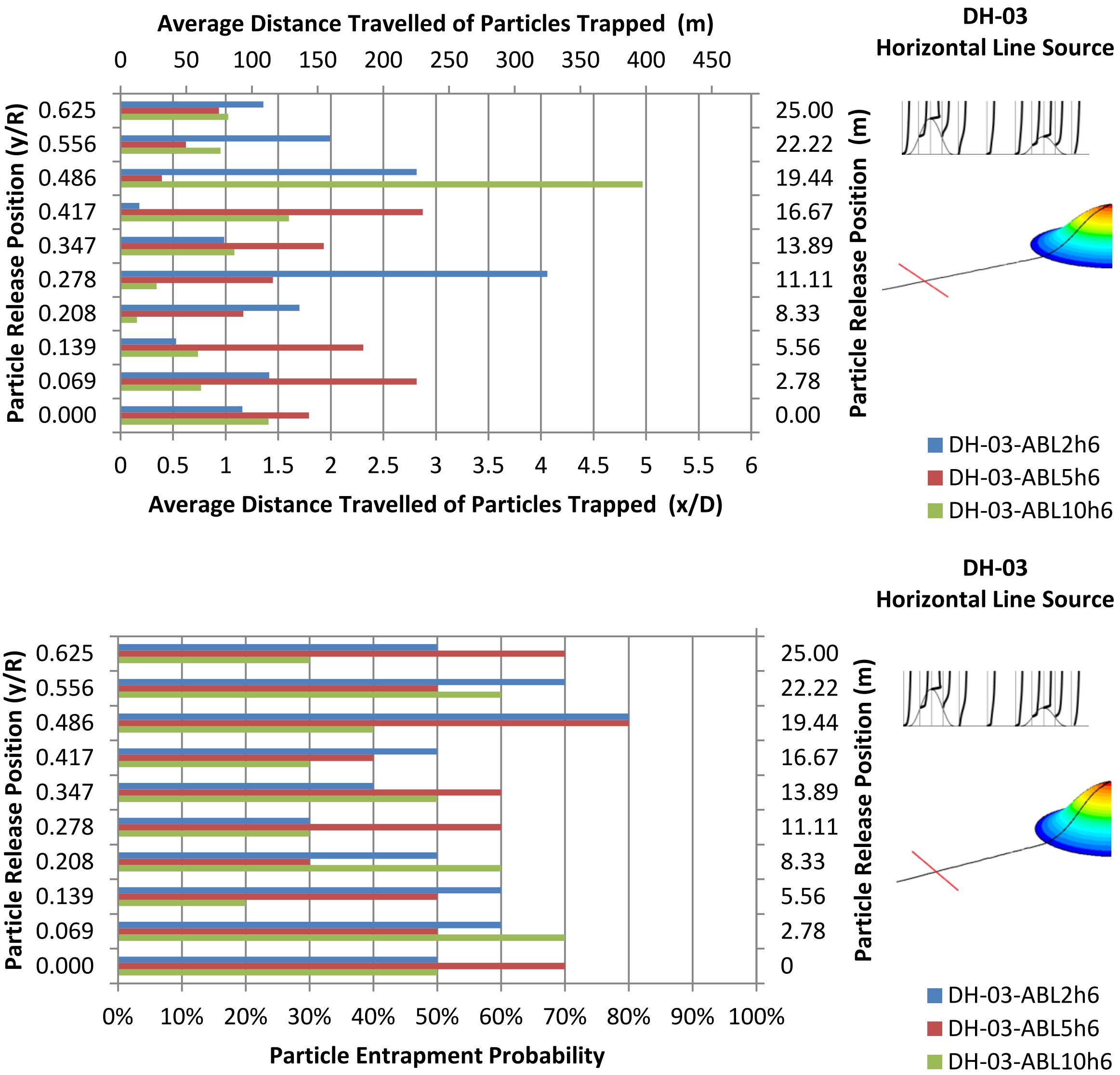

Figure 80 : Average distance travelled of particles trapped (top) and particle entrapment probability (bottom) plots for particles released from a horizontal line source upstream steep and shallow 3D hills for three ABL inlet conditions.

5.5.3 Species Transport over Double 3D Hills

Following the examination of wind flow and particle tracking for domains with double sinusoidal hills, species transport simulations were carried out. The inlet ABL condition of ABL2h6 was selected because wind at lower mean velocity was seen to take high mole fractions further than the first hill (evident from single 3D hill cases). Solver details and boundary conditions for these simulations where similar to those for species transport for a single 3D hill.

Mole fraction of wood species was seen to rapidly decrease by 18% for domains with steep Hill 1: DH-01 and DH-03 which both had identical mole fraction plots until they reached Hill 2 (Figure 81). DH-01 had a steep Hill 2 causing another big drop (compared to the same hill for the other domains) in mole fraction of wood by 2%. The drop was smaller for DH-03 (1%) which had a shallow Hill 2 (Figure 82). For DH-02 with shallow Hill 1, the wood mole fraction was reduced by 15% and had larger percentage values in-between hills than DH-01 and DH-03. Reaching the steep Hill 2, values dropped by 4% to the same value as DH-02. The combined effect of both hills for DH-02 (shallow and steep hills) and DH-03 (steep and shallow hills) was equal for both resulting to a drop of mole fraction to 4% at 4D downstream the first hill (or 5.25D from the ground source). The domain DH-01 with double steep hills had a greater effect on reducing the wood mole fraction with the value at the same distance downstream dropping to 3%.

Contour plots of wood mole fractions at different heights above ground level are presented in Figure 83, Figure 84 and Figure 85 for all domain cases. Results show that wood species travelled downstream the domain reaching the windward face of Hill 2. However, when Hill 1 was steep (DH-01 and DH-03) the mole fraction of species reaching Hill 2 was smaller as seen by the plots described above. For both these cases with steep Hill 1, mole fraction reached higher altitudes (up to 25m) above ground. In DH-02, shallow Hill 1 was again seen to act as a damper to Hill 2 but not ‘blocking’ as much of the wood species as a steep hill would do.

The above results clearly show that flat and hilly terrains cannot be treated with a single approach. Hills of different slopes (shallow 1:4 and steep 1:2) have different effects to wind flow, particle dispersion and species spread. Thus, when topography is complex (steep / shallow multiple hills) site specific investigation is essential.

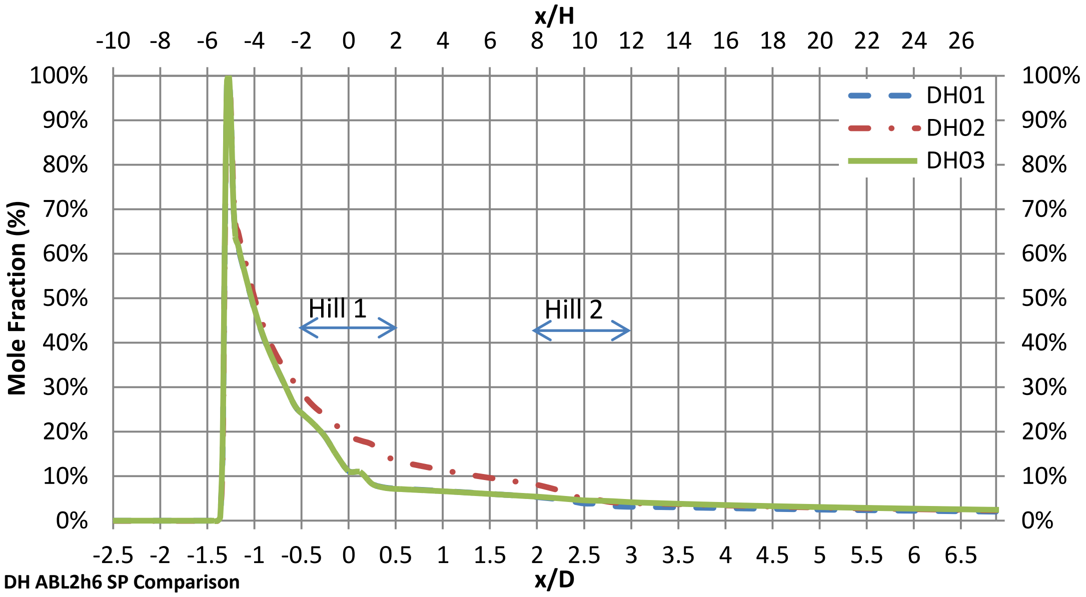

Figure 81: Wood mole fraction comparisons at lower ground and hill faces on symmetry plane for 3D double hills for inlet condition ABL2h6.

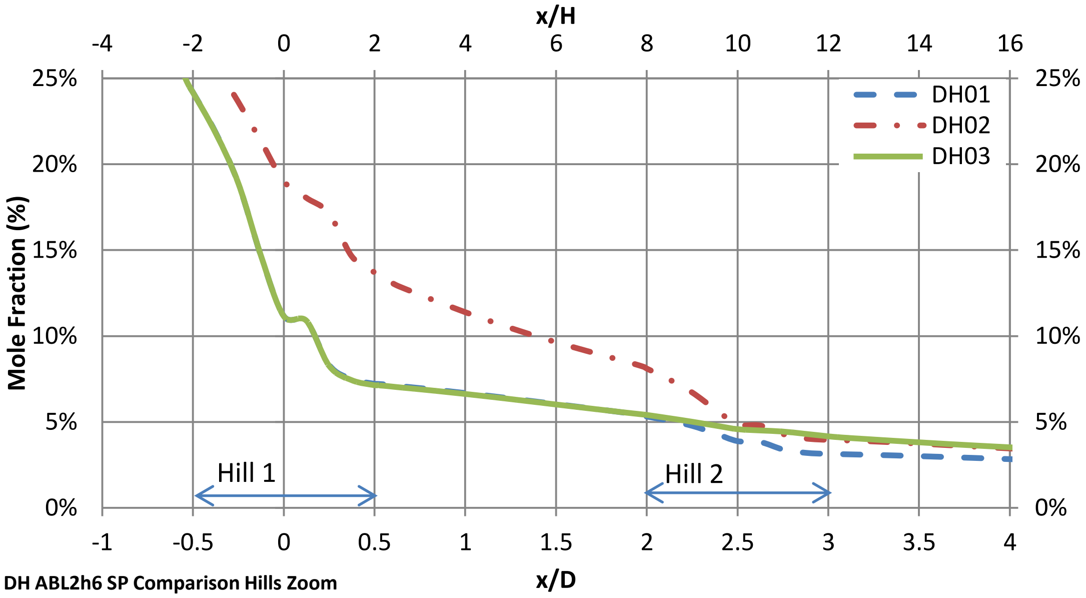

Figure 82 : Detailed plots of wood mole fraction comparisons at lower ground and hill faces on symmetry plane for 3D double hills for inlet condition ABL2h6.

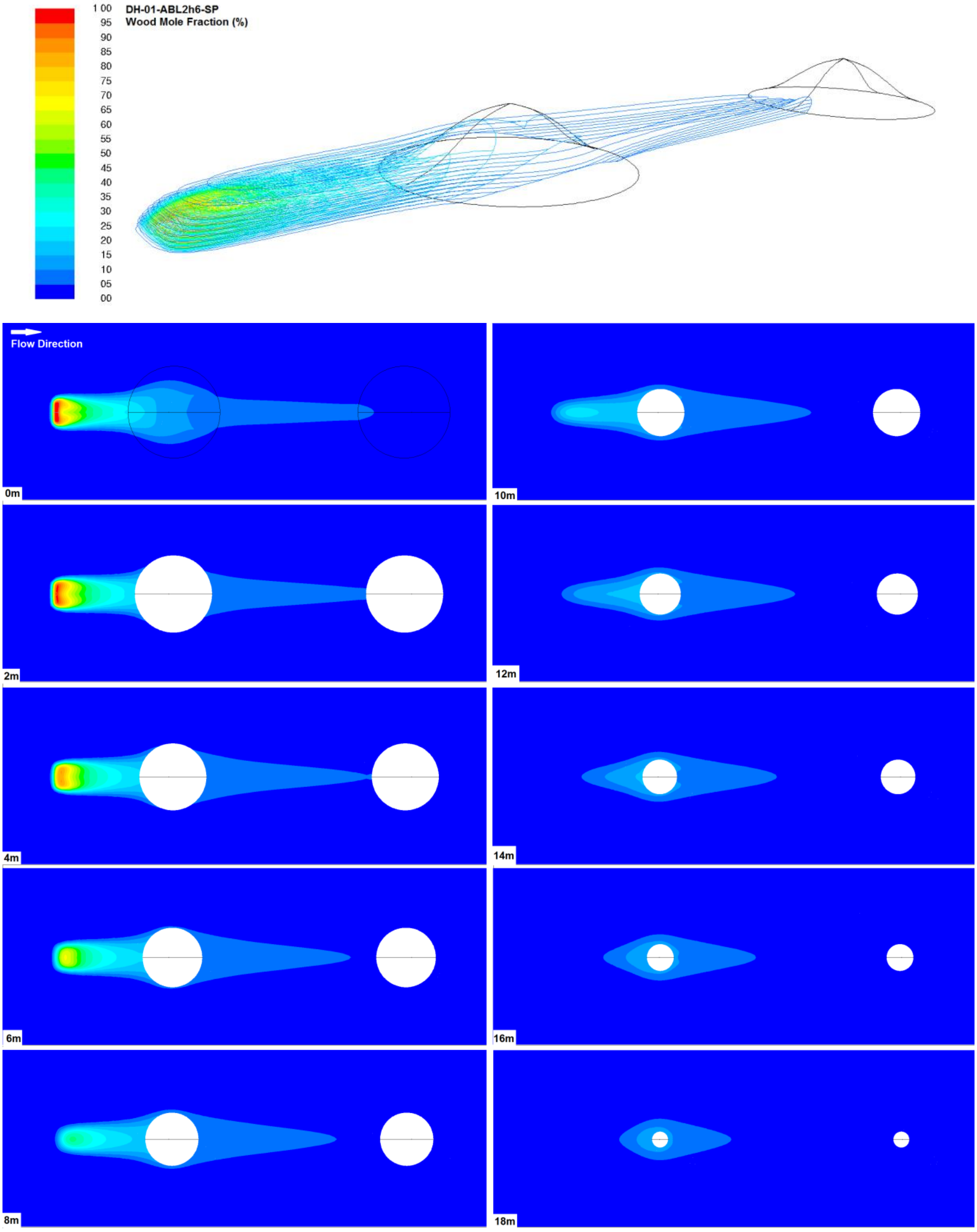

Figure 83 : Contour plots of wood mole fraction (%) on and above ground level for double steep sinusoidal 3D hills (case DH-01) with inlet ABL2h6 (isometric and top views).

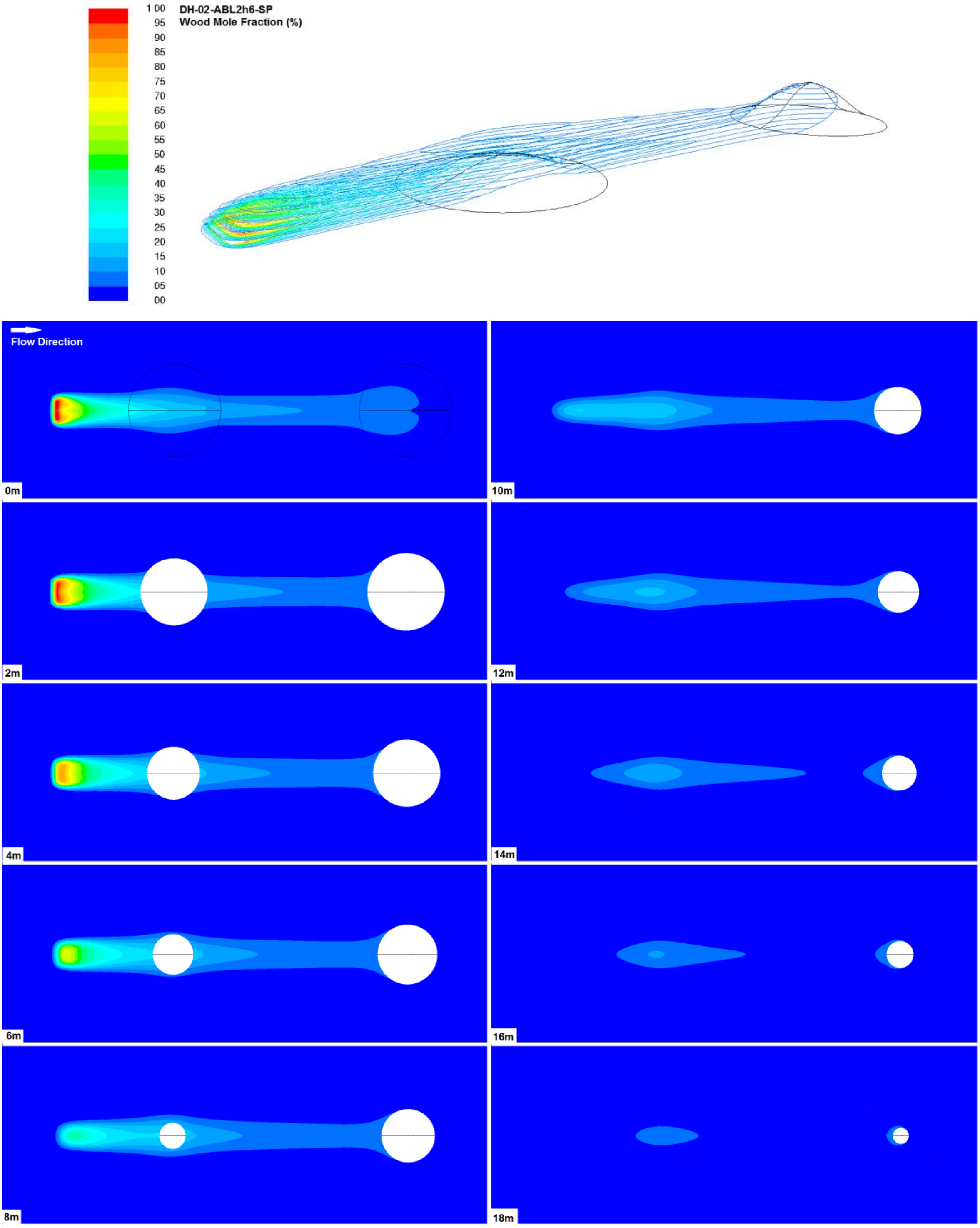

Figure 84 : Contour plots of wood mole fraction (%) on and above ground level for shallow and steep sinusoidal 3D hills (case DH-02) with inlet ABL2h6 (isometric and top views).

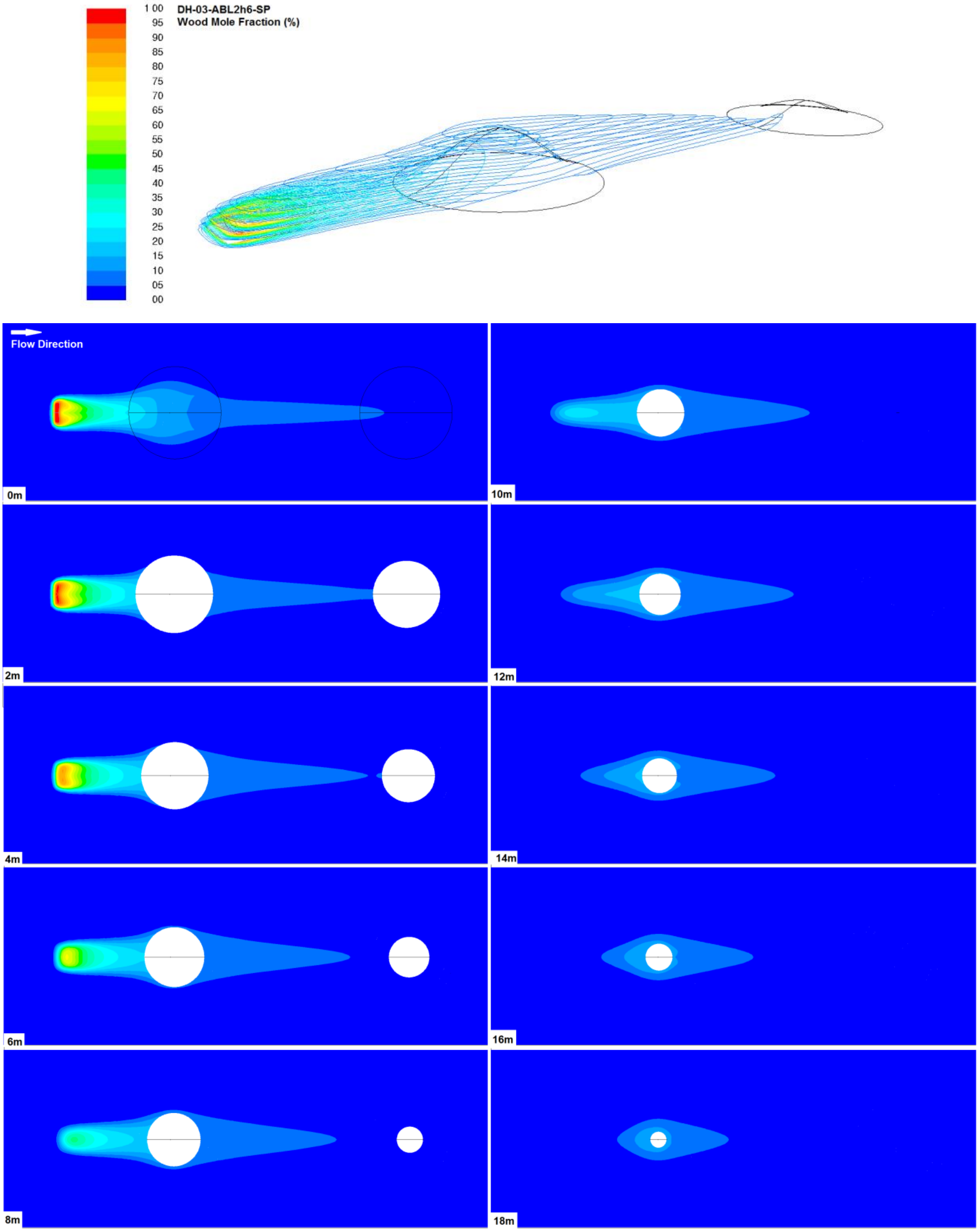

Figure 85 : Contour plots of wood mole fraction (%) on and above ground level for steep and shallow sinusoidal 3D hills (case DH-03) with inlet ABL2h6 (isometric and top views).

Chapter 6

CFD SIMULATION OF OPEN WINDROW COMPOSTING SITES

6.1 Introduction

Proposals for a waste management strategy for ‘green bin’ contents in South Yorkshire, UK involve four near town green processing facilities: two proposed open windrow composting sites and two green waste collection depots. The proximity of these sites to near towns and villages, prompted for a review of past practices and procedures relevant to the open windrow composting numerical modelling.

In South Yorkshire three important conditions come together to challenge the ‘universal’ approach of risk assessment only in the presence of sensitive receptors within 250m from the source. These conditions are: *a.* the terrain is hilly (more than 1:10 which is the limit specified by Pollard et al. (2004)); *b.* it is characterized by near continuous light winds; and *c.* there are many susceptible patients.

Interestingly, there were between 10 to 15 residents admitted to the hospital with primary or secondary *Aspergillosis* in the 3 years to March 2008 in the greater area of the examined region. From 2001 to 2008 there were between 5 to 10 cases where *Aspergillosis* has appeared on death certificates as a contributory cause to death [NHS Public Health Directorate]. In addition there is a plan to build four near-town sites on the presumption that this would save on transport costs for the incoming green waste and outgoing compost.

From the total of four facilities, one (Site A thereafter) was chosen to be examined here by the use of CFD due to available data and time limitations. This site is at a hilly location near three residential areas. A second existing open windrow composting site in West Midlands (Site B thereafter) was chosen for comparison as it is surrounded by flat land. The names of these facilities are not mentioned in this work nor in the publications of the author to keep confidentiality (see Table 23 below for site descriptions).

Site	Terrain Characteristics	Facility Type
A	Hilly	Proposed Compost Site
B	Flat Land	Existing Compost Site

Table 23 : Terrain characteristics for open windrow compost sites examined.

Wind flow for both Site A and B has been previously simulated by the author [Katsanis et al., 2009, 2010]. For Site A both two-dimensional and three-dimensional simulations were conducted. For Site B only two-dimensional simulations were run (2D slices for worst case scenario, i.e. slices passing from source and nearby receptors). These two sites are described below and were studied further in this thesis after taking into consideration all the factors that could influence wind flow and effluent pollution dispersion as presented in Chapter 3.

Present results are additional to the work previously published [Katsanis et al., 2009, 2010] and aim to analyse and explain the necessary assumptions for the multi variable problem of effluent pollution dispersion in depth. This will be achieved based on lessons drawn from simulations of idealised terrain and the optimisation of numerical parameters in Computational Fluid Dynamics.

6.2 Modelling Approach

For both sites, domain areas were carefully examined with the help of satellite pictures, Ordnance Survey maps and where possible by visiting the location. For 3D models, a square domain was chosen after examining the terrain and deciding where the boundaries should be set. Criteria mainly include wind breaks and substantial topographical features that could influence wind flow within the studied area.

Domain characteristics and mesh density were as detailed as possible given the computational resources and time available. The Ordnance survey map of each modelled area was divided into small squares and elevations were recorded for the corners of each of them to create the geometry (about 200 points); the computational mesh was then created with hexahedral cells with an increasing mesh interval size of 1m starting from the ground and growing up to 15m at the top (sky) of the domain.

For all simulations, the boundary conditions were set as described for the 3D ideal terrain in Chapter 5. Richards and Hoxey (1993) logarithmic profiles were set at the inlet of domains, symmetry conditions for the sides and top of the domain and finally the outlet as a pressure outlet. Ground, building and forest/tree faces were set as walls with a surface roughness of 0.2m [Hargreaves and Wright, 2007].

Modelled domains of both sites have a top boundary of 600m and included major characteristics that were likely to influence the flow such as: woods, rows of houses and the compost pads. Three piles of compost were modelled at the area of the presumed and existing compost site at Site A and Site B. These are 100m long, 6m wide and 3m high having a flat top (100m long, 3m wide and 3m high) to avoid problems during the mesh process of domains.

6.3 Weather Data

In order to accurately model wind flow and pollution dispersion, weather phenomena have be taken into account. As weather is a continuously changing system, the assembly and proper processing of weather data is essential.

For the examined site in South Yorkshire, inlet conditions were set according to weather data obtained from the Weston Park Museum in Sheffield, UK which has a weather station. Data processed and used in this work correspond to data for the year 2006. Although only a single set of data for a single year was supplied, wind speeds are representative of daily average and daily maximum wind speeds and directions.

The same data were used for simulating and comparing results for the existing compost Site B in West Midlands, UK for comparison reasons. Data was statistically processed to calculate frequencies for annual maximum wind speed and direction. The daily regular, calm wind speed of $2ms^{-1}$ along with the maximum wind speed and directions were of most importance since these would be used as the two extreme weather scenarios for simulations herein.

Maximum wind speed results are presented by a histogram in Figure 86 and wind directions for these speeds, by a wind rose in Figure 87. The most common maximum wind speed was $8ms^{-1}$, occurring at a frequency of 10.9% in 2006. The wind speed of $10ms^{-1}$ follows with a frequency of 10.8%. As for wind direction, the most common was the Northern-Western (NW) with a frequency of 15.6% followed by Southern-Western with a frequency of 13.7%. Note that the wind rose shows that maximum wind speeds mostly occur from the following directions: NW, WNW, W, WSW and SW.

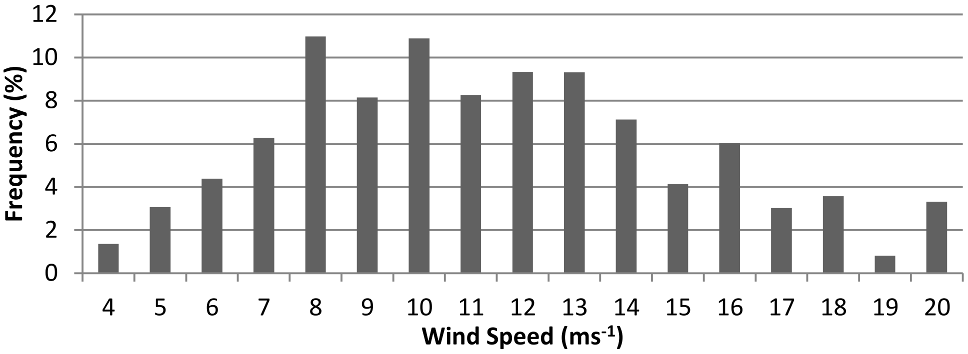

Figure 86 : Histogram of frequencies (%) of maximum wind speeds during 2006 for Sheffield, UK.

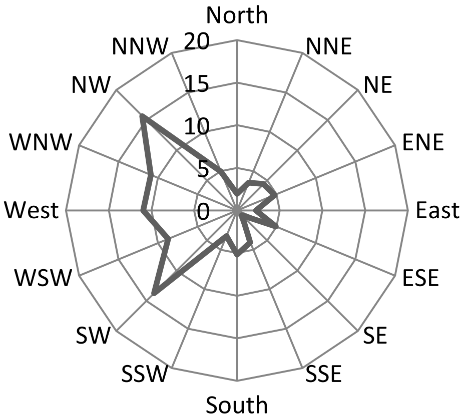

Figure 87 : Wind rose of wind direction frequencies (%) for maximum wind speeds during 2006 for Sheffield, UK.

6.4 Site A

6.4.1 Introduction

Regarding this particular location, a planning application for a green waste composting plant and the associated storage zones was submitted. The site is of great importance as many of the significant factors that could influence the health of nearby residents come together. The hilly topography, the nearby college, the close proximity of Village A and the very high woods suggest challenging factors for effluent pollution dispersion modelling for this area.

The terrain is hilly, with the suggested position of the plant at the lower ground below two hills (see Figure 88); this area has suffered serious floods in the past, causing the area of the proposed site to be underwater. Nearby villages exist with a large percentage of people who suffer from breathing impediments, including former deep mine workers (35% of over 60 year old male people).

A residential hill village, Village A, is located at just 300m to the south and above the proposed open windrows (slope of about 15%). This village has two large woods on the sides which could potentially form a channelling effect of wind to the houses. To the west, two more housing developments exist: these surround a primary and junior school and a railway station. A college is also situated further up the hill close to Village A (about 450m away). Next to the college a double line of 25m high trees (and adjacent gardens) attract visitors and students. Other nearby villages have primary and junior schools at a distance of about 1km to the north east.

Onsite, wind velocity readings were taken at the area of the pine trees on Saturday 10 July 2008; an anemometer (TSI VelocCalc 8344-M-GB) was used to record air velocity at several points along the line of trees and at the top of the hill [Katsanis et al., 2009]. The wind velocity at the top was much higher than the one between the lines of trees. Noticeably, the direction of the wind in-between the double row of trees was opposite to the direction at the top of the hill (presumed recirculation). The day after, the procedure was repeated only to show approximately the same reading and variation in wind direction.

The domain studied covered an area of 1.15x1.6km^2 with the sky boundary placed 600m above sea level. It included two 20m high woods and two rows of houses from the nearby Village A. The computational domain consisted of nearly 2 million cells with 1m^3 cells at the ground and around areas of interest.

6.4.2 Wind Flow and Particle Tracking at Site A

Wind flow simulation for Site A included two ABL inlet conditions as specified in Chapter 5 for 3D idealised terrains studies: ABL2h6 and ABL10h6. A Northern wind was simulated to represent the worst case direction of pollutant released from the compost piles with wind blowing and spreading pollutant particles directly towards the nearby Village A.

Figure 89 and Figure 90 show static pressure and turbulent kinetic energy contours for ground, house and compost faces at Site A with an inlet condition of ABL10h6. For the same inlet condition, Figure 91, Figure 92 and Figure 93 present contour plots of static pressure and mean velocity magnitude concerning different planes (slices) of the domain studied; for the x, y and z direction respectively showing the effects of terrain on wind flow.

Woods and buildings induced flow recirculation. At near ground parts of the domain static pressure was high and velocity was close to those of the inlet ABL values. As the wind accelerated up the hill the static pressure dropped and velocity increased. A channelling effect was also seen for the wind passing between the two woods located at 50m elevation above Village A houses. Wind flow results for ABL10h6 are representative for wind flow at Site A; results for ABL2h6 showed minor differences and thus are not included here; these can be found in Appendix 3.

Particle tracking was enabled together with the Random Walk Model and ground absorption following the method described earlier in Chapter 5 for 2D and 3D ideal hill studies. A total of 5000 particles were instantly released from the compost pad faces.

For the inlet condition of ABL10h6, particles travelled uphill towards the village which is situated approximately 300m away. Most of the particles (74%) were trapped on the windward face of the hill before reaching the houses in Village A, 2% of which were trapped immediately after release on the compost pile surfaces; 9% of particles were trapped on house faces or in the recirculation zones behind houses and 5% were trapped on the leeward face of the hill behind the village. Finally, 12% of particles were seen to escape the domain.

Particle tracking results were similar for ABL2h6. Although the mean inlet velocity was smaller, particles travelled slightly longer distances before being trapped. 59% of the released particles were trapped on the windward face of the hill, 11% at Village A houses, 7% on the leeward face of the hill behind Village A and finally, 23% of particles left the domain.

Figure 94 presents two isometric enlarged views of the domain, with particle tracks coloured by velocity magnitude for the compost source and for the nearby Village A houses.

Results are similar to those from idealised terrain simulations where the terrain has a greater effect on particle spread than the mean inlet velocities, as the range of wind speeds in the real environment under normal atmospheric conditions is considered small (normal conditions when mean ABL inlet velocities are below $10ms^{-1}$).

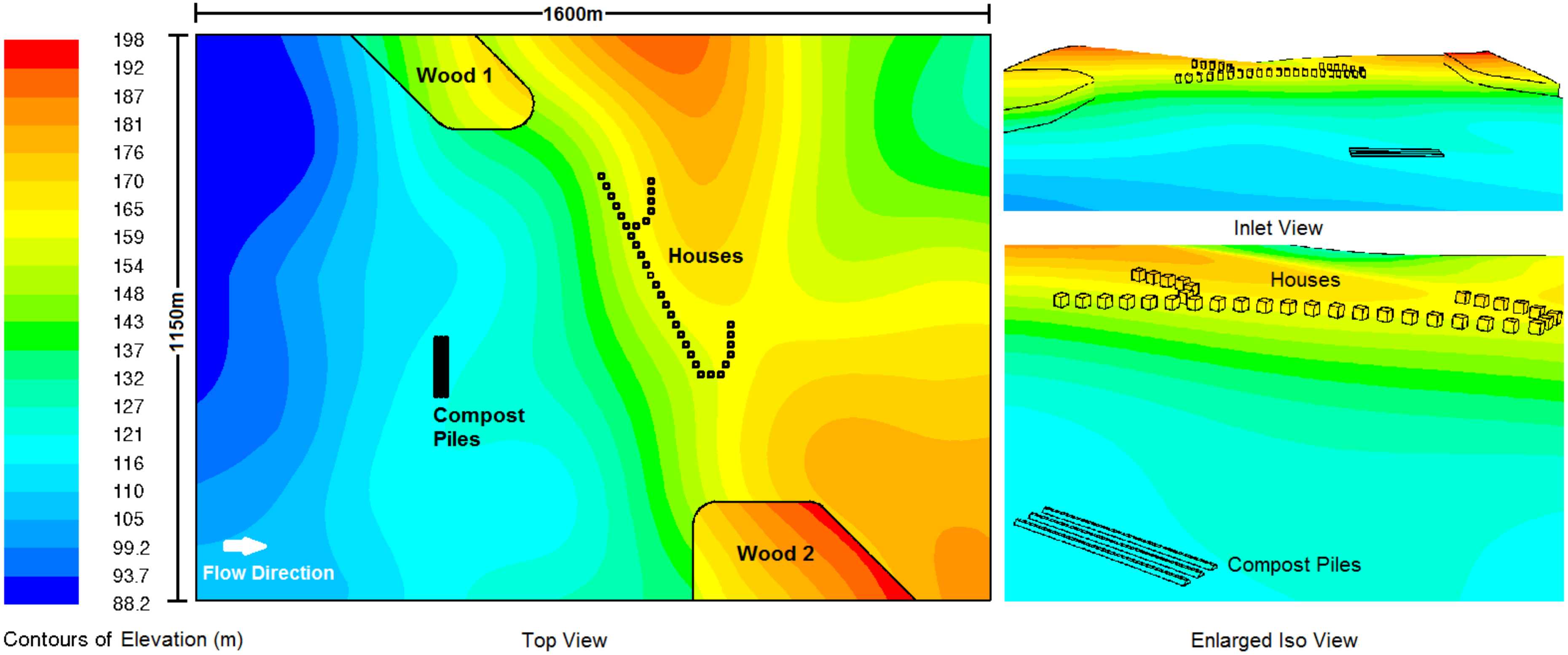

Figure 88 : Site A - Contours of terrain elevations for studied domain with location of proposed compost piles and nearby Village A houses and woods.

(top, inlet and enlarged isometric views)

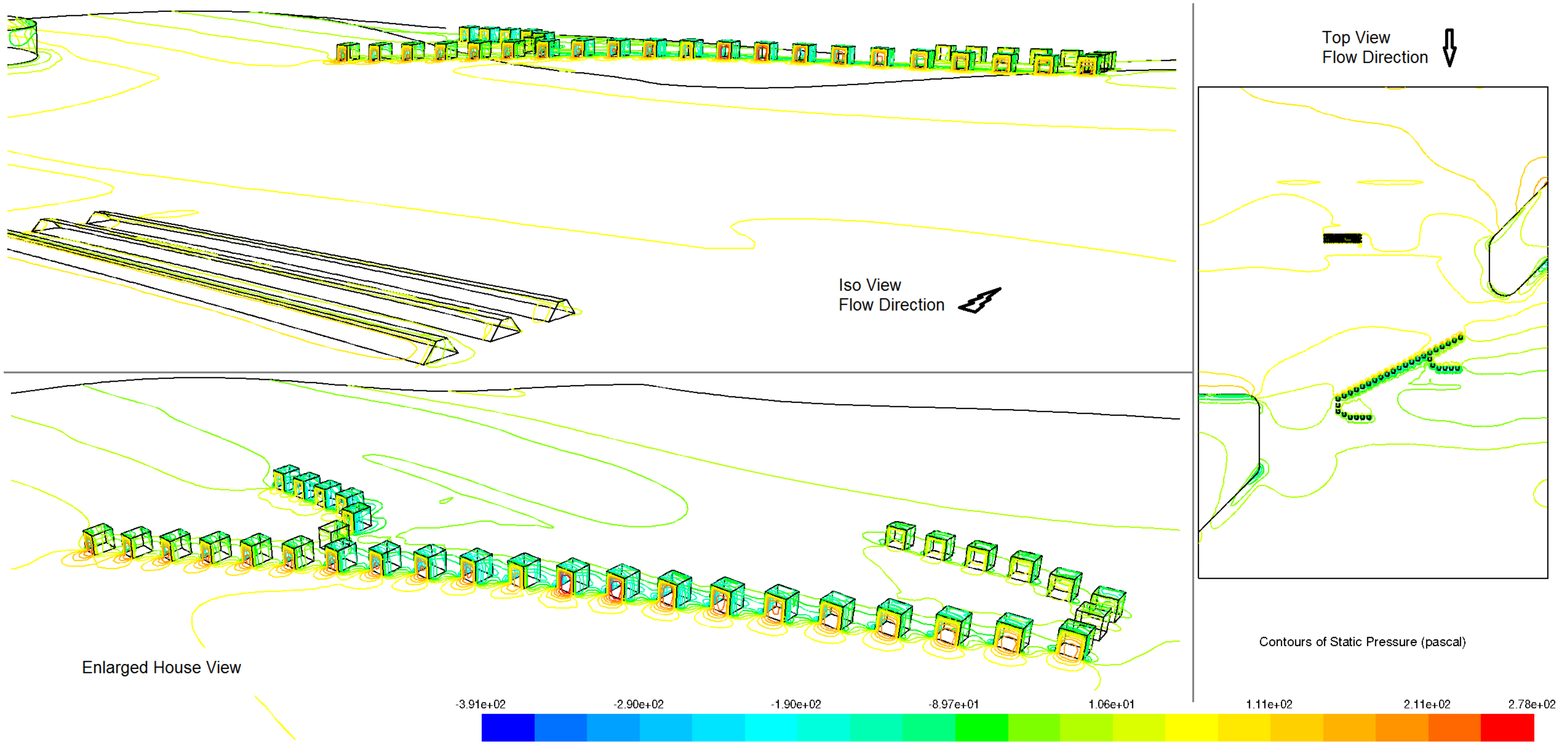

Figure 89 : Site A - Contours of static pressure p_{stat} *for ground level of studied domain (isometric compost view, enlarged house view and top view) for inlet condition ABL10h6.*

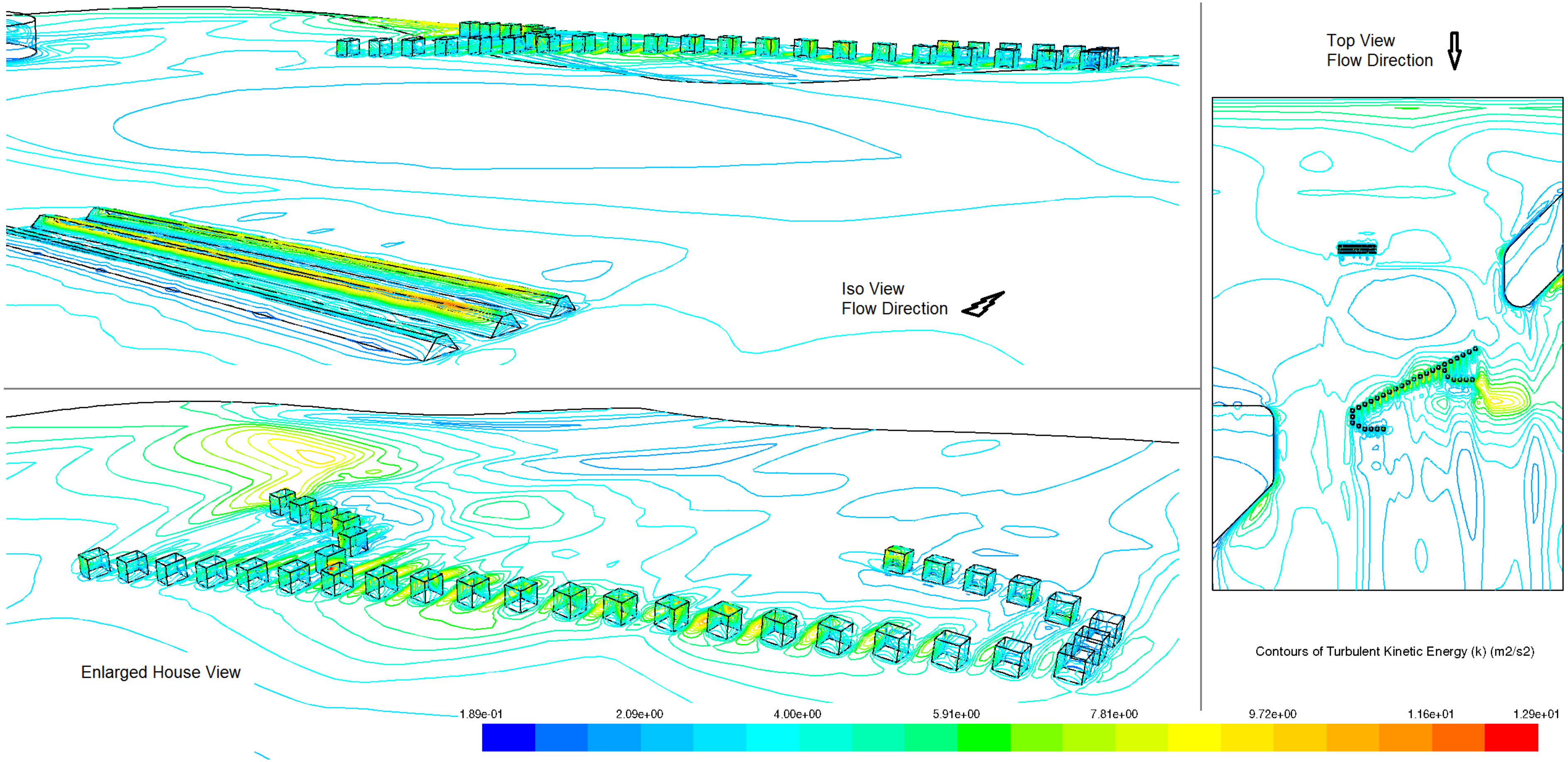

Figure 90 : Site A - Contours of turbulent kinetic energy k for ground level of studied domain (isometric compost view, enlarged house view and top view) for inlet condition ABL10h6.

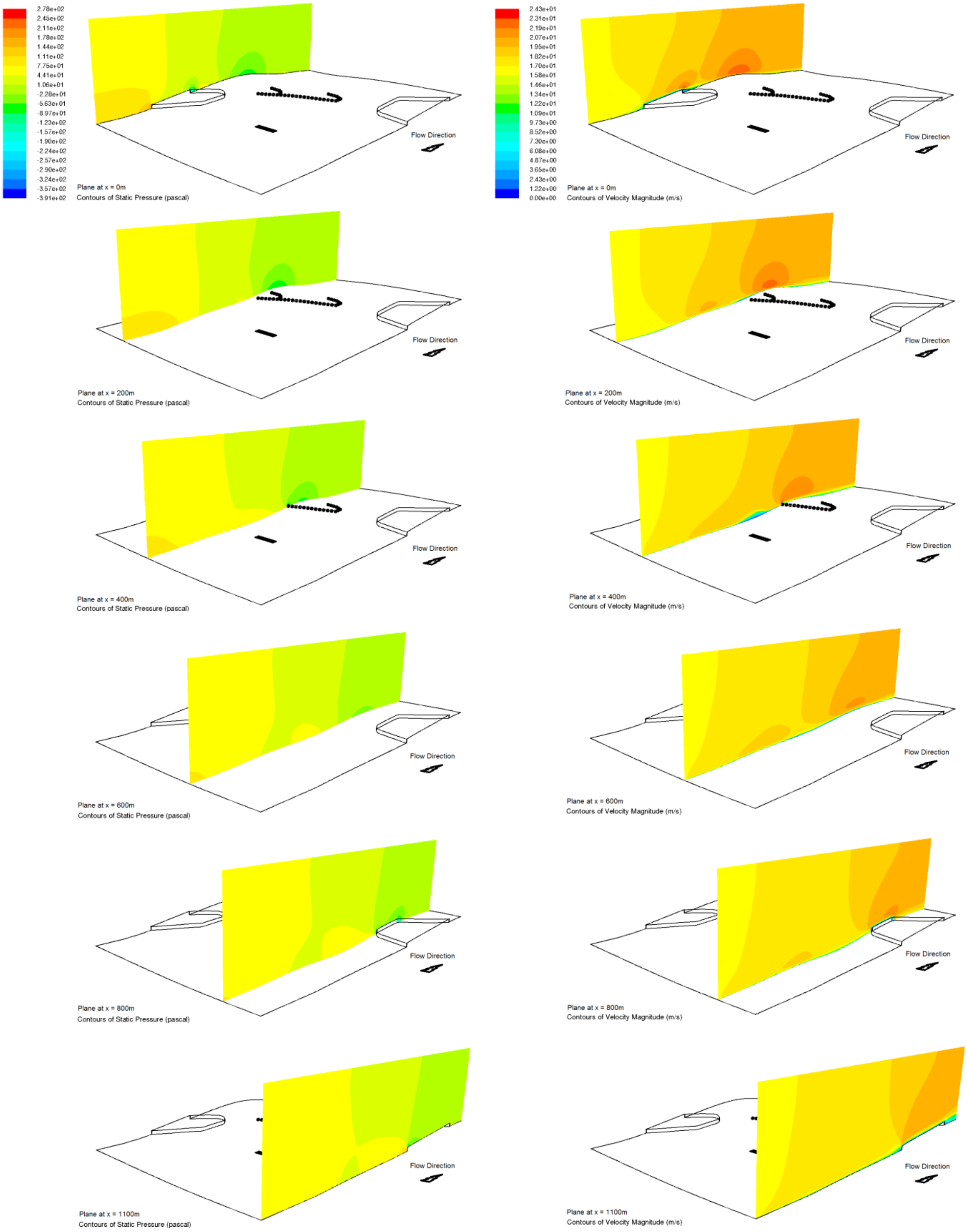

Figure 91 : Site A - Contours of (left) static pressure p_{stat} and (right) mean velocity magnitude $\overline{u}$ for selected planes along the x axis for inlet condition ABL10h6.

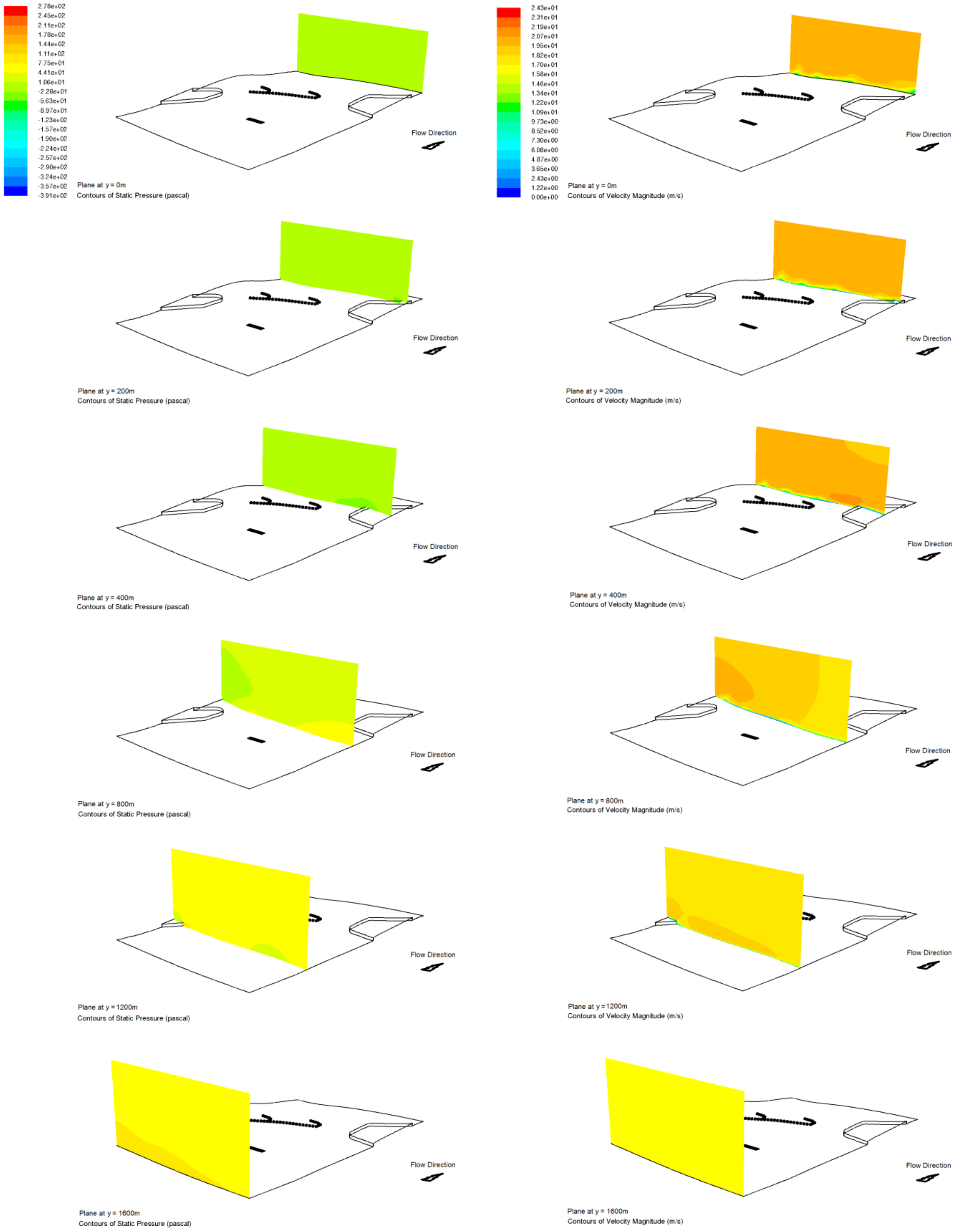

Figure 92 : Site A - Contours of (left) static pressure p_{stat} and (right) mean velocity magnitude $\overline{u}$ for selected planes along the y axis for inlet condition ABL10h6.

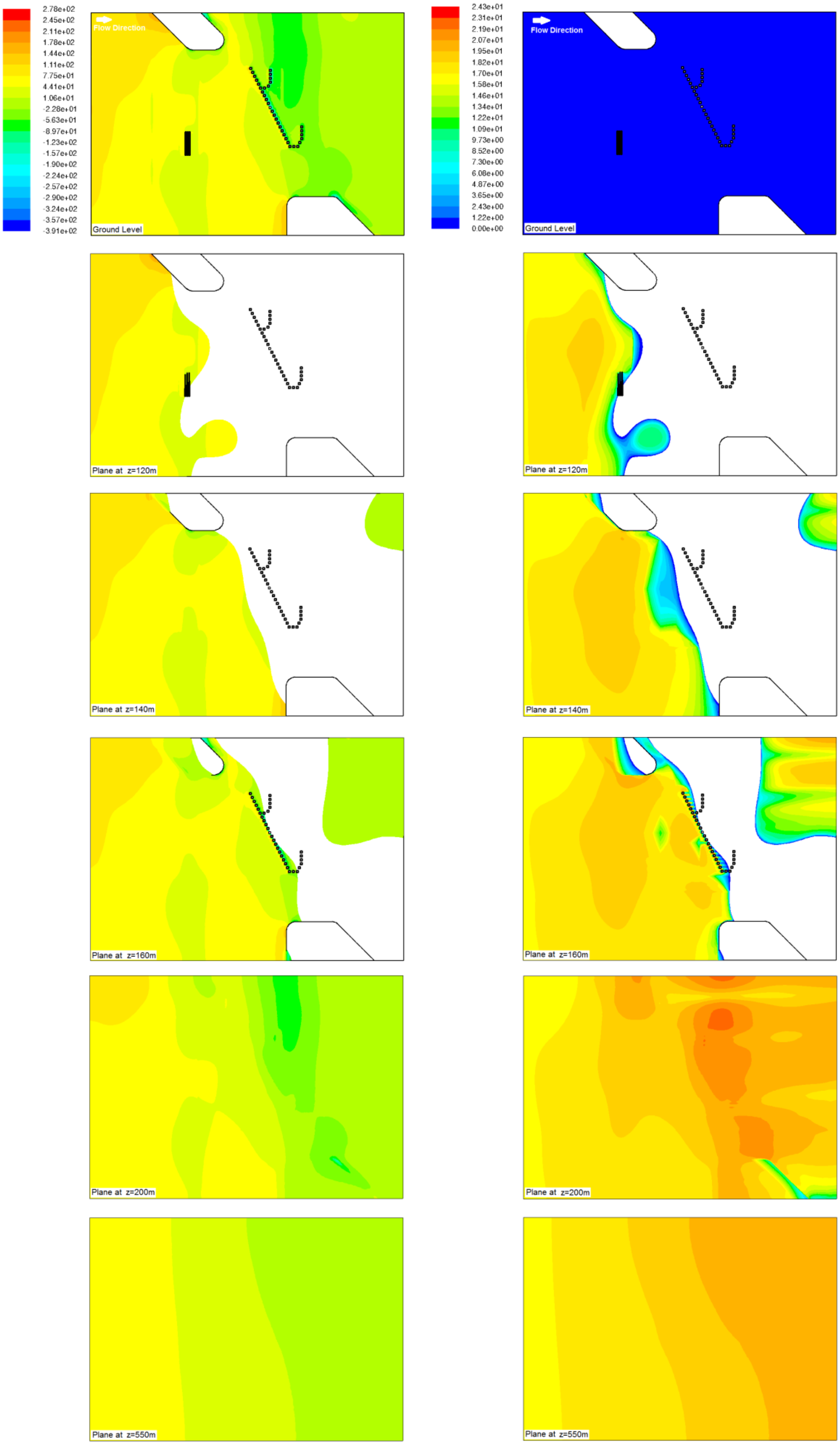

Figure 93 : Site A - Contours of (left) static pressure p_{stat} and (right) mean velocity magnitude $\overline{u}$ for selected planes along the z axis for inlet condition ABL10h6.

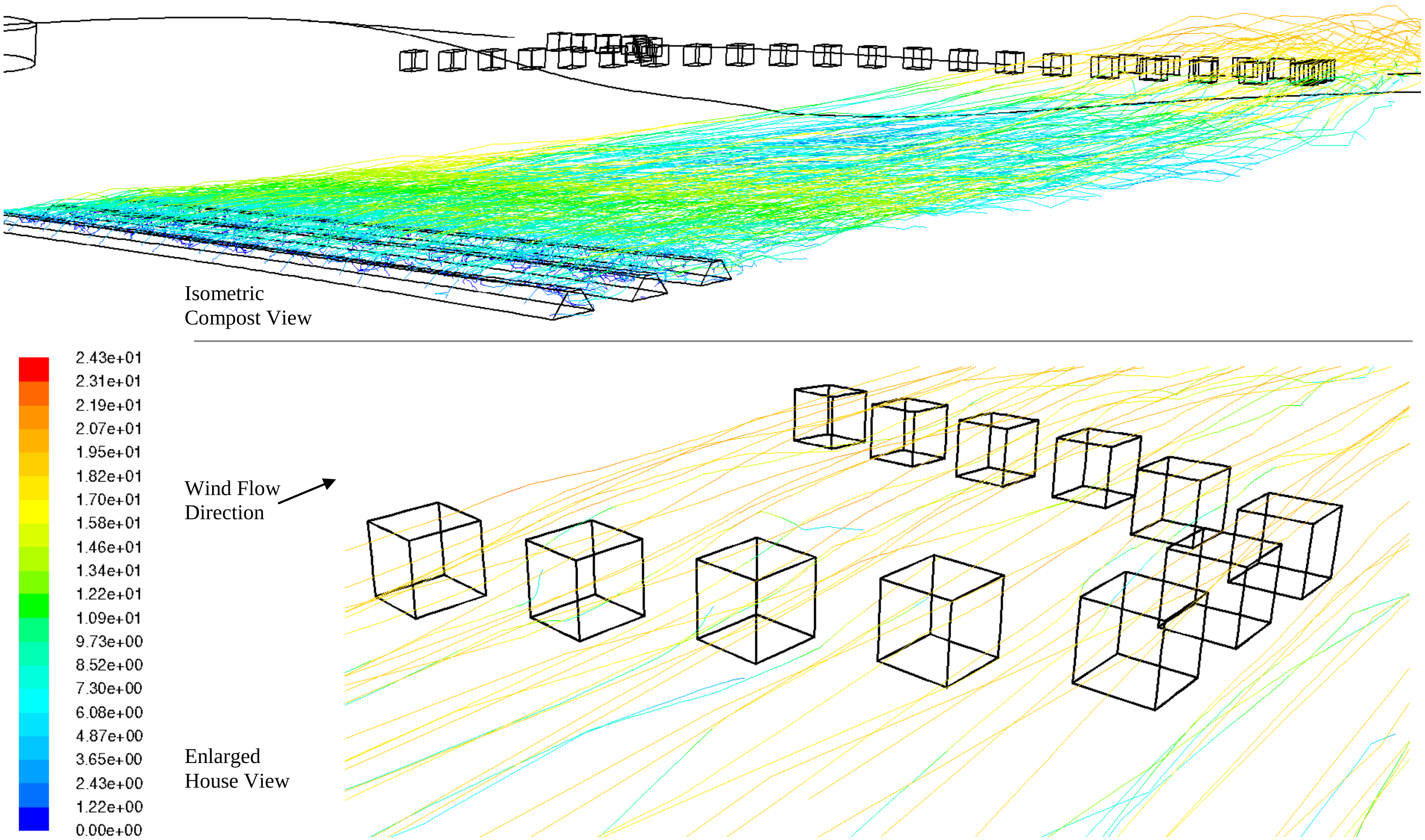

Figure 94 : Site A – Tracks of particles released from compost piles coloured by velocity magnitude (ms^{-1}) for inlet condition ABL10h6. (top - isometric compost view and bottom – enlarged house view)

6.4.3 Species Transport at Site A

Transport of wood species has also been studied for Site A for ABL2h6 and ABL10h6 inlet profiles. Solver settings for species transport were set as previously described in Chapter 5 for 3D idealised hill simulations.

For the vertical direction (upwards) and the case of ABL2h6, 70% of wood species mole fraction was seen to reach a height of 20m before starting to decay and drop to less than 50% (Figure 95). This did not seem to be the case for ABL10h6 for which wood species returned to background levels in the first 10m (Figure 95).

For the horizontal direction and the case of ABL10h6, wood species were seen to travel much less and reached background fraction levels (0%) within 200m from the compost pad while on the windward face of the hill and before reaching the nearby houses (Figure 96).

Fraction percentages in-between compost piles were also lower than ABL2h6 with species forced to the ground. In the case of ABL2h6, wood species were seen to travel further before reaching background levels; in this case the wood mole fraction at Village A houses was 5% with the 10% contour reaching approximately 280m on the windward face of the hill (Figure 96). Mole fraction was seen to drop to 50% just 50m from the compost piles. The highest mole fraction -as expected- was present within the three compost piles where values did not drop less than 90%.

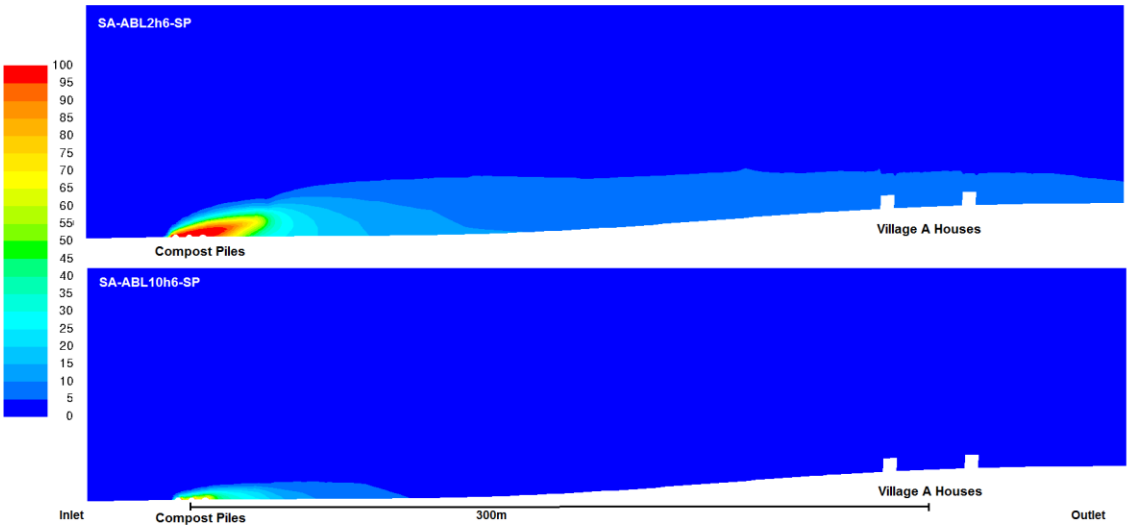

Figure 95: Site A - Contours of wood mole fraction (%) on vertical cross sectional plane passing from both compost piles and houses for the examined domain with inlet conditions of (top) ABL2h6 and (bottom) ABL10h6.

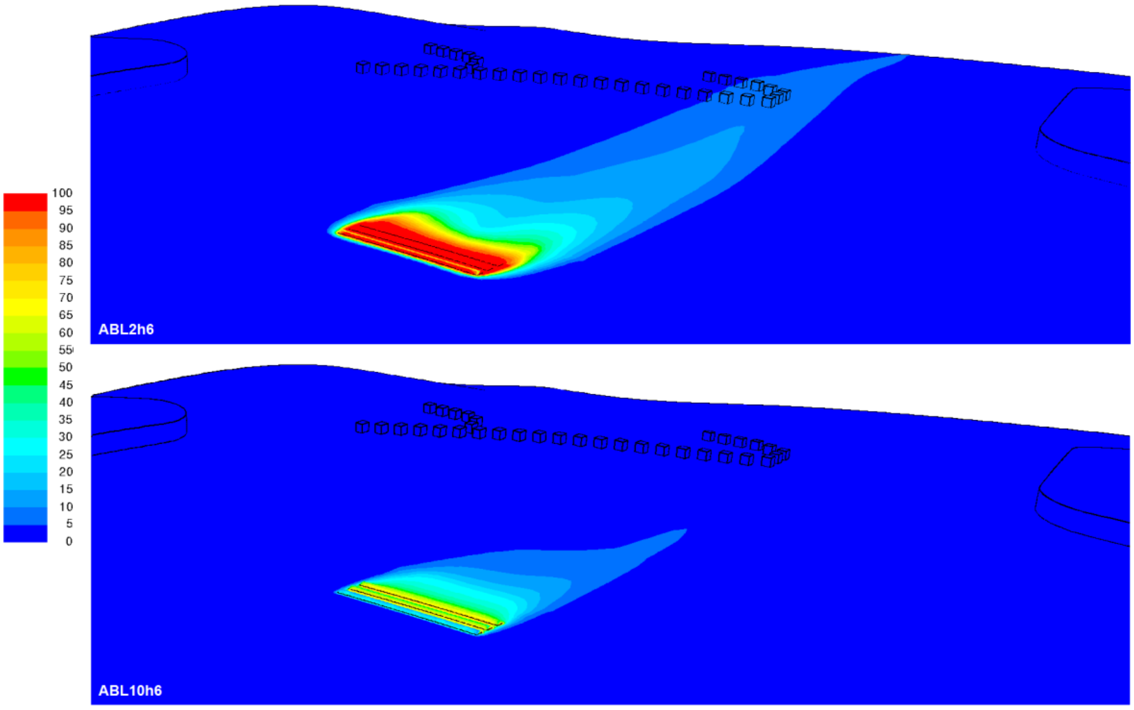

Figure 96 : Site A - Contours of wood mole fraction (%) on ground face for the examined domain with inlet conditions of (top) ABL2h6 and (bottom) ABL10h6.

6.5 Site B

6.5.1 Introduction

Site B has been chosen for its flat terrain (altitudes of about ±10m from the compost pads) and it's functioning open green waste composting facility. Its topography is in contrast to Site A with nearby Village B slightly higher than the existing compost site (+5m, see Figure 97). A questionnaire completed by residents living between 200 and 600m from the existing compost site showed an increased percentage of allergies supposedly attributed to AF spores.

Consultants to the site operator stated that the direction of the predominant incident wind is from the compost site to the nearby main road with a typical wind speed of 2ms^{-1}. As for Site A, possible reversed flow at the rear of the nearby houses could entrap effluent pollutants at ground level.

The domain studied covered an area of 0.8x1.13km^2 with the sky boundary placed 600m above sea level; similar to the domain for Site A. It included a row of houses in the Village B where health problems have been reported. The computational domain consisted of 2.2 million cells with 1m^3 cells on the ground as well as on the compost pile and house surfaces.

6.5.2 Wind Flow and Particle Tracking at Site B

Wind flow simulation for Site B also included two ABL inlet conditions; ABL2h6 and ABL10h6. The wind inlet direction simulated was NNW, in order to examine the worst spread direction of particles leaving the modelled compost piles and flying straight towards the nearby houses (similar approach adopted as for Site A). The domain boundaries were set accordingly to allow perpendicular NNW wind profile direction to the inlet face.

Figure 98 and Figure 99 show static pressure and turbulent kinetic energy contours for ground, house and compost faces at Site B with an inlet condition of ABL10h6. For this specific inlet condition, Figure 100, Figure 101 and Figure 102 present contour plots of static pressure and mean velocity magnitude regarding different planes (slices) of the domain studied; for the x, y and z directions respectively showing the little effect of the flat terrain on wind flow.

Static pressure and mean wind speed were found almost constant with small exceptions around the compost piles and houses from which there was little disturbance to the flow (Figure 98, Figure 99); small recirculation zones are formed at the leeward sides of the three compost piles and houses but these do not significantly influence wind flow at higher levels (Figure 102). Wind flow results for ABL2h6 are similar to those for ABL10h6 and therefore not presented here; they can be found in Appendix 3.

A total of 5000 particles were released from the compost pad faces similar to simulations of Site A. For the inlet condition of ABL10h6, particles travelled towards the nearby Village B houses which are located about 280m away.

A small percentage of particles (3%) was trapped on faces of compost piles due to nearly zero velocities and recirculation near ground level. The largest percentage of particles (50%) were trapped on the ground face and about 7% at the house faces (windward or leeward recirculation areas). Finally, 40% of particles were seen to escape the domain. Figure 100 shows an isometric and a side view of the examined domain with particle tracks coloured by velocity magnitude for the compost source and for the nearby Village B houses. Particle tracking results were similar for the simulation with inlet conditions ABL2h6, with a slightly larger percentage of particles escaping the domain through the outlet.

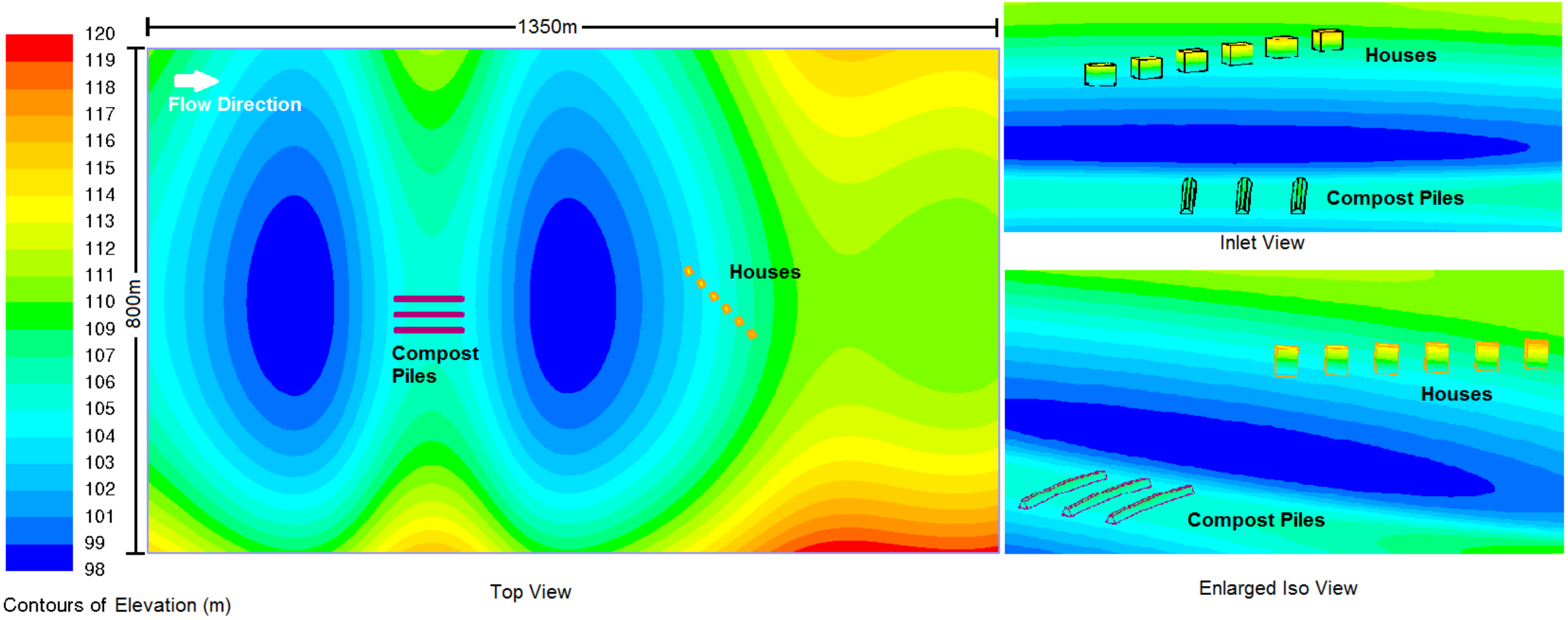

Figure 97 : Site B - Contours of terrain elevations for studied domain with location of existing compost piles and nearby Village B houses. (top, inlet and enlarged isometric views)

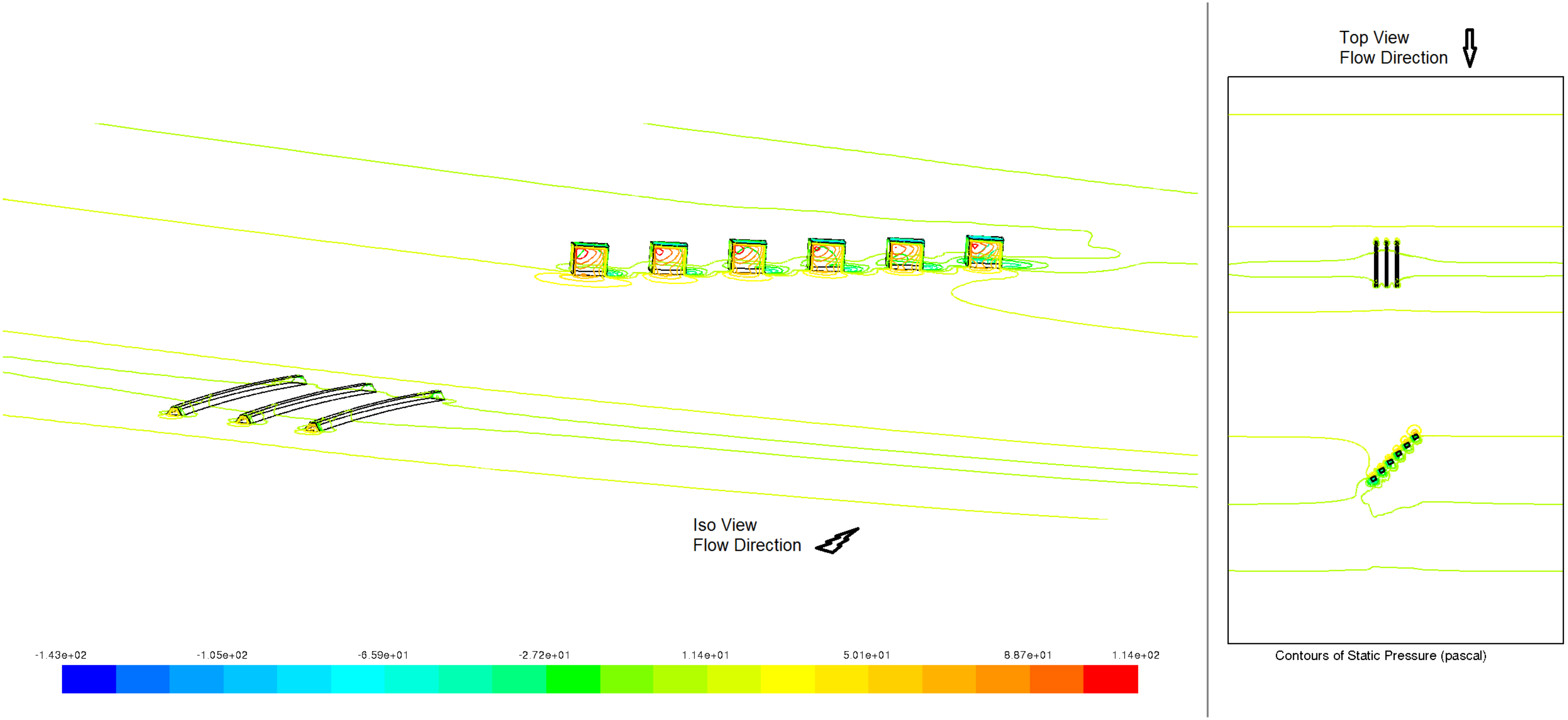

Figure 98 : Site B - Contours of static pressure p_{stat} for ground level of studied domain (isometric compost-house view and top view) for inlet condition ABL10h6.

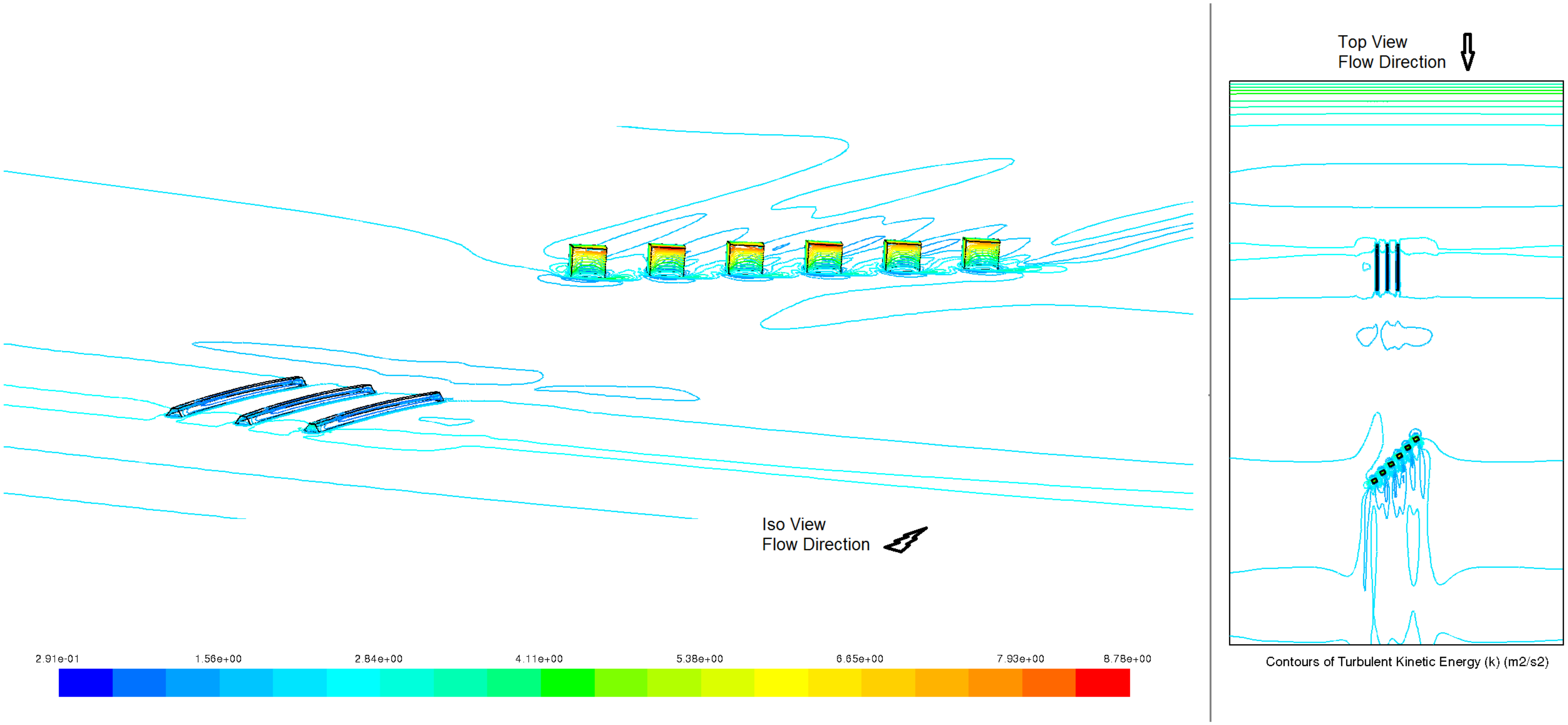

Figure 99 : Site B - Contours of turbulent kinetic energy k for ground level of studied domain (isometric compost-house view and top view) for inlet condition ABL10h6.

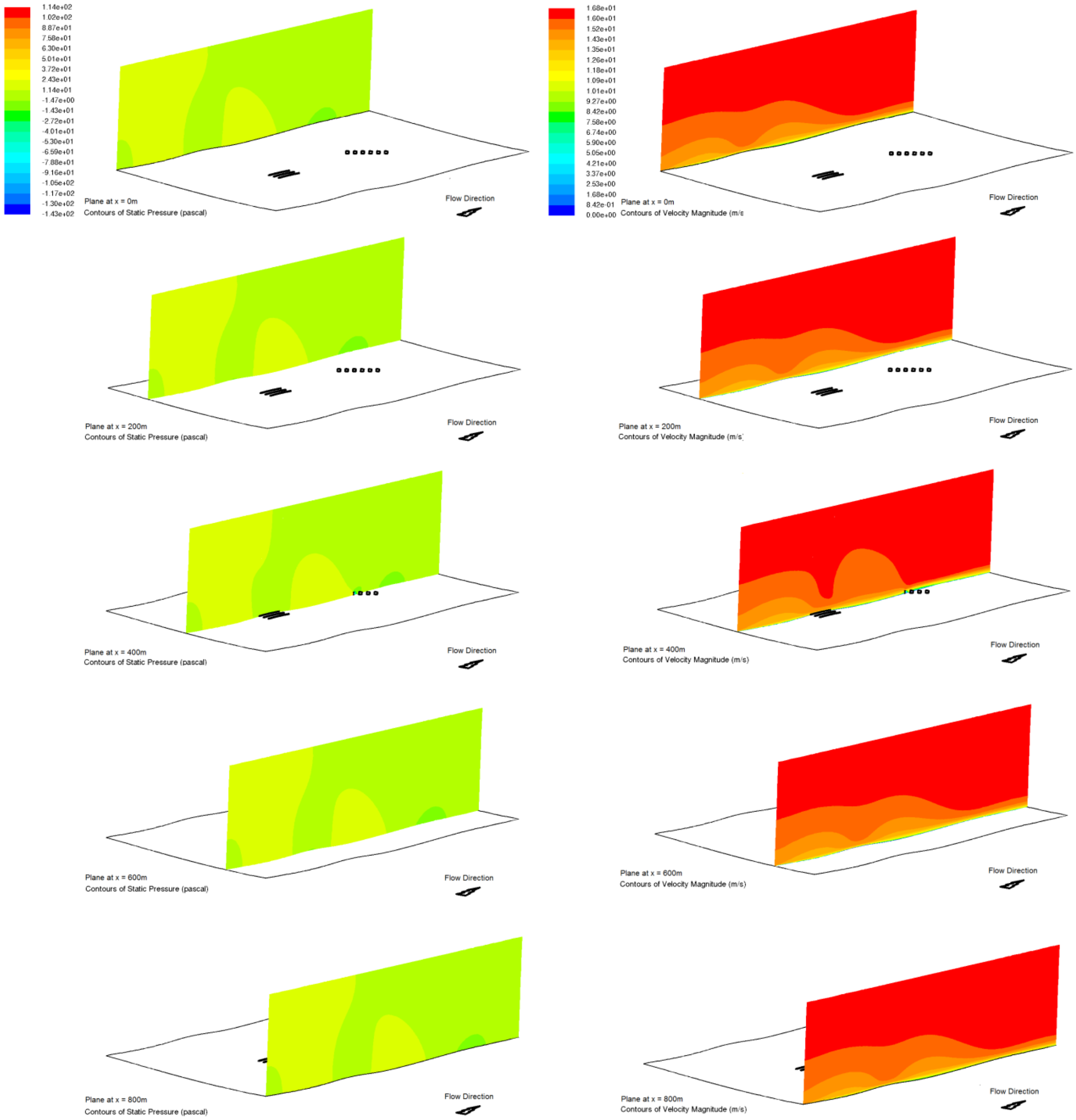

Figure 100 : Site B - Contours of (left) static pressure p_{stat} and (right) mean velocity magnitude $\overline{u}$ for selected planes along the x axis for inlet condition ABL10h6.

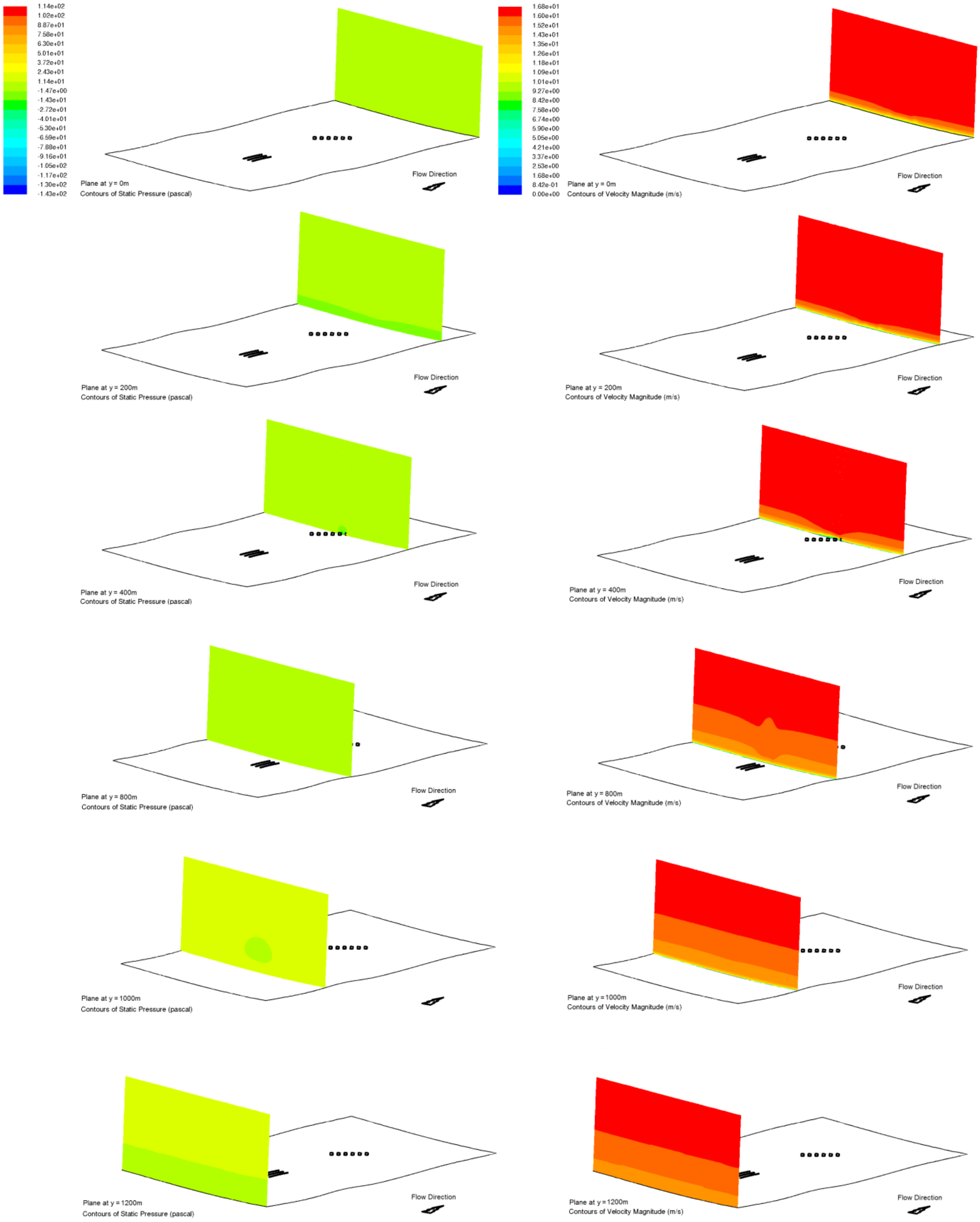

Figure 101 : Site B - Contours of (left) static pressure p_{stat} and (right) mean velocity magnitude $\overline{u}$ for selected planes along the y axis for inlet condition ABL10h6.

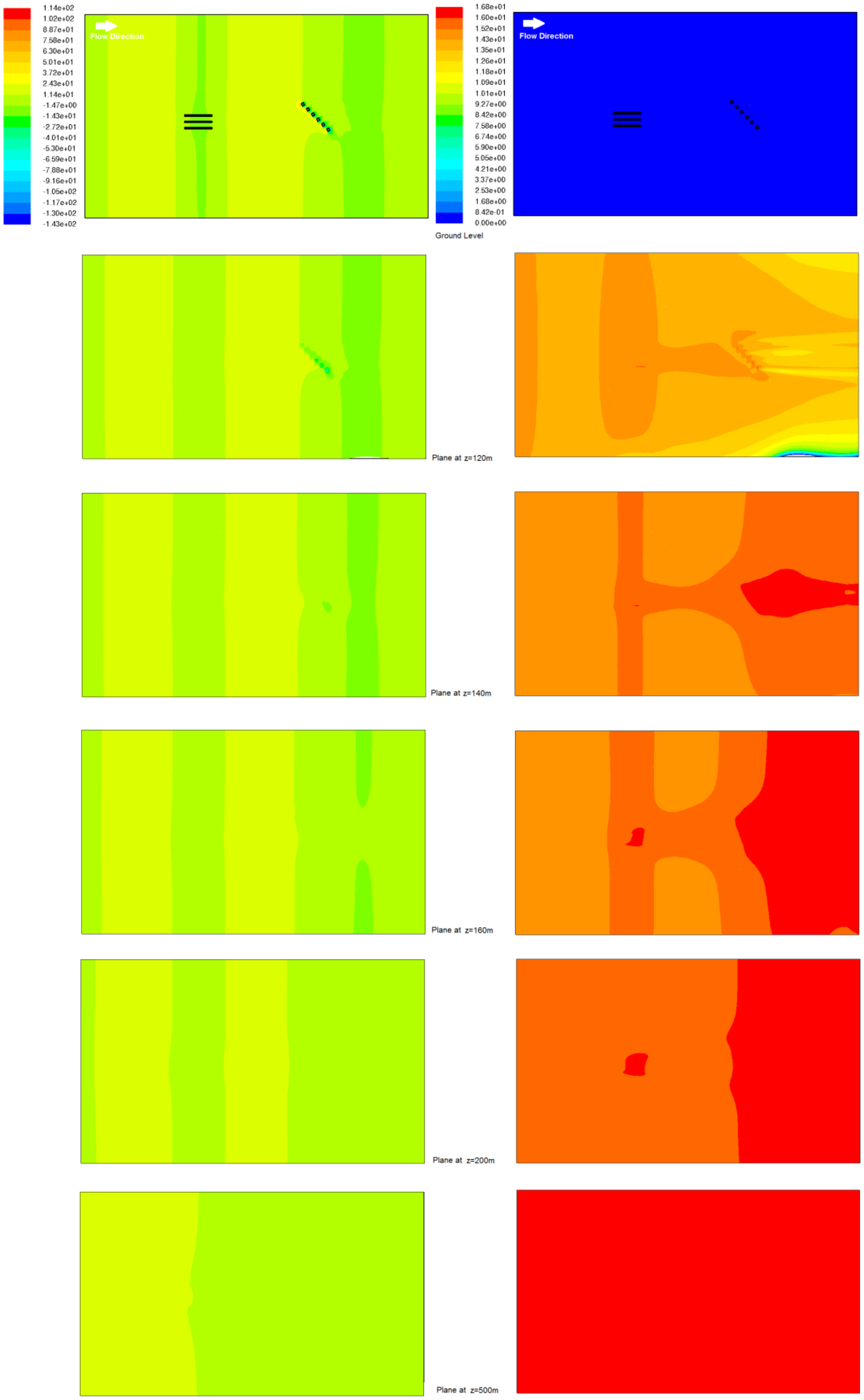

Figure 102 : Site B - Contours of (left) static pressure p_{stat} and (right) mean velocity magnitude $\overline{u}$ for selected planes along the z axis for inlet condition ABL10h6.

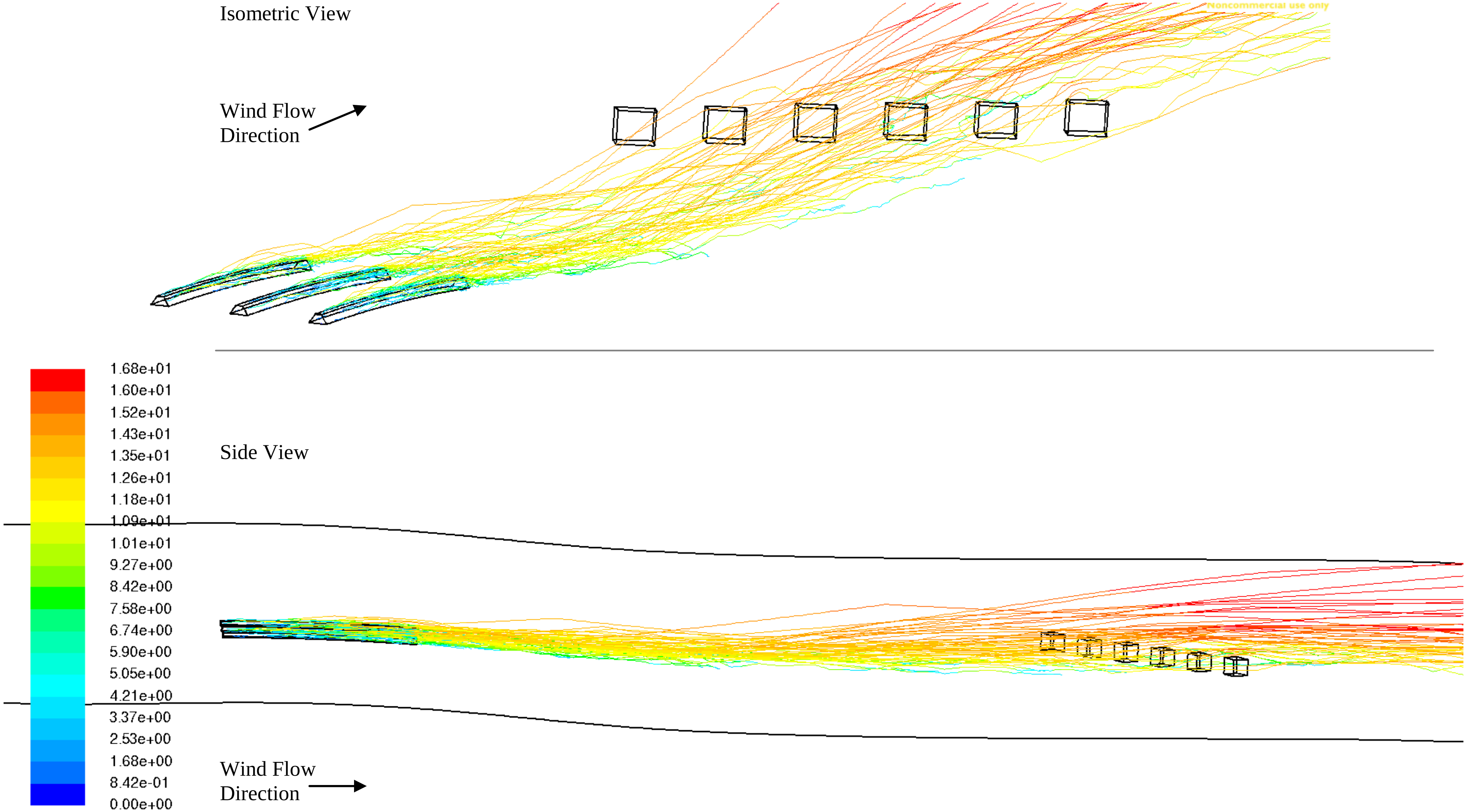

Figure 103 : Site B – Tracks of particles released from compost piles coloured by velocity magnitude (ms^{-1}) for inlet condition ABL10h6. (top - isometric view and bottom – side view)

6.5.3 Species Transport at Site B

Species transport simulations for both inlet conditions were run with similar conclusions drawn when compared to Site A; the effect of inlet condition on species transport was alike with the lower inlet velocity spreading wood species further. However, in the case of Site B wood species reached the end of the domain for both inlet conditions; mole fraction of wood at the outlet boundary was higher for ABL2h6 (15%) than for ABL10h6 (5%).

Regarding the vertical direction and the case of ABL2h6, high percentages of wood species mole fraction (80%) were seen to reach a height of 30m before starting to decay rapidly and drop to less than 50% (Figure 104). This did not seem to be the case for ABL10h6 for which wood species returned to background levels in the first 10m (Figure 104).

For the horizontal direction and in the case of ABL10h6 species were seen to travel much less and decreased below 5% within 280m from the compost piles nearly touching Village B houses (Figure 105). Fraction percentages in-between compost piles were also lower than ABL2h6 with species forced to the ground.

Finally, as for the case of ABL2h6, wood species were seen to travel further distances than ABL10h6 before reaching background levels; so wood mole fraction at Village B houses was 5% to 10% (Figure 105). Mole fraction was seen to drop to 50% within a distance of 100m from the source. The highest mole fraction – as expected - was present at and within the three compost piles.

6.6 Conclusion

Results of particle tracking and species transport presented in this chapter for Sites A and B create questions for the suitability of the - rather simplistic - EA rule for risk assessment of proposed compost plant when sensitive receptors are situated within 250m of the plant borders and the need of modelling slopes less than 1:10.

Particles and concentration percentages were seen to reach nearby houses at both sites at different intensities depending on the examined wind speed, direction and topographical factors taken into consideration in the modelling process.

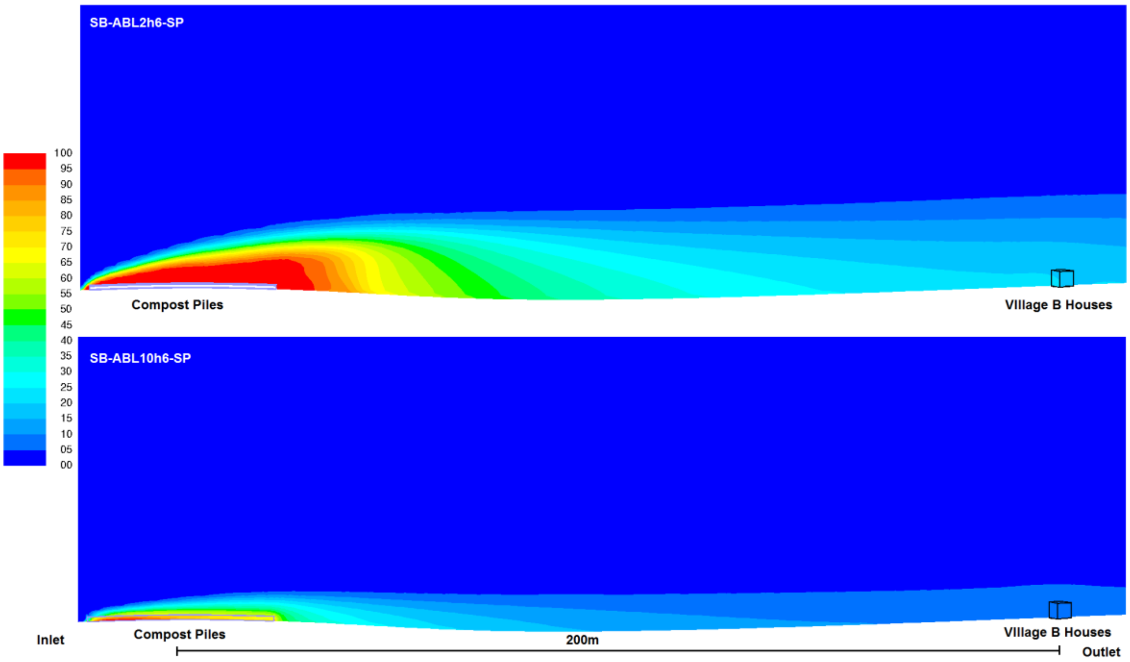

Figure 104: Site B - Contours of wood mole fraction (%) on vertical cross sectional plane passing from both compost piles and houses for the examined domain with inlet conditions of (top) ABL2h6 and (bottom) ABL10h6.

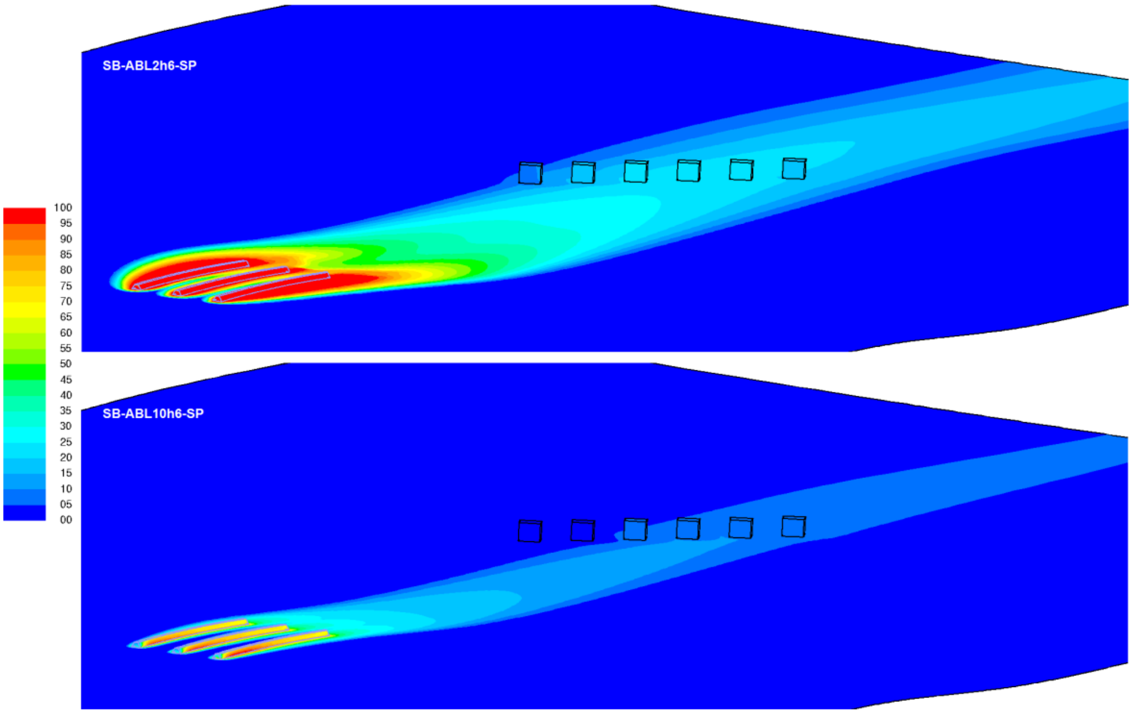

Figure 105 : Site B - Contours of wood mole fraction (%) on ground face for the examined domain with inlet conditions of (top) ABL2h6 and (bottom) ABL10h6.

Chapter 7

DISCUSSION

7.1 Introduction

Based on literature review of available methods for wind flow modelling and air pollution dispersion, present work has demonstrated the necessary initial steps of the proposed CFD method to tackle such complicated problem. By utilising ideal topographical scenarios, in combination with wind profiles for the atmospheric boundary layer, particle dispersion and species concentration over axisymmetric sinusoidal hills were studied. The same technique was used to examine two real-life locations in the UK: an existing green waste processing plant in West Midlands and a proposed location for an industrial scale, open windrow composting site in South Yorkshire.

Current, Chapter 7 discusses challenges and problems of the CFD technique employed for environmental wind flow and pollution dispersion investigation. Moving on from the literature review presented in Chapters 2 and 3, the computational approach described in Chapter 4 and simulations presented in Chapters 5 and 6 for ideal and real topographies respectively, this chapter interrelates final results that lead to useful conclusions for such multi-variable problem.

ABL profiles, type of sources and topography factors influencing wind flow are further discussed herein. Results from the two methods employed for effluent pollutant modelling in CFD program FLUENT (Lagrangian Particle Dispersion and Species Transport) are integrated to give a better understanding of the behaviour of particulate pollutants when released from near-ground sources like open windrow compost piles of several meters in length (compost pile 100m long, 3m high).

Finally, advantages of the proposed CFD approach to currently used dispersion programs are presented in relation to the range of modelling problems that such technique can cover. This ensures the meaningful use of the CFD examination method for simulating cases that should not be tackled with the currently operational programs, taking under consideration today's available computational processing power and wide accessibility to CFD programs.

7.2 CFD Numerical Modelling Challenges

By employing computational program FLUENT, the use of the herein proposed CFD approach has brought up the problems which a researcher and/or a modeller will encounter and have to overcome when modelling wind flow and pollution dispersion during an environmental risk assessment study.

For simple modelling cases with low complexity (flat terrains, absence of natural or manmade wind breaks), the CFD approach should not be chosen. Particularly for the study of simple 2D real life problems, any CFD program would require more resources and processing time compared to frequently used and previously mentioned (Chapter 3.10) approved programs such as ADMS and AERMOD.

As suggested by Pullen et al. (2005), Di Sabatino et al. (2007 and 2008) and Riddle et al. (2004), CFD performs better in complicated modelling cases where geometry plays an important role to the wind flow which largely affects pollution dispersion near ground. On the other hand, it is already established that ADMS can accurately model effluent pollutants when results are compared to data collected from full scale measurements [Taha et al., 2007; Righi et al., 2009; Connan et al.,2011] and to wind tunnel data [Carruthers et al.,1999; Hajra et al.,2010]. However, the assumptions of the wind flow and dispersion models used in ADMS and especially the limits on topographical resolution, number of buildings and sources need to be taken under consideration and designers or regulators need to set the limits for modelling such multi variable problem using these programs.

Thus, the question 'when' to use CFD arises, followed by how to correctly setup the modelling process and appropriately specify all necessary simulation settings. Such careful and step by step procedure should produce meaningful results which later can be interpreted to get conclusions regarding air pollution dispersion from near ground sources.

Moving on from standard requirements of a CFD study such as definition of domain size, mesh density, boundary conditions and dispersion model to use, further questions come up regarding the complexity of the problem and how much information to include in simulations, such as: source and emission alternatives; topographical factors to design and include (high buildings, large density of small houses, trees, forests); weather phenomena for which to simulate; number of wind directions and conditions (calm, windy, variant); time scale of the simulation (instantaneous, 1hour, 24hours, several months, etc.); and other significant factors mentioned and discussed earlier in Chapter 3.

The above topics - amongst others - are discussed below based on simulations run for this work and conclusions withdrawn during the modelling progression as well as from wind flow and pollution dispersion results for both ideal and real terrains.

7.2.1 Topography and Geometry Selection

For simulations of wind flow and pollutant dispersion over theoretical and ideal terrains, choice of resolution and characteristics to include is rather simple: most of the times topographical features and factors (cubes, hills, cylinders) that could influence results are chosen and deliberately placed in the flow path. This approach is similar to wind tunnel experiments and widely used for replication or comparison of numerical, experimental and on-site data collected.

However, this is not the case for real terrain problems requiring modelling in order to acquire some meaningful results - especially for pollutant concentrations. Urban but also rural topographies require careful selection of the area modelled, deciding whether or not certain wind obstacles will be included and at what resolution. This is the case for large trees, forests, hills, ridges, houses, villages, etc.

In the open environment, challenges connected to topographical characteristics such as high buildings and other man-made obstacles are less common. In most cases, the difficulty lies in choosing the right geographical area to cover. The source of pollutant is always the main focus of the simulation together with nearby sensitive receptors. There should be enough domain length upwind and downwind to enable the full or maximum presentation and examination of pollutant spread to the surroundings. Hills, ridges and other features that could influence the wind flow at source must be carefully examined in order to decide whether to include, neglect or substitute these with related boundary conditions. Certainly these assumptions/choices cover a single wind direction. For examining several wind directions these factors need to be further considered and inspected prior to starting simulations - in some cases adjustments per wind direction are necessary.

It should be noted however, that in most modelling cases, no matter the long planning, most of the problems with setup of the geometrical and mathematical model arise during the -rather normal- repeating simulation process. Small corrections and adjustments after every (un)successful simulation lead to the final and approved computational model which consists of a balance between realistic information and necessary assumptions - both in geometry and in represented physical phenomena.

7.2.2 2D vs. 3D Domain Modelling

Simple modelling cases with low topographical complexity could be modelled in 2D with the use of any CFD program. However, as mentioned above such cases would be quicker and more economically and appropriately examined with the help of a fast-turnaround program such as ADMS. Yet, it is important to understand the difference between 2D and 3D modelling which affects results for wind flow and eventually pollutant spread.

To further investigate effects of terrain dimensionality to wind flow, simulations were run at early stages of this work comparing wind flow over a single sinusoidal, axisymmetric hill in both 2D and 3D terrains. A logarithmic ABL wind inlet profile was used with mean velocity $2ms^{-1}$ (ABL profile and its characteristics are described in Chapter 3.2.5). All dimensions, conditions and solver settings were identical for both domains in order for such comparison to be analogous.

Figure 106 presents wind flow ribbons (coloured by mean velocity magnitude) over the same hill (2D vs. 3D comparison). As shown in the 2D case, wind can only travel over the hill, with the full fluid volume passing over the top of the hill where the maximum velocity point is. This is also the point of maximum velocity magnitude for the 3D domain examined, however, as the domain is three dimensional wind not only travels above the hill but also around it. This effect, decreases the maximum velocity value atop the hill resulting to a lower velocity magnitude for the complete 3D domain.

The dissimilar effects of single 2D and 3D hills to the wind flow is further presented by Figure 107 which displays horizontal (parallel to the ground) wind velocity profiles at height H (atop the hill) and at height 2H for the two domains described above. Maximum velocity magnitude atop the centre of the hill (at x/D=0) has little difference between 2D and 3D cases: only 0.1 at height H and 0.15 at height 2H with values of wind magnitude for the 2D terrain always greater than the others.

The dimensional dissimilarity of domains is seen to affect the wind phenomena at the windward and leeward faces of the hill as also as the relevant reattachment length.

For this examined hill and the specific ABL inlet condition there was no recirculation neither on the windward nor on the leeward faces of the hill. More specifically, at height H, the decrease of wind magnitude upwind the hill starts earlier at -2.5D for the 2D domain rather than that at -2D for the 3D domain. Similar behaviour is seen on the leeward face and downwind the hill towards the outlet of the domain. The wind velocity magnitude returns to approximately the original inlet value at height H: this takes place earlier for the 3D terrain at 4.5D than for the 2D terrain at 5.5D.

Figure 108 shows contours of mean velocity magnitude and coefficient of pressure for a single 3D hill as described above for inlet condition ABL2h6. Front (inlet) views of the domain show contours on the mid-plane and on the windward face of the hill. Top view for coefficient of pressure shows contours on hill and ground faces. As already presented in Chapter 5, Figure 108 illustrates contours of mean velocity magnitude and coefficient of pressure that show pressure dropping as velocity increases on the windward face of the hill. At the highest point of the hill, velocity has its maximum value and pressure coefficient its minimum. Finally on the leeward face of the hill velocity drops and the pressure coefficient increases again.

From results presented in Figure 108 about single sinusoidal axisymmetric hill, it is clearly visible that the modelled 3D hill is shown to create symmetrical wind flow patterns around itself and towards all three directions. This symmetry should be expected and assumed correct when modelling an axisymmetric wind obstacle (hill or cube) with a steady state RANS approach as herein [Ishihara and Hibi, 2002; Parker and Kinnersley, 2004]. However, it is well known that wind flow is not completely symmetrical. This 'non-symmetry' can be further studied by numerical methods that take under consideration previous behaviour of the flow (i.e. unsteady RANS approach) or examine the domain -and specific parts of it- in more detail such as by Tessicini et al. (2007) (i.e. LES approach or hybrid approach: RANS for the domain and LES for closer and more detailed examination at areas of interest).

For actual wind flows in the open environment, complexity of phenomena such as geometry, roughness and weather largely affect wind characteristics and the existence of symmetry is very rare. Thus, the simulation of any domain that provides symmetric results may not be accurate but it gives a good indication of phenomena for this isolated part of terrain. A nearby hill, large lake etc. could always be present and would always affect final results. Such drawback forms the need for an infinite in size domain to examine the complete topography, a task which is by principal impossible and would require infinite amount of time and resources to accomplish.

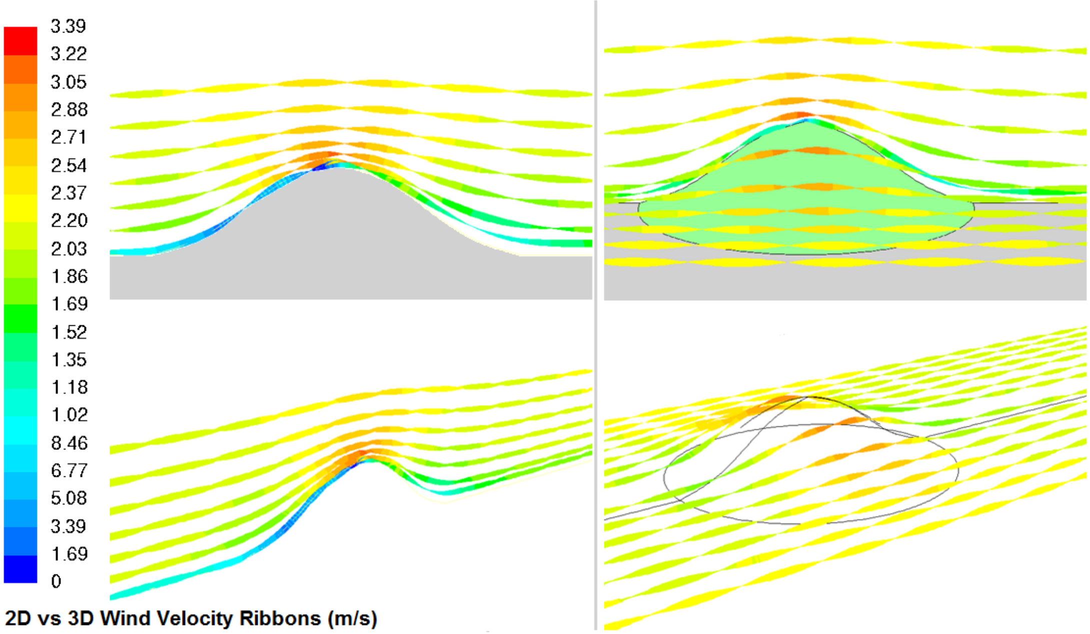

Figure 106 : Wind flow ribbons coloured by mean velocity magnitude $\overline{u}$ for wind flow simulation over 2D (left) and 3D (right) sinusoidal hill (comparison of side and isometric views).

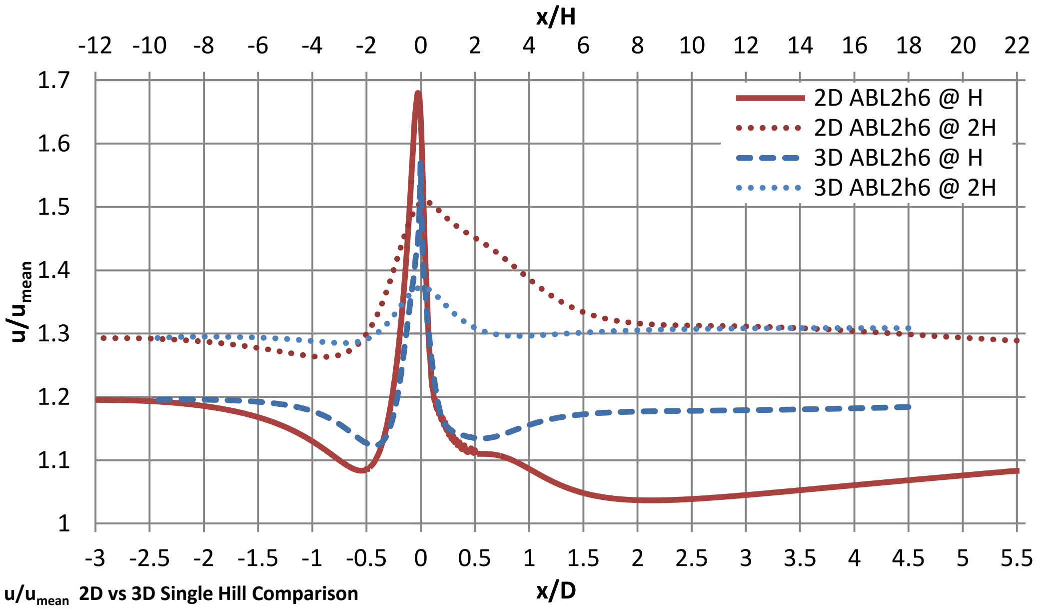

Figure 107 : Comparison of horizontal profile plots for wind velocity at heights H and 2H above ground for wind flow over 2D and 3D sinusoidal hill.

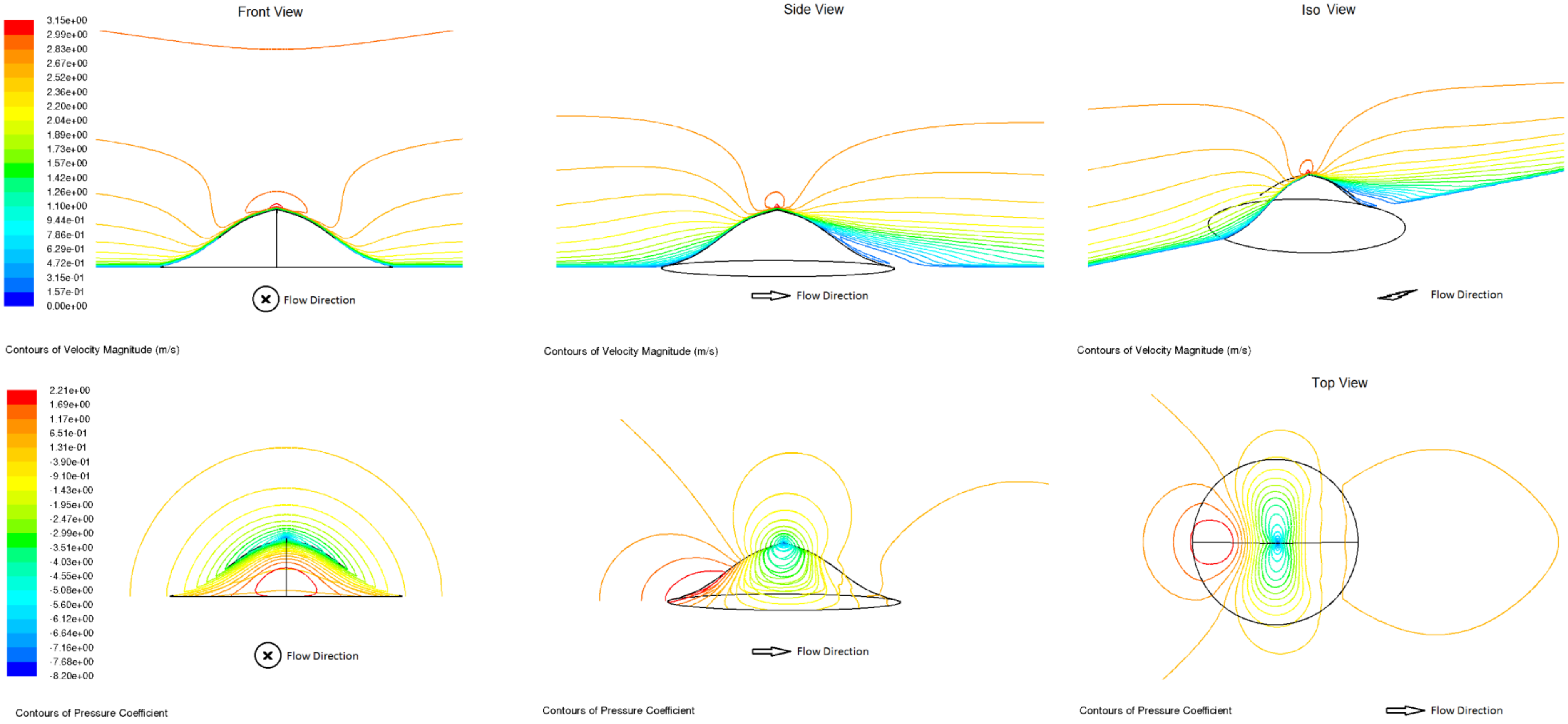

Figure 108 : Contour plots of mean velocity magnitude $\overline{u}$ and pressure coefficient Cp over single 3D hill for inlet condition ABL2h6.

(Front and side views show contours on hill face and mid-planes and top view shows contours on hill and ground faces)

7.2.3 Accuracy vs. Precision

Accuracy and precision in a given time frame are often difficult to achieve both when modelling environmental flows. Most of the real terrain modelling cases are undertaken for risk assessment of a possibly dangerous plant, site or stack that could influence the quality of life of neighbouring sensitive receptors. Thus, these studies have a deadline by which meaningful results must be produced and explained.

Limiting factors for accuracy and precision within a time frame are, as earlier discussed in Chapter 3, the modelling program, the computational power available and the complexity of the problem being studied. Usually, the more localised the phenomena, the more resolution is required in the simulation. This could often lead to long processing times and vast computational requirements.

Theoretically, for a very complicated problem, if the modeller had infinite time and computational resources, at some point in time he/she would achieve a great detail of accuracy and precision. Given that such careful examination requires continuous development of the geometrical and numerical model and that accurate and precise results are reached after a series of hit and miss simulations that can be compared to hitting or missing a target (see Figure 109), after an infinite amount of time and available equipment, one will be able to achieve the perfect result.

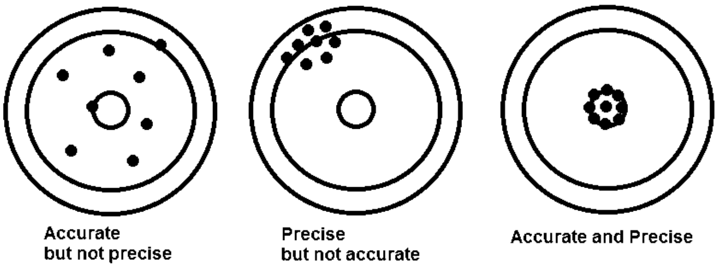

Figure 109 : Accuracy and precision after infinite time and number of tries.

However, this is not the case for real life examination problems for which certain assumptions and retreats need to be considered. In the case of CFD modelling of any open environment, these are mostly related to the numerical model of wind flow, topography and source representation and largely to weather phenomena that cannot yet be fully included/represented in simulations.

Final results must always be accompanied by all assumptions considered and these must be always presented and explained to clients / end users / risk assessors clearly.

7.2.4 Domain Size, Resolution and Mesh Density

The complete set of ideal terrain results presented in Chapter 5, after introducing the use of ideal terrain in Chapter 4.5, show that wind flow is affected at great distances around the ideal hill in both 2D and 3D terrains with the wind disturbance in some cases reaching the user assumed and set boundaries.

Therefore, the need for correct domain size when modelling such problems is created. It is important to consider that the case described above is a flat domain with a single axisymmetric sinusoidal hill - one of the most simple terrains encountered in theoretical research. When modelling several hills, non-flat terrains or overlapping hills, special attention should be given in order to choose appropriate distances upwind, downwind and sideways wind obstacles and adjoining boundaries to avoid possible interference with wind flow results.

Consecutively, to ensure that there will be no interaction between the studied hill and the surrounding boundaries, domain size studies were completed and presented both for the 2D and 3D hill in Chapters 5.3.2 and 5.4.2 respectively. This is a necessary process designed to show the correct choice of domain dimensions after several tries (2D: Table 16 and 3D: Table 18) and comparison of wind flow results and in specific mean wind velocity profiles (2D: Figure 30 and 3D: Figure 43).

Such comparison of results direct to specific domain dimensions of the problem and dimensionality (F5-S0-A12-B10 for 2D single hill and F4-S3-A4-B8 for 3D single hill) and are used to further set the final numerical domain by feeding it to the mesh density study. A domain study is meaningful when the mesh density amongst domains compared remains constant. For that purpose, a structured grid of 1x1m throughout the domains was used for both 2D and 3D studies. This ensures that no matter how the domain dimensions change, the resolution of the examination remains constant and therefore the comparison is valid.

Following the choice of domain size, a mesh density study has to be undertaken. This ensures that results are mesh independent and that the highest mesh density is concentrated in areas of interest - in this case at and around the hill. Such study was undertaken for both 2D and 3D hill domains in Chapters 5.3.3 and 5.4.3 respectively. The selected 2D domain was separated in five areas to assist towards the required high mesh density before, after and on the hill (Figure 32). A variety of mesh intervals (from 0.5x0.5m to 2x2m) and strategies (uniform and expanding) were selected to examine the domain with resolution from 15,400 to 662,880 cells (Table 17). Taking under consideration the longitudinal wind velocity profiles along the top boundary and at two hill heights above ground level (Figure 33 and Figure 34) a uniform mesh of $1m^2$ at and above the hill was used; for the remaining part of domain upwind and downwind the hill, an expanding mesh from 1 to 10m was used.

A similar method was employed for the mesh study of the 3D domain with lessons learned from the 2D study. The domain was separated into six volumes (2D domain was separated into five areas; see Figure 32 versus Figure 44) to allow for structured evenly expanding mesh. Three mesh densities at the hill were examined (0.75, 1 and 2m) with expanding mesh intervals in the direction of outer boundaries; the most dense domain had 2,455,560 cells and the less dense 715,000. An intermediate mesh density of 1,285,000 cells was chosen to compensate between computational cost and resolution required.

An important aspect to consider when meshing any domain -2D or 3D- and particularly an open environment problem is the cell size and shape at the ground/ wall faces. More specifically, the height of the first cell adjacent to a wall boundary largely affects y^+ values (see also standard wall function described in Chapter 4.4.3) which indicate the quality of the created mesh/grid. The setting of y^+ within range of recommended values, suggested by the designers of each program, ensures good quality results of simulations.

However, as previously discussed in Chapter 5.2, several authors have discovered the difficulty of achieving recommended values without the use of a custom wall function especially designed for environment flows. When the creation and incorporation of such custom wall function is not possible, an increased mesh density must be concentrated on wall boundaries. This creates an added complication to the already difficult problem to represent mathematically, as the designer must compromise between high density mesh on wall faces and also in areas of interest in order to increase quality of results but at the same time decrease as much as possible the total number of cells to save on required processing time and power.

The above summarised procedure is mainly followed for simple -mostly theoretical-terrains. Domain and mesh density studies for open environment flows and real topographies require a different approach due to their size and complexity. Sometimes domain size and boundaries are set by the problem itself - a larger area covered by the examined domain would rapidly increase computational cost: Banks (2005) has studied flow around the Art's Tower in Sheffield and has included only surrounding buildings that influence the flow reaching the tower - resolution of buildings was low except the tower itself, see also Figure 19; Blocken and Persoon (2009) have examined the flow around a football stadium modelling the stadium and the main shape of surrounding buildings within a radius of 300m; Turpin and Harion (2009a and 2009b) have first modelled wind flow over bulk material stockpiles and later modelled the complete site complex presenting interactions between stockpiles and buildings for several wind directions (again only main rough shapes of buildings were modelled - no complexity). It is apparent that domain size and resolution of topography characteristics to be included depends on the problem itself, nearby wind breaks, suspected problematic areas and most importantly wind speed and angle.

Site A's description and results presented in Chapter 6, will be used below as an example to demonstrate possible problems during the selection of the modelled topographical area. In regards to this site, the author has previously simulated 2D vertical planes of this topography with results presented in Katsanis (2008). That work took an initial step towards 3D modelling by examining a domain area of 3km^2 based on terrain elevations from Ordnance Survey maps and some rough shapes of the adjoining forests that can influence wind flow over the houses of Village A.

This initial domain had very large dimensions: 3x3km ground area and a height of 1.5km. The presumed compost site was located and was noted on the domain with a single dot - no windrow piles were designed. The same happened with Village A which was represented by a black shaded area with no houses modelled. The two large forests were designed as large wind breaks with sharp corners due to limitations on available time and problems with the meshing procedure; this is largely influencing wind flow as later evident by results.

Figure 110 (top) presents the initial 3km^2 domain firstly examined by the author in previous work and (bottom) the final -updated- domain used in this work for simulation of wind flow with three different ABL inlet profiles and pollutant spread from three presumed compost piles.

The modernized geometry and domain is the result of a series of runs and improvements of the design of topography modelled. The domain area was decreased to 1.15x1.6km and the height to 600m to save computational time and power - the extra area was simply not adding any information to the results. That helped concentrate high mesh density at areas of interest and especially close to the ground face, the three modelled windrow piles and nearby -simplified square- houses. The big neighbouring forests received smooth corners and all wind breaks (piles, houses, forests) had flat tops to help with the volume meshing process. Figure 111 presents detailed views of these improvements and the mesh structure on and around them.

Specific attention was given to the volume mesh of the domain which consisted of approximately 2 million cells with nearly half of them on the ground and on and around areas of interest. The difficulty with meshing large 3D domains with geometry that has curves and multiple wind breaks attached to the ground is the continuity of cells. The top boundary (sky) needs to have the same number of nodes and very similar node alignment to the full ground surface along with the top faces of the modelled forests, houses and compost piles. Such task required the separation of Site A domain into six different volumes which were connected (no intermediate face exists) but would be meshed separately to help the meshing process in regards to time and quality (see Figure 44).

Finally, such choices, assumptions and difficulties defined for the vital process of the numerical model to be utilised have to be repeatedly visited after every successful or unsuccessful simulation in order to adjust or improve and ultimately get the best available and meaningful final result.

All of the above must be considered in order to create a model of a real topography which will give satisfactory results (quality answers to the problem) within a reasonable amount of time, using realistic -and available- computational power.

The topography, geometry, dimensionality, boundary conditions and mesh created, are all fed into the solver of the CFD program which then utilises the selected equations and assumptions to simulate wind flow and pollutant dispersion as presented and discussed in the following part.

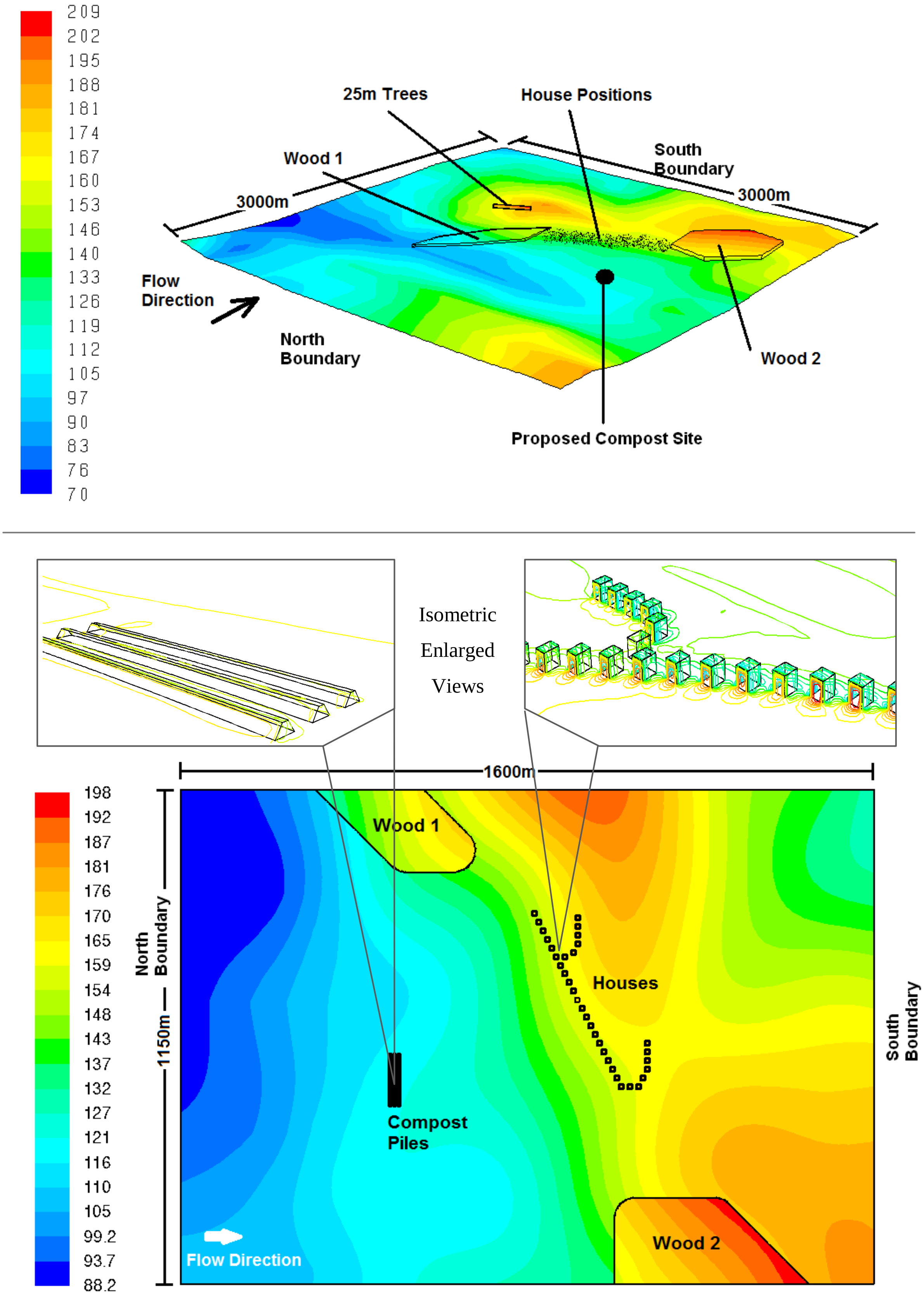

Figure 110 : Site A - Comparison of domain size and modelled terrain characteristics for (top) initial simulations and (bottom) final simulations. Contours show elevation above sea level in meters.

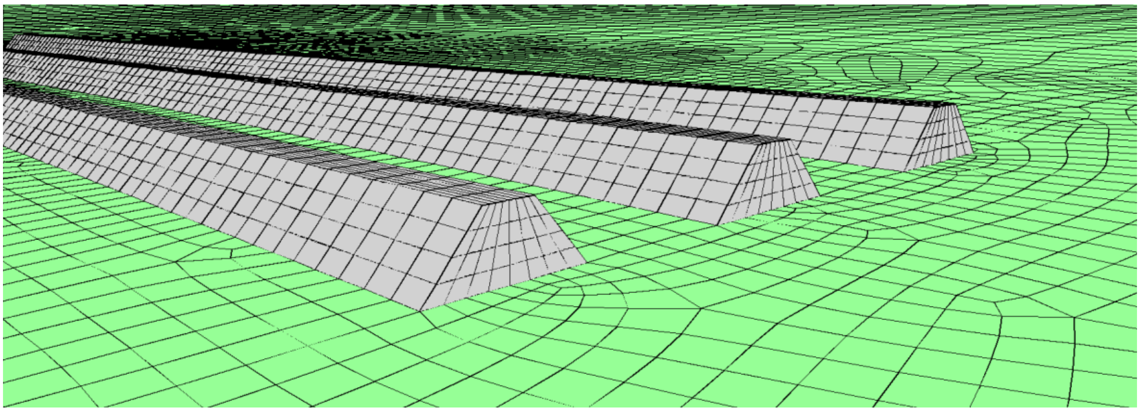

(a) Presumed compost piles detailed view.

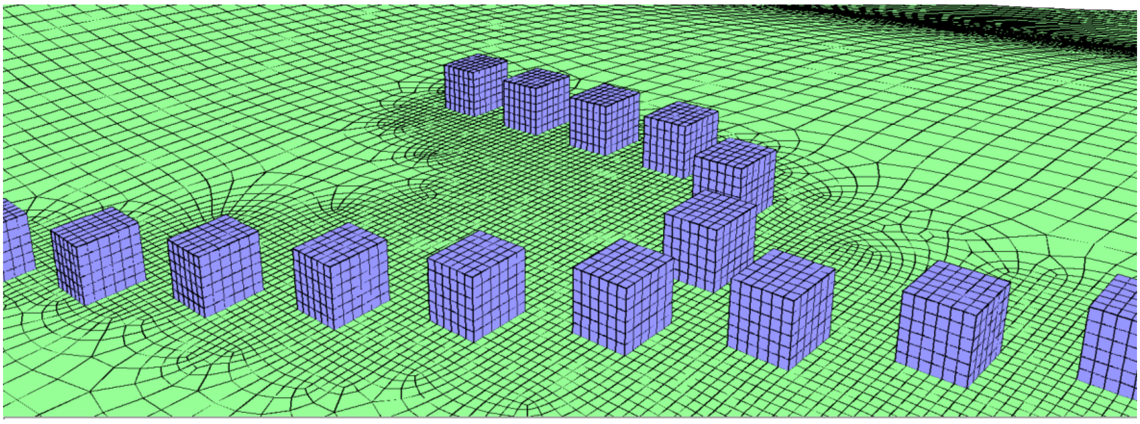

(b) Houses at Village A detailed view.

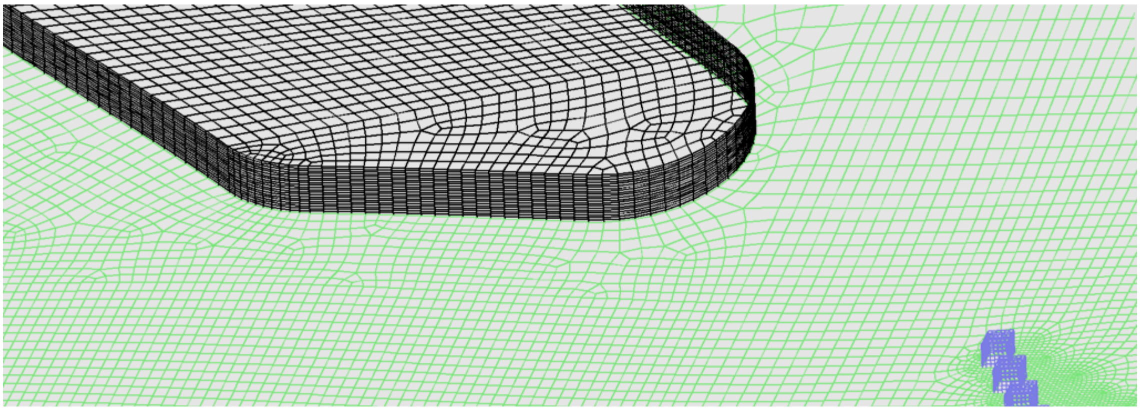

(c) Nearby forest detailed view.

Figure 111 : Detailed views of the final domain for Site A with structured mesh and improved design. (a) view of the three presumed windrow compost piles; (b) view of the houses at Village A; (c) view of one of the forests. All wind obstacles have a structured mesh and a flat top face to allow for structured cells in the vertical direction and therefore in the volume of the domain.

7.2.5 Boundary Conditions

Following the numerous complications for choosing and placing the boundaries of a domain, as discussed in previous parts of this chapter, the mathematical representation of the environmental conditions modelled needs to be selected.

Chapter 4 has already discussed boundary conditions chosen by other / previous authors for correct representation of open environmental flows and several types regularly selected for use with CFD programs. These boundary conditions are picked following assumptions on the real conditions at each boundary, sometimes representing phenomena that would occur outside the domain such as disturbances to wind flow due to hills, buildings etc. Such disturbances are represented by calibrating the relative mathematical options and assumptions of each boundary.

For instance, the wind profile at the inlet boundary of the domain would be altered and numerically represented by a curve according to real measurements or previous simulation results of this part of the area examined. Taking as an example the setup presented in Figure 112 which would be used to study the effects of Building 2 to the wind flow, and assuming that a uniform wind velocity profile is necessary at inlet 1, the arrows at inlets 2 and 3 show how wind profiles would change because of Building 1. It is clear that a choice between inlet 1, 2 or 3 would require a choice of the correct wind profile based on the previous wind breaks (in this case the changes to the wind flow because of Building 1). Such technique should apply to all open environmental flows for which it must be ensured that the original wind inlet conditions are represented as accurately as possible and later only affected by the domain characteristics downwind.

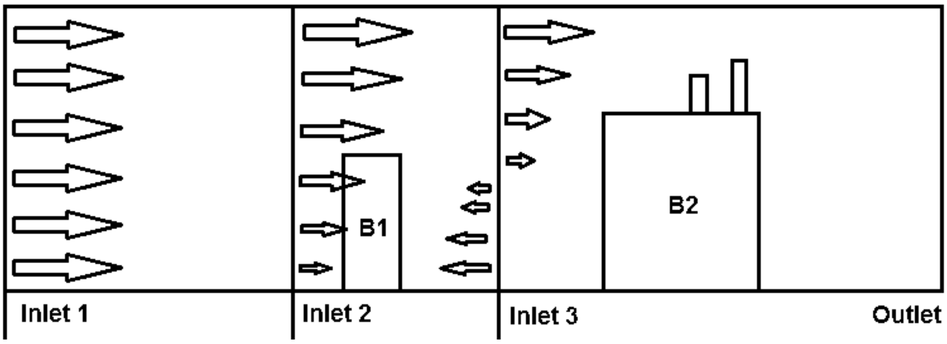

Figure 112 : Graphical representation of wind profiles at different inlets upwind and downwind Building 1, starting from an assumed uniform inlet profile at Inlet 1.

Such adaption of wind profiles to critical topographical factors, clearly shows that a uniform profile cannot be applied for numerical modelling of open environment flows as it would indicate that wind speeds on and near the ground are of the same value as at a few hundred meters above that. Moreover, if a uniform profile is defined at the inlet of a domain, this must be placed at a sufficient distance upwind the area that needs modelling in order for the wind profile to develop and adapt to the topographical factors included in the domain. For most environmental simulations, real wind data is used either from experimental results or from available data recorded at nearby weather stations (the approach followed in this work). Using data recorded at the exact location that requires modelling is very rare and expensive.

Changes to wind flow downwind in any open environment domain are very much dependent on the ground face of the examined area. As previously described in Chapter 3 and presented in Chapter 4, ground characteristics significant to the wind flow and pollutant dispersion can be represented either geometrically or mathematically. In most cases a combination of these two methods is used. Rough geometries of buildings, hills, forests are modelled and in addition, a surface roughness value is used on these faces/volumes to further describe their effect to wind flow. Values are selected for different surface types, from water to urban settings. For simulations presented in this work the value of $K_s = 0.2$m was used as previously described in Chapter 4.4.3 while taking under consideration the grass land examined and the necessary correction factor for FLUENT (typical values of roughness factors presented in Table 11).

7.2.6 Wind Flow and Pollutant Dispersion Approach

Mathematic representation of wind flow, weather phenomena and pollutant dispersion is a complicated process. RANS equations are used as described in Chapter 3.3 in combination with a turbulence model for mathematical closure of these equations as described in Chapter 3.4. Pollution dispersion has many advantages and there are Eulerian, Gaussian and Lagrangian models available in simulation programs, as previously discussed in Chapter 3.5. The choice of the dispersion model to be employed mainly depends on complexity of dispersion and complexity of effects introduced as illustrated earlier in Figure 12.

Pollutant source, topography and weather, as previously stated in Chapters 3.7 to 3.9, largely affect wind flow and pollution dispersion, in principal defining the choice of strategy to be followed for correct numerical representation of real-life open environment flows - the problem that this work mainly examines. Further analysis can be included for some pollutant spread modelling cases, such as dry deposition (deposition at the Earth’s surface) or wet deposition (incorporation into cloud droplets during formation of rainfall) which can also be mathematically represented when necessary according to each program's capabilities.

The numerical approach followed for CFD simulations in this work was presented in Chapter 4.3. RANS equations in combination with the standard k-ε turbulence model as originally suggested by Richards and Hoxey (1993), were employed for numerical examination of wind flow. Lagrangian Particle Tracking was utilised to predict dispersion of particles under turbulent conditions, in combination with the Discrete Random Walk Model to calculate instantaneous velocities. Later, the Species Transport approach was employed to model pollutant concentration spread.

The selected numerical approach for wind flow examination (RANS with standard k-ε turbulence model) for idealised and later real topographies, produced good results when compared to those by Hargreaves and Wright (2007). The ability of the numerical wind flow model to generate constant wind flow characteristics when examining the simple case of flat terrain in Chapter 5.2 (Figure 23) was tested and further connected to domain size choice by trying to maintain constant ABL characteristics for the longest possible distance. Past several simulations and after altering the height of the 3D flat domain (Figure 24, Figure 25, Figure 26, Figure 27) it was concluded that in order to maintain such characteristics using the described wind flow model, turbulence model and boundary conditions, the minimum simulated domain height should be at least one third of the domain length (Equation 5.1). Such requirement is understood to be connected to the process FLUENT uses to calculate flow variables within the domain examined (Figure 28) as discussed in Chapter 5.2. This recommendation clearly depends on the choice of CFD program and numerical approach selected in this work and should not be considered as a general rule. However, it is a good practise point to initially examine the abilities of the simulation program to be used and compare its results to already established and accepted data published by other authors.

Particle tracking in combination with the RWM was later enabled to track particles departing from theoretical vertical and horizontal line sources. As described in Chapter 5.4.4, the combination of these approaches introduced turbulence to the particle release overcoming the initial and rather simple approach that pollutant particles follow the exact same path of air particles. Such particles were considered massless and unaffected by gravitational forces as the size of single bacteria and fungi released from compost operations is negligible (see Table 9 and Appendix 2). Due to their small size, these were assumed to get absorbed when hitting an obstacle or the ground face of the domain. In real life, bacteria and fungi (groups) may get stuck to trees, etc. and may be set free again. However, these will most probably be inactive due to their short lifetime when not under certain conditions (especially temperature). Thus, the need and setting for absorbing particles numerically modelled when touching any boundaries in the simulations of this work.

Lagrangian particle tracking results give a good indication on how particulate pollutants would travel and in which areas of the domain (according to geometry complexity) these are more likely to get trapped, recirculate and get reattached to the flow. Such modelling technique requires only a short processing time and is completely dependent on wind flow results. There is no need for further simulation of the examined domain when the examined particles are small and do not affect air particles. Nevertheless, there is no indication on the concentration spread and reach of pollutant releases from compost processes. This is when species transport modelling (described in Chapter 4.3.5) needs to be employed at the cost of longer processing times and computational power. Such technique can graphically and numerically show the release of pollutants (single or mixed gases and solids but also reactions) with defined properties (density, viscosity, thermal properties, etc.) and how these spread within the domain examined, when affected by wind flow magnitude and direction.

Comparison of the two pollutant dispersion methods is meaningless as these produce results for different parts of the problem. However, the joint use of these two methods can be a powerful tool. The Lagrangian particle tracking technique can be used to initially examine particle trajectories, average distance travelled and entrapment possibility, given the selected setup and simulation options. Such results can assist in improving the domain geometry in order to further investigate pollutant spread and concentrations using available species transport models. Both methods combined can produce additional meaningful results for the comprehensive understanding of the multi variable pollution dispersion problem.

7.3 Wind Flow and Pollution Dispersion over Idealised Terrain

Wind flow and pollutant dispersion results over 2D and 3D steep and shallow hills were discussed previously in Chapter 5. The effects of domain and especially hill geometry on wind flow have already been proven to be significant for effluent pollutant spread and concentration. This was initially shown by 2D flat versus 2D single steep hill simulation and later by 3D flat versus 3D single steep hill results. Finally, combinations of double 3D steep/shallow hills in a row were simulated to examine the influence of the first to the second hill.

Results for wind flow and species transport over an ideal 2D flat terrain versus a 2D single steep hill terrain showed that the hill is acting as a barrier to the spread of wood species downstream (Figure 39 and Figure 40). Percentages of wood mole fraction were seen to suddenly drop just after the hill helping the mole fraction decrease more rapidly downwind. Evidently, the hill also had an effect to species transport under all inlet conditions examined but the largest concentration drop was seen for ABL10h6 for which wood mole fraction decreased by 90% until reaching the peak of the 2D steep hill.

Moving on to the examined ideal case of 3D single steep hill, wind flow results presented in Chapter 5 -Figure 50 to Figure 53- showed the common characteristics of wind obstacle influence to the surrounding environment: as velocity increases on the windward face of the hill, pressure drops. Atop the hill wind speed reaches its maximum value and the pressure coefficient is minimum. On the leeward face of the hill, velocity decreases and pressure coefficient increases again until they both reach levels prior to encountering the hill. In some cases and due to the shape of the hill (very steep hill) or due to the high mean velocity of the ABL profile at the inlet, recirculation may occur at the leeward face of the hill. Such case requires a longer reattachment length so that the flow properties and their magnitudes return to their initial values (prior to encountering the hill) -usually- further downstream the examined domain.

Based on the wind flow simulation results for the ABL inlet conditions, the Lagrangian particle tracking method was employed to study massless particle releases from two line sources: one horizontal and one vertical which were positioned 100m upwind the single 3D steep hill (see also Chapter 5.4.4). In this current chapter, only the horizontal line source results are further discussed and compared to the horizontal ground area source later used for species transport examination. These are both very similar to a long, open windrow compost pile afterwards examined for the real terrains simulated for Sites A and B.

Statistical analysis was done to process the particle travelling distance and also the entrapment possibility. Data was collected from multiple results and number of tries of the particle tracking method (see Chapter 4.3.3 and 4.3.4 for mathematical modelling approach). Figure 59 presents these results for all three ABL profiles simulated. Particles released upwind the peak of the sinusoidal hill (on the symmetry plane and close to it) were seen to get trapped more often for all wind speeds due to being stuck on the windward face of the hill. However, if these were to pass by the top of the hill they had the greatest chances to cover a longer distance and potentially escape the domain. For ABL conditions of larger wind speed, particles released from positions close to symmetry plane often enter recirculation zones until being trapped on ground faces or being reattached to the main flow. Particles released further away the symmetry plane and upwind the lowest parts of the hill generally travel longer distances and get trapped less easily as they pass by the hill and any significant wind disturbance created by the hill geometry. Indicative particle tracks are shown in Figure 113 for all three ABL inlet conditions simulated.

A common mistake takes place when processing results for distance travelled by each particle when this particle gets trapped into recirculation zones and then released back to the flow: the distance travelled by the particle is recorded instead of the final position of the particle within the domain. This can be prevailed by monitoring and recording the final position of the particles by means of their Cartesian coordinates thus finding the distance travelled between the original (source) and final (trapped) coordinates. This is the method employed in this work to calculate the average distance travelled by trapped particles released from the previously specified horizontal line source.

Following the statistical analysis of the particle tracks, wood species were released from a ground area source replacing the horizontal line source (see Figure 60 for positioning). The 3D hill was seen to act as a barrier to wood species spread as previously shown by 2D steep hill results. Figure 114 presents a comparison of wood mole fraction percentages downstream 2D and 3D single steep hills. It is clearly shown that mole fractions are lower in-between the source and the hill regarding the 3D domain than they are in the 2D domain. This is due to the wood species also moving around the hill in all directions (x, y and z) in the 3D case and not only in the x and z directions as in the 2D case.

The steep hill is seen to have the effect of suddenly lowering the mole fraction percentage from 3 to 10% for 2D domains and 1 to 3% for 3D domains and according to the ABL inlet velocity (Figure 114). These reductions are valid for the percentage decrease of wood mole species for the ground and wall faces on the symmetry plane of the domain. In comparison to the 2D domain, the 3D domain species result presented above does not give the complete picture of the barrier effect of a hill to the pollutant spread, as all other directions must be plotted and examined.

To aid the above task of understanding the 3D spread of wood species around the hill, contour plots at different heights above ground must be plotted. These were presented analytically in Figure 63 to Figure 65. Figure 115 shows contours of wood mole fraction on the ground, hill and symmetry faces for wind flow over single steep 3D hill as described above: side and top views for all three ABL inlet profiles simulated give a complete picture of species spread over and around the hill and how this alters due to wind speed introduced at the inlet. In addition, Figure 116 presents wood species at 4 and 8m above ground level. Mole fraction results are seen to reach background levels after passing over the hill for ABL2h6 and on the hill for ABL5h6 and ABL10h6. For all three cases, the largest reduction of species percentage was upwind the hill and on the leeward face of it.

From the above discussed results and the combined understanding of Lagrangian particle tracking and species transport it is shown that pollutants travel shorter distances when wind speed is high. On the other hand, steady and low wind speed carries pollutants further down the domain, frequently exiting the studied area.

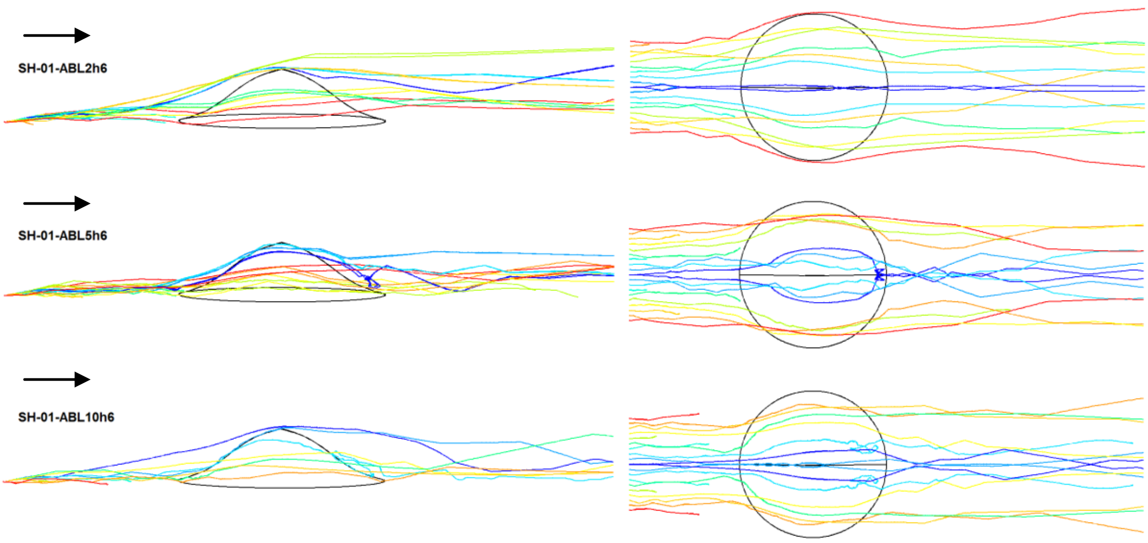

Figure 113 : Side view (left) and top view (right) of indicative particle tracks released from a horizontal line source upstream a single 3D steep hill: SH-01-ABL2h6; SH-01-ABL5h6; SH-01-ABL10h6 (paths coloured by particle ID).

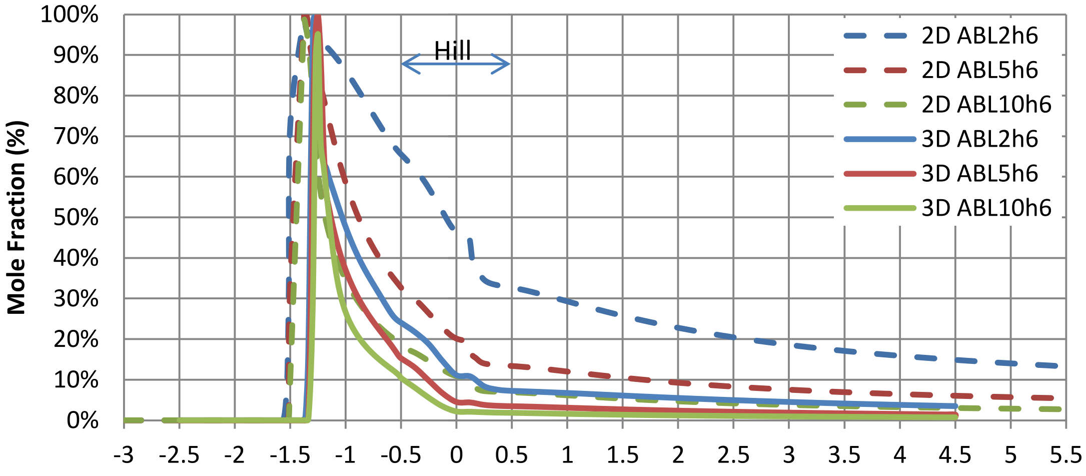

(a) 2D vs 3D Single Hill

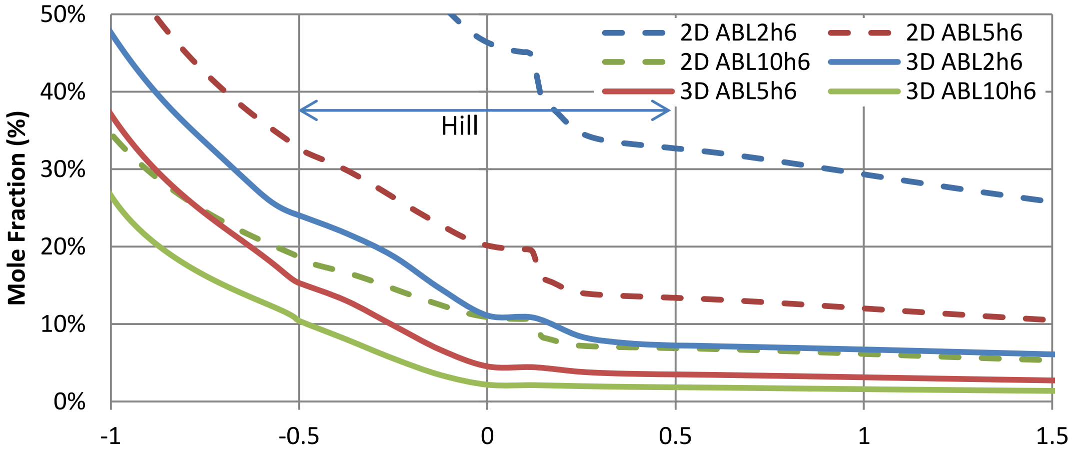

(b) 2D vs 3D Single Hill Enlarged

Figure 114 : Full (a) and enlarged (b) views of wood mole fraction (%) at lower ground and hill faces on symmetry plane for 2D and 3D single hill cases simulations and for three ABL inlet conditions examined.

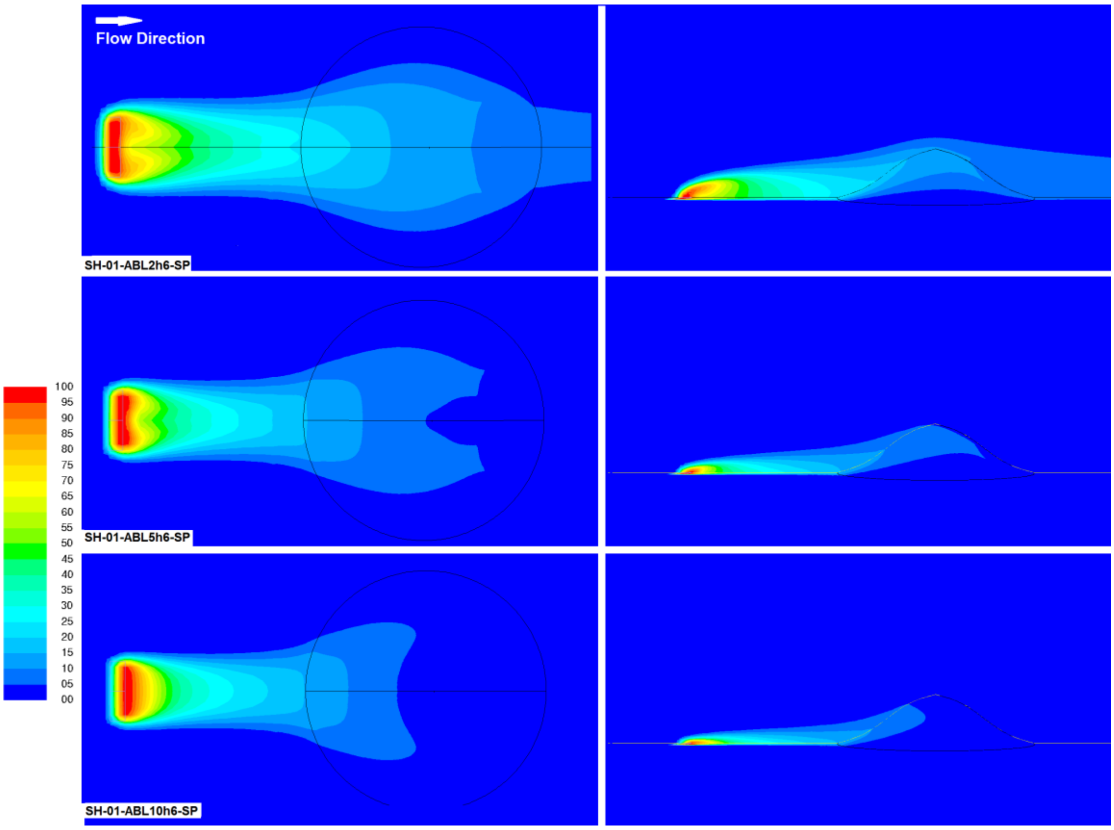

Figure 115 : Contours of wood mole fraction (%) downwind single 3D steep sinusoidal hill. Top and side views for three wind inlet profiles: ABL2h6, ABL5h6 and ABL10h6.

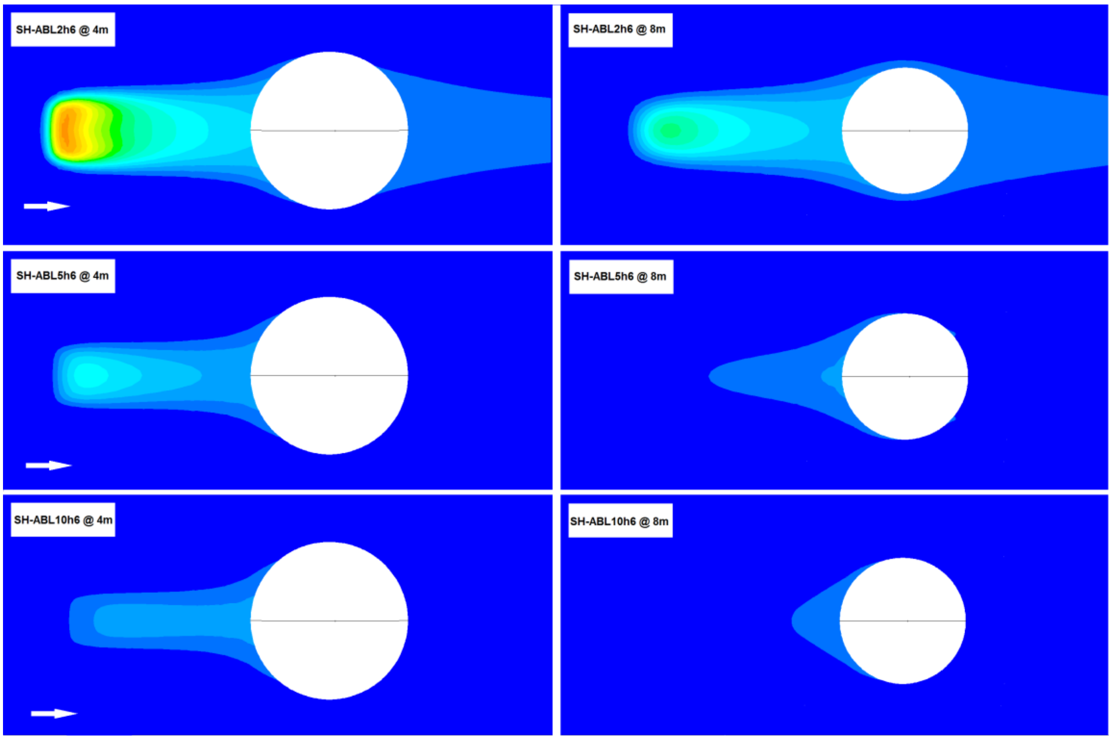

Figure 116 : Contours of wood mole fraction (%) downwind single 3D steep sinusoidal hill at 4m (left) and 8m (right) above ground level. For three wind inlet profiles: ABL2h6, ABL5h6 and ABL10h6.

To further investigate the effect of geometry on pollutant dispersion, combinations of steep and shallow hills in a single row were simulated as described in Chapter 5.5. Wind flow results presented previously in Figure 67, Figure 68 and fully listed in Appendix 3.2 show that the first hill works as a damper to the wind flow approaching the second hill. Such effect helps ease wind phenomena reaching the second in row hill, decreasing the area of recirculation or reducing the reattachment length.

Lagrangian particle tracking was utilised similarly to the single steep hill case in order to examine behaviour of particles released from a horizontal line source 100m upwind the first hill. Results were analytically presented previously in Chapter 5.5. Figure 117 shows indicative particle tracks for the three hill combinations simulated. Particles were seen to enter recirculation zones on the leeward face of the steep hill when this was the first hill of the examined row. Results were different when the steep hill was placed behind a shallow hill: the shallow hill helped smooth the wind flow reaching the steep hill thus almost eliminating recirculation on the leeward face of the second steep hill.

Figure 118 groups results of particle tracks released from a horizontal line source upwind double hill combination cases simulated for inlet profile ABL2h6 (which was shown to carry particles further than other ABL profiles). The double steep hill case (DH-01-ABL2h6) was seen to trap most of the particles released from the line source: up to 80% for release positions further away from the symmetry plane and up to 40% for release positions close to the symmetry plane.

Figure 119 presents results of wood mole fractions downstream the examined hill combinations also for inlet profile ABL2h6. Percentage coloured mole fraction contours show that first hill of the row plays a significant role to what happens to the spread of wood species at the second hill and whether or not these reach the latter. Results for both DH01 and DH03 are almost identical as both have a steep first hill; species concentration reaches 10% atop Hill 1 and drops down to 5% on the windward face of Hill 2 (steep or shallow) before reaching background levels. Results differ for case DH02 where Hill 1 is shallow and although it buffers the species spread, it allows 10% of mole fraction to reach the point in-between the two hills. The concentration drops down to 5% atop shallow Hill 2 and reaches background levels at the leeward face of the latter.

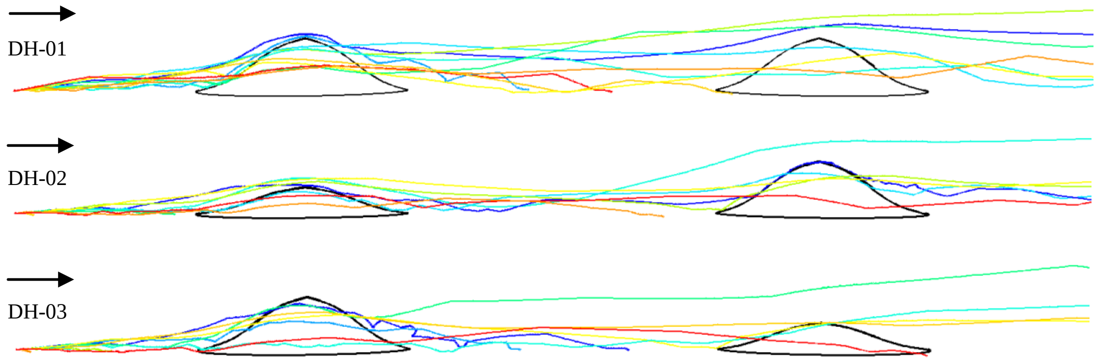

Figure 117 : Side view comparison of indicative particle tracks released from a horizontal line source upstream double 3D hill combinations: DH-01 double steep hills; DH-02 shallow and steep hills; DH-03 steep and shallow hills (paths coloured by particle ID).

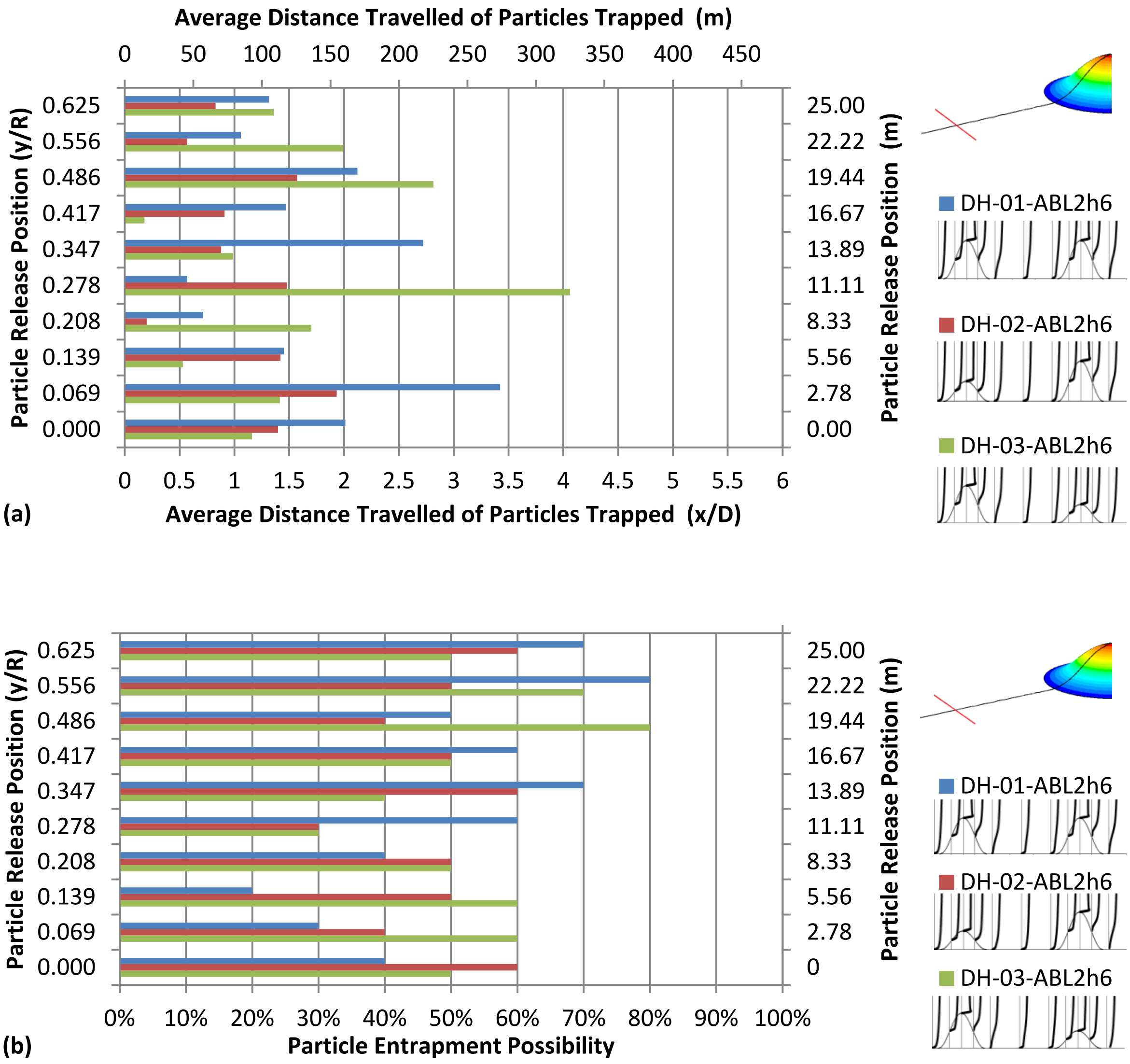

Figure 118 : Average distance travelled of (a) particles trapped and (b) particle entrapment probability plots for particles released from a horizontal line source upstream double 3D hill combinations: DH-01 double steep hills; DH-02 shallow and steep hills; DH-03 steep and shallow hills.

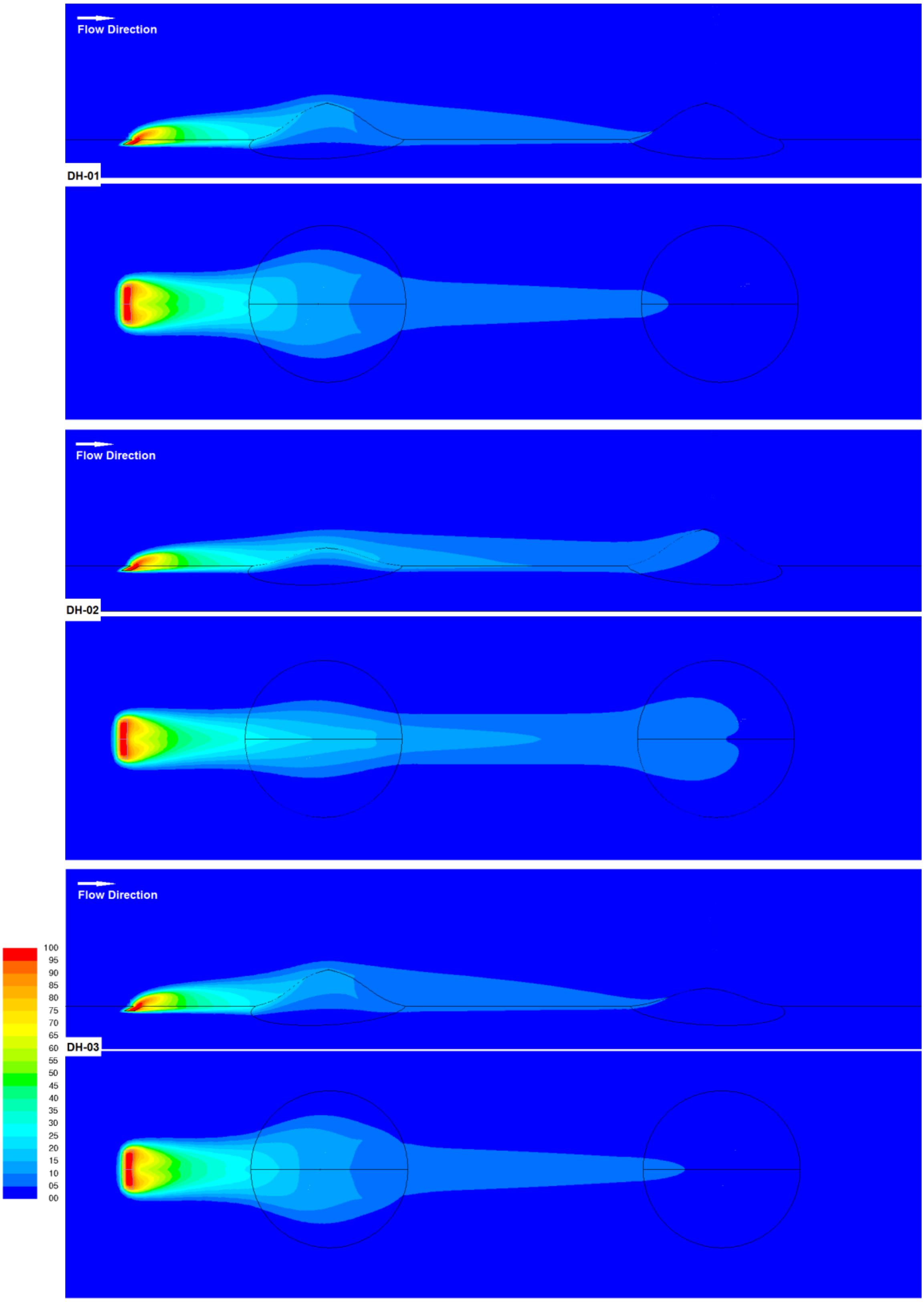

Figure 119 : Contours of wood mole fraction (%) on ground and hill faces for species spread downwind double 3D hill combinations for wind inlet profile ABL2h6. From top to bottom: DH-01 double steep hills; DH-02: shallow and steep hills; DH-03 steep and shallow hills.

Comparison of particle tracking and species transport results for "worst case scenario" wind inlet ABL2h6 (Figure 118 and Figure 119) and assessment of results previously presented in Chapter 5 for all hill combinations and wind inlets, shows a pattern of pollutant behaviour when released from near ground sources over shallow and steep hill combinations. Most particles and species are trapped on the windward face of the first wind break (Hill 1). Shape and dimensions of the first obstacle largely influence wind flow and pollutant spread downstream the domain and the arrival of pollutants at the second obstacle (Hill 2). High wind speeds are seen to create larger recirculation areas driving pollutants to ground faces where these get trapped. On the contrary, low wind speeds are seen to carry pollutants to further distances by avoiding high pressure areas where wind speed has very low - almost zero - values; for most cases examined at low wind speed, pollutants travel further with large percentages exiting the area studied.

The above conclusions for both wind flow and pollutant spread over ideal axisymmetric hills show a clear resemblance to the results of similar studies over 3D cubes. Yang and Shao (2008) also used CFD to simulate 3D idealised canyons by employing cubes in rows to represent buildings. When compared, results show that wind flow over two 4m long cubes in a row with an in-between distance of 16 to 2 meters, is very similar to hills: vertical and horizontal vortices appeared above and sideways of the cubes having recirculation areas formed in the canyon between cubes. Pollutant dispersion concentrations (ground source at zero elevation similar to the author's work) show that values are greatly influenced by the first building and significantly reduced till reaching the second building when the in-between distance is large. This pollutant behaviour is similar to the spread of wood species released upwind the herein studied hills and largely influenced and reduced by Hill 1 prior reaching Hill 2 at nearly background levels.

Mavroidis (2000) has studied wind flow and concentration spread over in-line and staggered cube arrays by performing wind tunnel and field experiments. Wind speed downstream the in-line array was found to reduce gradually after five rows of cubes; similarly the double hill wind flow examined in Chapter 5.5 presented how horizontal wind profiles change at hill's height over the three combinations simulated (Figure 67). The staggered array was proven to be more capable of decelerating wind flow, in comparison to the in-line array, and therefore concentrations were reduced further at shorter distances. This clearly showed the effect of obstacle height to wind velocity decrease, similar to the herein study of steep and shallow hills and how these affect wind flow and pollutant dispersion (see Chapter 5.5 for results and current chapter for discussion). Moreover, it was noted that source position within the cube array plays an important role to concentration results in regard to the relative receptor (pollutant detector) and at what percentages the pollutant would reach this receptor. The current work has not examined different source locations because of the axisymmetric nature of hills examined; as earlier mentioned in Chapter 5.4, any transition of the source away from the centreline would actually cause a change in the wind direction. However, the study of a source in-between hills would be beneficial presenting how the affected air flow downwind Hill 1 would carry pollutants to Hill 2 and further down the domain.

7.4 Wind Flow and Pollution Dispersion over Open Compost Sites

Real topographies have been simulated for a proposed open windrow compost site and an existing green waste processing facility in South Yorkshire, UK. Individual results were previously presented in Chapter 6, starting from collected and processed weather data from Sheffield's Weston Park Museum and moving on to description, simulation and presentation of wind flow and pollutant dispersion results.

Weather data, although collected and processed, were only used to figure out minimum, maximum but most importantly average yearly wind speeds. Average wind direction and frequency of incoming wind was examined and a wind rose was presented in Figure 87. However, conclusions of this study were not employed in the real topography simulation because the examined problem called for a specific wind direction to model: that of driving particles released from the presumed/existing compost piles directly to nearby houses. Other wind directions including the most occurring NW wind can be studied in future work to determine how wind direction for Sites A and B alter results not only for wind flow but also for pollution dispersion. Similar work has been undertaken by Turpin and Harion (2009a) by rotating the modelled stockpiles and later by the same authors (2009b) for an industrial site complex which was simulated for several wind directions and speeds.

The above is a good example of how the case under examination rules some of the settings/assumptions for the simulation that will be computed: in this case the wind direction. Thus, wind data herein were mostly used for understanding wind speeds involved in open environmental flows and towards choosing the mean wind magnitude of the three ABL inlet profiles modelled (for both ideal and real terrain cases studied in this work): ABL2h6, ABL5h6 and ABL10h6.

Wind flow simulation and results for both actual topographies under investigation was straight forward after overcoming problems mentioned earlier in this chapter regarding modelling and establishing a way of conduct to process data and compare wind flow intensities. Analytical wind flow results were presented in Chapters 6.4 and 6.5 for Site A and Site B respectively. Figure 89 and Figure 90 presented static pressure and turbulent kinetic energy on ground, house and compost faces for Site A. Figure 98 and Figure 99 have presented the same set of results for Site B. Further investigation in regards to mean wind flow values throughout the domain was done by plotting and comparing selected planes along the x, y and z axis of both sites: Figure 91 to Figure 93 for Site A and Figure 100 to Figure 102 for Site B.

Figure 120 illustrates a comparison of wind velocity on two vertical planes for both sites; results presented for ABL10h6. The first plane at x=200m shows vertical behaviour and changes of wind flow due to the terrain itself as there are no intermediate wind obstacles. For Site A the changing, sloping terrain is seen to affect the flow: wind accelerates as it travels up the hill. At the valley (close to the presume compost piles) wind has a mean velocity of 15ms^{-1} at approximately 20m above ground. As it moves up the hill it accelerates to 20ms^{-1} before reaching its maximum value of 24ms^{-1} just after the top behind the village houses (see also Chapter 3.2.8 for speed up effect over hills). Passing the hill, wind decelerates again to 15ms^{-1} before reaching the outlet boundary. On the contrary, for Site B, which is almost flat, wind speed hardly changes downstream the domain with values ranging from 14 to 16ms^{-1} due to the very small elevation changes. Contours of wind speed on the second plane, at x=400m which is more closely examined and compared also in Figure 120, are seen to be influenced by compost piles and houses included. Again, the change in average wind magnitude is greater for the hilly domain than for the flat. In both cases, houses create an obstacle that causes velocity to reach maximum values above their roof and small recirculation zones on their windward and leeward faces (these zones could correspond to front and back yards or gardens).

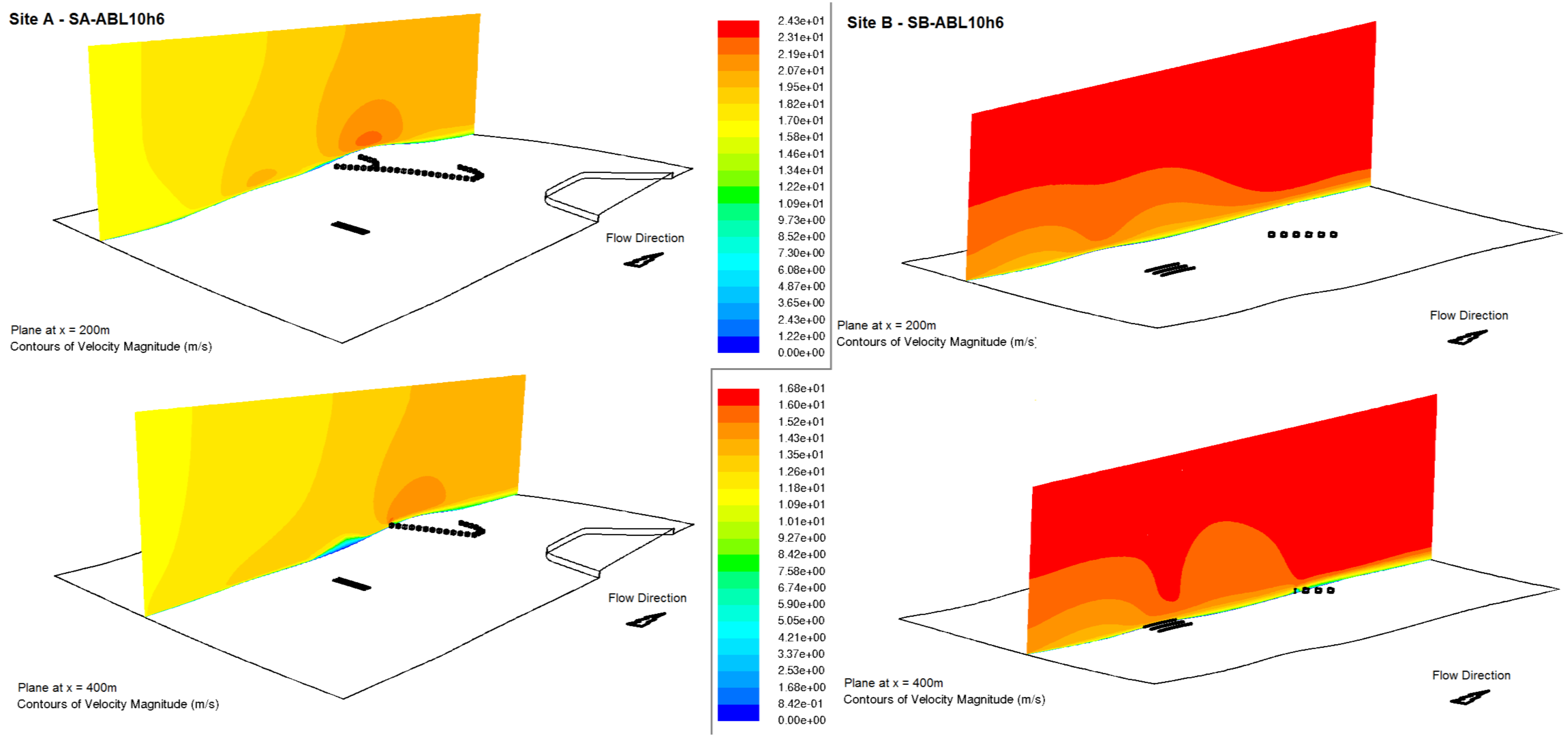

Figure 120 : Site A (hilly) and Site B (flat) wind flow comparison. Contours of mean velocity magnitude $\overline{u}$ for two planes along the x axis for inlet condition ABL10h6. Planes at x=200m free of wind breaks and at x=400m crossing compost piles and nearby houses. (presented plots not in scale)

Progressing from wind flow to pollutant dispersion modelling and based on results presented in Chapters 6.4 and 6.5, Table 24 summarises percentages of particles which got trapped (and at what face) and those that escaped the studied domains of the two locations. For all combinations of topography and wind inlet conditions, a large percentage of particles (45 to 74%) was seen to get trapped immediately after being released and during the distance travelled between the compost piles and the nearby village houses. A small percentage (4 to 11%) was always getting trapped at the villages after getting trapped in recirculation zones at the windward or leeward faces of the houses or being delivered to the ground in-between. Finally the rest escaped the domain with percentages within the range of 12 to 51%.

More analytically, wind flow over the hilly terrain at Site A is seen to deliver most of the particles towards the ground before these can reach the nearby village and especially when the weather is windy (condition ABL10h6): 74% of particles get trapped and 12% of particles escape through the outlet. On the contrary, for the flat terrain at Site B, the windy condition delivers 53% of particles to the ground prior to reaching Village B and allow 40% of particles to escape the domain. Particles travel further distances when the wind condition at the inlet is calm (ABL2h6) and especially in the case of Site B which is flat and causes little disturbance and changes to wind phenomena downstream (also discussed earlier based on Figure 120).

Particle Tracking	**Site A - Hilly Terrain**		**Site B - Flat Terrain**	
Trapped Area	**ABL2h6**	**ABL10h6**	**ABL2h6**	**ABL10h6**
Before Village	59%	74%	45%	53%
Houses	11%	9%	4%	7%
After Village	7%	5%	-	-
Escape	23%	12%	51%	40%

Table 24 : Analytical percentages per area of particles trapped and escaped for simulations of Site A and Site B for ABL2h6 and ABL10h6 inlet conditions.

Moreover, Table 25 presents wood mole fraction percentages for both real topographies examined and compares fraction percentages at different distances starting from the designed compost piles which are acting as the source. Percentage results of hilly Site A, show that wood more fraction reaches background levels faster and especially in windy conditions. On the other hand, fractions at flat Site B do not reach less than 20% during calm conditions. For both sites, concentration percentages reaching nearby houses are lower when wind intensity is high. The flat terrain and calm wind condition combination present the worst case scenario with

40% of wood mole fraction reaching the houses of Village B (200 meters downstream of the compost piles) and 20% reaching the outlet boundary without approaching background levels. The "best case scenario" for quick return of the wood species down to background levels, was presented for hilly Site A, which largely influences wind flow, as argued earlier, in combination with windy ABL10h6 condition which causes a drop to the mole fraction percentages to less than 5% within the first 100 meters from the modelled source compost piles.

Species Transport	**Site A - Hilly Terrain**		**Site B - Flat Terrain**	
Trapped Area	**ABL2h6**	**ABL10h6**	**ABL2h6**	**ABL10h6**
50m	20%	10%	70%	30%
100m	15%	< 5%	50%	40%
Houses	10% (300m)	< 5% (300m)	40% (200m)	10% (200m)
Outlet	10% (600m)	< 5% (600m)	20% (400m)	< 5% (400m)

Table 25 : Wood mole fractions (%) at different distances downstream the real topographies simulated at Site A and Site B for ABL2h6 and ABL10h6 inlet conditions.

In addition to the above Table 25, Figure 121 presents a comparison of contours showing wood mole fraction on the vertical plane crossing both compost pads and houses in both domains. As already mentioned, results for ABL2h6 are presented and compared since this inlet condition presents the longest distance of wood mole fraction travel.

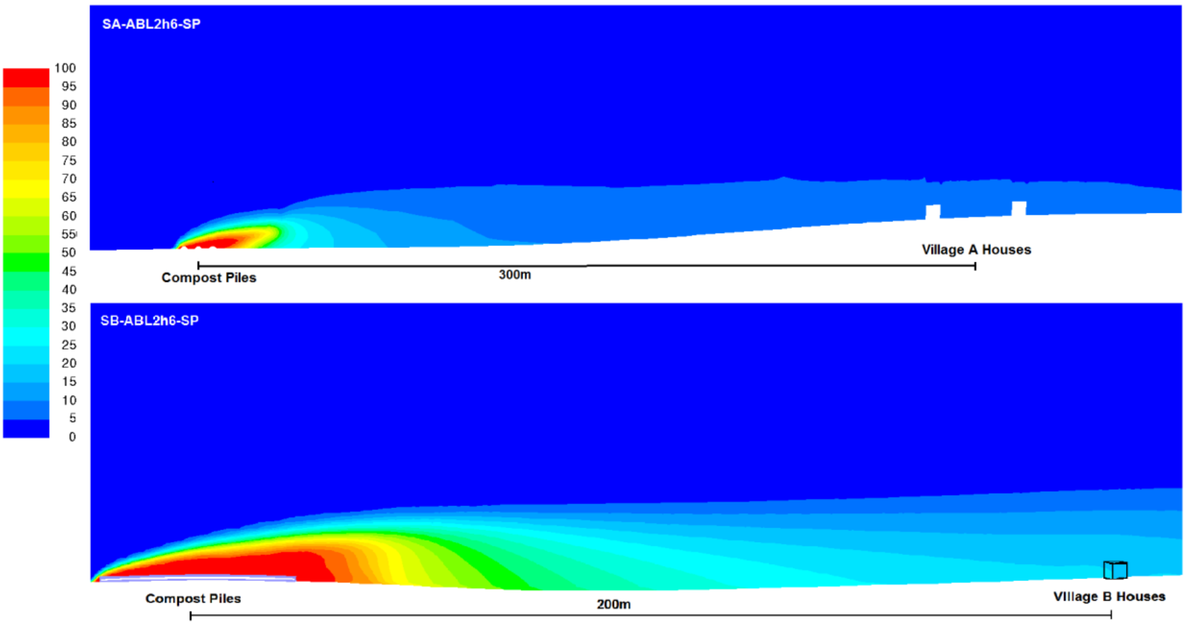

Figure 121 : Contours of wood mole fraction (%) on vertical cross sectional plane for the examined Site A (top) and Site B (bottom) with an inlet condition of ABL2h6. (presented plots not in scale)

Chapter 8

CONCLUSION

Examining the current practices suggested by the EA on risk assessments of pollutant dispersion for green waste processing facilities and following the literature review of work undertaken by other authors on this subject, the guidelines issued by the Environment Agency were examined.

Furthermore, the capabilities and limits of regularly used and EA approved dispersion program ADMS were studied, from which it is evident that existing challenges on topographical resolution, number of buildings and sources are vital for the accurate modelling and collection of meaningful results when studying pollution dispersion problems in the open environment.

It is clear that every case under examination has features and difficulties which make it unique, requiring an individual, more specific approach. Therefore, the use of a widely available CFD program like FLUENT was suggested in this work in order to study more accurately and precisely wind flow and pollution dispersion over real topography.

Furthermore, the use of a case study helped examine the problem: a proposed open windrow compost site at a challenging and hilly location in South Yorkshire, UK was modelled with results presented and discussed. Wind flow was simulated by solving the RANS equations and effluent pollution dispersion was examined by employing both the Lagrangian particle tracking and Species Transport equations.

As a starting point and prior to examining complicated 3D real terrains, simple 2D ideal hills were simulated to verify and study the capabilities of FLUENT and the approach that needed to be adopted. Following the concluded angle of attack on boundary conditions, boundary placement, source, inlet conditions, modelling approach and assumptions to employ within the study, a series of combinations of double steep and shallow ideal axisymmetric sinusoidal hills were simulated. Successful wind flow runs were followed by pollution dispersion simulations to examine how the combination of terrain and wind intensity affect pollutant spread behaviour.

Wind flow results for double ideal hills in a row show that the first hill "smooths" the wind intensity reaching the second hill. Especially when the first hill is steep, the reduction of maximum wind velocity magnitude atop the second hill is clear. Such depressing effect also affects pollution dispersion when the source is located upwind the first hill. Pollutants travel shorter distances before getting trapped on the ground or on hill faces. Naturally, in an open environment flow, some pollutants will carry on and travel further distances but ultimately they will be delivered to an obstacle and get trapped; and maybe re-released later on.

Moreover, the proposed open windrow facility at hilly Site A was simulated and the results were compared to another green waste processing facility situated on flat ground at Site B. Site A is a proposed area for an open windrow composting facility unlike Site B where there was an operational -shut down- green processing facility which is said to have caused health problems to the tenants of the nearby houses at Village B.

CFD results showed that air flow adapts to different topologies and terrain elevations, unmistakably concluding that there is no connection with the simple case of flow on a flat plane (assumption undertaken for small terrain changes by EA approved guidelines and programs).

However, all cases discussed, demonstrate flow disturbance due to sudden changes in the terrain: by trees, woods and buildings. These disturbances can exist in the form of recirculation. Any large bluff body or obstacle can significantly change the flow direction locally and produce unfavourable environments around it. Such disturbances largely influence pollutant spread and entrapment. Detailed results for pollution releases from modelled compost piles at both Sites A and B show that pollutants travel further under calm wind conditions and when the terrain is flat with no critical to the flow wind breaks.

The "250m rule" set by the EA which requires a risk assessment when sensitive receptors are within the 250m radius of the pollutant source needs to be further studied. Results herein demonstrate that under certain assumptions and when wind is calm over flat terrain, pollutants can reach distances further than 250 meters.

Additionally, the general flat land examination approach based on terrain slopes of less than 1/10 needs to be completely re-evaluated. Flat land at Site B was shown to carry pollutants modelled further and present these to houses 300 meters away from the compost piles. On the other hand, hilly terrain, and in fact any terrain with wind obstacles, will cause recirculation at certain areas and also entrapment of particles and thus total reduction of the spread and distances travelled before an acceptable or background level of bioaerosols, bacteria etc. is reached.

It seems that more attention must be given to the examination of such multi-variable complicated problem that requires a case sensitive examination with the appropriate approach in order to examine different topographies (proposed plants at possible problematic areas). Nevertheless, the basic approach to study open environment wind flow and pollution dispersion using any CFD program which is readily and easily accessible nowadays, is described by the current work, offering the correct initial principals and steps for further and more detailed examination of the problem.

Results and conclusions herein suggest that not all terrain examinations can be approached with the same method using general models and assumptions covering a range of cases. Examination must be site specific (topography - source - weather - pollutant - receptors) and every case needs to be carefully studied prior to selection of assumptions, models and simulation techniques in order to present sufficient, informative and accurate results within a given timeframe.

Towards the direction of improving the process of green waste compost production for use as a fertiliser, other processes than that of open windrows can be adopted. Closed composting in huge warehouses with filtered exhaust air has been proven to control emissions, reduce risk and suppress complains of nearby residents. However, such solution is much more expensive than open windrow stockpiles where little infrastructure is necessary. Regarding existing open air compost facilities, simple measures could be implemented to reduce possible spread of pollutants; by creating further man made wind breaks that will disturb wind flow and restrict pollution transfer; by building high walls on the borders of the facilities and also at reasonable distances between the facility and populated areas will help towards containing most of the bioaerosol spread; such walls would cause recirculation zones that would be able to trap pollutants and deliver them to the ground.

Much work remains on assessing the influence of local topography and meteorology on the dispersion of bioaerosols in an open environment. The limitations and effectiveness of various simulation techniques have yet to be quantified to ensure that the risk for passersby's, nearby residents and workers is eliminated.

Chapter 9

RECOMMENDATIONS

Further to the work herein, Computational Fluid Dynamics can also be employed to simulate odour releases from compost operations. Such type of examination is very close to bioaerosol modelling and is based on approximately the same assumptions and techniques. Noise simulations could also be carried out; industrial scale sites emit noise at increased levels with nearby populations complaining and people responsible trying to implement solutions. Both odour and noise problems which are very similar but have to be examined separately would apply to industrial size composting operations and other similar cases of waste processing. Results would help in the risk assessment and regulation of such emissions which at the moment are not well known and examined.

Wind tunnel and field experiments for air pollution modelling can be conducted in the future and compared to computational results. Wind tunnel tests are easy to perform but require high precision of a series of models. The necessity of a specialised wind tunnel with the ability to create ABL conditions is obvious. Partial field data is already available from using the Andersen filters and other techniques for comparison to onsite measurements; but these are known to underestimate concentrations (this is the only approved method at the moment). However, both experimental procedures are costly and time consuming with almost non–existent data. All these important factors should be taken into consideration.

Moreover, unsteady simulations of wind flow and effluent pollution dispersion should also be conducted following the conclusions of this work. Such simulations would give a greater insight to wind flow above hilly terrain and effluent pollutant dispersion released from a source with variable emission types or rates. Most importantly, the behaviour of wind and pollutant phenomena could be studied based on the history of the flow within the computational domain for variable ABL characteristics within a day, month or other regular time intervals. Unsteady simulations would also indicate temperature variations of waste processes within a day or from season to season. Such results would demonstrate if heat plays an important role when the waste material has greater temperature than the surrounding environment (this is the case of compost piles which reach temperatures up to 60 degrees Celsius during the decomposition process).

Following the in-program procedure in FLUENT CFD code, a more suitable and customised code could be designed. Similar specialised codes have been developed for aeronautical applications. By using the same principle for a number of specific application of equations to specific problems, the equivalent could be done for waste processing and other similar bioaerosol release problems. Together with the constantly increasing commercial computing capabilities, the creation of a custom, high speed, Large Eddy Simulation (LES) code should also be examined - such level of detail would give the opportunity to closely examine pollutant behaviour near the source and in close proximity to the compost plant. By overcoming the difficulty of implementing such type of computational technique and the increased requirements in processing power and time, risk planners and researchers would have a high precision tool to work with in the future.

Finally, further research could be conducted in the biological behaviour of bioaerosols and their lifetime. A biology/medical research group could collaborate with environmental scientists and engineers to further understand the spread of bioaerosol pollutants emitted from waste processing. It would be essential to combine results from research in all different aspects of the problem (wind flow and pollutant spread from computational and experimental data as well as biological pollutant behaviour and life time) in order to validate and improve knowledge on the modelling practices and provide further understanding of the problem which would result in a better establishment of all associated factors endangering workers and nearby sensitive receptors.

REFERENCES

Abo El-Azm, A. M. S. (2008). Study of the dispersion of heavy-particle sets in turbulent flows and of the fractal geometry of heavy-particle line using Kinematic Simulation to enhance Fluid Power Systems. Department of Mechanical Engineering. Sheffield, The University of Sheffield. PhD Thesis.

Arya, S. P. (1999). Air pollution meteorology and dispersion. New York, Oxford University Press.

Banks, N. J. (2005). Computational Fluid Dynamics Analysis of the Airflow around the University of Sheffield's Arts Tower Building. Department of Mechanical Engineering. Sheffield, The University of Sheffield. MEng Thesis.

Baxter, L. L. and P. J. Smith (1993). "Turbulent Dispersion of Particles - the Stp Model." Energy & Fuels **7**(6): 852-859.

Blocken, B., J. Carmeliet, et al. (2007a). "CFD evaluation of wind speed conditions in passages between parallel buildings - effect of wall-function roughness modifications for the atmospheric boundary layer flow." Journal of Wind Engineering and Industrial Aerodynamics **95**(9-11): 941-962.

Blocken, B. and J. Persoon (2009). "Pedestrian wind comfort around a large football stadium in an urban environment: CFD simulation, validation and application of the new Dutch wind nuisance standard." Journal of Wind Engineering and Industrial Aerodynamics **97**(5-6): 255-270.

Blocken, B., T. Stathopoulos, et al. (2007b). "CFD simulation of the atmospheric boundary layer: wall function problems." Atmospheric Environment **41**(2): 238-252.

Bluett, J., N. Gimson, et al. (2004). Good Practice Guide for Atmospheric Dispersion Modelling. New Zealand, Ministry for the Environment.

Byeon, J. H., C. W. Park, et al. (2008). "Size distributions of total airborne particles and bioaerosols in a municipal composting facility." Bioresource Technology **99**(11): 5150-5154.

Carpenter, P. and N. Locke (1999). "Investigation of wind speeds over multiple two-dimensional hills." Journal of Wind Engineering and Industrial Aerodynamics **83**: 109-120.

Carruthers, D. and S. Dyster (March 2009). Boundary Layer Structure Specification. ADMS 4 Technical Specification, CERC. **P09/01U/09**.

Carruthers, D., A. Mckeown, et al. (1999). "Validation of ADMS against wind tunnel data of dispersion from chemical warehouse fires." Atmospheric Environment **33**: 1937-1953.

Carruthers, D., W. S. Weng, et al. (March 2009). Complex Terrain Module. ADMS 4 Technical Specification, CERC. **P14/01O/09**.

Carruthers, D., W. S. Weng, et al. (March 2009). Plume/Puff Spread and Mean Concentration Module Specification. ADMS 4 Technical Specification, CERC. **P10/01V/09 P12/01V/09**.

Carruthers, D. J., D. R. J. Holroy, et al. (1994). "UK-ADMS - A New Approach to Modelling Dispersion in the Earths Atmospheric Boundary-Layer." Journal of Wind Engineering and Industrial Aerodynamics **52**(1-3): 139-153.

Cartwright, C., S. Horrocks, et al. (2009). Review of methods to measure bioaerosols from composting sites, Environment Agency.

Casey, M. and T. Wintergerste (2000). ERCOFTAC Special Interest Group on "Quality and Trust in Industrial CFD" Best Practice Guidelines, European Research Community On Flow, Turbulence And Combustion.

Castro, I. P. and W. H. Snyder (1982). "A Wind-Tunnel Study of Dispersion from Sources Downwind of 3-Dimensional Hills." Atmospheric Environment **16**(8): 1869-1887.

Castro, I. P., W. H. Snyder, et al. (1988). "Wind Direction Effects on Dispersion from Sources Downwind of Steep Hills." Atmospheric Environment **22**(10): 2229-2238.

Chang, C. H. and R. N. Meroney (2003). "Concentration and flow distributions in urban street canyons: wind tunnel and computational data." Journal of Wind Engineering and Industrial Aerodynamics **91**(9): 1141-1154.

Chiang, C.-F., H.-H. Yang, et al. (2003). "Monitoring of Bioaerosol Emission from a Sludge Composting Facility." International Journal of Applied Science and Engineering **1**(2): 148-159.

Chin, S. B. (2005). MEC404 Lecture Notes - Computational Fluid Dynamics, The University of Sheffield.

Chu, A. K. M., R. C. W. Kwok, et al. (2005). "Study of pollution dispersion in urban areas using Computational Fluid Dynamics (CFD) and Geographic Information System (GIS)." Environmental Modelling & Software **20**(3): 273-277.

Connan, O., C. Leroy, et al. (2011). "Atmospheric dispersion of an elevated release in a rural environment Comparison between field SF6 tracer measurements and computations of Briggs and ADMS models." Atmospheric Environment **45**: 7174-7183.

Crook, B., S. Stagg, et al. (2008). Bioaerosols in waste composting: deriving source terms and characterising profiles, Environment Agency.

DEFRA (2007). Waste Strategy for England 2007, Department for Environment Food and Rural Affairs.

Di Sabatino, S., R. Buccolieri, et al. (2007). "Simulations of pollutant dispersion within idealised urban-type geometries with CFD and integral models." Atmospheric Environment **41**(37): 8316-8329.

Di Sabatino, S., R. Buccolieri, et al. (2008). "Flow and pollutant dispersion in street canyons using FLUENT and ADMS-Urban." Environmental Modelling & Assessment **13**(3): 369-381.

Dimov, I., K. Georgiev, et al. (2004). "Computational challenges in the numerical treatment of large air pollution models." Ecological Modelling **179**(2): 187-203.

Dixon, N. S. and A. S. Tomlin (2007). "A Lagrangian stochastic model for predicting concentration fluctuations in urban areas." Atmospheric Environment **41**(37): 8114-8127.

Drew, G. H., P. Longhurst, et al. (2008). Development of Amenity Risk Assessments at Organic Waste Treatment Facilities, Environment Agency.

Drew, G. H., A. Tamer, et al. (2006). Dispersion of bioaerosols from composting facilities. Waste 2006 Conf. Integrated Waste Management and Pollution Control, Stratford-upon-Avon, UK.

European Union Council Directive 1999/31/EC on the landfill of waste. Official Journal of the European Communities**:** L 182/1 - L182/19. (26 April 1999).

European Union Directive 2001/81/EC of the European Parliament and of the Council on national emission ceilings for certain atmospheric pollutants. Official Journal of the European Communities**:** L 309/22 - L 309/30. (23 October 2001).

European Union Directive 2008/50/EC of the European Parliament and of the Council on ambient air quality and cleaner air for Europe. T. E. P. a. t. C. o. t. E. Union. Official Journal of the European Union**:** L 152/1 - L 152/44. (21 May 2008).

Fischer, G., A. Albrecht, et al. (2008). "Analysis of airborne microorganisms, MVOC and odour in the surrounding of composting facilities and implications for future investigations." International Journal of Hygiene and Environmental Health **211**(1-2): 132-142.

Fischer, J. L., T. Beffa, et al. (1998). "Aspergillus fumigatus in windrow composting: effect of turning frequency." Waste Management & Research **16**(4): 320-329.

Fluent Inc., (2006). Fluent 6.3 User's Guide

Fracchia, L., S. Pietronave, et al. (2006). "The assessment of airborne bacterial contamination in three composting plants revealed site-related biological hazard and seasonal variations." Journal of Applied Microbiology **100**(5): 973-984.

Franken, J., A. Hellsten, et al. (2007). Best Practice Guideline for the CFD Simulation of Flows in the Urban Environment. Belgium, COST Action 732.

Gorle, C., J. van Beeck, et al. (2009). "CFD modelling of small particle dispersion: The influence of the turbulence kinetic energy in the atmospheric boundary layer." Atmospheric Environment **43**(3): 673-681.

Gouesbet, G. and A. Berlemont (1999). "Eulerian and Lagrangian approaches for predicting the behaviour of discrete particles in turbulent flows." Progress in Energy and Combustion Science **25**(2): 133-159.

Gousseau, P., B. Blocken, et al. (2011). "CFD simulation of near-field pollutant dispersion on a high-resolution grid: A case study by LES and RANS for a building group in downtown Montreal." Atmospheric Environment **45**(2): 428-438.

Graham, D. I. and P. W. James (1996). "Turbulent dispersion of particles using eddy interaction models." International Journal of Multiphase Flow **22**(1): 157-175.

Gromke, C., R. Buccolieri, et al. (2008). "Dispersion study in a street canyon with tree planting by means of wind tunnel and numerical investigations - Evaluation of CFD data with experimental data." Atmospheric Environment **42**(37): 8640-8650.

"Guidelines issued by the Royal Meteorological Society. Atmospheric Dispersion Modelling: Guidelines on the justification of choice and use of models and the communication and reporting of results." (1995). Meteorol. Appl. **2**: 83-88.

Hajra, B., T. Stathopoulos, et al. (2010). "Assessment of pollutant dispersion from rooftop stacks: ASHRAE, ADMS and wind tunnel simulation." Building and Environment **45**: 2768-2777.

Hargreaves, D. M. and N. G. Wright (2007). "On the use of the k-epsilon model in commercial CFD software to model the neutral atmospheric boundary layer." Journal of Wind Engineering and Industrial Aerodynamics **95**(5): 355-369.

Herr, C. E. W., A. zur Nieden, et al. (2003). "Effects of bioaerosol polluted outdoor air on airways of residents: a cross sectional study." Occupational and Environmental Medicine **60**(5): 336-342.

Holmes, N. S. and L. Morawska (2006). "A review of dispersion modelling and its application to the dispersion of particles: An overview of different dispersion models available." Atmospheric Environment **40**(30): 5902-5928.

Hu, C. H. and F. Wang (2005). "Using a CFD approach for the study of street-level winds in a built-up area." Building and Environment **40**(5): 617-631.

Huang, H., R. Ooka, et al. (2008). "CFD analysis on traffic-induced air pollutant dispersion under non-isothermal condition in a complex urban area in winter." Journal of Wind Engineering and Industrial Aerodynamics **96**(10-11): 1774-1788.

Hurley, P. (2002). The Air Pollution Model (TAPM) Version 2: User Manual. CSIRO Atmospheric Research Internal Paper No. 25. Melbourne, CSIRO.

Ishihara, T. and K. Hibi (2002). "Numerical study of turbulent wake flow behind a three-dimensional steep hill." Wind and Structures **5**(2-4): 317-328.

Jackson, P. S. and J. C. R. Hunt (1975). "Turbulent Wind Flow over a Low Hill." Quarterly Journal of the Royal Meteorological Society **101**(430): 929-955.

Kaimal, J. C. and J. J. Finnigan (1994). Atmospheric boundary layer flows : their structure and measurement. New York, Oxford University Press.

Katestone-Scientific (1998). Peak to Mean Ratios for Odour Assessments. Report from Katestone Scientific to Environment Protection Authority of New South Wales.

Katsanis, S. (2008). Environmental Impact of Open Windrow Composting in South Yorkshire. Department of Mechanical Engineering. Sheffield, The University of Sheffield. MSc Thesis.

Kim, H. G., C. M. Lee, et al. (1997). "An experimental and numerical study on the flow over two-dimensional hills." Journal of Wind Engineering and Industrial Aerodynamics **66**(1): 17-33.

Kim, H. G., V. C. Patel, et al. (2000). "Numerical simulation of wind flow over hilly terrain." Journal of Wind Engineering and Industrial Aerodynamics **87**(1): 45-60.

Kim, J. J., J. J. Baik, et al. (2001). "Two-dimensional numerical modelling of flow and dispersion in the presence of hill and buildings." Journal of Wind Engineering and Industrial Aerodynamics **89**(10): 947-966.

Kobayashi, M. H., J. C. F. Pereira, et al. (1994). "Numerical Study of the Turbulent-Flow over and in a Model Forest on a 2d Hill." Journal of Wind Engineering and Industrial Aerodynamics **53**(3): 357-374

Launder, B. E. and D. B. Spalding (1974). "The Numerical Computation of Turbulent Flows." Computer Methods in Applied Mechanics and Engineering **3**: 269-289.

Lemelin, D. R., D. Surry, et al. (1988). "Simple Approximations for Wind Speed-up over Hills." Journal of Wind Engineering and Industrial Aerodynamics **28**(1-3): 117-127.

Lun, Y. F., A. Mochida, et al. (2003). "Numerical simulation of flow over topographic features by revised k-epsilon models." Journal of Wind Engineering and Industrial Aerodynamics **91**(1-2): 231-245.

Mandas, N., F. Cambuli, et al. (2004). Numerical Simulation of the Atmospheric Boundary Layer (ABL) over Complex Terrains. European Wind Energy Conference & Exhibition, London, UK.

Mandurino, C. and P. Vestrucci (2009). "Using meteorological data to model pollutant dispersion in the atmosphere." Environmental Modelling & Software **24**: 270-278.

Markiewicz, M. (2006). Modelling of the Air Pollution Dispersion. Models and Techniques for Health and Environmental Hazard Assessment and Management**:** 304-348.

Mavroidis, I. (2000). "Velocity and concentration measurements within arrays of obstacles." Global Nest: the Int. J. **2**(1): 109-117.

Maxey, M. R. and J. J. Riley (1983). "Equation of Motion for a Small Rigid Sphere in a Nonuniform Flow." Physics of Fluids **26**(4): 883-889.

McHugh, C. (March 2009). Multiple Sources, Species and Particle Sizes. ADMS 4 Technical Specification, CERC. **P24/01H/09**.

Mennink-Kersten, M. A. S. H., D. Ruegebrink, et al. (2006). "In vitro release by Aspergillus fumigatus of galactofuranose antigens, 1,3-beta-D-glucan, and DNA, surrogate markers used for diagnosis of invasive Aspergillosis." Journal of Clinical Microbiology **44**(5): 1711-1718.

Meroney, R. N., B. M. Leitl, et al. (1999). "Wind-tunnel and numerical modelling of flow and dispersion about several building shapes." Journal of Wind Engineering and Industrial Aerodynamics **81**: 333-345.

Mohan, R., G. S. Leonardi, et al. (2009). "Evaluation of methodologies for exposure assessment to atmospheric pollutants from a landfill site." J Air Waste Manag Assoc **59**(4): 490-501.

Mousiopoulos, N., F. Barbas, et al. (2009). A study for the effect of source treatment on numerical results for pollutant dispersion in urban areas. 11th International Conference on Environmental Science and Technology. Chania, Crete**:** A-962 - A-968.

Neofytou, P., M. Haakana, et al. (2008). "Computational fluid dynamics modelling of the pollution dispersion and comparison with measurements in a street canyon in Helsinki." Environmental Modelling & Assessment **13**(3): 439-448.

Nicolleau, F. C. G. A. (2009). MEC427 Lecture Notes - Theory and Application of Turbulence, The University of Sheffield.

Nielsen, E. M., B. H. Nielsen, et al. (1995). "Occupational Bioaerosol Exposure During Collection of Household Waste." Ann Agric Envron Med **2**: 53-59.

Ohya, Y. and T. Uchida (2008). "Laboratory and numerical studies of the atmospheric stable boundary layers." Journal of Wind Engineering and Industrial Aerodynamics **96**(10-11): 2150-2160.

Okuniewski, M. and V. Dennis (2007). Environment Agency Policy: Our position on composting and potential health effects from bioaerosols. E. Agency. United Kingdom. **405_07**.

Parker, C. and N. Gibson (2009). Good Practice and Regulatory Guidance on Composting and Odour Control for Local Authorities, Department for Environment, Food and Rural Affairs.

Parker, S. T. and R. P. Kinnersley (2004). "A computational and wind tunnel study of particle dry deposition in complex topography." Atmospheric Environment **38**(23): 3867-3878.

Pelegry, A., I. Diego, et al. (2009). "Simultaneous CFD evaluation of wind flow and dust emission in open storage piles." Applied Mathematical Modelling **33**(7): 3197-3207.

Pollard, S. J. T., R. Smith, et al. (2006). "Recent developments in the application of risk analysis to waste technologies." Environment International **32**(8): 1010-1020.

Pollard, S. J. T., S. Tyrrel, et al. (2004). An Environmental Risk Management Framework for Composting Facilities in England and Wales, Environment Agency.

Pullen, J., J. P. Boris, et al. (2005). "A comparison of contaminant plume statistics from a Gaussian puff and urban CFD model for two large cities." Atmospheric Environment **39**(6): 1049-1068.

Richards, P. J. and R. P. Hoxey (1992). "Computational and Wind-Tunnel Modelling of Mean Wind Loads on the Silsoe Structures Building." Journal of Wind Engineering and Industrial Aerodynamics **43**(1-3): 1641-1652.

Richards, P. J. and R. P. Hoxey (1993). "Appropriate boundary conditions for computational wind engineering models using the k-ε turbulence model." Journal of Wind Engineering and Industrial Aerodynamics **46**: 145-153.

Richards, P. J., S. Fong, et al. (1997). "Anisotropic turbulence in the atmospheric surface layer." Journal of Wind Engineering and Industrial Aerodynamics **71**: 903-913.

Richards, P. J., R. P. Hoxey, et al. (2000). "Spectral models for the neutral atmospheric surface layer." Journal of Wind Engineering and Industrial Aerodynamics **87**(2-3): 167-185.

Richards, P. J., R. P. Hoxey, et al. (2007). "Wind-tunnel modelling of the Silsoe cube." Journal of Wind Engineering and Industrial Aerodynamics **95**(9-11): 1384-1399.

Richards, P. J. and R. P. Hoxey (2008). "Wind loads on the roof of a 6 m cube." Journal of Wind Engineering and Industrial Aerodynamics **96**(6-7): 984-993.

Riddle, A., D. Carruthers, et al. (2004). "Comparisons between FLUENT and ADMS for atmospheric dispersion modelling." Atmospheric Environment **38**(7): 1029-1038.

Righi, S., P. Lucialli, et al. (2009). "Statistical and diagnostic evaluation of the ADMS-Urban model compared with an urban air quality monitoring network." Atmospheric Environment **43**: 3850-3857.

Roberts, O. F. T. (1923). "The theoretical scattering of smoke in a turbulent atmosphere." Proceedings of the Royal Society of London Series a-Containing Papers of a Mathematical and Physical Character **104**(728): 640-654.

Robins, A. G. and D. D. Apsley (March 2009). Modelling of Building Effects in ADMS. ADMS 4 Technical Specification, University of Surrey, National Power, CERC. **P16/01S/09**.

Rotach, M. W. (2008). Lecture Notes - Boundary Layer Meteorology and Air Pollution Modelling. Switzerland, Institute for Atmospheric and Climate Science.

Sanchez-Monedero, M. A. and E. I. Stentiford (2003). "Generation and dispersion of airborne microorganisms from composting facilities." Process Safety and Environmental Protection **81**(B3): 166-170.

Scaife, H., B. Crook, et al. (2008). PPC bioaerosols (dust and particulates) potentially emanating from intensive agriculture and potential effects on human health, SC040021/SR4, Environment Agency.

Schnelle, K. B. and P. R. Dey (1999). Atmospheric Dispersion Modelling Compliance Guide, McGraw-Hill.

Schroeder, W. H., M. Dobson, et al. (1987). "Toxic Trace-Elements Associated with Airborne Particulate Matter - a Review." JAPCA-the International Journal of Air Pollution Control and Hazardous Waste Management **37**(11): 1267-1285.

Seinfeld, J. H. (1986). Atmospheric chemistry and physics of air pollution. New York, John Wiley & Sons.

Seinfeld, J. H. and S. N. Pandis (2006). Atmospheric Chemistry and Physics: From Air Pollution to Climate Change. New York, John Wiley & Sons.

Slater, R. A. and J. Frederickson (2001). "Composting municipal waste in the UK: some lessons from Europe." Resources Conservation and Recycling **32**(3-4): 359-374.

Smith, F. B. and J. S. Hay (1961). "The Expansion of Clusters of Particles in the Atmosphere." Quarterly Journal of the Royal Meteorological Society **87**: 82-101.

Stagg, S., A. Bowry, et al. (2010). Research Report 786 - Bioaerosol Emissions from Waste Composting and the Potential for Workers Exposure, Health and Safety Executive

Sutton, O. G. (1953). Micrometeorology; a study of physical processes in the lowest layers of the earth's atmosphere. New York,, McGraw-Hill.

Swan, J. R. M., B. Crook, et al. (2002). Microbial Emissions from Composting Sites. Issues in Environmental Science and Technology, The Royal Society of Chemistry.

Swan, J. R. M., A. Kelsey, et al. (2003). Research Report 130 - Occupational and environmental exposure to bioaerosols from composts and potential health effects - A critical review of published data, Health and Safety Executive.

Taha, M. P. M., G. H. Drew, et al. (2006). "Bioaerosol releases from compost facilities: Evaluating passive and active source terms at a green waste facility for improved risk assessments." Atmospheric Environment **40**(6): 1159-1169.

Taha, M. P. M., G. H. Drew, et al. (2007). "Improving bioaerosol exposure assessments of composting facilities - Comparative modelling of emissions from different compost ages and processing activities." Atmospheric Environment **41**(21): 4504-4519.

Taha, M. P. M., S. J. T. Pollard, et al. (2005). "Estimating fugitive bioaerosol releases from static compost windrows: Feasibility of a portable wind tunnel approach." Waste Management **25**(4): 445-450.

Tessicini, F., N. Li, et al. (2007). "Large-eddy simulation of three-dimensional flow around a hill-shaped obstruction with a zonal near-wall approximation." International Journal of Heat and Fluid Flow **28**(5): 894-908.

Technical Guidance on Composting Operations v3 (2001). Environment Agency.

Thomson, D. (March 2009). The Met Input Module. ADMS 4 Technical Specification, The Met Office. **P05/01P/09**.

Thomson, D. J., C. McHugh, et al. (March 2009). Implementation of Area, Volume and Line Sources. ADMS 4 Technical Specification, The Met Office, CERC. **P25/03H/09**.

Turpin, C. and J. L. Harion (2009a). "Numerical modeling of flow structures over various flat-topped stockpiles height: Implications on dust emissions." Atmospheric Environment **1-9**.

Turpin, C. and J. L. Harion (2009b). Numerical Modelling of flow structures over an industrial site: effect of the surroundings buildings on dust emissions. 11th International Conference on Environmental Science and Technology, Chania, Crete, A-1471 - A1477.

Versteeg, H. K. and W. Malalasekera (1995). An introduction to computational fluid dynamics: the finite volume method. Harlow, Essex, England Longman Scientific & Technical ;, New York : Wiley.

Viz, A. (2011). Numerical Modelling of Wind Flow and Air Pollution Dispersion over Idealised Terrain: A CFD Approach. Department of Mechanical Engineering. Sheffield, The University of Sheffield. MEng Thesis.

Ward, M. M. (2002). Composting: A Beginner's Guide. T. J. Reynolds, The Robert A. Macoskey Center for Sustainable Systems Education and Research at Slippery Rock University of Pennsylvania.

Wheeler, P. A., I. Stewart, et al. (2001). Health Effects of Composting - A Study of Three Compost Sites and Review of Past Data. Technical Report P1-315/TR, Environment Agency.

Xie, H. M., Z. Huang, et al. (2006). "The impact of urban street layout on local atmospheric environment." Building and Environment **41**(10): 1352-1363.

Yang, Q.-s. and J. Zhang (2009). Simulation of Horizontally Homogeneous Atmosphere Boundary Layer Based on k-e Variant Models Combined with Modified Wall Functions. The Seventh Asia-Pacific Conference on Wind Engineering. Taipei, Taiwan.

Yang, Y., M. Gu, et al. (2009). "New inflow boundary conditions for modelling the neutral equilibrium atmospheric boundary layer in computational wind engineering." Journal of Wind Engineering and Industrial Aerodynamics **97**: 88-95.

Yang, Y. and Y. P. Shao (2008). "Numerical simulations of flow and pollution dispersion in urban atmospheric boundary layers." Environmental Modelling & Software **23**(7): 906-921.

Zannetti, P. (1990). Air Pollution Modelling, Theories, Computational Methods and Available Software. New York, Von Nostrad Reinhold.

LIST OF PUBLICATIONS

Conferences with proceedings (peer reviewed):

Katsanis, S., S. B. Chin, F. C. G. A. Nicolleau and W. A. Bullough (2011). Numerical Simulation of Air Pollution Dispersion over Hilly Terrain: The Influence of Topography. 12th International Conference on Environmental Science and Technology. Rhodes, Greece: A918 – A925.

Katsanis, S., S. B. Chin, F. C. G. A. Nicolleau and W. A. Bullough (2009). Particle Dispersion from a Compost Site in the UK: A Numerical Simulation. 11th International Conference on Environmental Science and Technology. Chania, Crete**:** A582 - A587.

Journal (peer reviewed):

Katsanis, S., W. A. Bullough and S. B. Chin (2010). "Wind Flow on Breezy Hills and Plains: A Computational Fluid Dynamics Approach." CWRM **10**(1): 22-27.

Workshop (presentation only - no proceedings):

Katsanis, S., S. B. Chin and F. C. G. A. Nicolleau (2010). Environmental Air Pollution Dispersion: Theory and Modelling. ERCOFTAC SIG42 - Workshop on Synthetic Models and Environment. LMFA, Ecole Centrale de Lyon, France.

APPENDIX 1 – AERMOD DESCRIPTION

The following description was extracted from Viz (2011) and was written based on the AERMOD Model Description Formulation (U.S Environmental Protection Agency, 2004)**.**

"In 1991 the American Meteorological Society (AMS) and the U.S Environmental Protection Agency (EPA) decided to form a joint team with the objective of collaborating planetary boundary layer (PBL) concepts into regulatory dispersion models. As a result, a new team which included scientists of both EPA and AMS was formed. This team was named AERMIC.

Prior to the formation of AERMIC in 1991, scientists spent most of their resources in understanding the atmospheric boundary layer (ABL), the convective boundary layer (CBL) and the stable boundary layer (SBL). The ABL is formed due to fluid flow over the earth's surface and hence contributes to the lower region of the atmosphere. The change in temperature of the earth's surface between daytime and night time influences the ABL characteristics. During the day, solar heating causes strong convection and the ABL is aptly known as the CBL. Similarly during the night where atmospheric conditions are more stable, the PBL is regarded as the SBL. The problem encountered by these scientists was with defining these boundary layers in the available dispersion models available at the time. A good understanding with regards to theoretical and experimental information was present. However when it came to numerical methods, the results did not match the observations and therefore AERMIC decided to design a state-of-the-art dispersion models. This new model was to include improved parameterisation of the PBL turbulence, development of dispersion in the CBL and techniques used to analyse plume interactions with the terrain.

AERMIC began by reviewing the existing model called ISC3 which was EPA's regulatory model. Therefore AERMIC's new model was named AERMOD. This model was an improved version of the previous model, ISC3. Basically, the input and output data along with algorithms were updated using the latest techniques.

The AERMOD modelling system is split into two sections. The first section is made up of two pre-processors which are known as AIRMET and AERMAP. The second section is the dispersion model. Exploring the pre-processors, AIRMET provides

AERMOD with relevant data to calculate boundary layer parameters. In others words meteorological data which are easily obtainable from National Weather Stations, are provided which must resemble the characteristics of the meteorological conditions in the actual domain. The terrain pre-processor, AERMAP is used to develop the terrain-influence height, h_c *, (also known as terrain height-scale) which resembles the modelling area in question.*

AERMOD is currently valid for modelling specific simulations. These include flat terrain, complex terrain and urban areas (which are the conditions of the region under examination of the author's project).

AERMOD is a steady-state plume model and was developed using the Lahey F77L – EM/32 FORTRAN Compiler. A plume model enables the estimation of the pollution concentration at ground level from a pollution source. AERMOD is capable of modelling various types of sources emissions including point, area and volume sources. Source emission rates can also be specified by the user.

In both the SBL and CBL, the concentration distribution in the horizontal direction is assumed to be Gaussian. However the vertical distributions are Gaussian and bi-Gaussian probability density function for the SBL and CBL respectively.

One aspect in which AERMOD differs with other models is with regards to flow and dispersion across complex terrain. AERMOD has simplified the approach by designing a realistic plume model which allows the user to avoid determining the terrain regime.

In order to characterise the PBL, AERMOD only requires basic information which can be obtained from National Weather Stations with ease. The vertical inhomogeneity which exists in the PBL is also taken into consideration. Although there are a few types of data inputs available for the model to run, AERMOD requires only one type of basic data input. One of these types could be a runstream setup file which encodes receptor locations, meteorological data specifications, source location along with modelling and output options. With regards to the meteorological data, AERMOD requires to extra files one of which contains surface scalar parameters and the other consisting of vertical meteorological data profiles.

However to account for the effects of elevated terrain, AERMAP needs to process the receptor and terrain data prior to any input to the AERMOD model.

With regards to plume modelling, AERMOD has the ability to model plumes in two distinctive cases. These are terrain impacting and terrain-following plumes. The use of the AERMAP pre-processor avoids the need to distinguish the plume models for various terrain types. This is due to the fact that AERMAP is able to determine a representative terrain-influence height, h_c *, for each receptor with the gridded terrain. Using this data, AERMOD then calculates receptor specific values,* H_c*, using Equation D.1:*

$$\frac{1}{2}u^2\{H_c\} = \int_{H_c}^{h_c} N^2(h_c - z)dz \qquad (D.1)$$

where:
$u\{H_c\}$ *= Wind speed at height* H_c
$N = \left[\frac{g\partial\theta}{\theta\partial z}\right]^{0.5}$ *is the Brunt – Vaisala Frequency*

The generalised concentration equation (Equation D.2) is displayed below. It is important to note that it is valid for both stable and/or convective conditions.

$$C_T\ \{x_r, y_r, z_r\} = f.C_{c,s}\ \{x_r, y_r, z_r\} + (1-f)C_{c,s}\{x_r, y_r, z_p\} \qquad (D.2)$$

where:
$C_T\ \{x_r, y_r, z_r\}$ *is the total concentration.*
$C_{c,s}\ \{x_r, y_r, z_r\}$ *is the contribution from the horizontal plume state (subscripts c and s refer to convective and stable conditions, respectively).*
f *is the plume state weighting function.*
$\{x_r, y_r, z_r\}$ *represents the coordinates of the receptor.*
Please note that for flat terrain: $z_p = z_r$.

For the CBL it is possible to model the plume flow with updrafts and downdrafts. This is possible by assuming that both vertical and horizontal velocities are random variables in each element and simultaneously described by their probability density function (PDF). This feature is considered to be a significant advance in plume modelling when compared to other regulatory models."

APPENDIX 2 – ADDITIONAL TABLES

Class	Primary Pollutants	Secondary Pollutants
Sulfur compounds	Sulfur dioxide (SO_2), sulfur trioxide (SO_3), hydrogen sulfide (H_2S), carbonyl sulfide (COS), carbon disulfide (CS_2), dimethyl sulfide ($(CH_3)_2S$)	Sulfur trioxide (SO_3), sulfuric acid (H_2SO_4), sulphate ion ($SO_4^=$), ammonium sulphate ($(NH_4)_2SO_4$), etc.
Nitrogen compounds	Nitric oxide (NO), nitrous oxide (N_2O), nitrogen dioxide (NO_2), ammonia (NH_3)	Nitric oxide (NO), nitrogen dioxide (NO_2), nitric acid (HNO_3), nitrate ion (NO_3^-), ammonium ion (NH_4^+)
Inorganic carbon compounds	Carbon monoxide (CO), carbon dioxide (CO_2)	Carbon dioxide (CO_2) oxygenated inorganic carbon compounds
Organic carbon compounds	Methane (CH_4), terpenes, isoprene, C1-C5 compounds classified as paraffins, olefins, and aromatics	Organic nitrates, peroxides (e.g., PAN), oxygenated hydrocarbons classified as aldehydes, ketones, and acids
Halogen compounds	Hydrogen fluoride (HF), hydrogen chloride (HCl), carbon tetrachloride (CCl_4), chlorofluorocarbons (CFCs), methyl chloride (CH_3Cl, CH_3CCl_3)	
Radioactive substances	Strontium ($^{90}S_r$), cesium ($^{137}C_s$), iodine (^{131}I), tritium (^3H) radon and radon daughters	

A classification of gaseous air pollutants based on their chemical properties [Arya, 1999]

	Fine Particles	**Coarse Particles**
Formation Pathways	Chemical reactions Nucleation Condensation Coagulation Cloud / fog processing	Mechanical disruption Suspension of dusts
Composition	Sulfate Nitrate Ammonium Hydrogen ion Elemental carbon (EC) Organic compounds Water Metals (Pb, Cd, V, Ni, Cu, Zn, Mn, Fe, etc.)	Re-suspended dust Coal and oil fly ash Crustal element (Si, Al, Ti Fe) oxides $CaCo_3$, NaCl Pollen, mold, spores Plant, animal debris Tire wire debris
Solubility	Largely soluble, hydroscopic	Largely insoluble and non-hydroscopic
Sources	Combustion (coal, oil, gasoline, diesel, wood) Gas-to-particle conversion of NO_x, SO_3 and VOCs Smelters, mills, etc.	Re-suspension of industrial dust and oil Suspension of soil (farming, mining, unpaved roads) Biological sources Construction / demolition Ocean spray
Atmospheric Lifetime	Days to weeks	Minutes to days
Travel Distance	100s to 1000s of km	< to 10s of km

Comparison of ambient and fine particles
[Seinfeld and Pandis, 2006]

	ADMS 4	**AERMOD**
Meteorological pre-processor	Yes	Yes
Boundary-layer structure	h, L_{MO} scaling	h, L_{MO} scaling
Plume rise	Advanced integral model	Briggs empirical expressions
Concentration distribution	Advanced Gaussian	Advanced Gaussian
Buildings	ADMS buildings module	PRIME buildings module
Complex terrain	Based on calculation of flow field and turbulence field by FLOWSTAR model	Interpolation between neutral flow approximate solution and stable flow impaction solution
Deposition (wet and dry)	Yes	Yes
Chemistry	Generic Reaction Set 8 reaction scheme	Ozone limiting model, assumes maximum conversion of NO to NO_2
Fluctuations	Yes	No
Visible plumes	Condensed plume visibility	No
Radioactivity	Radioactive decay / γ-ray dose; decay chain database	Simple decay
Puff model	Yes	No
Coastline module	Yes	No
Input of vertical profiles of meteorological data	Yes	Yes

Comparison between ADMS and AERMOD capabilities
[Data from http://www.cerc.co.uk/environmental-software/ADMS-model.html]

APPENDIX 3 – COMPLETE WIND FLOW CFD PLOTS

A3.1 Plots for Single 3D Hill

A3.1.1 SH-01-ABL2h6

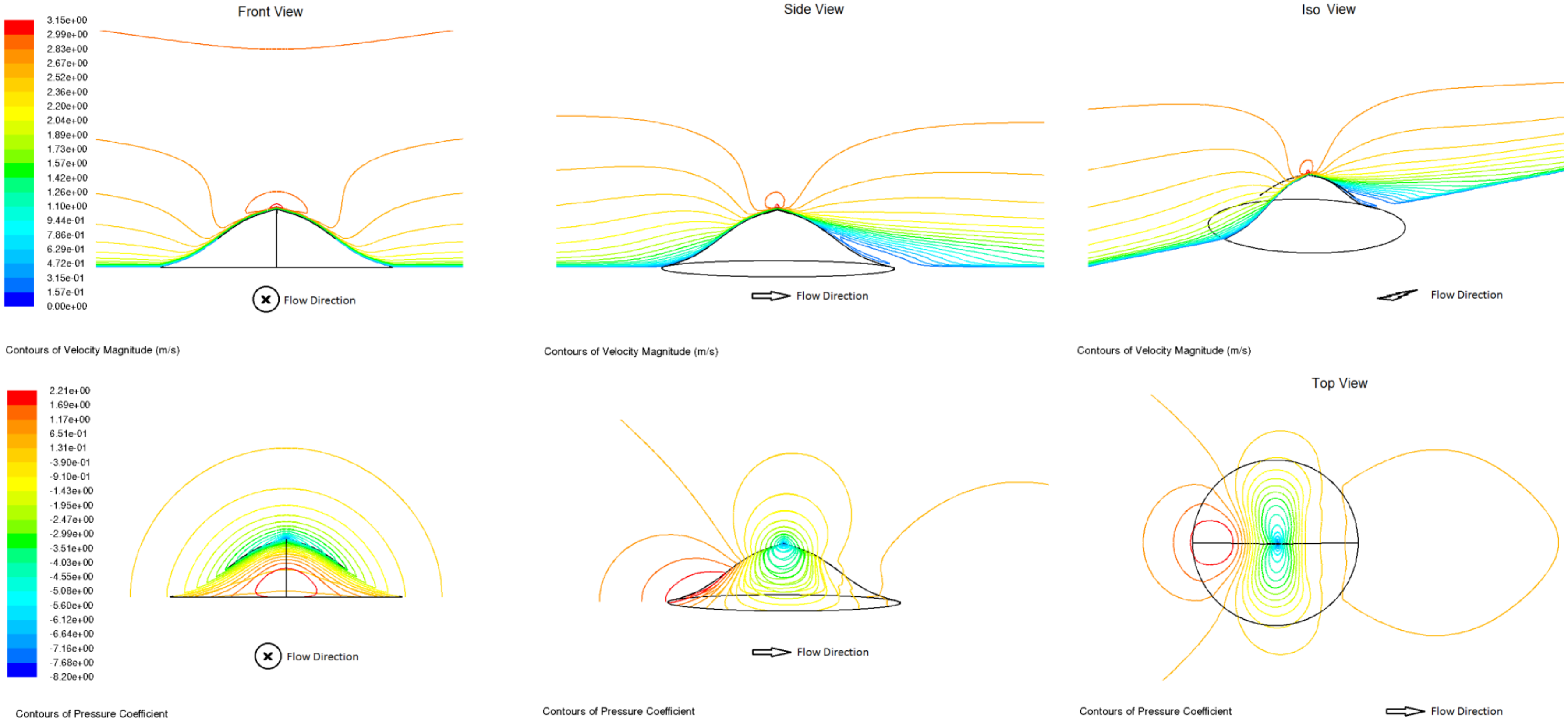

SH-01-ABL2h6 : Contour plots of mean velocity magnitude $\overline{u}$ and pressure coefficient Cp over single 3D hill.

(Front and side views show contours on hill face and mid-planes and top views show contours on hill and ground faces)

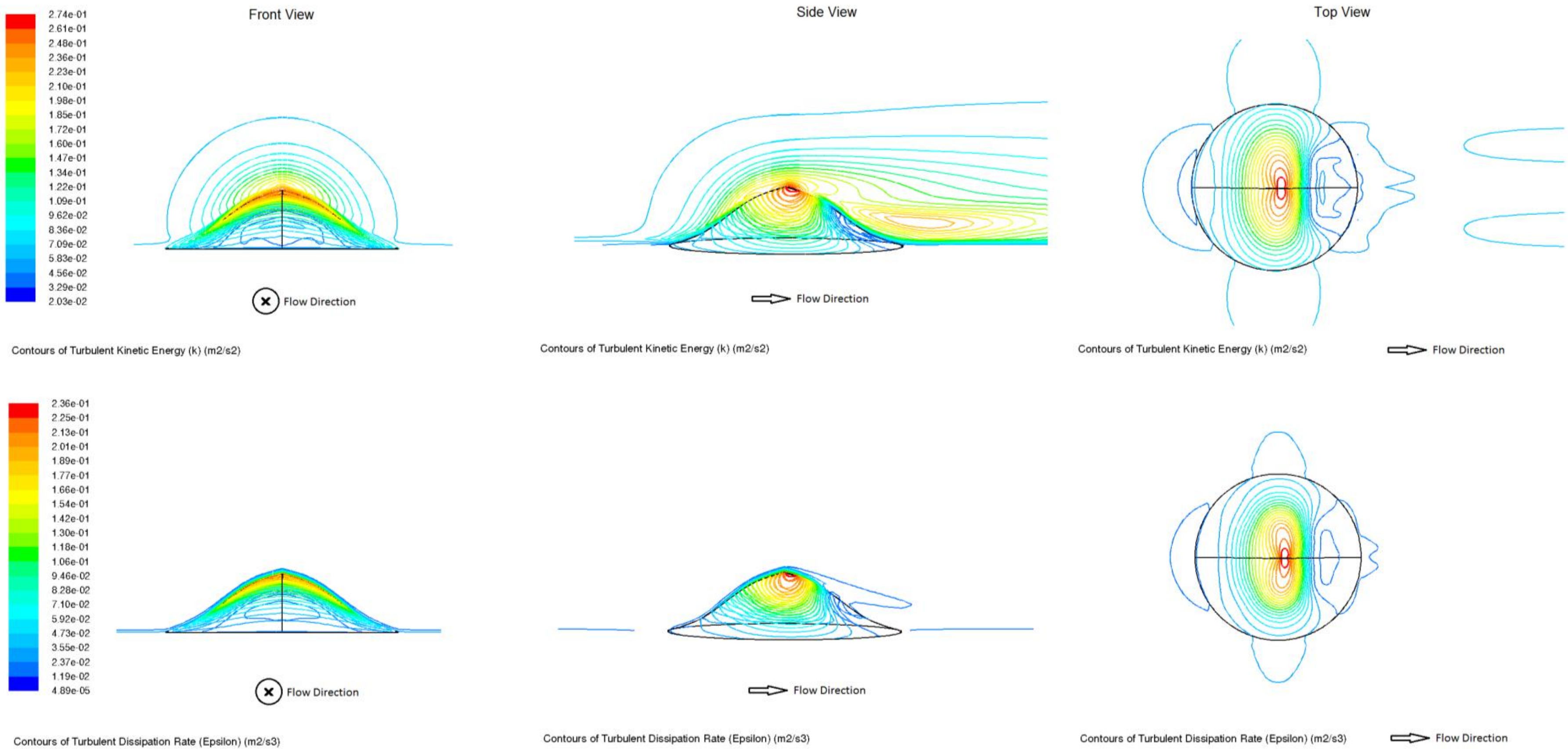

SH-01-ABL2h6 : Contour plots of turbulent kinetic energy k and dissipation rate ε over single 3D hill.

(Front and side views show contours on hill face and mid-planes and top views show contours on hill and ground faces)

A3.1.2 SH-01-ABL5h6

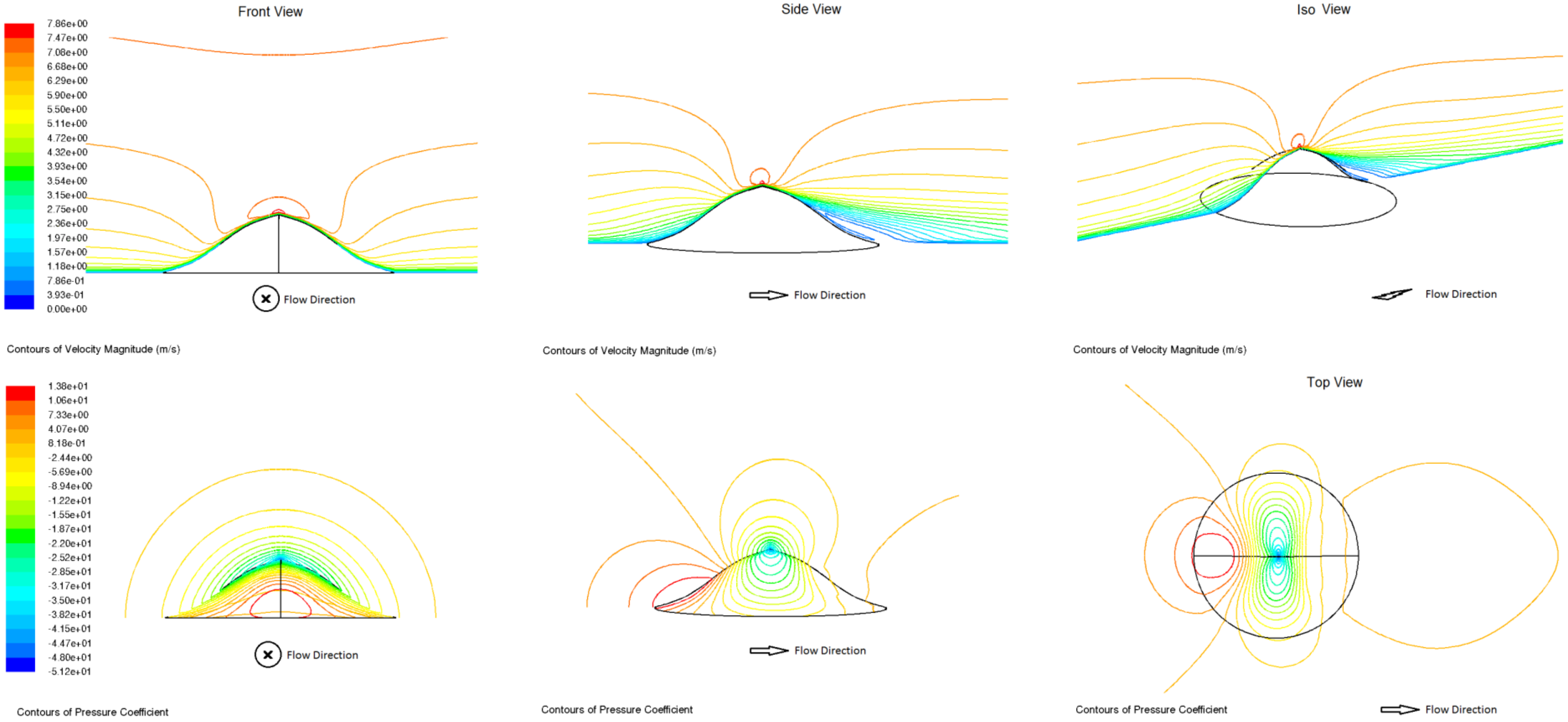

SH-01-ABL5h6 : Contour plots of mean velocity magnitude $\overline{u}$ and pressure coefficient Cp over single 3D hill.

(Front and side views show contours on hill face and mid-planes and top views show contours on hill and ground faces)

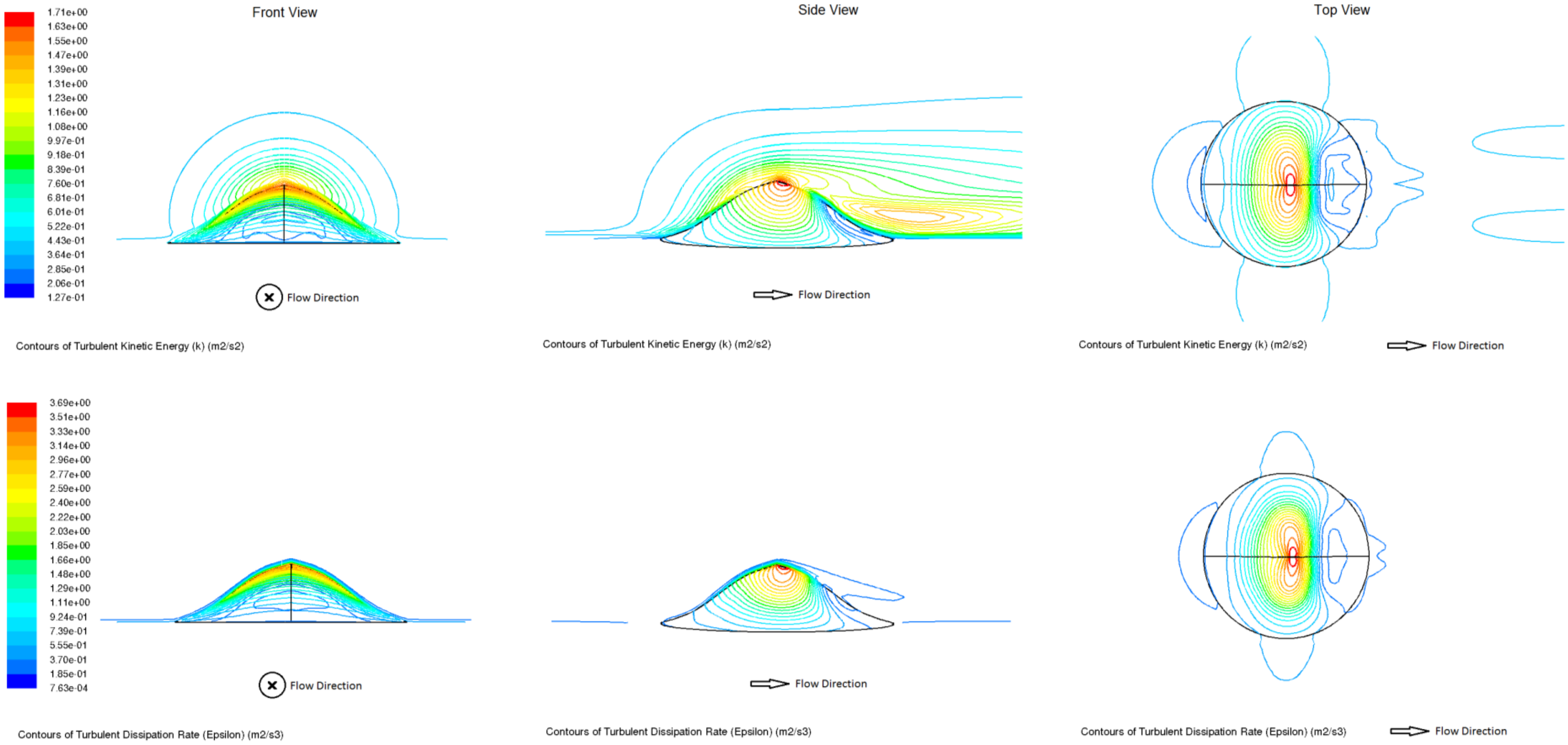

SH-01-ABL5h6 : Contour plots of turbulent kinetic energy k and dissipation rate ε over single 3D hill.

(Front and side views show contours on hill face and mid-planes and top views show contours on hill and ground faces)

A3.1.2 SH-01-ABL10h6

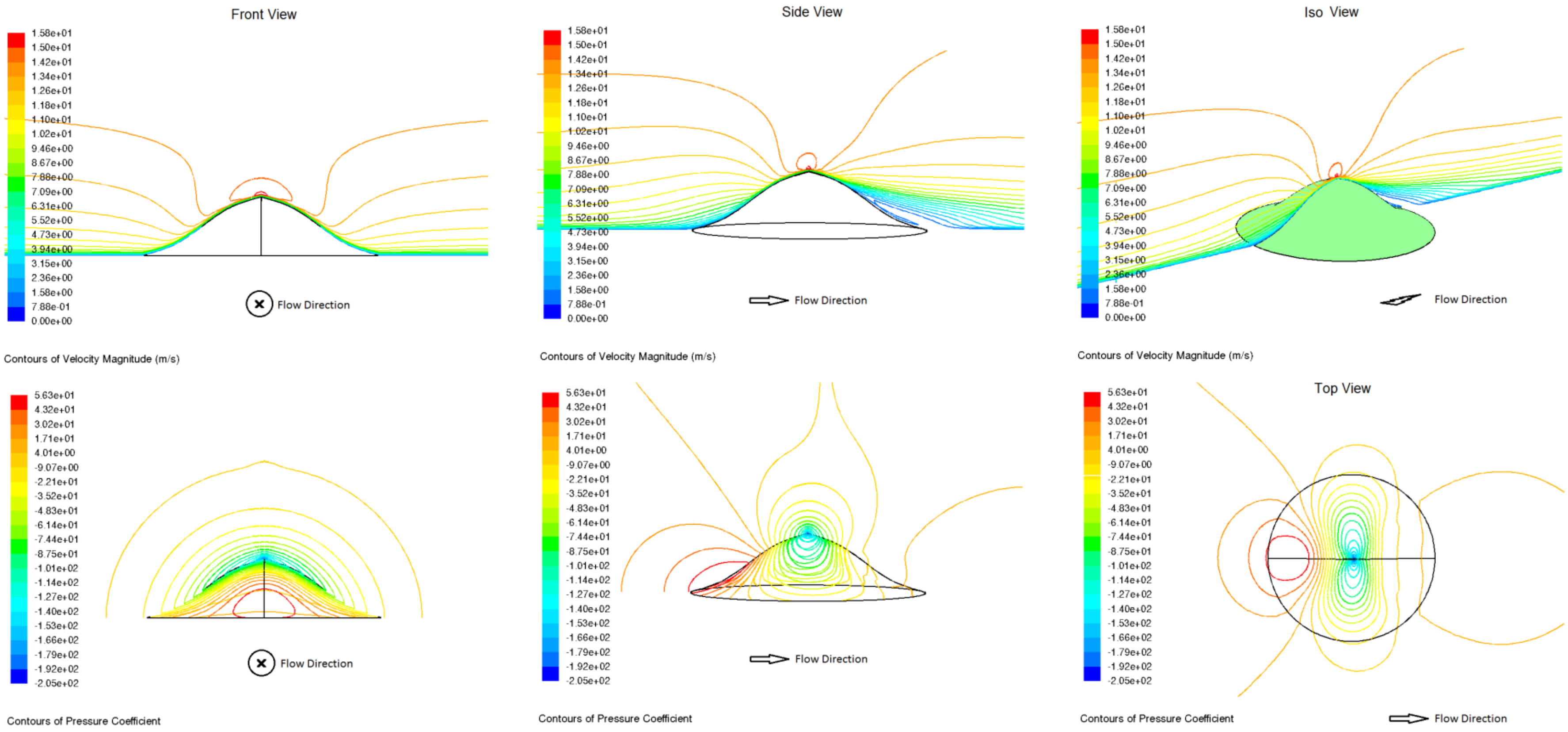

SH-01-ABL10h6 : Contour plots of mean velocity magnitude $\overline{u}$ and pressure coefficient Cp over single 3D hill.

(Front and side views show contours on hill face and mid-planes and top views show contours on hill and ground faces)

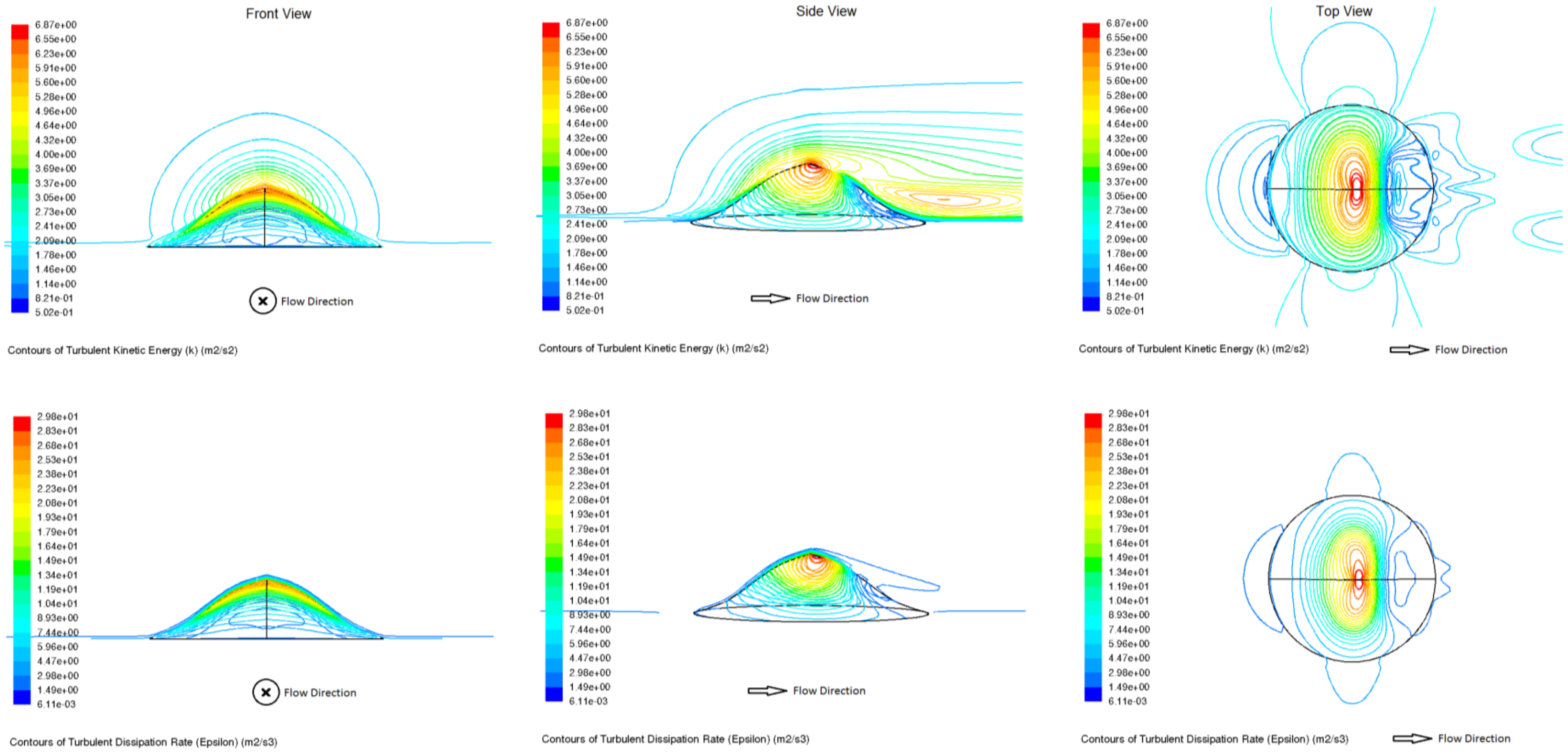

SH-01-ABL10h6 : Contour plots of turbulent kinetic energy k and dissipation rate ε over single 3D hill.

(Front and side views show contours on hill face and mid-planes and top views show contours on hill and ground faces)

A3.2 Plots for Double 3D Hills

A3.2.1 DH-01-ABL2h6

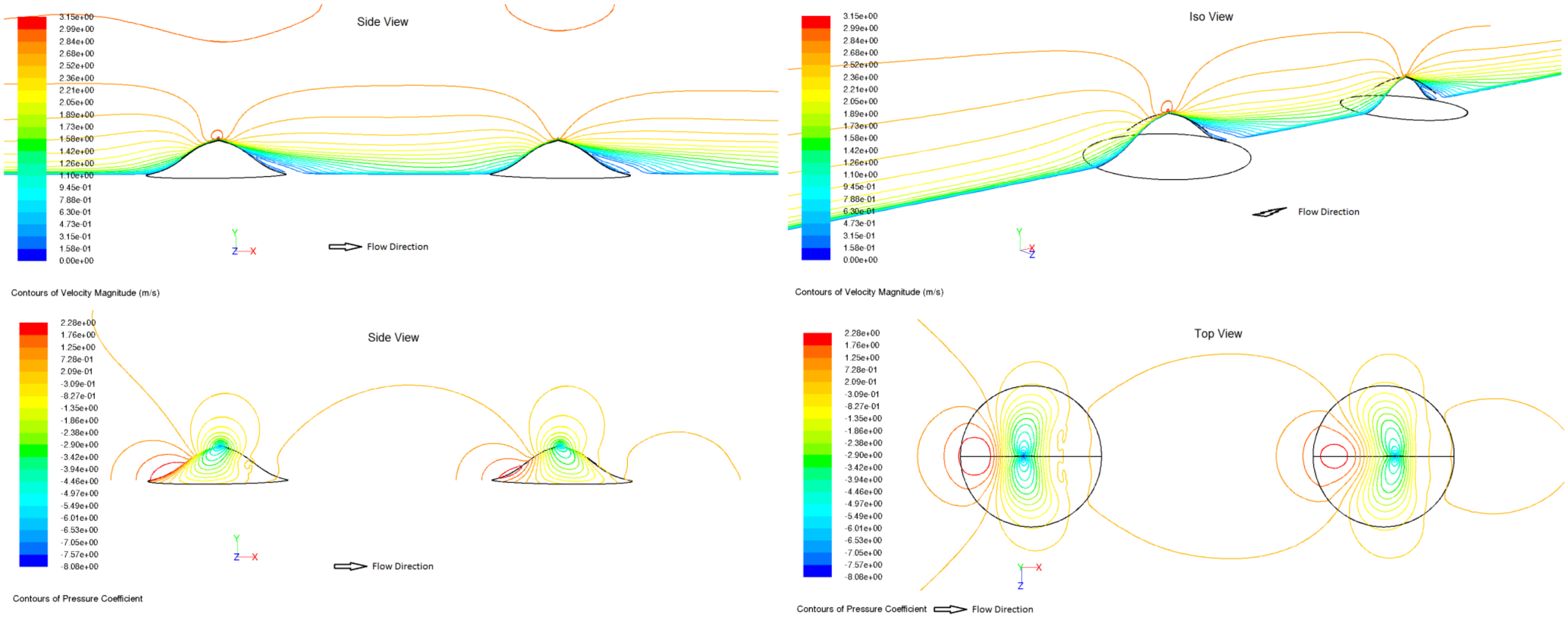

DH-01-ABL2h6 : Contour plots of mean velocity magnitude $\overline{u}$ and pressure coefficient Cp over two steep 3D hills.

(Side views show contours on hill faces and mid-plane and top views show contours on hill and ground faces)

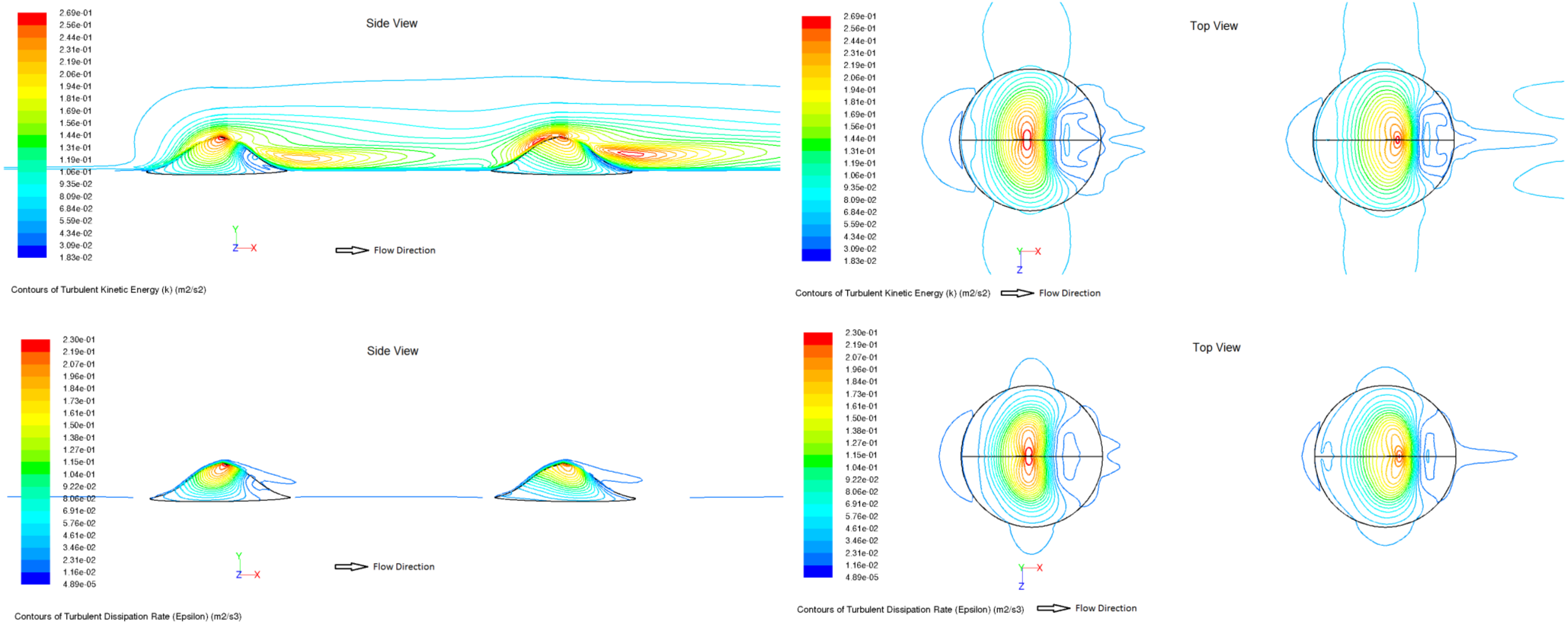

DH-01-ABL2h6 : Contour plots of turbulent kinetic energy k and dissipation rate ε over two steep 3D hills.

(Side views show contours on hill faces and mid-plane and top views show contours on hill and ground faces)

A3.2.2 DH-01-ABL5h6

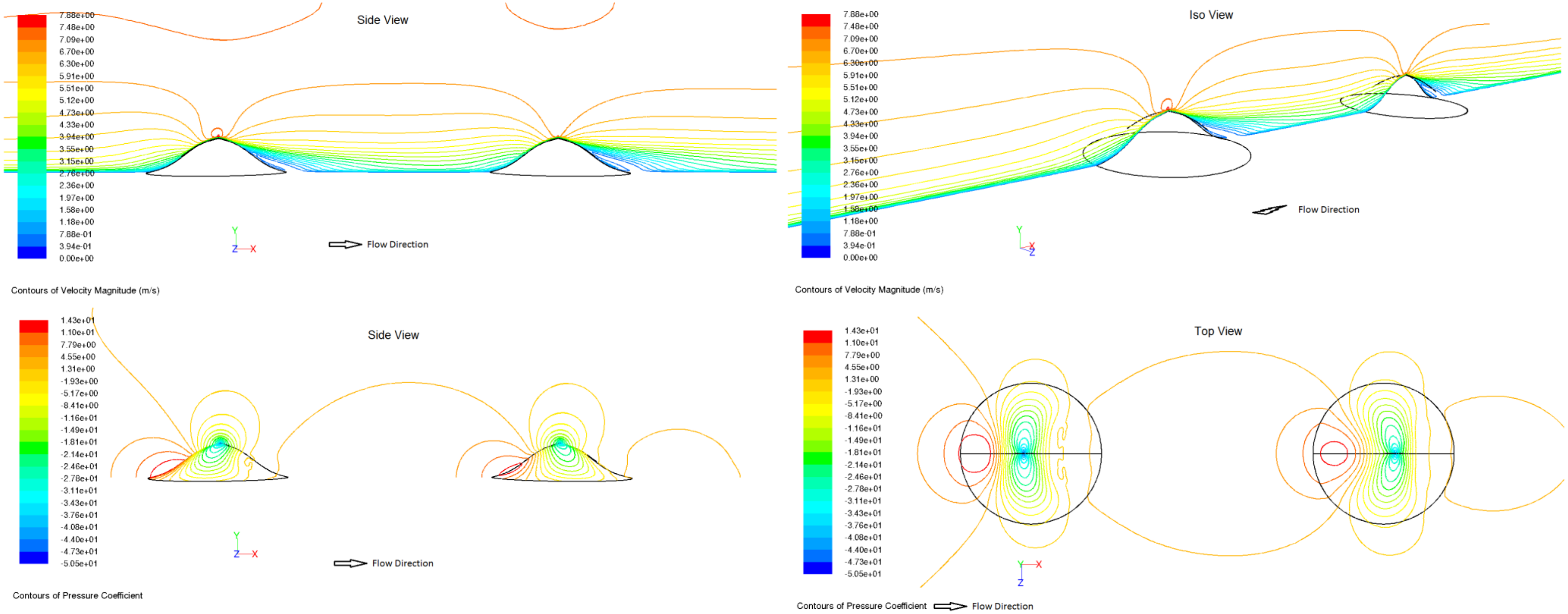

DH-01-ABL5h6 : Contour plots of mean velocity magnitude $\overline{u}$ and pressure coefficient Cp over two steep 3D hills.

(Side views show contours on hill faces and mid-plane and top views show contours on hill and ground faces)

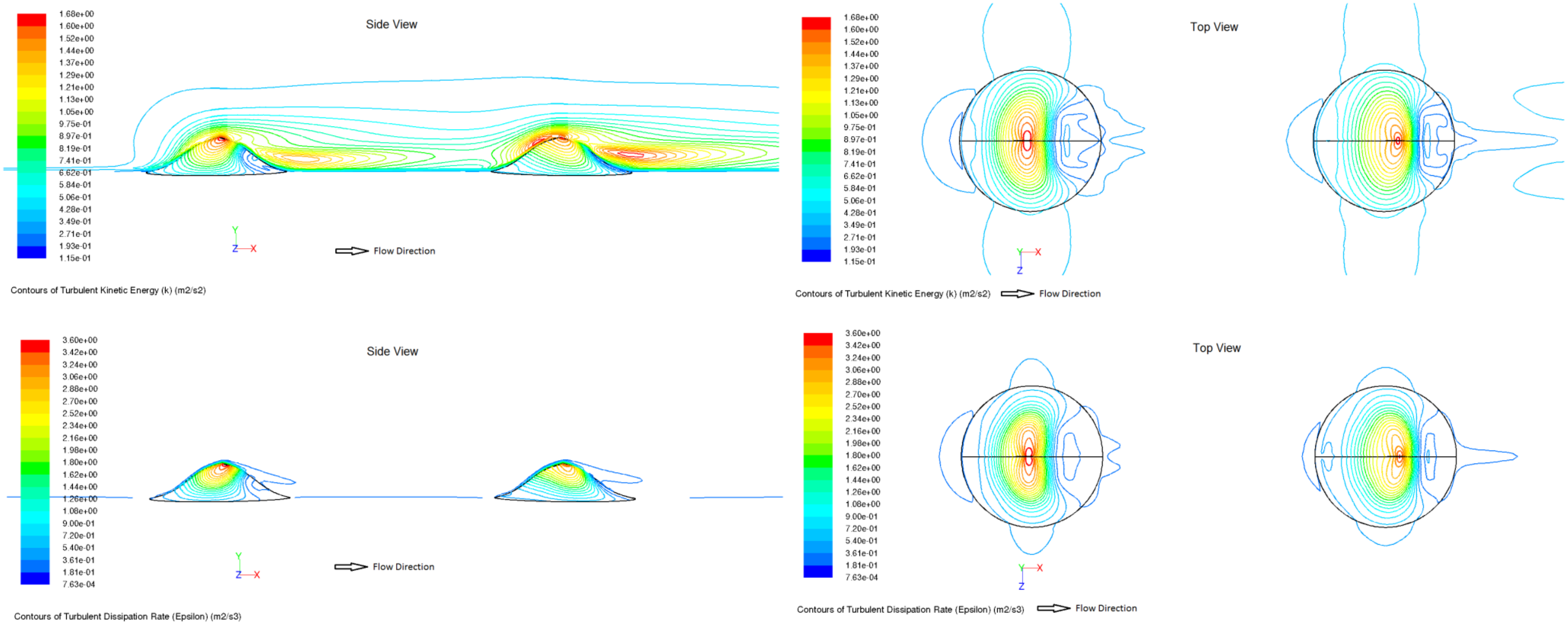

DH-01-ABL5h6 : Contour plots of turbulent kinetic energy k and dissipation rate ε over two steep 3D hills.

(Side views show contours on hill faces and mid-plane and top views show contours on hill and ground faces)

A3.2.3 DH-01-ABL10h6

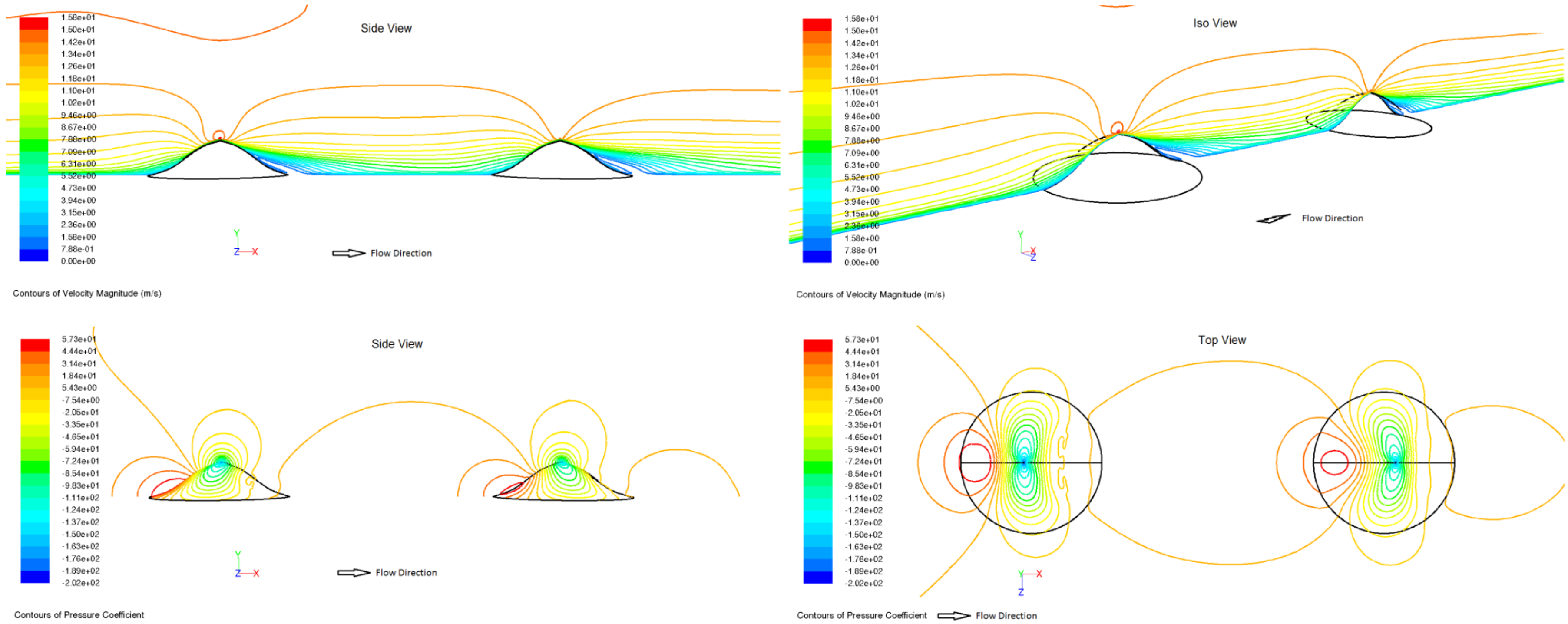

DH-01-ABL10h6 : Contour plots of mean velocity magnitude $\overline{u}$ and pressure coefficient Cp over two steep 3D hills.

(Side views show contours on hill faces and mid-plane and top views show contours on hill and ground faces)

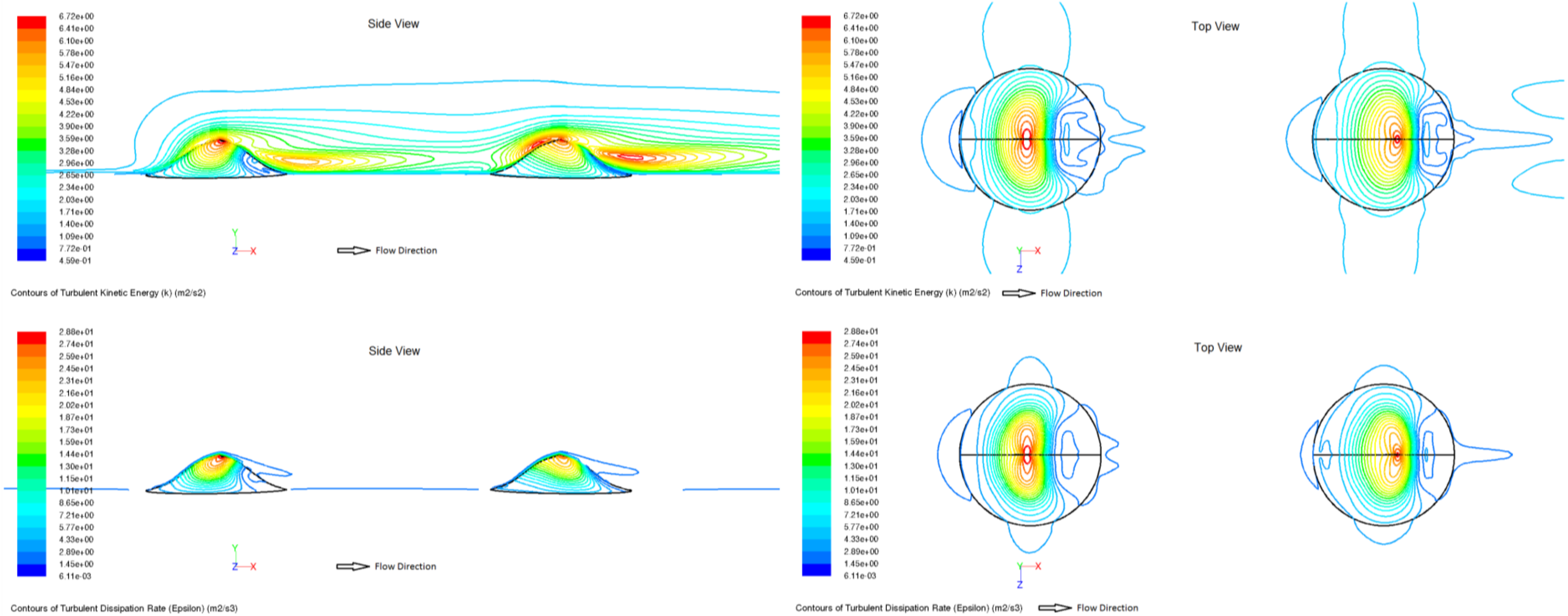

DH-01-ABL10h6 : Contour plots of turbulent kinetic energy k and dissipation rate ε over two steep 3D hills.

(Side views show contours on hill faces and mid-plane and top views show contours on hill and ground faces)

A3.2.4 DH-02-ABL2h6

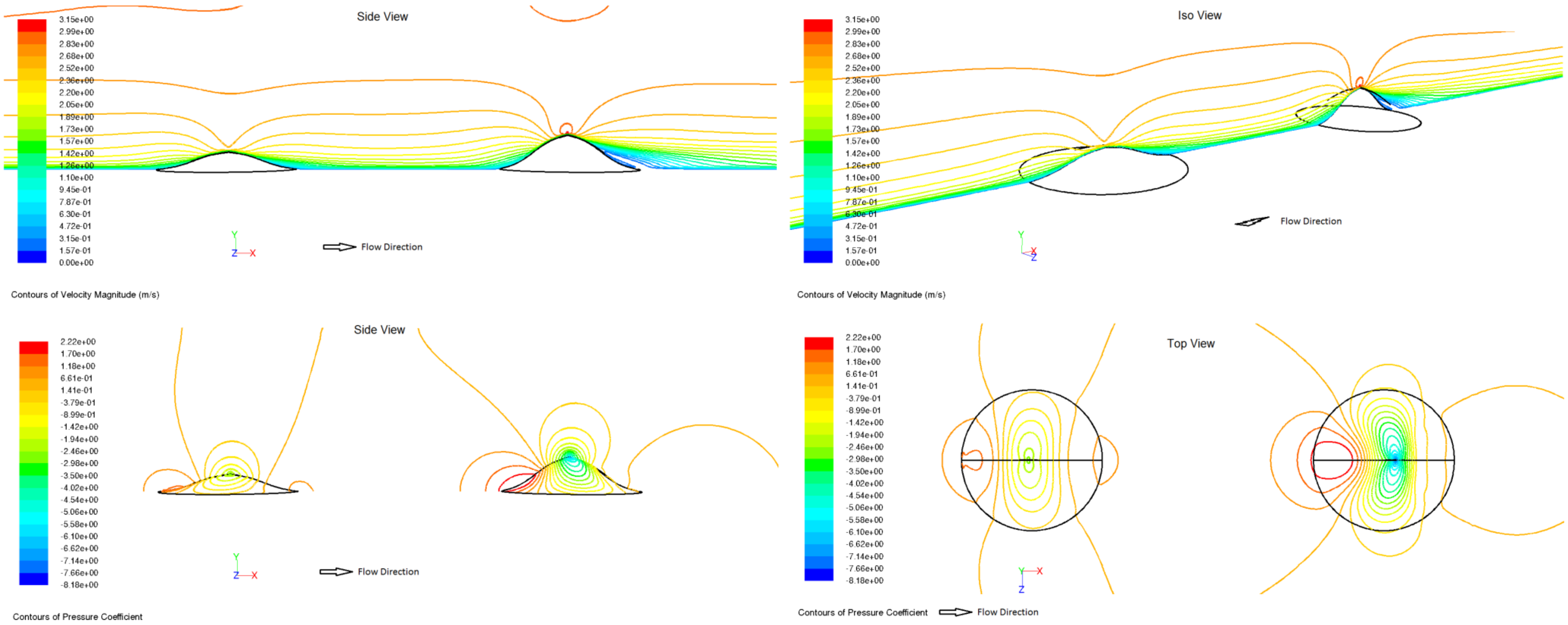

DH-02-ABL2h6 : Contour plots of mean velocity magnitude $\overline{u}$ and pressure coefficient Cp over shallow and steep 3D hills.

(Side views show contours on hill faces and mid-plane and top views show contours on hill and ground faces)

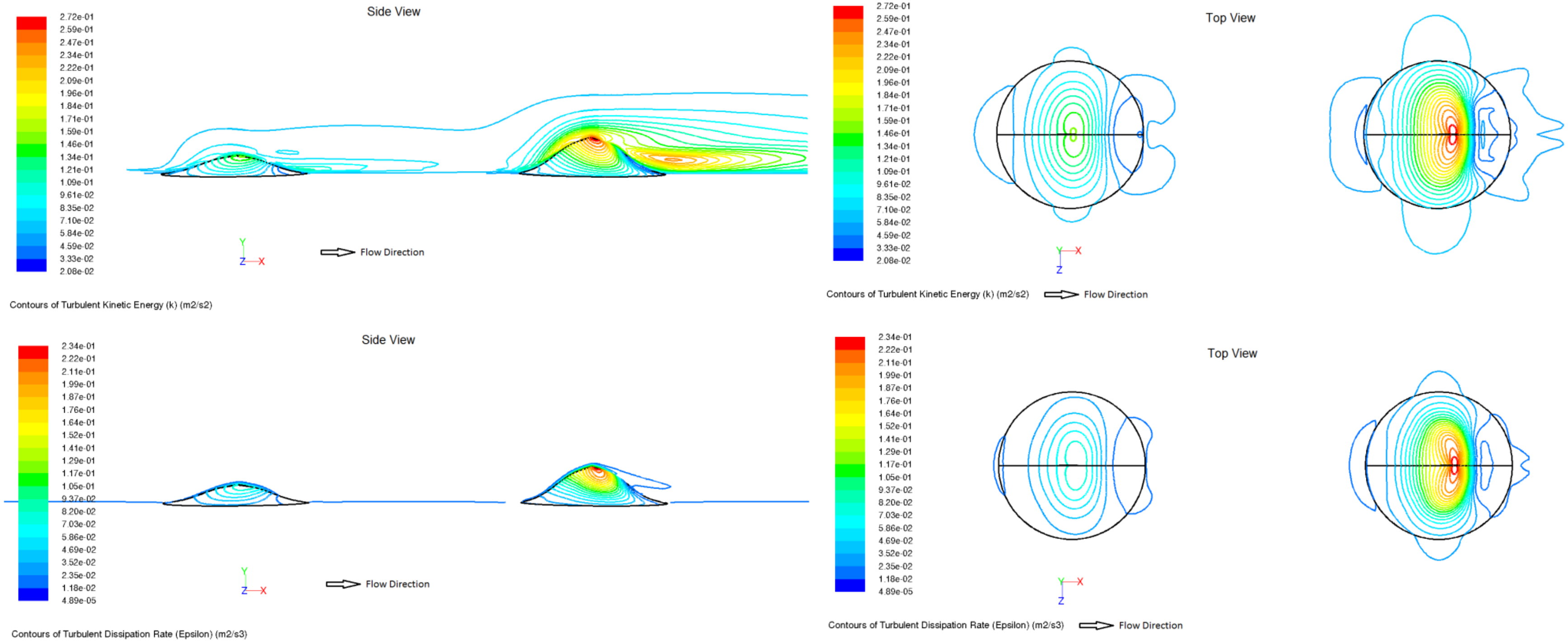

DH-02-ABL2h6 : Contour plots of turbulent kinetic energy k and dissipation rate ε over shallow and steep 3D hills.

(Side views show contours on hill faces and mid-plane and top views show contours on hill and ground faces)

A3.2.5 DH-02-ABL5h6

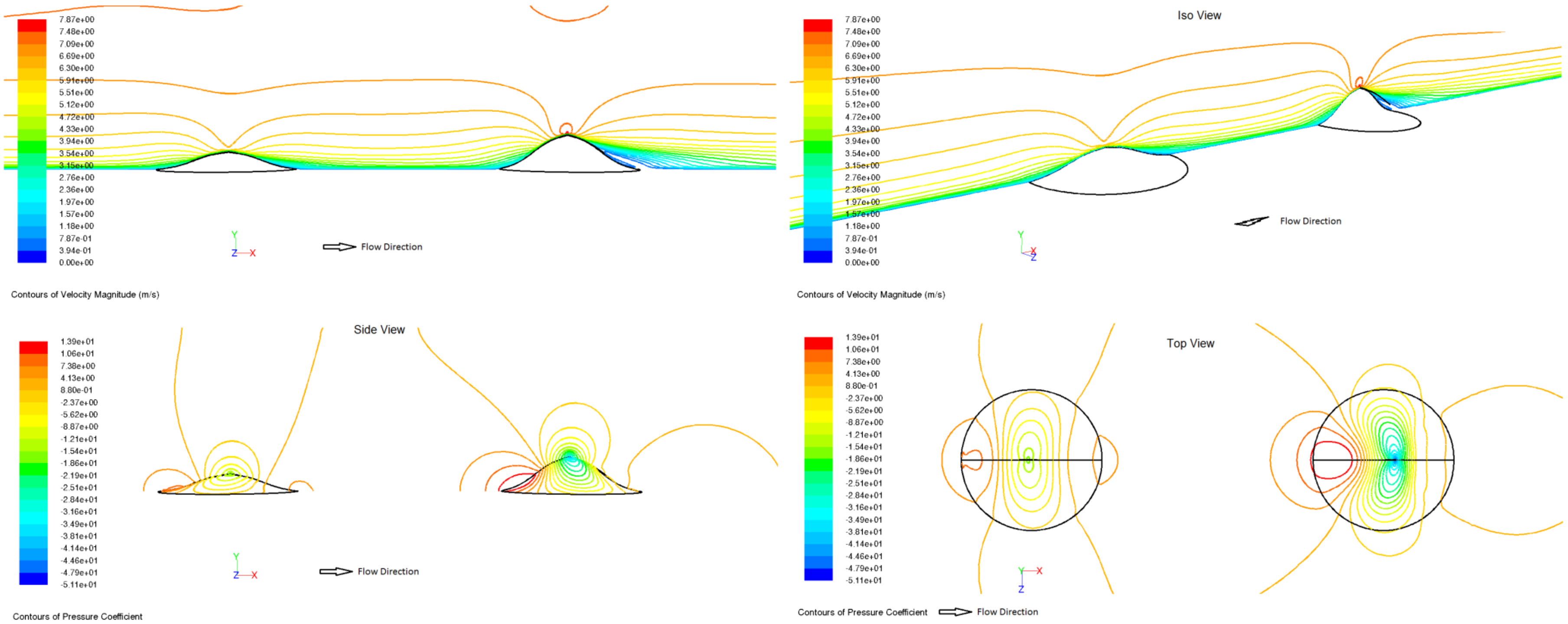

DH-02-ABL5h6 : Contour plots of mean velocity magnitude $\overline{u}$ and pressure coefficient Cp over shallow and steep 3D hills.

(Side views show contours on hill faces and mid-plane and top views show contours on hill and ground faces)

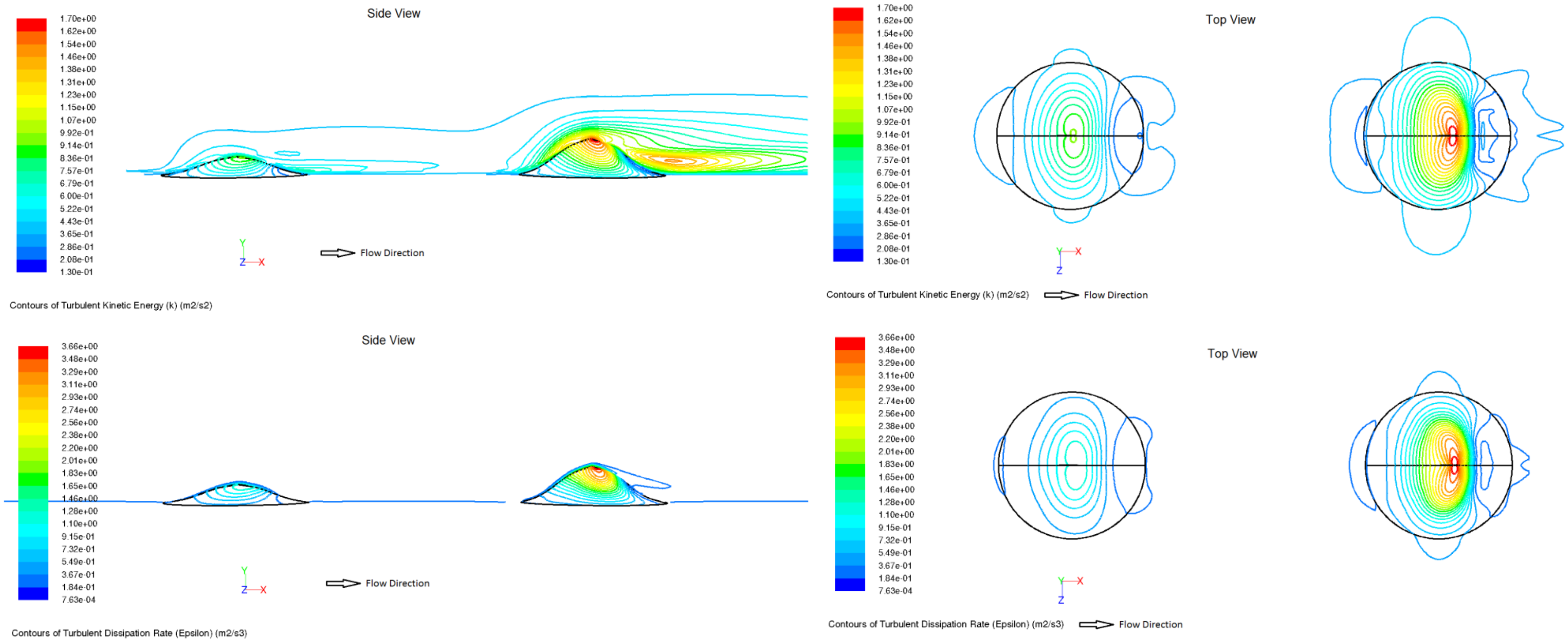

DH-02-ABL5h6 : Contour plots of turbulent kinetic energy k and dissipation rate ε over shallow and steep 3D hills.

(Side views show contours on hill faces and mid-plane and top views show contours on hill and ground faces)

A3.2.6 DH-02-ABL10h6

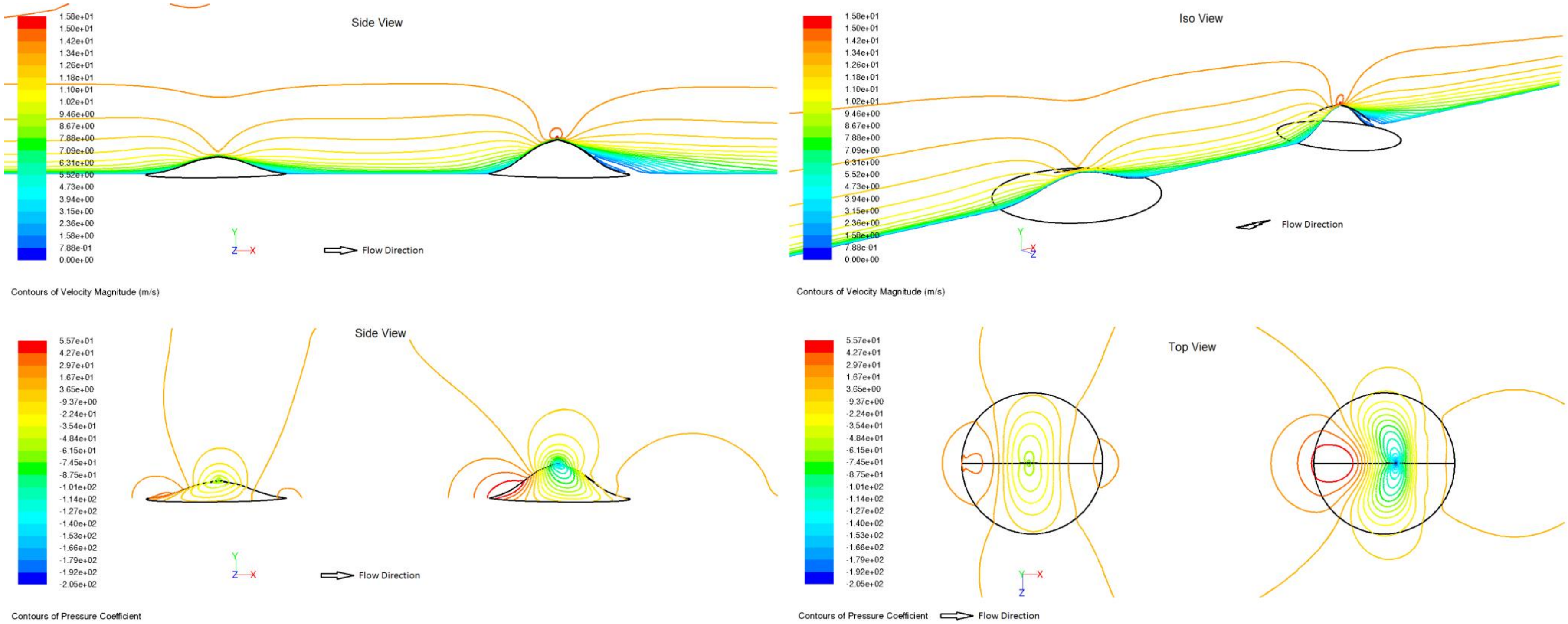

DH-02-ABL10h6 : Contour plots of mean velocity magnitude $\overline{u}$ and pressure coefficient Cp over shallow and steep 3D hills.

(Side views show contours on hill faces and mid-plane and top views show contours on hill and ground faces)

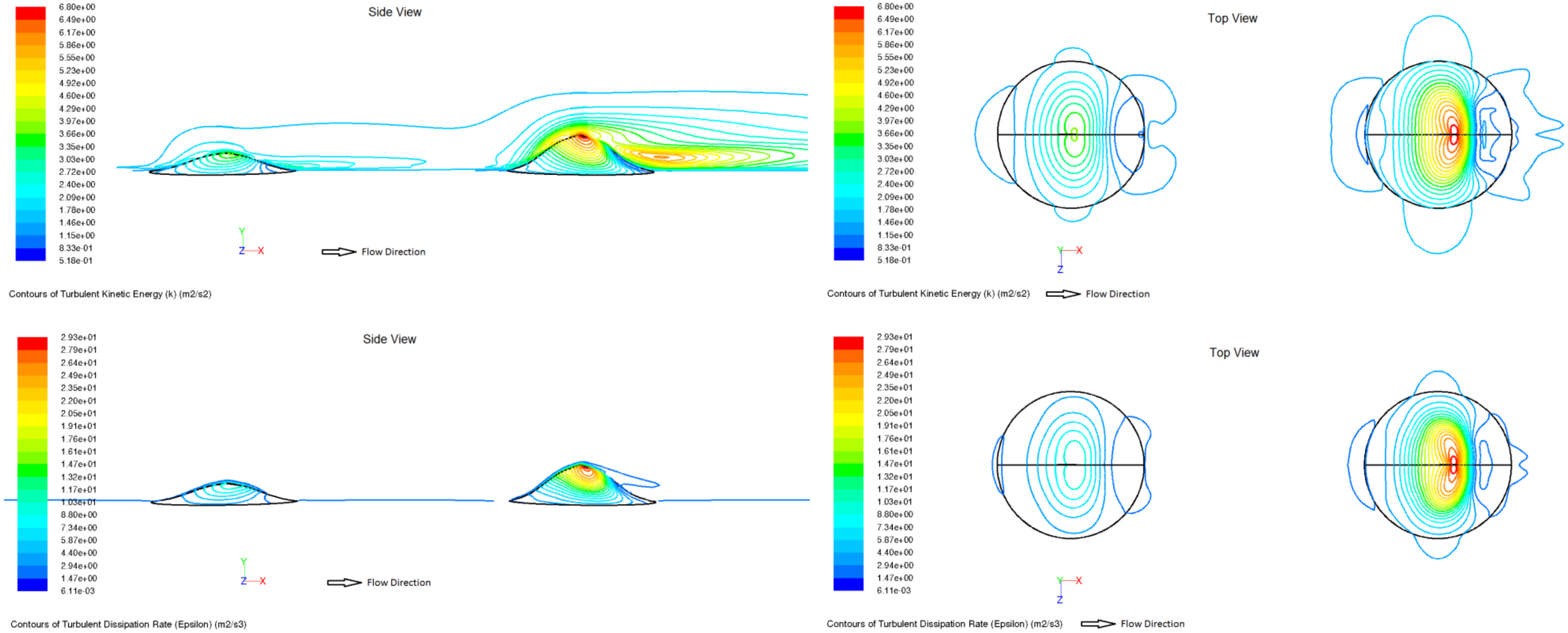

DH-02-ABL10h6 : Contour plots of turbulent kinetic energy k and dissipation rate ε over shallow and steep 3D hills.

(Side views show contours on hill faces and mid-plane and top views show contours on hill and ground faces)

A3.2.7 DH-03-ABL2h6

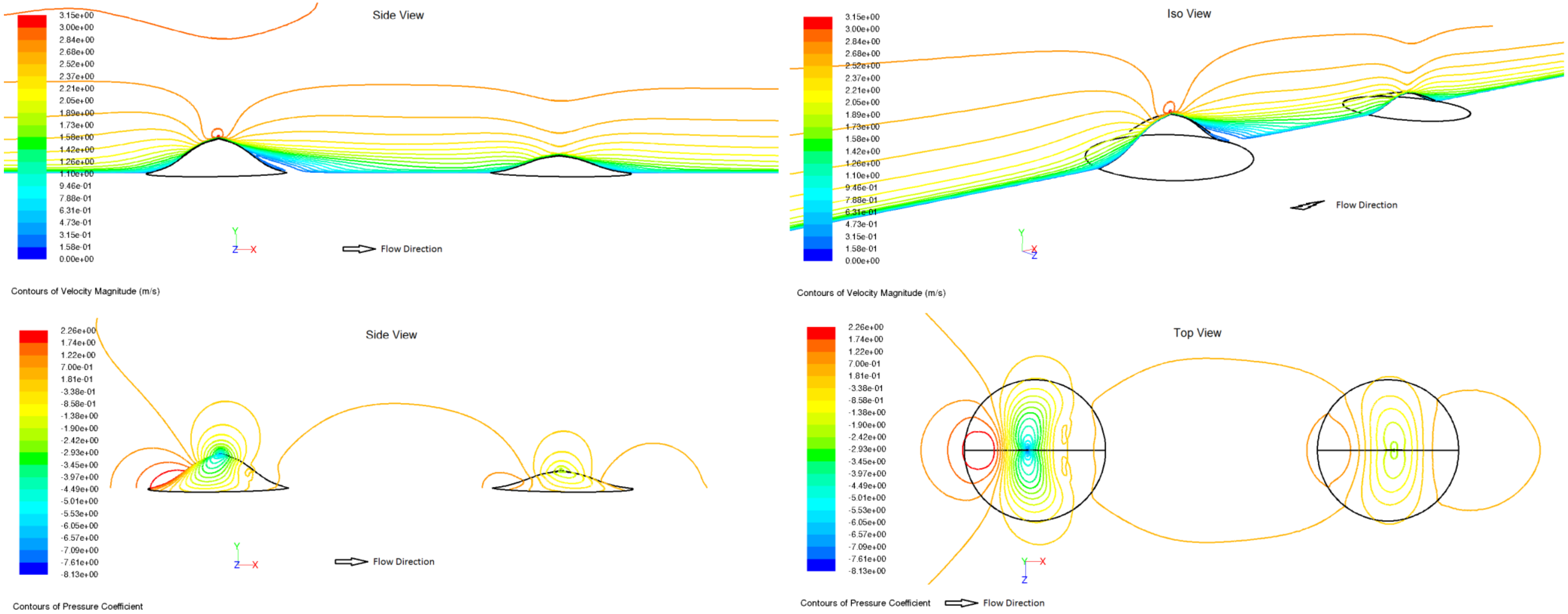

DH-03-ABL2h6 : Contour plots of mean velocity magnitude $\overline{u}$ and pressure coefficient Cp over steep and shallow 3D hills.

(Side views show contours on hill faces and mid-plane and top views show contours on hill and ground faces)

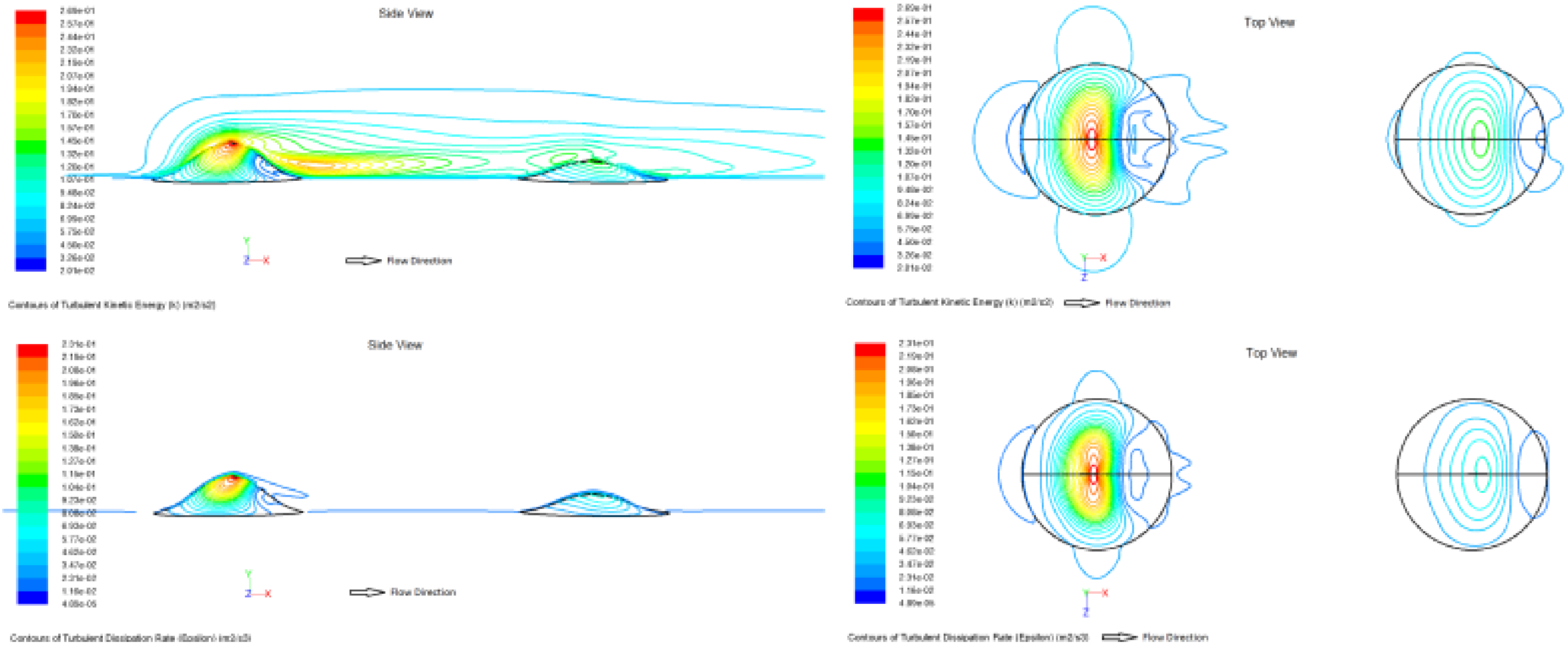

DH-03-ABL2h6 : Contour plots of turbulent kinetic energy k and dissipation rate ε over steep and shallow 3D hills.

(Side views show contours on hill faces and mid-plane and top views show contours on hill and ground faces)

A3.2.8 DH-03-ABL5h6

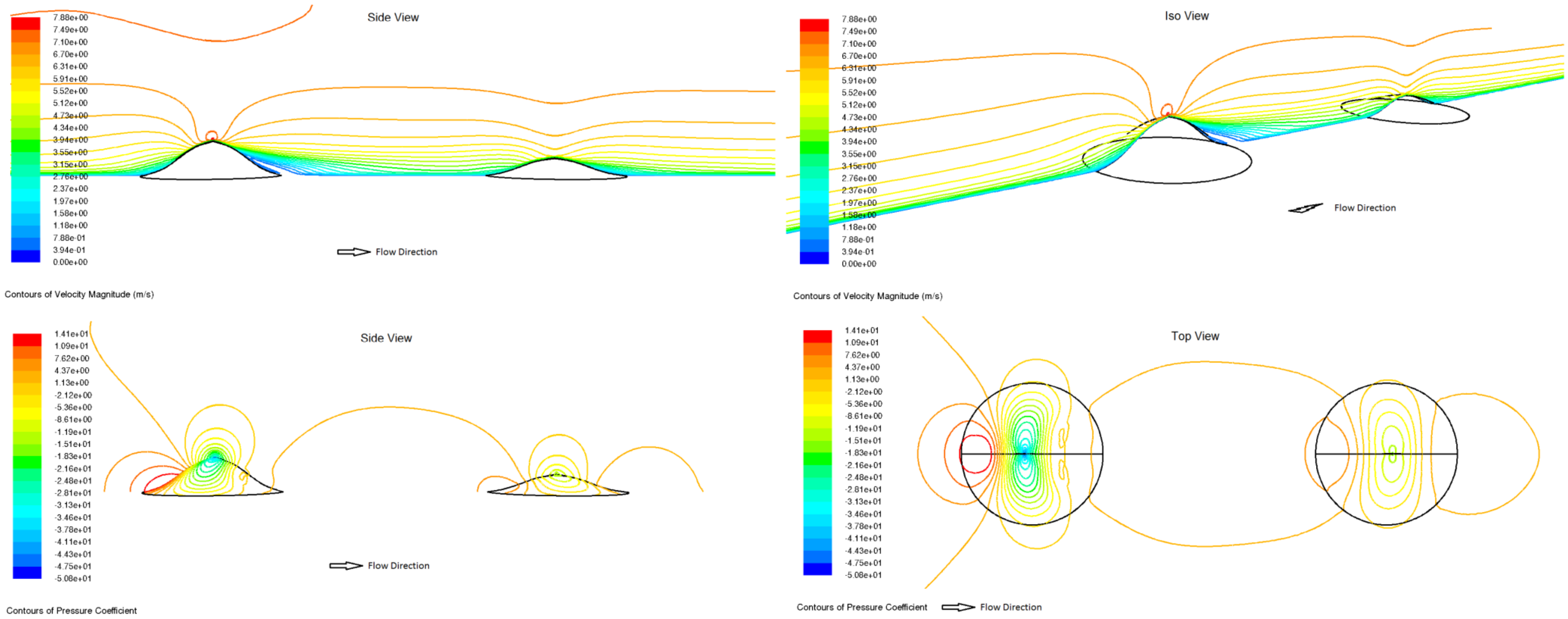

DH-03-ABL5h6 : Contour plots of mean velocity magnitude $\overline{u}$ and pressure coefficient Cp over steep and shallow 3D hills.

(Side views show contours on hill faces and mid-plane and top views show contours on hill and ground faces)

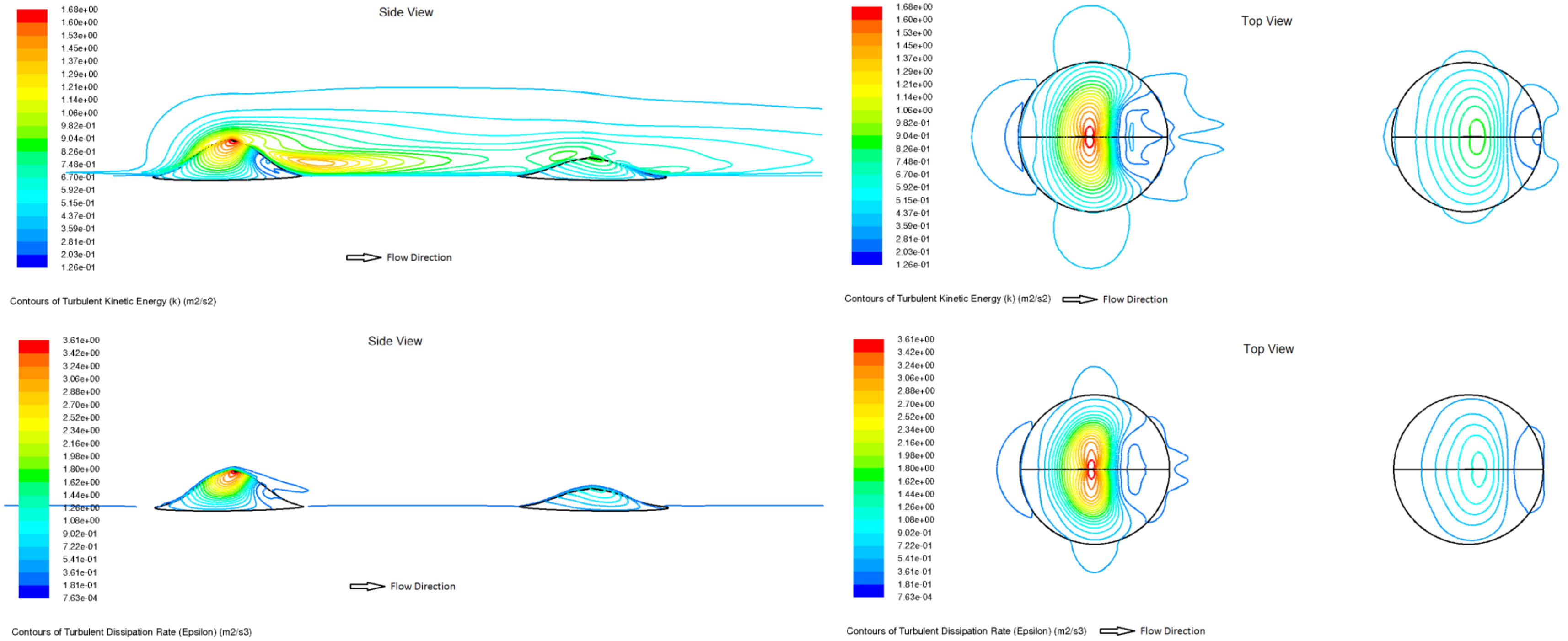

DH-03-ABL5h6 : Contour plots of turbulent kinetic energy k and dissipation rate ε over steep and shallow 3D hills.

(Side views show contours on hill faces and mid-plane and top views show contours on hill and ground faces)

A3.2.9 DH-03-ABL10h6

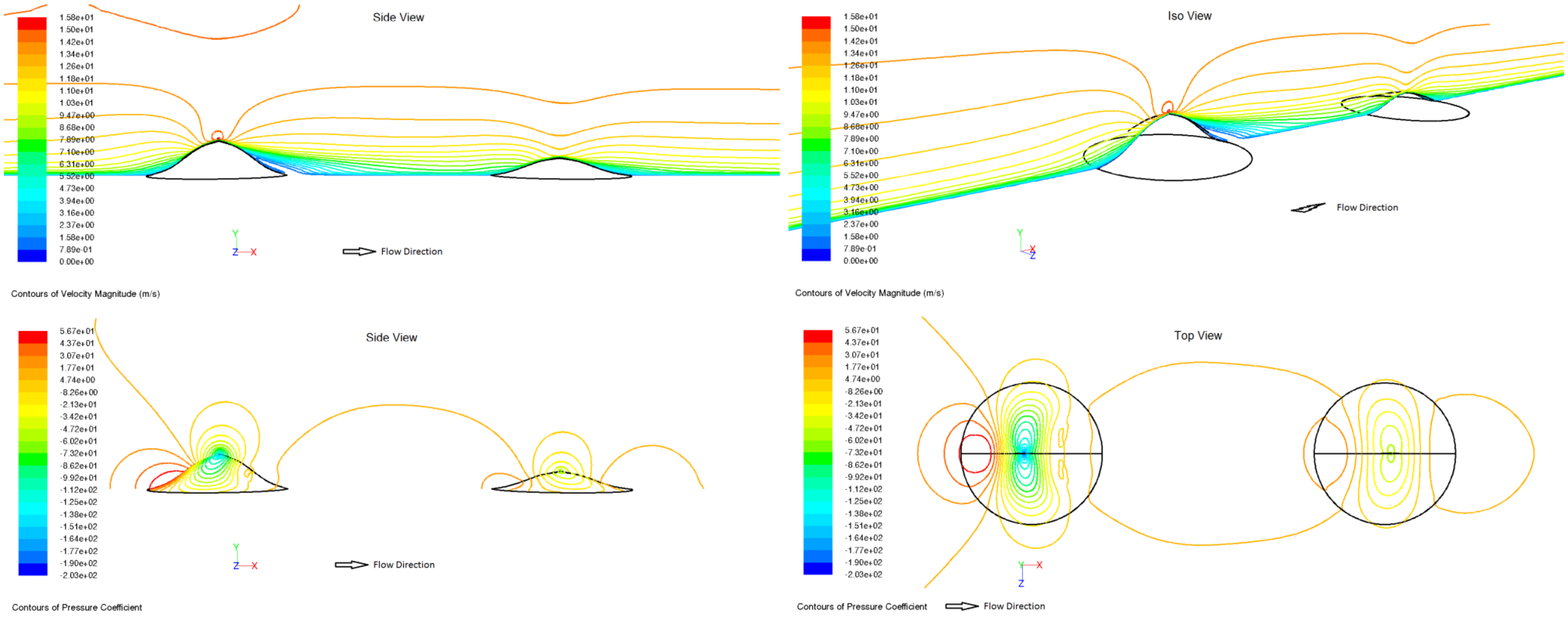

DH-03-ABL10h6 : Contour plots of mean velocity magnitude $\overline{u}$ and pressure coefficient Cp over steep and shallow 3D hills.

(Side views show contours on hill faces and mid-plane and top views show contours on hill and ground faces)

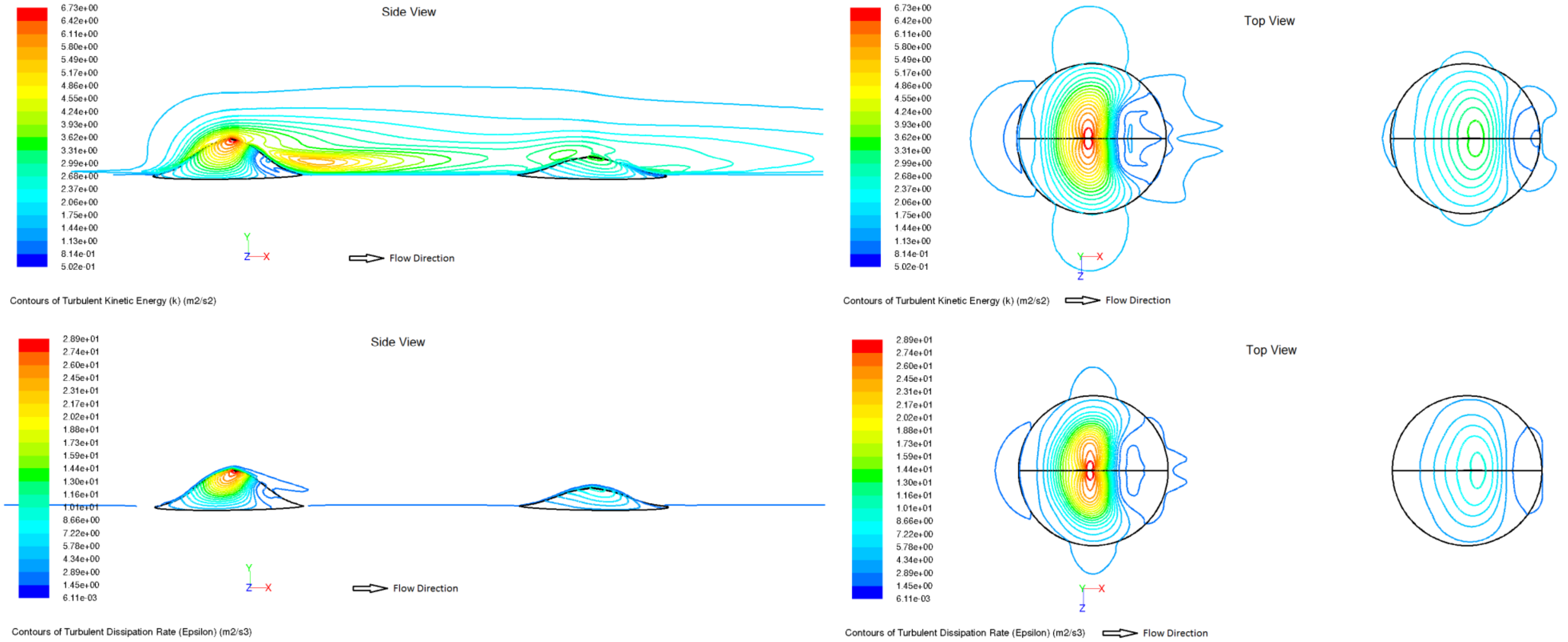

DH-03-ABL10h6 : Contour plots of turbulent kinetic energy k and dissipation rate ε over steep and shallow 3D hills.

(Side views show contours on hill faces and mid-plane and top views show contours on hill and ground faces)

A3.3Plots for Site A (SA-ABL2h6)

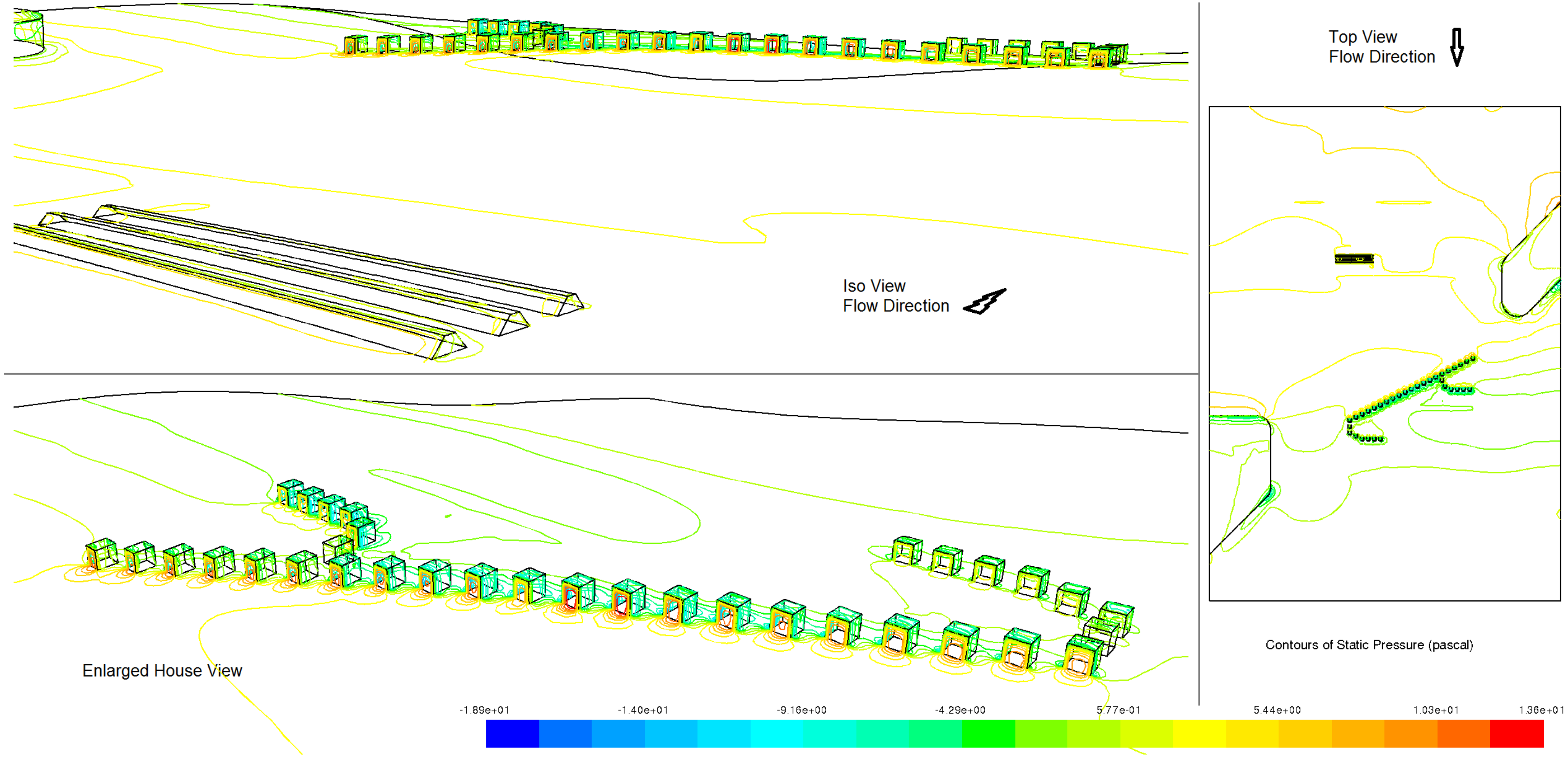

SA-ABL2h6 : Site A - Contours of static pressure p_{stat} for ground level of studied domain (isometric compost view, enlarged house view and top view) for inlet condition ABL2h6.

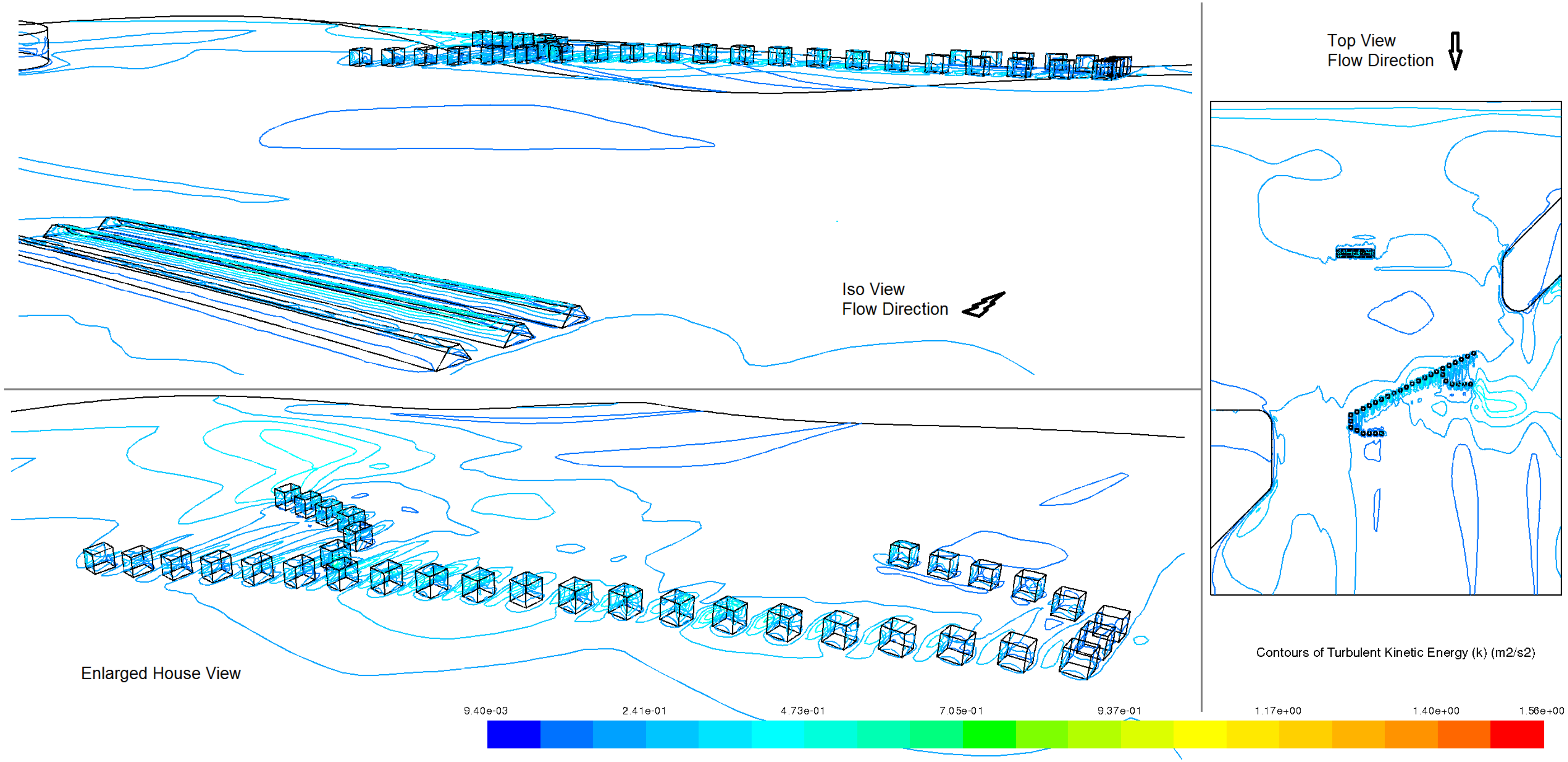

SA-ABL2h6 : Site A - Contours of turbulent kinetic energy k for ground level of studied domain (isometric compost view, enlarged house view and top view) for inlet condition ABL2h6.

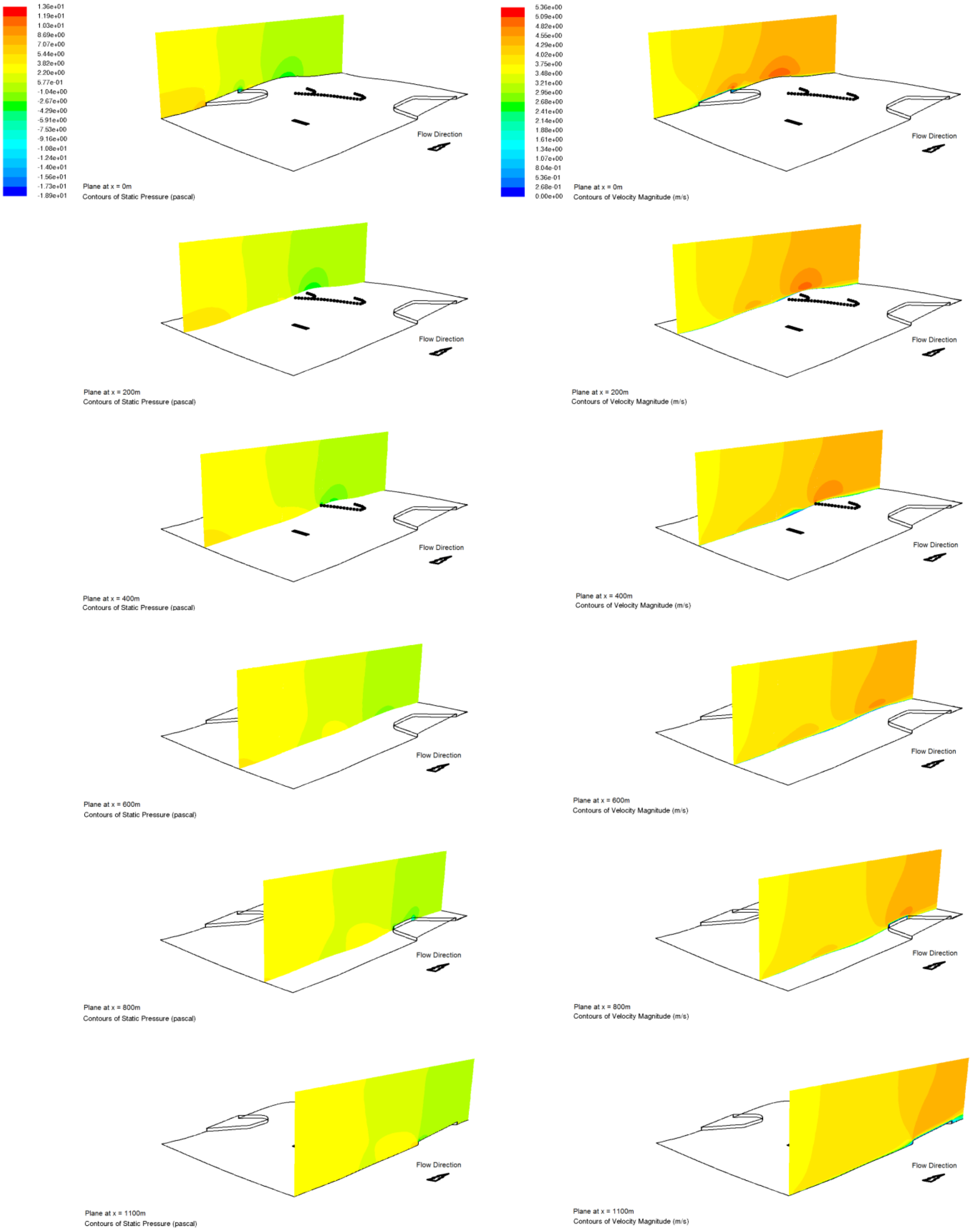

SA-ABL2h6 : Site A - Contours of (left) static pressure p_{stat} and (right) mean velocity magnitude $\overline{u}$ for selected planes along the x axis for inlet condition ABL2h6.

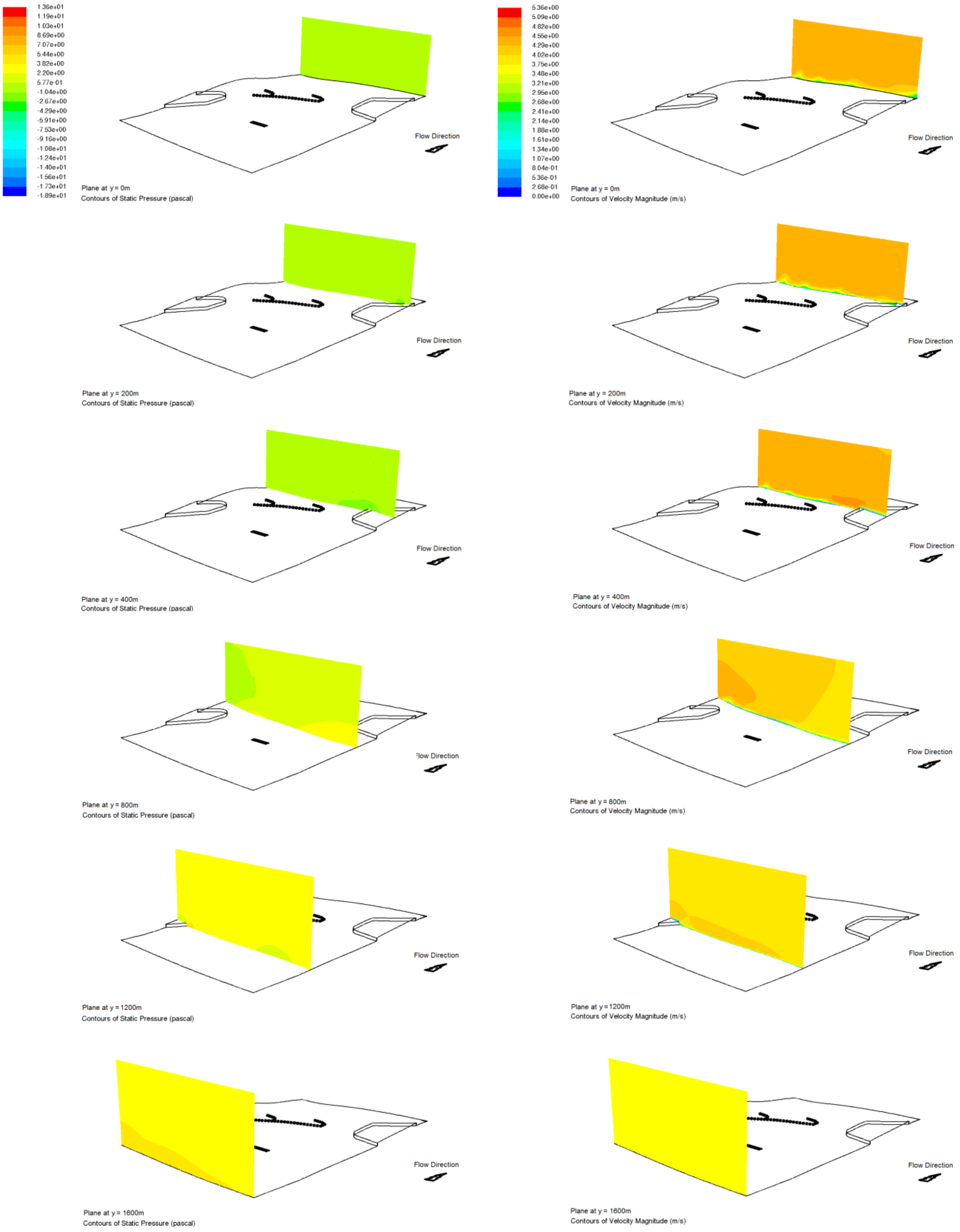

SA-ABL2h6 : Site A - Contours of (left) static pressure p_{stat} and (right) mean velocity magnitude $\overline{u}$ for selected planes along the y axis for inlet condition ABL2h6.

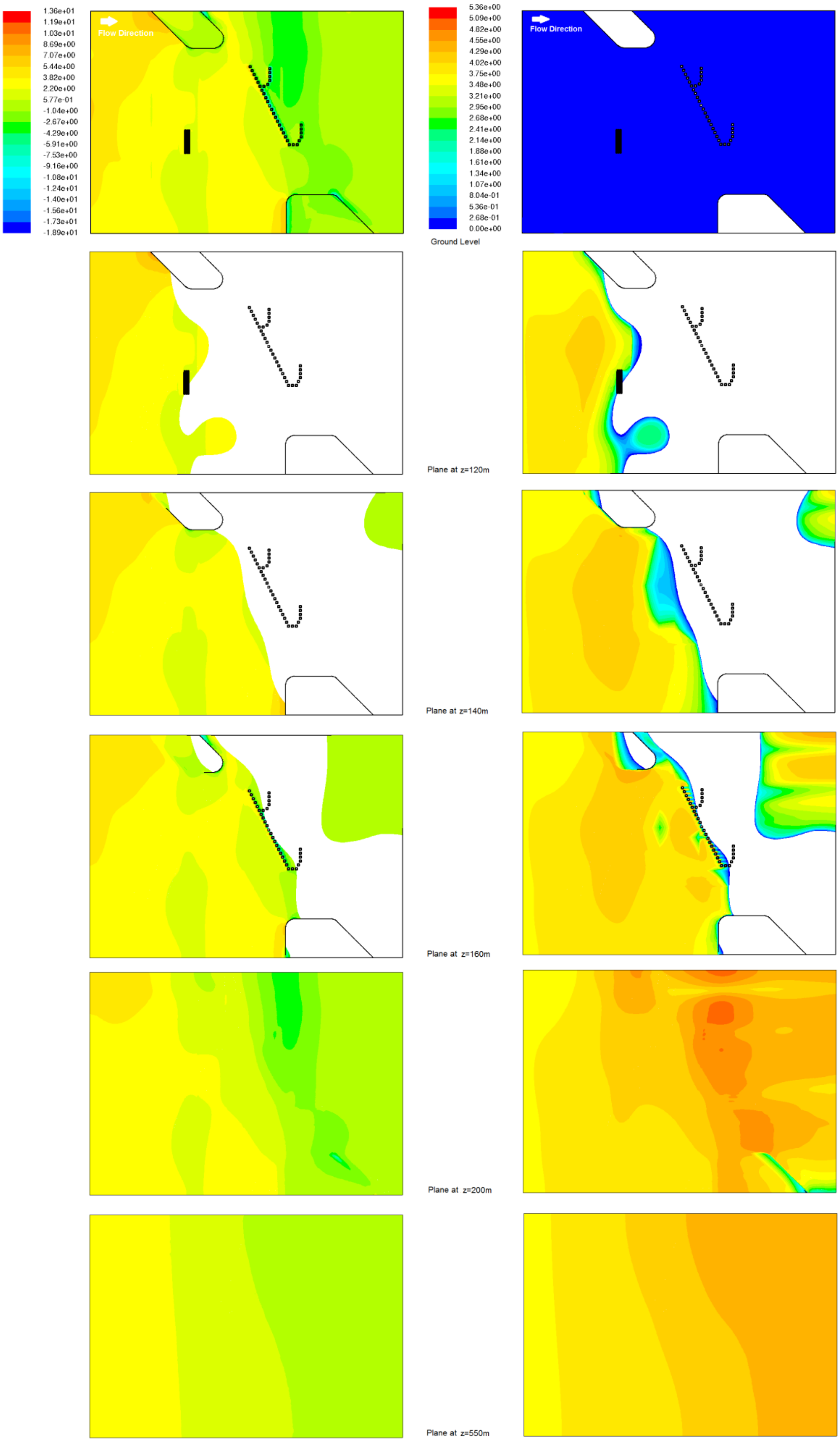

SA-ABL2h6 : Site A - Contours of (left) static pressure p_{stat} and (right) mean velocity magnitude $\overline{u}$ for selected planes along the z axis for inlet condition ABL2h6.

A3.4Plots for Site B (SB-ABL2h6)

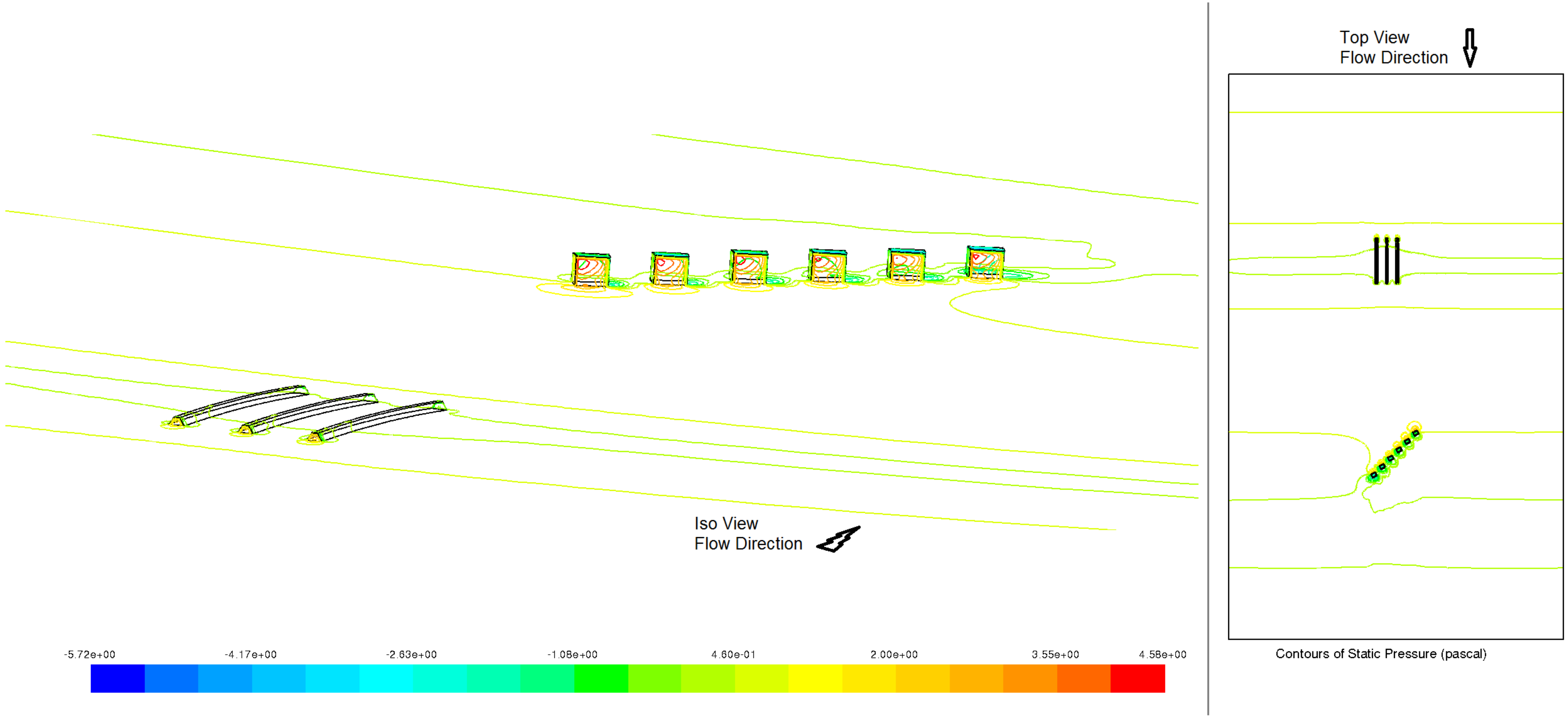

SB-ABL2h6 : Site B - Contours of static pressure p_{stat} *for ground level of studied domain (isometric compost-house view and top view) for inlet condition ABL2h6.*

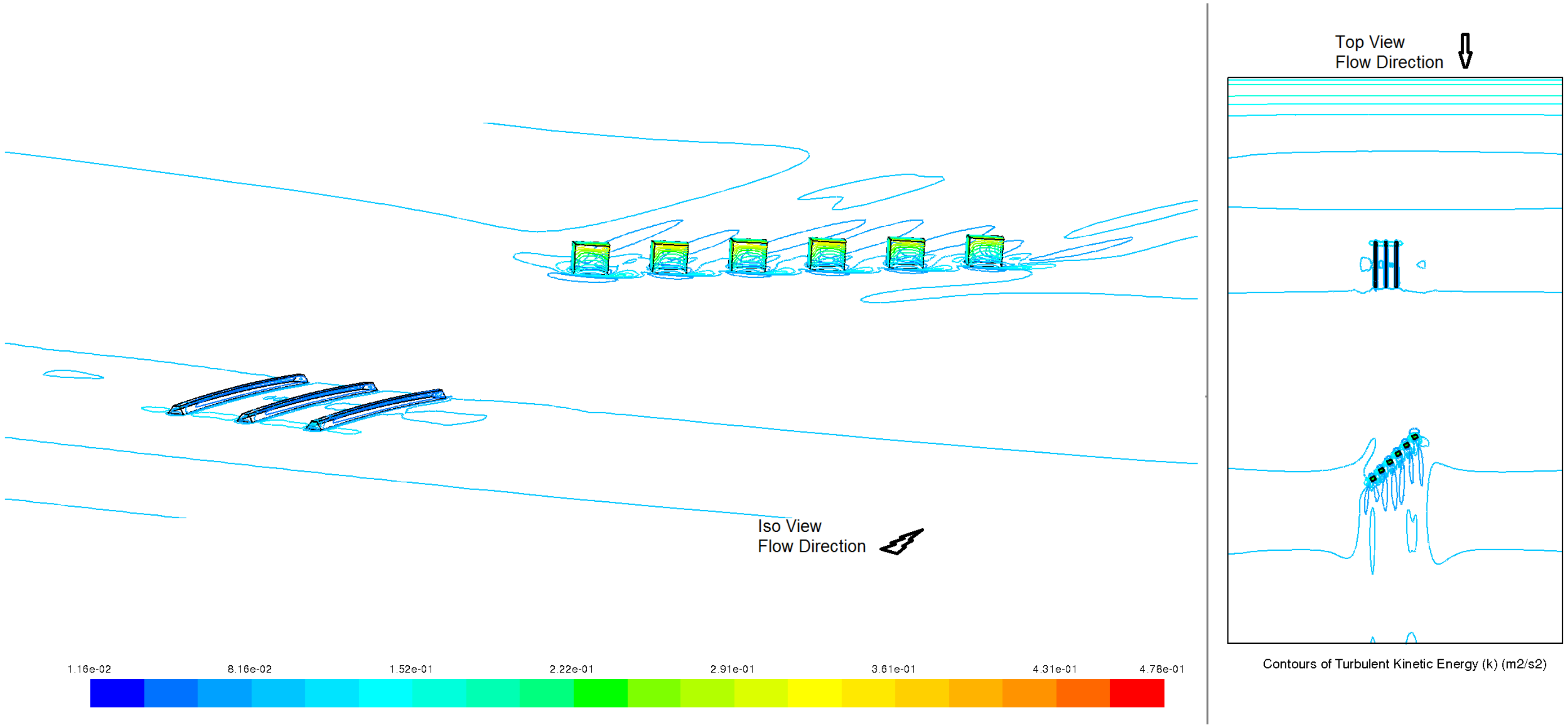

SB-ABL2h6 : Site B - Contours of turbulent kinetic energy k for ground level of studied domain (isometric compost-house view and top view) for inlet condition ABL2h6.

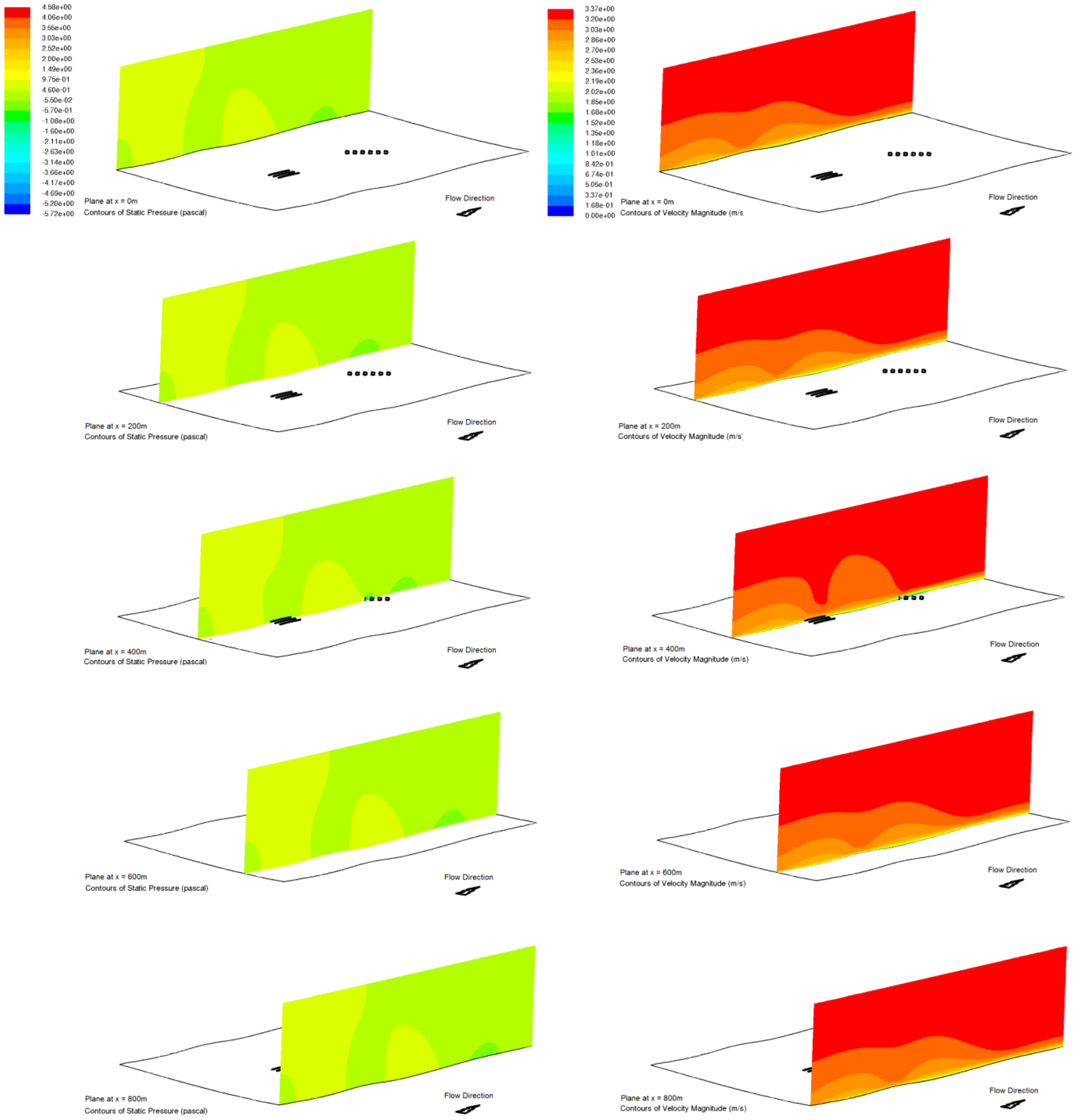

SB-ABL2h6 : Site B - Contours of (left) static pressure p_{stat} and (right) mean velocity magnitude $\overline{u}$ for selected planes along the x axis for inlet condition ABL2h6.

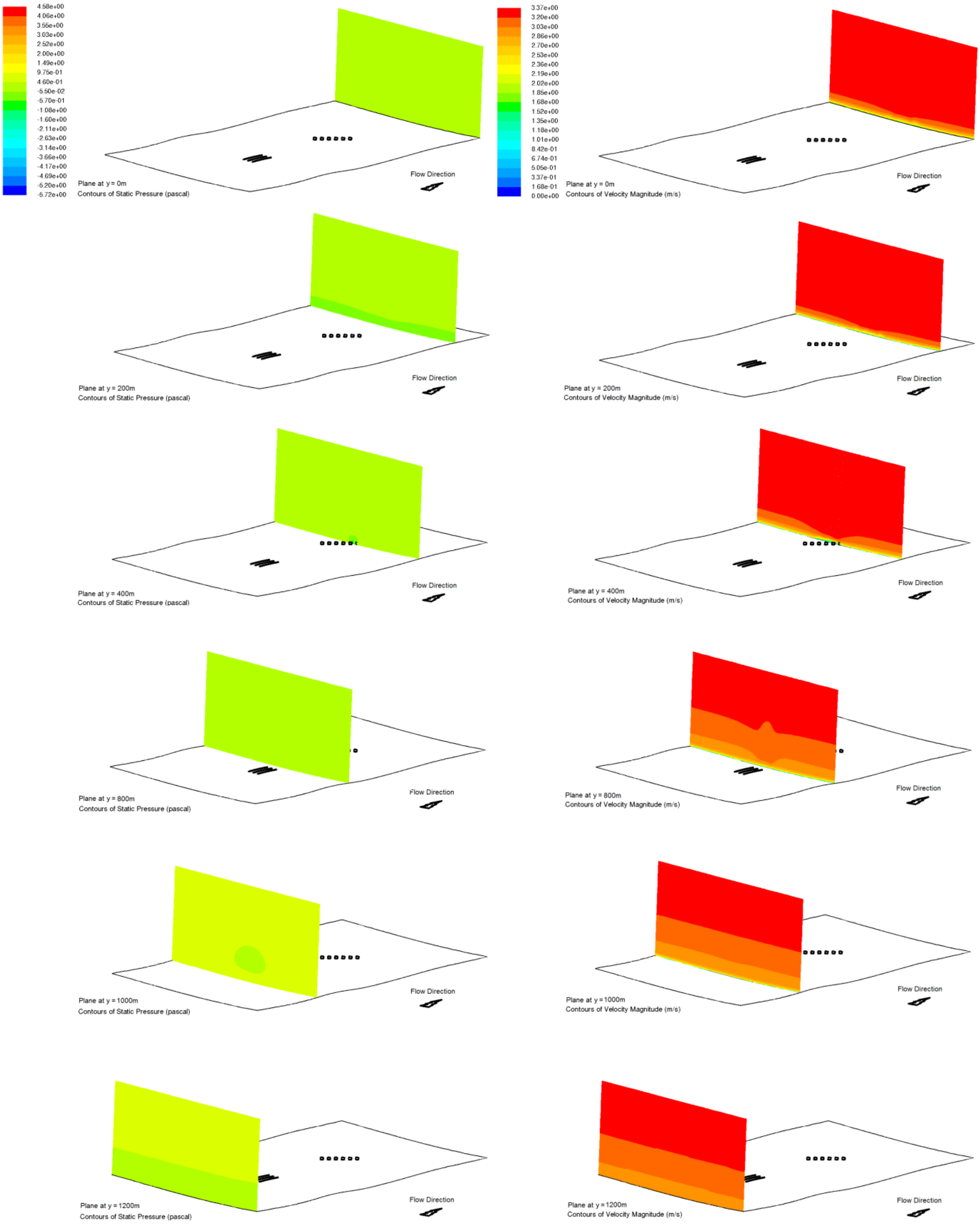

SB-ABL2h6 : Site B - Contours of (left) static pressure p_{stat} and (right) mean velocity magnitude $\overline{u}$ for selected planes along the y axis for inlet condition ABL2h6.

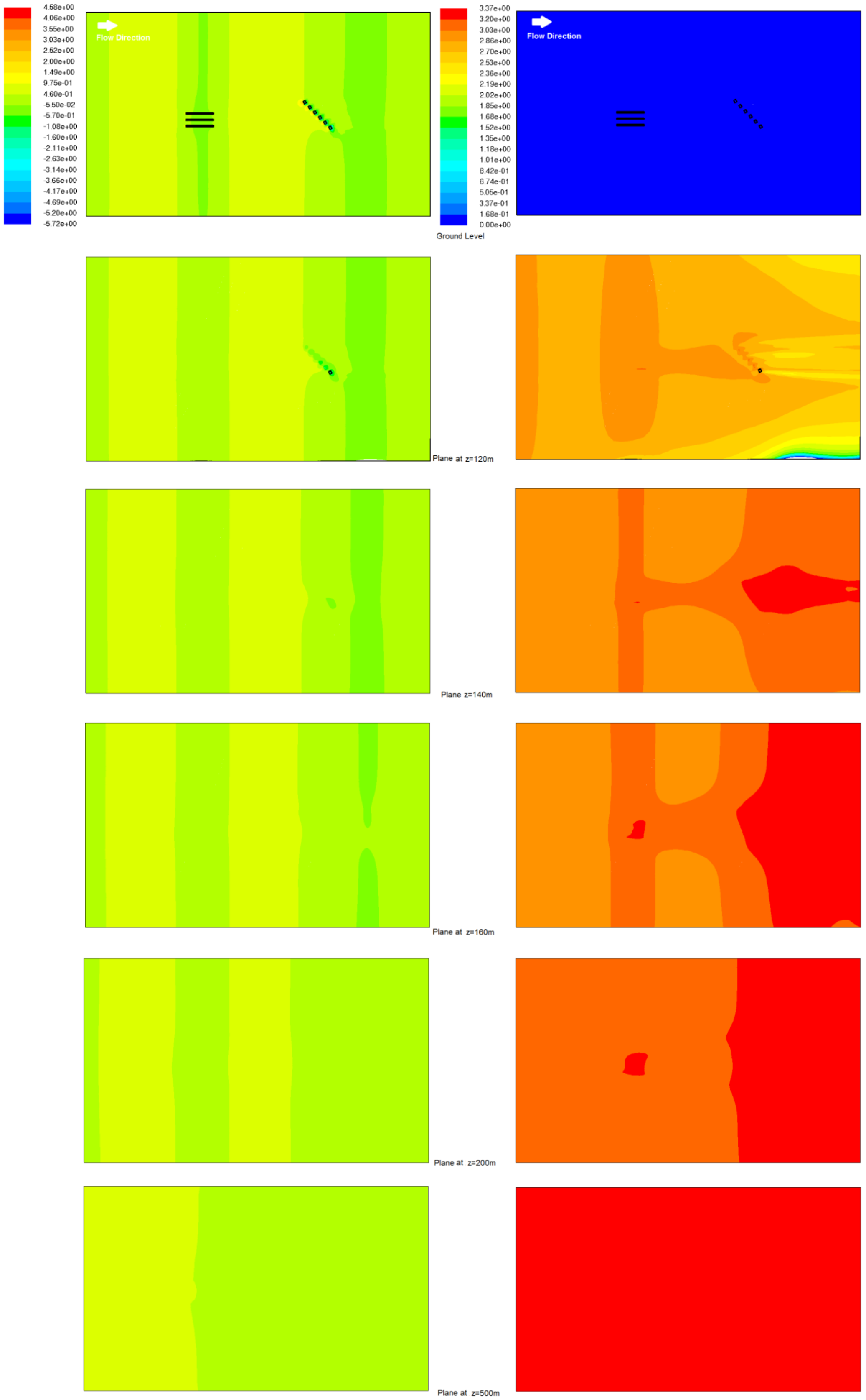

SB-ABL2h6 : Site B - Contours of (left) static pressure p_{stat} and (right) mean velocity magnitude $\overline{u}$ for selected planes along the z axis for inlet condition ABL2h6.